Afferent Connectivity of the Zebrafish Habenulae

Katherine Jane Turner

University College London
PhD Supervisor: Prof Stephen Wilson

A thesis submitted for the degree of
Doctor of Philosophy
University College London
February 2018

Declaration

I, Katherine Jane Turner confirm that the work presented in this thesis is my own. Where information has been derived from other sources, I confirm that this has been indicated in the thesis. Part of the work of this thesis has been published in:

Turner KJ., et al. Afferent Connectivity of the Zebrafish Habenulae. Front Neural Circuits. 2016 Apr 26;10:30. doi: 10.3389/fncir.2016.00030

Frontiers articles are published under a Creative Commons licence (CC-BY version 4.0) and all copyright remains with the author. I confirm that this article was written by me so some of the content may overlap partly with my thesis.

Abstract

The habenular nuclei are bilateral nuclei located in the dorsal diencephalon. The habenulae and their associated circuitry, the dorsal diencephalic conduction system (DDC) are conserved across all vertebrates. As part of the DDC, the habenulae act as a major relay station between forebrain regions and monoaminergic centres in the midbrain.

Zebrafish habenulae display prominent neuroanatomical asymmetries and asymmetries in circuit microarchitecture have been described in both afferent and efferent projections. In this study, I characterise two of the main forebrain afferent nuclei of the habenula: the ventral entopeduncular nucleus (vENT) and nucleus rostrolateralis (RL).

Through fate mapping, transgenic line analysis and gene expression studies, I show that the vENT is diencephalic in origin and extends into the telencephalon. vENT is the main afferent telencephalic nucleus of the habenula in zebrafish and is homologous to the entopeduncular nucleus in mammals.

I show the afferent nucleus conveying visual information to the habenula is RL. RL is prethalamic and retina and tectal recipient. RL and parapineal afferents asymmetrically innervate the left dorsal habenula. Using parapineal ablations and mutants in which habenula asymmetry is disrupted, I show that RL asymmetric innervation is not parapineal dependent. RL afferents arborise close to differentiating “left sided” habenula neuronal sub-types.

Previous studies in zebrafish claim the habenula receives pallial innervation. Using a pan-pallial enhancer -trap line, Tg(gata2:EGFP)^{bi105}, I show that this is not the case. I mapped the insertion to *egr3,* a gene linked to schizophrenia and important for hippocampal learning and memory and characterise the expression pattern of this line at larval stages.

To look at the morphologies and projection patterns of individual habenula afferent and pallial neurons I have adapted a method for switching EGFP to Gal4 in transgenic lines using CRISPR/Cas9.

The neuroanatomical characterisation of these habenulo-afferent areas lays important groundwork for further functional characterisation of this important circuit.

Acknowledgements

My biggest thank you goes to my PhD supervisor and boss of 15 years, Steve Wilson. Thank you for always employing me, despite my tendency to wander off down various other non-scientific paths from time to time. Thank you for supporting me financially and academically to study for my doctorate. Lastly, thank you for creating such a fantastic work environment that attracts other inspiring scientists and humans. The Wilson Lab is like a very agreeable tarpit from which no one ever quite escapes….and I love it there.

Thank you to my thesis committee; Masa Tada, Yoshiyuki Yamamoto aka Yama and Isaac Bianco for your great input on my project. Thanks also to UCL for their financial and administrative support. I benefitted immensely from my undergraduate UCL Neuroscience tutors, John Scholes and Jon Clarke, who first inspired me to work in academia and in zebrafish neural development in particular. The zebrafish group at UCL goes from strength to strength. Pooling our resources and most importantly our brains has been a great success and I heartily thank all members of the Wilson, Rihel, Tada, Bianco, Gestri and Hawkins labs for all the help and sweet treats they have given me.

When you have worked somewhere for so long you see many friends come and go. Thankfully Wilsonites never seem to go too far and if they do, they always come back at regular intervals. Too many past and present members I can't name you all. Special thanks to my undergraduate supervisor Florencia Cavodeassi, thank you for teaching me the right way to do all my experimental work and being infinitely patient and sweet. Tom Hawkins, thank you for then teaching me all the shortcuts! Tom, I wouldn't like to tot up how many hours we have spent together in pitch black microscope rooms and steamy fish rooms throughout the world. Somehow, we always make it fun and I never tire of your company. Gaia, I love you my curry queen. Monica, thank you for teaching me more about fish neuroanatomy than any book ever has and for being a brilliant friend. Swim team, Tom and Ricardo, thanks for making me want to swim every morning, no matter how hungover or pregnant I was- I love you guys…and PRET chocolate croissants. Beijos to the Piccolo Crew, obrigada!

I would like to thank my loving family. Mum and Dad, thank you for being endlessly supportive parents and grandparents to Joe. To Dave my very very funny brother. Mary and Bill who taught me not to work too hard. Thank you to my grandfather Francis Ludden for being the best human and my grandmother Dymphna for being a force of nature. The last thank you goes to the loves of my life…James and Joe who bring me joy every day. I love you so much.

Table of Contents

List of figures

List of Tables

Abbreviations

ac, anterior commissure; BNSM, bed nucleus of the stria medullaris; BSTdm, dorsomedial part of the bed nucleus of the stria terminalis; BNST, bed nucleus of the stria terminalis: CC, cerebellar corpus; D, diffuse nucleus of the hypothalamus; DBB, diagonal band of Brocca; DDC, dorsal diencephalic conduction system; dENT, dorsal entopeduncular nucleus; dHbL, lateral subnucleus of the dorsal habenula; dHbM, medial subnucleus of the dorsal habenula; Dl, lateral area of the pallium; Dm, medial area of the pallium; Dp, posterior area of the pallium; EmT, emminentia thalami; ENT, entopeduncular nucleus; fr, fasciculus retroflexus; GL, glomerular layer of the olfactory bulb; Hb, habenula; Hc, habenula commissure; Hd, dorsal zone of the periventricular hypothalamus; HL, lateral hypothalamic lobe; IPN, interpeduncular nucleus; I, intermediate thalamic nucleus; lfb, lateral forebrain bundle; lHb, left habenula; LF, longitudinal fascicle; LH, lateral hypothalamus; LPO, lateral pre-optic area; MLF, medial longitudinal fasicle; MR, median raphe; OB, olfactory bulb; och, optic chiasm; OT, optic tectum; Otr, optic tract; P, pineal; PAG, periaqueductal grey; Pal, pallium; PG, preglomerular complex; PGZ, periventricular grey zone; PHL, posterior hypothalamic lobe; PO, preoptic region; Pp, parvocellular preoptic nucleus; PP, parapineal; PT, posterior tuberculum; PTh, prethalamus; PTN, posterior tuberal nucleus; rHb, right habenula; RL, nucleus rostrolateralis; S, septal area; SFGS, stratum fibroseum et griseum superficiale; SG, secondary gustatory nucleus; StMed, stria medullaris; Tel, telencephalic lobes; Th, thalamus; tHC, tract of the habenular commissure; TL, longitudinal torus; TLa, lateral torus; TS, semicircular torus; V, subpallium; VC, valvula cerebelli; Vd, dorsal area of the subpallium; vENT, ventral entopeduncular nucleus; vHb, ventral habenula nucleus; Vl, lateral area of the subpallium; VL, ventro-lateral thalamic nucleus; VM, ventro-medial thalamic nucleus; Vs, supracommissural area of the subpallium; Vv, ventral area of the subpallium; ZLI, zona limitans intrathalamica.

Chapter 1. Introduction

1.1 The dorsal diencephalic conduction system

1.1.1 Overview

Why are we interested in studying the habenula?

The habenulae are components of highly conserved circuitry, the dorsal-diencephalic conduction system (DDC) that interconnects sites in the limbic forebrain with the ventral midbrain and hindbrain. The habenulae have started to attract a lot of interest of late due to its role in modulating both the dopaminergic and serotinergic systems (Hikosaka., 2008).

The habenulae are important in a range of behaviours including the modulation of fear behaviours, avoidance learning and attention (Agetsuma et al, 2010, Lee et al, 2010). The habenulae regulate monoaminergic activity and consequently have been implicated in psychosis, depression, anxiety, schizophrenia and addictive behaviours. They also play a role in circadian rhythms, sleep initiation and duration and reproductive and maternal behaviours (Bianco & Wilson 2009; Hikosaka 2010).

The habenular nuclei exhibit left-right asymmetries in most vertebrates (Concha & Wilson 2001). In zebrafish, the habenulae display differences in the proportion of neuronal subtypes with distinct gene expression profiles, projection patterns and axon terminal morphologies (Reviewed in (Roussigné et al. 2012). The functional consequences of habenular asymmetry are not known although disrupting these left-right asymmetries in zebrafish reduces exploratory behaviour and increases cortisol levels, two factors associated with increased anxiety (Facchin et al. 2015). Correlations between habenular laterality and certain behaviours in zebrafish (Barth et al. 2005; Facchin, Burgess, et al. 2009; Facchin, Argenton, et al. 2009) and other fish (Gutiérrez-Ibáñez et al. 2011) have also been observed.

The goal of my research is to identify the habenula-associated circuitry in zebrafish. Although afferent inputs into the habenula have been anatomically well described in higher vertebrates, these connections are currently not well defined in the larval zebrafish. Using transgenic tools to label specific neuronal populations, we hope to identify key brain areas projecting to the epithalamus and to define any neuroanatomical asymmetries in these projecting neurons.

Why study this circuitry in the fish?

Studies unravelling the function of the habenula are sparse in mammals due to the small size and inaccessibility of this structure. Until recent advances in fMRI and positron emission tomography (PET) the activity of human habenula could not be visualised. Following improvements in the resolution of these imaging techniques, the activity of habenular neurons have been shown to play a role in reward based learning (Salas et al. 2010) and also in several pathologies such as depression (Savitz et al. 2011), schizophrenia (Shepard et al., 2006; Holcomb et al., 2008) and drug induced psychosis. Comparatively, in zebrafish the habenula is relatively large and amenable to genetic and cellular manipulation during embryonic development. Moreover, this structure displays overt molecular and anatomical asymmetries thus giving us the unique opportunity to assess the functional significance of the observed neuroanatomical asymmetries, and how these asymmetries are linked to lateralised behaviours.

1.1.2 Habenula

The habenulae along with the pineal complex are part of the epithalamus. These bilaterally paired nuclei are located in the dorsal diencephalon next to the third ventricle, rostral to the posterior commissure. The habenular commissure runs between the left and right habenular nuclei (Butler & Hodos, 1995). Each habenular nucleus can be further subdivided into a medial (MHb) and lateral (LHb) subnucleus. These distinct subnuclei for the most part receive different afferent inputs and project to different regions in the midbrain, and so form part of distinct sub-circuits within the DDC (Herkenham & Nauta 1977b; Bianco & Wilson 2009). In birds and mammals where pineal and parapineal innervation of the habenulae is not present the habenular nuclei are overtly symmetric (Sutherland 1982) but functional asymmetries have been described in both mice (Ichijo et al. 2015; Ichijo et al. 2016) and humans(Hétu et al. 2016; Hennigan et al. 2015; Lawson et al. 2014) .

The habenulae in zebrafish:

The habenulae are ovoid nuclei sitting either side of the dorsal midline of the diencephalon containing monopolar projection neurons (Bianco et al. 2008). Habenular projection neurons direct their dendrites inwards forming an internal neuropil core that the cell bodies surround. Habenular neurons project their axons via the fasiculus retroflexus to the interpeduncular nucleus (IPN) and the median raphe.

The habenulae are divided into dorsal and ventral subnuclei. In both habenulae a dorsal (dHb) and ventral (vHb) nucleus can be distinguished. The dHb is considered the homologue of the mammalian medial habenula and the vHb, the homologue of the lateral habenula. The dorsal habenula nucleus can be further subdivided into lateral (dHbL) and medial subnuclei (dHbM)(Figure 1) (Amo et al. 2010).

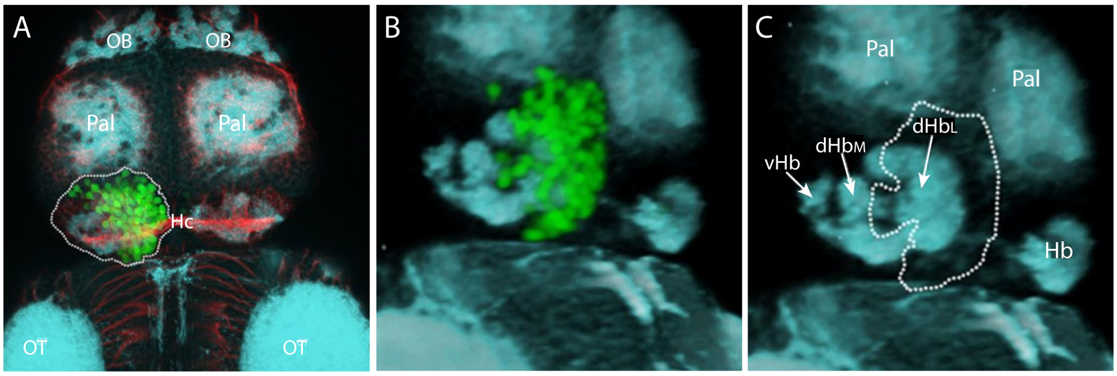

Figure 1.1: **The habenular subnuclei. (A)** Dorsal view of the brain of a 4dpf Tg(mp558b:GFP) embryo co-labelled with anti-acetylated tubulin(red) and SV2(blue) and shown in a z-projection of a confocal stack (A). This line expresses GFP only in the left dHbL nuclei (marked by the dashed white line in A). **(B & C)** show the same confocal stack rendered into 3D. By tilting the stack to the right and displaying only SV2 (C) or SV2 and GFP (B), we can see the synaptic neuropil of the three subnuclei (vHb, dHbm, dHbl; C) and their relative positions at this stage of development. In panel C, the region that would be GFP positive is indicated by the dashed white line.

The relative positions of the habenular subnuclei change throughout development. By observing the expression pattern of a vHb specific marker *diamine oxidase (dao*) throughout development it is possible to see that the dorso-ventral orientation of the fish habenula is a result of a morphogenetic process. At 5dpf expression of *dao* in the primordium is lateral to the dorsal habenula nuclei. This region then migrates ventro-medially to result in the arrangement we observe in the adult zebrafish (Figure 2) (Amo et al. 2010).

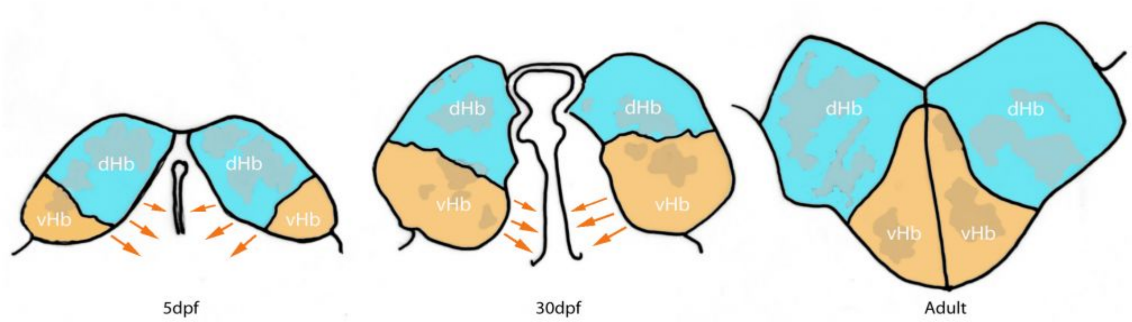

Figure 1.2: Morphogenesis of the habenula in zebrafish. Schematic showing the relative positions of the dorsal and ventral habenulae subnuclei at different stages of development. At 5dpf the vHb subnucleus (orange) is lateral to the dorsal habenular nuclei (cyan) in the habenular primordium. This region then migrates ventro-medially to produce the arrangement we observe in the adult zebrafish. dHb (blue) and vHb(orange)(Schematic adapted from (Amo et al. 2010)).

The dorsal habenula (dHb)

The dHb is homologous to the mammalian medial habenula. The dHb in the zebrafish and the mammalian medial habenula both innervate the interpeduncular nucleus (IPN) and show conserved patterns of gene expression that suggest homology(Aizawa et al., 2005). In the zebrafish, the dHb can be further subdivided into medial (dHbM) and lateral (dHbL) subnuclei. These subnuclei have different size ratios on the left and the right and innervate different regions of the IPN (Aizawa et al. 2005; Gamse 2005; Bianco et al. 2008). In the adult, the dHbL subnucleus is much larger on the left side and is the main source of projections to the dorsal region of the interpeduncular nucleus. The dHbM subnucleus that is larger on the right, projects mainly to the ventral IPN. In the adult IPN, there is an intermediate region that receives innervation from both the dHbM and dHbL (Reviewed in (Okamoto et al. 2012). These distinct projects from dHbM and dHbL are also evident at larval stages although the intermediate zone of the IPN is not clearly defined.

The ventral habenula (vHb)

The vHb is homologous to the mammalian lateral habenula and projects to the median raphe. In zebrafish the vHb nucleus is initially positioned lateral to the dHb in embryonic/larval stages but morphogenetic movements within the epithalamus eventually position this nucleus ventral to the dHB in the adult (Figure 1.2). This nucleus is overtly symmetrical in the zebrafish (Amo et al. 2010). The efferent projections from the vHb travel to the median raphe in the outer sheath of the fasciculus retroflexus surrounding the efferents from the dHb (Amo et al., 2010).

In mammals, neurons of the lateral habenula project to the dorsal and median raphe, substantia nigra and the ventral tegmentum. Homology of the mammalian lateral habenula and the zebrafish vHb is further supported by homologous gene expression in addition to connectivity (Amo et al. 2010).

1.1.3 Organisation and function of habenula circuitry in mammals

N.B our understanding of habenula circuitry is mostly based on the rat as it is well resolved in this system (Herkenham & Nauta 1977b).

The medial and lateral habenular subnuclei receive distinct afferent inputs and project to different downstream targets. Thus, the functions of these two parallel pathways are distinct. The following section describes what is known of the connectivity and function of MHb and LHb associated circuitry.

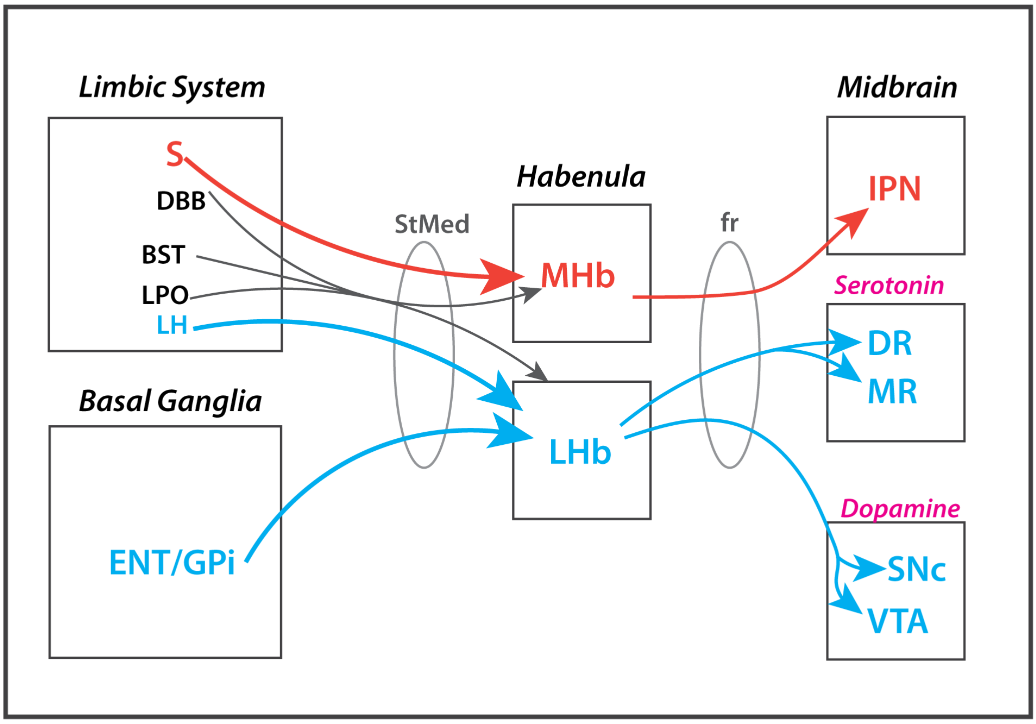

Figure 1.3 Afferent and efferent connections of the habenula (adapted from Hikosaka et al., (2008)). The MHb, LHb, and pineal body (PB) are collectively called the epithalamus. The MHb receives inputs mainly from the supracommissural septum (S) and sends outputs to the interpeduncular nucleus (IP). The LHb receives inputs mainly from the basal ganglia and limbic regions and sends outputs to the brain structures containing DA neurons and serotonin neurons. Afferent and efferent connections of the habenula are conveyed by the stria medullaris (sm) and fasciculus retroflexus (fr), respectively. Green and blue lines indicate the axonal connections associated with the MHb and LHb, respectively; black lines are associated with both. The thickness of the line implies the strength of the connec- tion. Many other connections are not shown, including reverse connections (e.g., from DR/VTA to LHb). DR, Dorsal raphe; MR, medial raphe; S, septum; DBB, nucleus of diagonal band of Broca; BST, bed nucleus of stria terminalis; LPO, lateral preoptic area; LH, lateral hypothalamus; GPi, globus pallidus internal segment; CPu, caudate and putamen; sm, stria medullaris; fr, fasciculus retroflexus. This figure was modified with permission from Hikosaka (2007a).

Limbic system →MHb→IPN/raphe

Various studies have implicated medial habenula circuitry in the control of fear and anxiety. The major afferent input to the medial habenula in mammals comes from septal nuclei. In particular from the posterior septal nuclei, the septofimbrial nucleus and the nucleus triangularis (Herkenham & Nauta 1977b).

A recent paper in mouse also showed innervation of the dMHb from the bed nucleus of the anterior commisure (BAC) (Yamaguchi et al. 2013). This paper dissected septohabenulo afferent pathways from the triangular septum (TS) and the BAC both anatomically and functionally. They were able to show that these septal nuclei project to different regions of the medial habenula and that ablating the TS-vMHb projection neurons impaired anxiety related behaviours. Ablation of the BAC-dMHb projection had no effect on anxiety but changed both fear responses and fear learning. Another study, using optogenetic stimulation of the glutamatergic MHb afferents from the posterior septum, also suggested a role in locomotion and anxiolysis (Otsu et al. 2018). These two septal nuclei receive distinct inputs. The TS receives most of its input from the hippocampus and median raphe while the BAC is innervated by the medial amygdala (Yamaguchi et al. 2013).

MHb neurons project to the IPN via the fasciculus retroflexus. How the MHb modulates fear and anxiety behaviours is likely to be complicated due to the multitude of targets innervated by the IPN. The IPN in the rat is composed of seven subnuclei that express several different neurotransmitters in a spatially organised pattern within the different subnuclei including somatostatin, met-Enkephalin and substance P (Morley 1986); Hamil et al, 1984). The major targets of IPN neurons are the dorsal tegmental region and the raphe. Regulation of serotinergic neurons in the raphe by the IPN could affect the response to aversive stimuli (Mathuru & Jesuthasan 2013). The dorsal tegmental region projects to many limbic regions throughout the brain (Groenewegen & Van Dijk 1984).

In zebrafish, similar projections from the IPN to the dorsal raphe have been described. These projections extend around the medial longitudinal fasciculus and extend throughout a longitudinal region called the griseum centrale. This region in the zebrafish is thought to be homologous to the periaqueductal grey, the dorsal tegmental nucleus and nucleus incertus in mammals, regions that are implicated in control of behaviour under stressful or fearful conditions (Okamoto et al. 2012). In mammals, different regions of the

PAG are responsible for different coping strategies in response to aversive stimuli. The different behaviours evoked in response to stressful situations can be separated into “active” coping strategies including confrontational or defensive postures and escape behaviours and “passive” coping strategies or freezing behaviours (Okamoto et al. 2012). In zebrafish, disruption of this pathway biases towards freezing behaviours rather than normal escape response to a fear conditioned stimulus (Agetsuma et al. 2010). These results have lead to the hypothesis that the habenula can act as a switch between these different coping strategies in response to previous experience of stressful situations.

Another study in which the same pathway was silenced in zebrafish looked at the behaviour of the fish in response to various aversive stimuli that had been designed to mimic natural stressors as opposed to repetitive unnatural aversive stimuli (Mathuru & Jesuthasan 2013). Under these conditions, the authors found that although the fish with silenced nuclei displayed a disproportionate response to mildly stressful novel stimuli compared to wildtypes they were able to show both active and passive responses indicating an increase in baseline anxiety rather than a particular bias to one coping strategy. In adult zebrafish, preferential silencing of dHbM/vIPN and dHbL/dIPN efferent pathways revealed that the activity of these two circuits antagonistically modulate the outcome of social conflict (Chou et al., 2016)

Ascending IPN afferents also innervate several forebrain regions that send projections to the habenula forming important feedback circuits. These areas include the lateral septal nucleus, diagonal band of Broca, preoptic area, dorsolateral hypothalamus, mediodorsal nucleus of the thalamus, hippocampus and entorhinal cortex (Shibata & Suzuki 1984; Groenewegen & Van Dijk 1984; Bianco & Wilson 2009).

The medial habenula and IPN are also implicated in addiction and withdrawal. Neurons in both structures express many nicotinic receptors. Activation of this pathway by nicotine and opioids results in increased levels of dopamine in the nucleus accumbens mediating the rewarding effects of these drugs (Glick et al. 2006; McCallum et al. 2012). Continuous use of nicotine results in the degeneration of MHb neurons specifically. Underactivation of this pathway results in the symptoms associated with nicotine withdrawal (Salas et al. 2010; R Baldwin et al. 2012).

Basal Ganglia→ LHb→ RMTg/raphe

The connections of the LHb are broader and less evolutionarily conserved when compared to the MHb. The LHb is an important point of convergence for pallidal and limbic forebrain afferents and thus may enable motivational and emotional information from limbic areas to influence motor behaviour through pallidal efferents (Bianco & Wilson 2009).

Major habenulopetal projections to the LHb derive from the entopeduncular nucleus, this is the non-primate equivalent of the globus pallidus interal segment (GPi). The GPi is the main output nucleus of the basal ganglia. This nucleus mainly projects to the motor thalamus and is integral for basal ganglia control of body movement. Work in primates has shown that basal ganglia neurons also have a non-motor role and are strongly modulated by expected reward (Hikosaka et al. 2006). Neurons in the LHb are excited by stimuli signifying the absence of reward and inhibited by stimuli indicating the presence of reward (Matsumoto & Hikosaka 2008). LHb circuitry is particularly important for reward-based learning. LHb neurons are activated when expected reward is not delivered or when unexpected punishment is received or positive feedback omitted (Bromberg-Martin & Hikosaka 2011). By communicating these reward prediction errors to midbrain dopamine circuits, the motivational value of salient stimuli can be learnt. Consequently, the LHb can suppress less rewarding motor behaviors by inhibiting dopamine neurons (Hong et al. 2011) resulting in the adjustment of behavioural strategies. Negative reward prediction errors in habenula neurons have also been recorded in humans (Salas et al. 2010).

Reward related information is conveyed to the LHb by ENT/GPi habenula afferents (Hong & Hikosaka 2008). Although the primary output of the ENT/GPi is thought to be inhibitory, recent work has shown that the GPi/ENT-habenulo afferent projection neurons, that make up 10% of the total GPi population (Parent et al, 2001), in rats are excitatory, glutamatergic neurons (Shabel et al. 2012). Firing patterns of these afferent neurons are similar to those of the LHb but reward related signals start earlier in GPi neurons. Other evidence for a reward related role for GPi/ENT neurons has come from a study looking at glucose sensitivity in GPi neurons. This study found that a subset of GPi neurons located at the border of the GPi (roughly matching where the LHb projecting neurons are located in rat and monkey) are glucose sensitive and modulate their activity relative to feeding behavior (Karadi et al, 1995).

The LHb in the rat sends both ascending and descending efferents to a broad range of targets. The major efferent connections of this pathway are descending and project to both the median and dorsal raphe and the rostromedial tegmental nucleus (RMTg). The majority of LHb neurons are glutamatergic but these descending projections act to inhibit monoaminergic signaling. LHb neurons inhibit serotinergic raphe nuclei directly through inhibitory interneurons within the raphe (Varga et al. 2003) whereas inhibitory action on dopaminergic neurons within the ventral tegmental area and the substantia nigra pars compacta is mediated through the GABAergic neurons of the RMTg (Jhou et al. 2009; Hong et al. 2011). Many of these projections are reciprocal, with dopaminergic neurons of the VTA projecting both directly to the LHb and providing feedback indirectly through projections to striatal and pallidal nuclei that innervate the LHb.

Limbic inputs to the LHb

Major limbic innervation of the LHb comes from the lateral preoptic area and the lateral hypothalamus (Herkenham & Nauta 1977b). The lateral preoptic area contains estrogen concentrating neurons and so habenulopetal projections from this area account for the important role the habenula has in reproductive behaviours. The lateral hypothalamus plays an important role control of feeding behaviours amongst other functions (Sutherland 1982). Smaller descending inputs from septal nuclei, the diagonal band of Broca and lateral septal nuclei, also innervate the LHb (Herkenham & Nauta 1977a).

Other minor projections to the lateral subnucleus arise from the frontal cortex, serotinergic input from the raphe and visual input from the retina and suprachiasmatic nucleus(Bianco and Wilson., 2009; Herkenham and Nauta., 1977b).

Several brain areas project to both habenula subnuclei including another septal nucleus, the diagonal band of Broca and the nucleus accumbens part of the basal ganglia. In addition to these forebrain nuclei the habenula receive ascending dopaminergic inputs from the ventral tegmental area, ascending pain and temperature fibres from the periaqueductal grey and noradrenergic input from the locus coerulus (Herkenham & Nauta 1977b; Sutherland 1982; Bianco & Wilson 2009).

1.1.4 Habenula afferent and efferent circuitry in zebrafish (in detail).

What afferent and efferent circuits are already described in zebrafish? What neuroanatomical asymmetries exist within this circuitry? Afferent projections to the habenulae arise from several forebrain regions. To date, afferent projections to the habenulae have been shown from parapineal neurons, mitral cells of the olfactory bulb and diencephalic neurons that may constitute the eminentia thalami or entopeduncular nucleus.

Parapineal

Parapineal neurons innervate the left dorsal habenula (dHb) (Concha et al. 2000)The left-sided parapineal nucleus forms part of the pineal complex along side the midline epiphysis (Concha et al 2003). The laterality of habenular asymmetry is always concordant with that of the parapineal (Concha 2000).

Parapineal migration determines the subsequent connectivity of dHb neurons to the dorsal IPN (Bianco et al. 2008; Gamse 2005).

Olfactory bulb

A subset of mitral cells of both left and right olfactory bulb asymmetrically innervate the right habenula (Miyasaka et al. 2009). These neurons extend their axons into the telencephalon via the lateral and medial olfactory tracts. Their axons arborize in the telencephalon and some cross the midline through the anterior commissure. Some of the axons also extend further caudally and asymmetrically innervate the medial portion of the central neuropil domain of the right habenula. These mitral cells are labelled in the transgenic line Tg(lhx2A:GapYFP)(Miyasaka et al., 2009).

Emminentia Thalami

Lipophilic tracing of habenular afferents in larval zebrafish by Hendricks and Jesuthasan (2007) identified habenulopetal projections from the eminentia thalami (EmT) that is thought to become the bed nucleus of the stria medularis (BNSM) in the adult. The BNSM is located at the border of the pallium and the thalamus surrounding the lateral forebrain bundle. This nucleus is calretinin positive and glutamatergic. The BNSM was formerly called the ventral part of the entopeduncular nucleus. The entopeduncular nucleus (formerly known as the dorsal entopeduncular nucleus) is of subpallial origin and contains GAD67 positive projection neurons and is likely homologous to the entopeduncular nucleus in non-primate mammals and the internal segment of the globus pallidus in primates (Mueller & Wullimann 2009; Wullimann & Mueller 2004a; Mueller 2012). DiI labeling in the habenula of trout also resulted in dense labeling of entopeduncular neurons (Yañez & Anadón 1996). There doesn’t appear to be a consensus on the origins of the EmT/BNSM and entopeduncular nuclei in zebrafish. As such a major contributor of habenula afferents this region definitely warrants further investigation.

Other

Other regions identified as habenula afferent sources in the zebrafish include the posterior tuberculum and potentially the pallium (Hendricks & Jesuthasan 2007; Hendricks & Jesuthasan 2011)). This study has several limitations and errors (mostly due to the technical limitations associated with DiI labelling) and does not show very convincing evidence for either of these projections. It also fails to find the olfactory bulb innervation of the right habenula found later by Miyasaka (Miyasaka et al. 2009). In trout, habenulopetal projections from the posterior tuberculum were also found along with afferents from a small telencephalic nucleus in the region of the anterior commissure (Yañez & Anadón 1996). The existence or lack of pallial and subpallial inputs to the habenula in the zebrafish still needs to be resolved. It would be particularly interesting to target subpallial regions thought to be homologous to striatal and septal areas in mammals to see the level of conservation of this circuitry. DiI labeling of the subpallium in adult zebrafish resulted in labelled fibers in the habenula and habenula commisure (Rink & Wullimann 2004).

Several papers looking at neurotransmitter systems in the zebrafish have shown innervation of the habenula by dopaminergic, noradrenergic *(Kastenhuber et al. 2010; Tay et al. 2011) and serotinergic (Lillesaar et al. 2009) neurons. These inputs could provide important feedback information from midbrain monoaminergic centers targeted by habenula efferents. Hypocretin neurons of the hypothalamus also innervate the habenula. Hypocretins/orexins are neuropeptides involved in regulating sleep and wakefulness and energy balance (Appelbaum et al. 2009) none of these studies show which specific subpopulations of neurons send these habenulopetal projections.

**personal observation of the data. Habenula innervation is not specifically discussed in the actual papers.*

In the lamprey, the prethalamus and posterior tuberculum send afferents to the habenula. These regions receive ascending sensory input from the octavolateral nucleus/lateral line system (Stephenson-Jones et al., 2012). This more direct sensory input to the habenula present in lamprey and to some extent in zebrafish (Miyasaka et al., 2012; Costa et al., 2003) is evolutionary interesting and is discussed in more detail below.

Habenula efferents described in zebrafish

The efferent projections of the habenulae in zebrafish are already fairly well resolved. As in mammals, the different habenula subnuclei project to different targets in the midbrain. The two main targets of habenula efferents are the interpeduncular nucleus (IPN) and the raphe in the ventral midbrain. Both of these regions are involved in the control of monaminergic signalling. A small projection to the griseum centrale has already been discussed above.

As stated above the dHb in the zebrafish and the mammalian medial habenula both innervate the interpeduncular nucleus (IPN). Medial and lateral dorsal habenula (dHbM and dHBL) neurons have different terminal morphologies(Bianco et al. 2008). Habenular efferents have two distinct patterns of terminal arborisation in the IPN. Axons from most left-sided habenula neurons terminate predominantly in the dorsal IPN with arbors formed like a 'domed crown' with branches extending over considerable dorso-ventral depth (L-typical arbors). Their terminals circle the interpeduncular nucleus (IPN) and extend colaterals directed internally into the IPN (Bianco et al. 2008).

Right-sided habenula neurons predominantly terminate in the ventral IPN. Their axon terminals also surround the IPN but in a more ovoid-like shape reminiscent of an electromagnetic coil (R-typical arbors). They are flatter than the L-typical arbors, extending over less depth. The branches of the right axon terminals concentrate more in the periphery, with relatively few branches in the centre of the IPN (Bianco et al. 2008).

Although single cell electroporation experiments have not been carried out in transgenic lines labelling the dHbL and dHbM, it is likely that the neurons innervating the dorsal IPN emanate from the dHbL and those innervating the ventral IPN emanate from the dHbM.

Anterograde tracers applied to the dorsal and ventral regions of the IPN suggest the existence of two parallel efferent pathways (Agetsuma et al. 2010). Neurons in the dIPN project axons dorsally to the dorsal raphe then continue on to reach and extend through the griseum centrale. The griseum centrale is a periventricular structure that is likely homologous to the mammalian periaqueductal gray (PAG), dorsal tegmental nucleus and nucleus incertus. This connection between the dIPN and griseum centrale appears to be reciprocal. Neurons in the ventral IPN (vIPN) have reciprocal projections to the median raphe.

1.2 Evolutionary conservation of habenula associated circuitry

1.2.1 Habenular circuitry in the lamprey

With their description of habenular circuitry in the lamprey, one of the phylogenetically oldest species, Stephenson-Jones et al (2012) aimed to determine the fundamental, ancestral circuitry and function of the habenula. They found that the lamprey homologues of the MHb and LHb and particularly their efferent connections were conserved in lamprey. They also found that an area homologous to the GPi projects to the LHb in the lamprey, projections from the lateral hypothalamus to the LHb were also present (conserved in zebrafish).

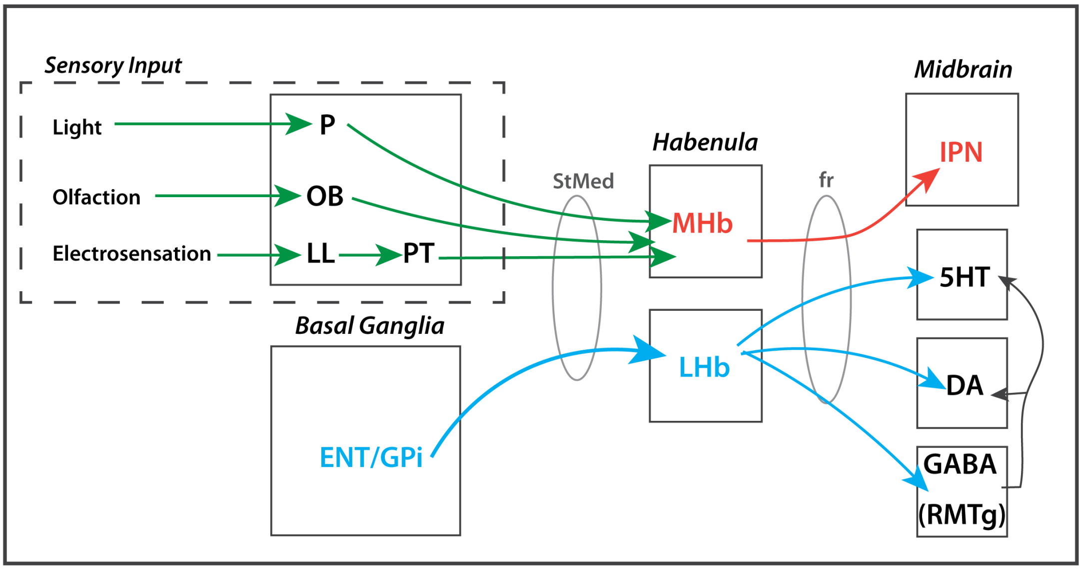

Figure 1.4: Evolutionary conserved habenula circuitry from lamprey (Schematic modified from Stephenson-Jones et al (2012). The lamprey homologs of the medial (lfHb and rmHb) and lateral (rvHb and rdHb) habenulae are represented by the central boxes with afferent nuclei on the left and efferent projections to the right. The dashed line indicates the circuit features that have been adapted during evolution. DA, dopamine; Hist, histamine; 5HT, 5-hydroxytryptophan; IPN, interpeduncular nucleus; LH, lateral hypothalamus; LL, lateral line receptors; MHb, medial habenula; OB, olfactory bulb; Pin, parapineal organ; PT, pretectum; RMTg, rostromedial mesopontine tegmental nucleus.

The afferent inputs to the MHb found in mammals (Described in 1.1.4 above) do not seem to be present in lampreys. MHb circuitry is used to regulate the flight response to fearful and aversive stimuli (Agetsuma et al., 2010; Reviewed in Hikosaka., 2010; Mathuru & Jesuthasan., 2013; Facchin et al., 2015). As discussed above this information in mammals is relayed to the MHb from the amygdala and hippocampus via septal nuclei. In lamprey, this septal input is not present, although a striatal input is seen. Instead the MHb receives primary sensory input from the olfactory bulb and parapineal. Other sensory information is relayed to the habenula by the pretectum. This region receives electroceptive and vestibular sensory input from the lateral line via the octavolateral nucleus (Stephenson-Jones et al. 2012).

Direct sensory input to the habenula present in lamprey appears to be missing in mammals and has been replaced with contextual information about sensory stimuli through hippocampal inputs to the septal nuclei. In zebrafish, habenular nuclei receive direct innervation from olfactory bulb neurons (Miyasaka et al. 2009) and studies in our lab looking at the activity of habenula neurons *in vivo* have shown that habenula neurons respond to both visual and olfactory stimuli (Dreosti et al., 2014).

Deciphering afferent inputs to the habenula in zebrafish compared to lamprey will highlight how this circuitry has been conserved in different vertebrate lineages. The conservation of the LHb and MHb and their associated circuitry throughout vertebrate phylogeny indicate that these circuits share a common function throughout the vertebrate lineage, namely the ability to select and adapt behavioural programs in response to motivational stimuli and the particular context (Stephenson-Jones et al. 2012).

1.2.2 Telencephalic organisation in teleosts: Eversion vs Evagination

The major brain nuclei with afferent inputs to the habenulae in mammals are telencephalic. Differences in the morphology of the forebrain among the vertebrate taxa are particularly pronounced compared to other brain regions. In order to define regions of the zebrafish telencephalon homologous to the septal and pallidal nuclei responsible for habenula innervation in mammals, a better understanding of teleost telencephalic organisation, particularly at larval stages, is required.

In teleost fish, the telencephalon develops by a process of eversion as opposed to the evagination of the neural tube that underlies telencephalic morphogenesis in most other vertebrate species (Butler & Hodos, 2005). During evagination, the lumen of the anterior neural tube enlarges to form the telencephalic ventricles creating two hollow telencephalic hemispheres each surrounding the expanded ventricle. For the zebrafish and other ray-finned fishes, the forebrain consists of two solid hemispheres separated by a midline ventricle that expands over the surface of the telencephalic lobes. In order to produce this anatomical arrangement another morphogenetic process takes place. In this scenario, the sub-pallium or basal telencephalon remains unchanged such that the different areas of the subpallium are considered to be homologous and aligned with all other vertebrate species. The dorsal telencephalon or pallium undergoes a process known as eversion. The classic view of eversion holds that the roof-plate of the neural tube will thin and elongate and the pallial region of the telencephalic hemispheres will bend outwards laterally. The result of this out-bending means that the medio-lateral positions of the hippocampal and olfactory areas are reversed in the ray-finned fishes with respect to other vertebrates (Butler & Hodos, 2005; (Northcutt 2008; Northcutt 2011; Wullimann & Mueller 2004b).

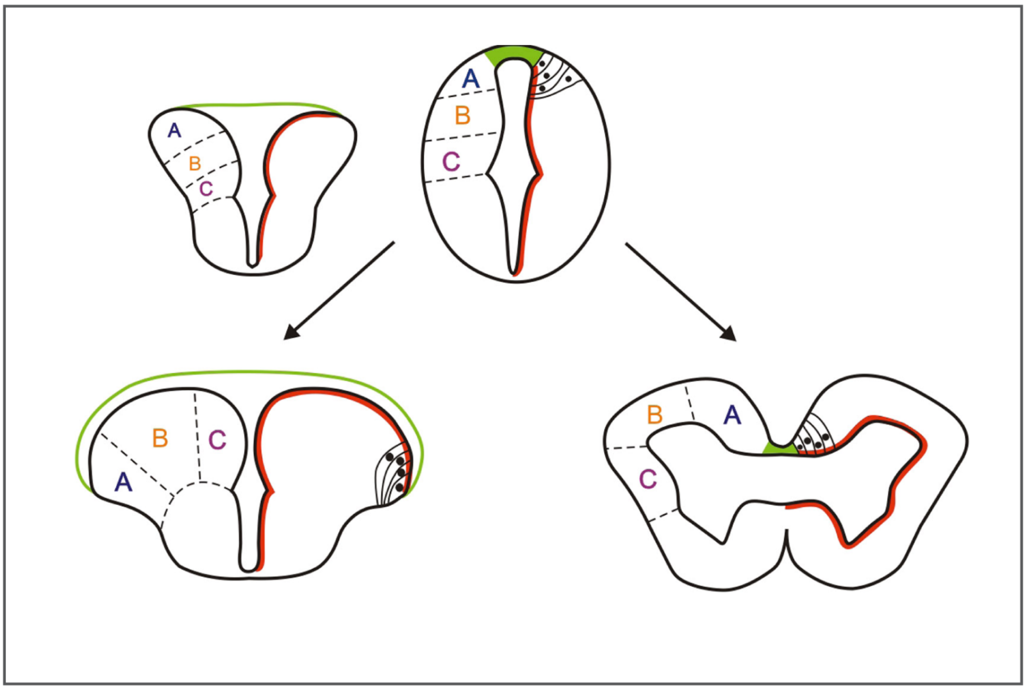

Figure 1.5. Conventional model for eversion in ray-finned fishes.
Cartoon showing the classic view for eversion in ray-finned fishes (left) in contrast to the evagination of the telencephalic vesicles that occurs in the rest of vertebrates (right). In ray-finned fishes, it is thought that the dorsal region of the telencephalic neural tube (pallium) folds over the ventral region (subpallium), stretching the dorsal roof plate region of the neural tube (green) to form the *tela choroidea*. This would also relocate some ventricular cells to the dorsal telencephalic surface (red dotted line) and cause medial to lateral rearrangements of pallial regions (compare the location of regions A, B and C between everted and evaginated telencephalons). (Taken from (Folgueira et al. 2012))

The Yamamoto group, looking at telencephalic homology in the adult zebrafish have also suggested that the position of some pallial areas in the adult do not support a simple medio-lateral out-folding of pallial regions, suggesting that the medio-lateral out-folding in posterior pallial regions is more complex than at the anterior pole (Yamamoto et al. 2007). In his review "Stalking the Everted Telencephalon: Comparisons of Forebrain Organisation in Basal Ray-finned Fishes and Teleosts", Braford tries to bring together and evaluate the several different hypotheses for Pallial eversion and resulting organisation and homology of the telencephalic areas in teleosti. Braford concludes that more analysis of gene expression data and morphogenesis during development are needed to resolve the exact morphogenetic movements and resulting organisation of telencephalic regions in order to confirm their homologies to tetrapods (Braford 2009).

A study in our lab into telencephalic eversion investigated the morphogenetic movements taking place in the zebrafish larvae and also found them to be more complex than a simple laterally directed out folding of the pallium. This study found that the early formation of the anterior-intraencephalic sulcus (AIS) between telencephalon and diencephalon creates a ventricular telencephalic wall at the level of the pallium and displaces the most posterior region of the pallium laterally. Secondly, they found the major axis of growth and extension of the pallium to be along the antero-posterior axis rather than laterally. This pallial expansion is coupled with a bulging of the posterior wall into the AIS resulting in the dorsal region of the telencephalic wall pushing up against the roof of the AIS forming the ventricular space and tela choroidea. The tela choroidea is formed from the initially narrow roof-plate of the telencephalon that expands to cover the dorsal surface of the pallium enclosing the ventricular space (Folgueira et al. 2012). It should be noted at these early stages, the pallium has yet to undergo a massive expansion seen at later stages (Furlan et al. 2017).

Furlan and coworkers (2017), using a genetic birthdating approach, described “a sequential stacking construction mode of the pallium”, where neurons are arranged in concentric age-related layers from a central core (Dc) generated at embryonic stages. This study found minimal radial migration involved in the development of the zebrafish pallium. The authors hypothesize that the simple method of pallium neurogenesis found in the zebrafish could form the basic generation process from which amniote pallial structures could evolve through the addition of radial migration in mammals and the regional control of neurogenic activity in birds and reptiles (Furlan et al. 2017).The majority of pallial neurons are generated by radial glia positioned at the ventricular surface. These cells continue to divide and produce pallial neurons throughout the lifetime of the zebrafish acting as adult neural stem cells (Dirian et al. 2014; Rothenaigner et al. 2011).

Due to these differences in telencephalic morphogenesis, homologies between mammalian and teleostian telencephalic organisation are difficult to resolve. In order to resolve homologies between habenula afferents originating in telencephalic regions in the zebrafish, using comparative afferents in mammals as a guide, further understanding of telencephalic organisation at larval stages will be required. These different telencephalic sub-domains are poorly described and defined at larval stages. Understanding the hodology of different areas within the larval telencephalon is a good way to resolve these homologies between zebrafish and other species.

Pallial homologies

The teleost pallium consists of four histogenetic units that are homologous to the same four pallial divisions present in mammals (Mueller et al, 2011).

Medial Pallium (MP/Dl) = mammalian hippocampus (Hip)
Dorsal Pallium(DP/Dc) = mammalian isocortex (Ctx)
Ventral Pallium(VP/Dm) =mammalian basolateral amygdala
Lateral Pallium(LP/Dp) = mammalian piriform cortex

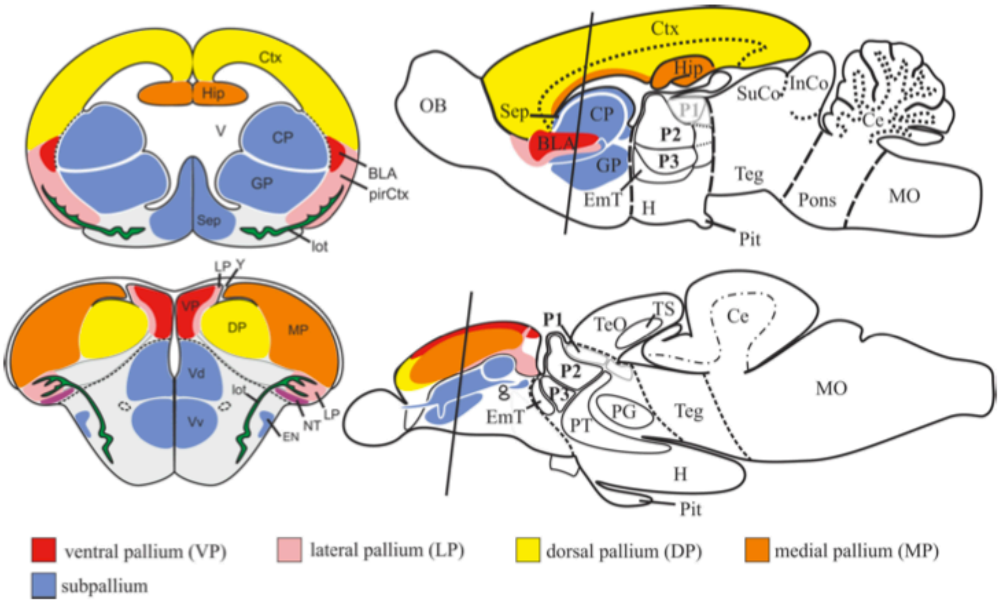

Figure 1.6: Cyprinid and rodent telencephala contrasted.
Schematic drawing illustrating topological correspondences between cyprinid (zebrafish/goldfish; teleostean) and rodent (mouse/rat; mammalian) telencephala From Mueller et al, 2011.

The eventual topological organisation of these areas is a result of complicated morphogenetic movements during development. As most research in zebrafish utilises embryonic and larval stage embryos to look at both circuitry organisation and function, the identification of key homologous regions such as the hippocampus, amygdala and piriform cortex needs to be resolved at early stages. With reference to this project, afferent input from both regions homologous to the hippocampus and amygdala to septal areas would provide important limbic input conveyed to the habenula via septal nuclei in the subpallium. Nomenclature for different pallial divisions in the above Figure from Mueller et al, 2011 differs from the more traditional nomenclature used in most communications. (See Figure below for traditional nomenclature)

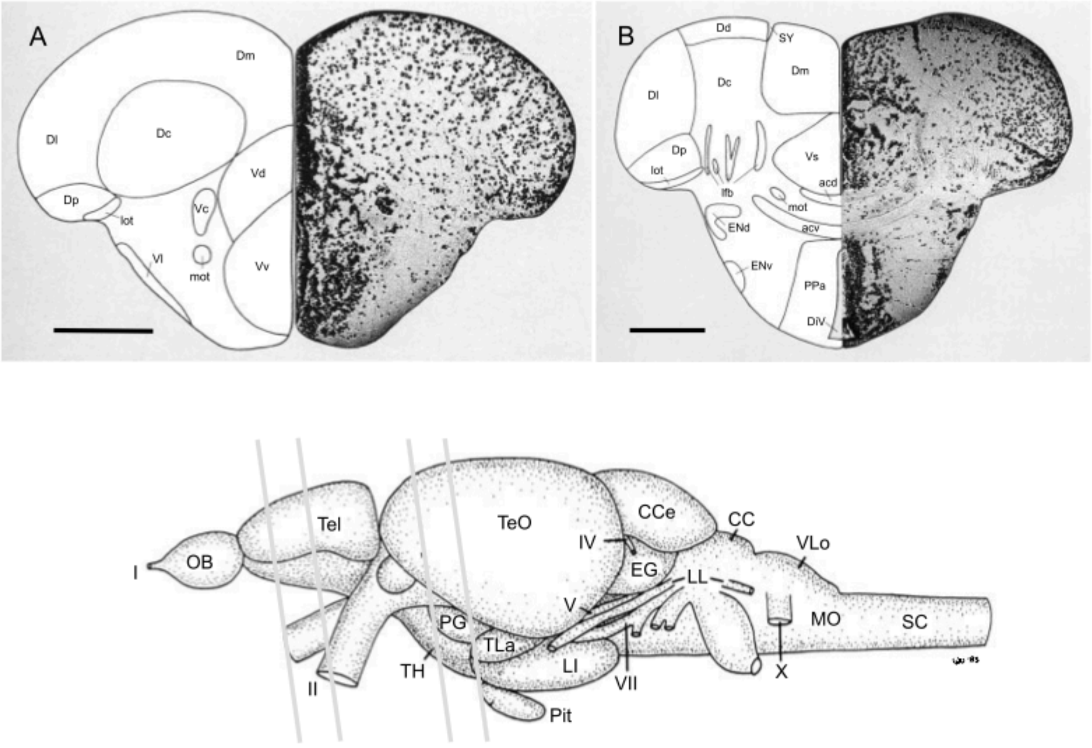

Figure 1.7: Subdomains of precommissural (A) and postcommisural (B) telencephalon in adult zebrafish. Section (A) most rostral section through telencephalon on brain schematic below. Section (B) more caudal section through the telencephalon.(From Wullimann et al,1996)

Subpallial homologies

Homologies between subpallial nuclei of teleosts and mammals are still quite unresolved. In the zebrafish, subpallial nuclei are named according to their topographical location rather than names homologous to mammalian nuclei. By looking at the relative expression patterns of conserved marker genes it is possible to delineate striatal-like, pallidal-like and septal-like areas within the zebrafish subpallium in both adults (Ganz et al. 2011) and larvae (Mueller et al. 2008). Ganz proposes that in zebrafish, the striatum and pallidum are stretched along the rostro-caudal axis of the telencephalon and that septal nuclei are derived from both pallial and subpallial regions.

The main forebrain afferents to the MHb in lamprey come from the striatum (Stephenson-Jones et al., 2012) and in mammals from septal areas (Herkenham and Nauta 1977 reviewed in Bianco and Wilson., 2009). With supracommisural septum axons “coursing in the stria medullaris” The most significant septal nuclei terminate in different MHb subdomains. The nucleus triangularis innervates the caudal MHb while the septofimbrial nucleus innervates the rostral MHb, more minor projections from the nucleus of the diagonal band is also present in rodents (Bianco and Wilson., 2009). Although a gene expression study in the adult subpallium identified striatal-like, pallidal like and septal-like domains within the zebrafish subpallium (Ganz et al., 2011) these areas have not been delineated at larval stages. These are listed below and separated into rostral and caudal subpallium.

Rostral and mid telencephalic regions

- Dorsal nucleus of area ventralis telencephali (**Vd**) = mammalian striatum (caudate/putamen)
- Ventral nucleus of area ventralis telencephali (Dorsal part) (**Vv**) = mammalian pallidum
- Ventral nucleus of area ventralis telencephali (Ventral part) (**Vv**) = mammalian pallidally derived septum

No clear homology for either the lateral nucleus of area ventralis telencephali (Vl) or the central nucleus of area ventralis telencephali (Vc) has been established between teleosts and mammals. As both of these nuclei are migrated it would be necessary to trace from which proliferative area they originate and which brain areas they connect to determine their homology to mammalian subpallial nuclei.

Subpallial homologies at the level of, and caudal to, the anterior commissure

- Supracommisural nucleus (**Vs**) of area ventralis telencephali= mammalian bed nucleus of the stria terminalis (**BST**) and ventral part of central amygdala.

- Postcommissural nucleus (**Vp**) of area ventralis telencephali= dorsal part of the mammalian central amygdala.
- Entopeduncular nucleus(**ENT**)= Entopeduncular N (rat)/Globus Pallidus internal segment (Primates)

Traditional tracing methods using DiI or other tracers can give us information on the broad connectivity of the whole subpallium (Rink & Wullimann 2004) but does not let us look at the connections of specific subnuclei. DiI labelling studies in the trout looking at the connections of the dorsal (Folgueira, Anad n, et al. 2004) and ventral (Appelbaum et al. 2009; Folgueira, Anadón, et al. 2004; Folgueira, Anadón, et al. 2004) telencephalon revealed putative habenulopetal projections from Vv and Vs. Folgueira et al (2004a and b) specifically highlight the particular problem of identifying telencephalo-habenulo projections either anterogradely or retrogradely using DiI. Telencephalic and olfactory bulb neurons both use the habenular commissure to cross the midline but do not necessarily synapse onto habenular neurons (Miyasaka et al. 2009; Folgueira, Anadón, et al. 2004; Folgueira, Anadón, et al. 2004) therefore any labelling either of habenula neurons or telencephalic neurons could result in the accidental labelling of these *en passant* fibres.

To definitively define homologies between the different subpallial nuclei, it is important to understand their connectivity. Looking at the projection patterns of neurons within these different telencephalic nuclei will help refine homologies between zebrafish and other vertebrates in addition to identifying habenula afferent nuclei. The schematic in Figure 1.8 shows the state of knowledge of zebrafish habenula circuitry prior to 2016, when our paper Turner et al (2016) was published, relative to homologous circuitry in lamprey and mammals. The habenula afferent brain areas or sensory inputs that are of relevance to this thesis are indicated by an orange box. The work in this thesis and adult data from Monica Folgueira contained within Turner et al (2016) place zebrafish habenular afferent inputs somewhere between mammals and lamprey. Some direct sensory afferents exist such as the olfactory inputs

(Miyasaka et al., 2009) but zebrafish habenulae also have afferent innervation from several limbic brain areas akin to mammals such as the hypothalamus and preoptic areas and also the subpallium (Vv), parts of which are homologous to septal areas in mammals.

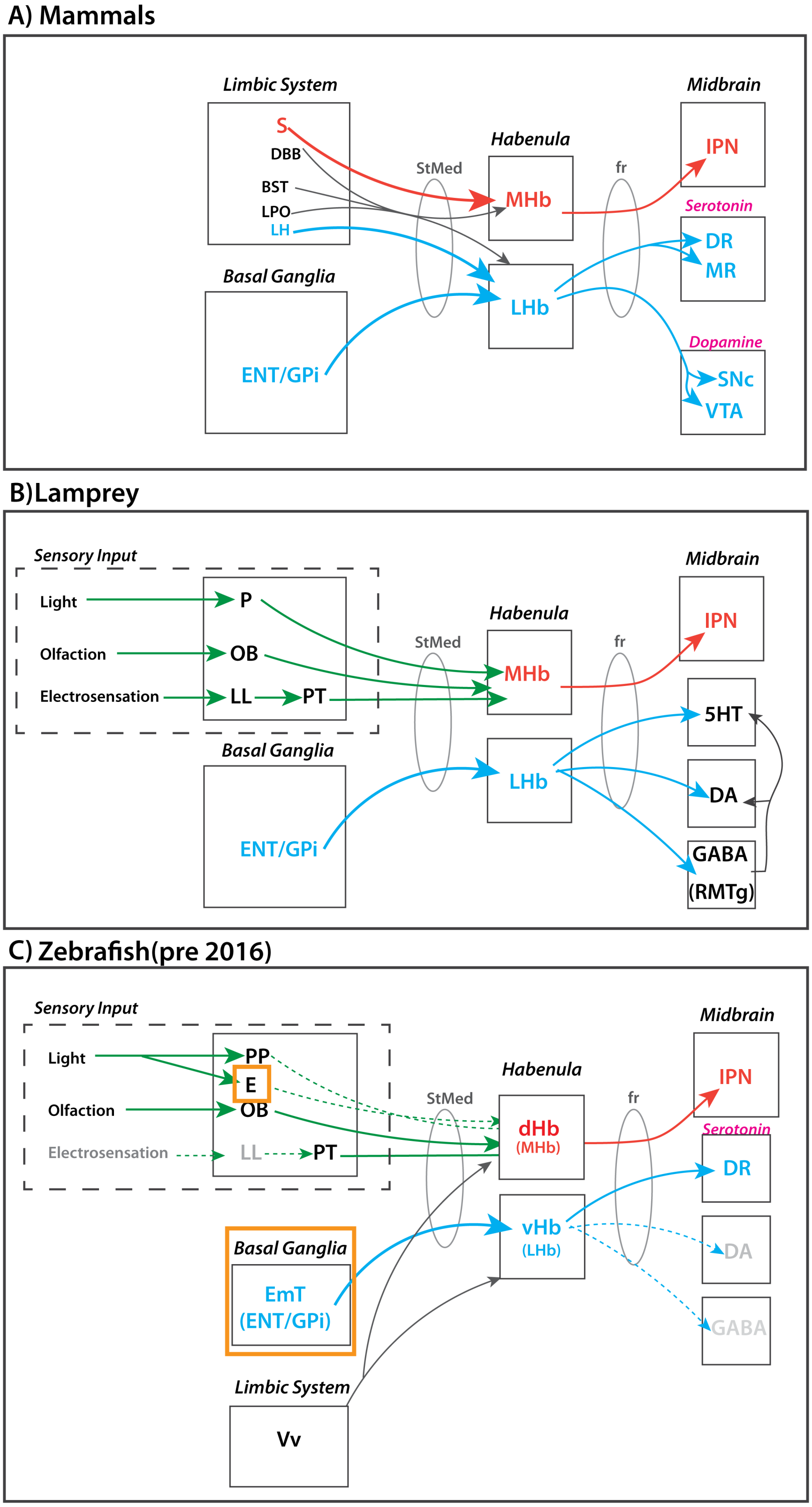

Figure 1.8 Schematic of comparative habenular circuitry between mammals, lamprey and zebrafish (prior to 2016). (A) Mammals. Adapted

from Hikosaka, 2008) For legend see Figure 1.3 **(B)** Lamprey. Adapted from Stephenson-Jones et al (2012). For legend see Figure 1.4 **(C)** Zebrafish known afferents and efferents prior to our paper Turner et al (2016) and this thesis. Dashed lines and grey brain regions are connections from lamprey not yet shown in zebrafish. Orange boxes indicate afferent areas investigated in this thesis.

1.3 Late-breaking results affecting this thesis

In addition to resolving the identity and developmental origin of the ventral entopeduncular nucleus, this thesis also focuses on the identification of a visual habenula afferent nucleus. Towards the very end of my doctorate, two studies identifying the same visual afferent circuit that my own work has determined have been published. One study has recently been published in Neuron (Zhang et al., 2017) and another published in BMC Biology (Cheng et al., 2017).

These two competing studies both arrived at essentially the same circuit by which visual information could be relayed to the LdHb as my own work has. In short, that visual information is relayed by “thalamic” afferents that connect with RGCs at AF4, also potentially at AF2, and send asymmetric projections to the left dHb subnucleus. I will summarise the key findings of these two studies below and then in the Discussion Chapter 6 detail how my own research into this afferent nucleus fits with or differs from these two recent studies

1.3.1 Zhang et al., (2017)

This study focused on the role of the habenula in light-preference behaviour. The light preference of freely swimming larvae was determined using a light/dark choice assay. Wildtype larvae prefer the light environment. This preference switches between larval and juvenile and adult stages when fish exhibit light-avoidance (Lau et al., 2011). The authors found that the LdHb was necessary and sufficient to drive this light preference behaviour.

Using calcium imaging and whole cell recordings of Hb neurons, they found that both the presence and intensity of light could be encoded dHb neurons. Both left and right dHb contain visually responsive neurons. Three different types of visual responses are seen in habenula neurons. These are sustained excitatory responses, transient excitatory and inhibitory responses. The authors state that neurons in both the left and right habenula display these sustained excitatory responses for the duration of the light stimulus and that they preferentially located to the L-dHb. This finding that light responses are stronger in the left dHb has also been found in other studies (Dreosti et al., 2014). Intensity of illumination was also found to be encoded in addition to stimulus duration. Coupled together, this means that habenula neurons can "persistently detect environmental illuminance, a pre-requisite for the generation of a light preference behaviour" (Zhang et al., 2017).

To determine the source of the visual input to LdHb the authors used the same Gal4 enhancer-trap line as I did in Chapter 5: Tg(Gal4s1020t). Mosaic labelling showed GFP+ neurons in the most anterior part of the ventral thalamus, that they label as larval EmT based on identification in Mueller and Guo, 2009), sent projections to the ipsilateral habenula and then to contralateral habenula via Habenula commisure. These EmT neurons sent "local" processes to contact RGC terminals at AF4. Calretinin was used as a marker for EmT (again citing Mueller and Guo, 2009). Several CR+ neurons were found to connect with RGC fibres at AF4 "within the EmT area." (Zhang et al., 2017). Silencing of pan-ventral thalamic neurons and ablation of EmT impaired the light-preference behaviour (described above). Functional imaging showed symmetrical visual responses in L and R EmTs. However, responses in EmT neuron terminals within the L-Hb were stronger than those in R-Hb and injection of DiO into either L or R-EmT showed an asymmetric projection to LdHb.

In accordance with the characterisation of AF4 by Robles et al., 2014, retrograde tracing of RGCs projecting to AF4 showed a predominent location in ventral retina. The majority of AF4-projecting RGCs analysed showed a sustained ON component that the authors state would be a requirement for detecting environmental luminance in a light-preference behaviour.

1.3.2 Cheng et al., (2017)

Calcium imaging of habenula neurons in response to light (blue light flashes) and darkness. Responses to blue light flashes were first seen in the LdHbl neuropil and then subsequently spread throughout the habenula including the vHb. Onset and offset of light evoked responses in different regions of the LdHbl neuropil and increasing illumination resulted in stronger responses in LdHbl neuropil and more habenula cells showing excitation. These light evoked responses were not dependent on the parapineal and DiI retrograde labelling of the LdHbl neuropil lead to bilateral labelling of “an anterior thalamic nucleus”. Specific labelling of entopeduncular neurons with the *Et(sqKR11)* line shows this thalamic nucleus overlaps with the ENT at its caudal edge and is located slightly dorsal and caudal to it. The anterior thalamic cells surround a neuropil that is also contacted by RGC axons. The authors state that these RGC terminals that form this neuropil relate to AF4 and AF2 based on their position relative to the optic tract (based on Burrill and Easter., 1996 and Robles et al., 2014).

The authors hypothesized that the thalamic afferent neurons should show non-overlapping responses to light and darkness. They did find these responses to be segregated in the thalamic cells with different subpopulations responding to light ON and light OFF. These responses were also segregated within the thalamic AF neuropil domain where darkness increased fluorescence in the anterior domain of the neuropil. Light intensity was also encoded by these thalamic neurons that showed increased activity in response to increases in illumination (Cheng et al., 2017).

Light ON thalamic responses were lost following bilateral enucleation but OFF thalamic responses persist. This lead the authors to hypothesise that there could be a non-retinal input to the anterior thalamic nucleus that they identified as the pineal organ. DiI studies in adult zebrafish looking at the overlap of pineal and retinal projections also show that the pineal innervates the largely the ventrolateral thalamic nucleus (VL) with some pineal terminals in the medial part of the anterior thalamic nucleus (A) (Yañez et al. 2009). Optogenetic activation of the thalamus disrupts a light-evoked vertical migration behaviour.

Unlike my solely neuroanatomical description of these Hb afferents, both these studies primarily focus on the functional characterisation of these Hb afferent neurons and their possible roles in driving visual behaviour. In this respect, even if I and the authors of Zhang et al (2017) disagree about the identity of this nucleus, the functional analyses of these neurons are complementary to this study and helps to confirm that this nucleus does convey visual information to the dHbm.

1.4 Aims and scope of this thesis

1) Identify main afferents to the habenula in zebrafish
2) Follow development of major afferent nuclei from embryonic stages through to adult stages* (collaboration with Monica Folgueira*).
3) Characterise the identity of habenulo afferent populations using expression of key developmental genes and neurotransmitters.
4) Describe any asymmetries in these afferent nuclei and their projections to the habenula.
5) Develop methods to image the dendritic morphologies of individual neurons and trace axons over long distances.

Chapter 2. Materials & Methods

2.1 Embryology

2.1.1 Fish stocks and maintenance

Adult zebrafish (*Danio rerio,* Cyprinidae) were maintained at University College London (UCL) Fish Facility under standard conditions: 28ºC and 14h light/10h dark periods (Westerfield, 2000). Embryos were obtained by natural spawning and raised in fish water at 28.5°C and staged according to Kimmel et al. (1995). To avoid pigment formation in larvae, 0.003% w/v Phenylthiocarbamide (PTU, Sigma) was sometimes added to the fish water at 24 hours post fertilization (hpf). Larvae were anesthetized using 50µg/mL tricaine methanesulfonate (MS-222) in fishwater. All experimental procedures were conducted following UK Home Office Guidelines on Animal Care and Experimentation and were approved by animal care and use committees.
The following zebrafish strains were used in this study:

Wild Types:

TUE, AB*,AB and TL.

Transgenic lines:

Tg(lhx5:GFP)^{b1205} and Tg(lhx5:Kaede)^{b1204} (Gao et al., 2012; Zhang et al., 2012), was used to study the development of habenular afferent areas (vENT, RL). Also labels the olfactory bulbs, pallium, preoptic area.

Tg(1.4dlx5a-dlx6a:GFP)^{ot1} (Zerucha et al., 2000), labels subpallial and preoptic neurons and was used to look at projections from these areas to habenula in adult zebrafish.

Tg(isl1:GFP)^{rw0} (Higashijima et al., 2000), also labels subpallial neurons and was used to look at projections from these areas to habenula in adult zebrafish.

Et(gata2:GFP)^{bi105} (Folgueira et al., 2012), an enhancer-trap line with dense pallial expression of GFP. This transgenic line was used to develop mosaic labelling technique and show pallial innevation of vENT.

Tg(slc17a6b:DsRed)^{nns9Tg} (Kani et al., 2010; Miyasaka et al., 2009), labels glutamatergic neurons.

Tg(-2.7shh:GFP)^{t10} (Albert et al., 2003), labels shh expressing neurons. Used in the study to show position of zona limitans intrathalamica to distinguish between prethalamus and thalamus proper.

Tg(-1.6flh:EGFP)^{u711}***;Tg(foxD3:GFP)***^{zf15} (Concha et al., 2003), labels the pineal and parapineal. Used in this thesis to perform parapineal ablations and check lateralty of asymmetry mutants.

Tg(-8.0cldnb:LY-EGFP)^{zf106} (Haas & Gilmore., 2006), the construct used to make this line is 8kb upstream of the *claudin B* gene cloned into a vector containing lynEGFP flanked by I-SceI sites. This line labels to the lateral line and neuromasts and has been principally used for that purpose. However, this particular allele also has lynGFP expression in the forebrain due to an unmapped positional effect. For the purposes of tis thesis this transgenic line has been used to look at forebrain regions afferent to the habenula.

Tg(Pet1:KalTA4), this transgenic line was made by me using the *pet1* promoter originally cloned by Lillesaar et al., (2009) to drive KalTA4. It labels serotinergic raphe neurons.

Tg(-10lhx2a:EGFP)^{zf176} (Miyasaka et al., 2012), ***Tg(-10lhx2a:GAP-EYFP)***^{zf177} (Miyasaka et al., 2012), these two transgenic lines label a subset of mitral cells that project to the habenula. Used in this study to show olfactory projections from olfactory bulb to the habenula in adult zebrafish.

Tg(14xUAS:mRFP,Xla.Cryg:GFP)^{tpl2} (Auer et al., 2014), very bright UAS:RFP line used to ID founder following Crisp/Cas conversion of GFP lines to Gal4.

Et(-0.6hsp70l:Gal4-VP16)^{s1020t} (Scott et al., 2007), “pan-thalamic” Gal4 driver line used to mosaiclally label habenular afferent neurons in this study.

Tg(UAS-E1b:Kaede)^{s1999t} (Scott et al., 2007), UAS:kaede used by Ethan Scott and Lucy Heap in conjunction with *Et(-0.6hsp70l:Gal4-VP16)*^{s1020t}

UAS:synaptophysin-GFP (Heap et al., 2013., Meyer and Smith., 2006), used by Ethan Scott and Lucy Heap in conjunction with *Et(-0.6hsp70l:Gal4-VP16)*^{s1020t} to show synapsing of thalamic afferents in the habenula.

Tg(atoh7:GAP-RFP)^{cu2Tg} (Zolessi et al., 2006), labels retinal ganglion cells and their projections to the optic tectum. Used in this study to show proximity of prethalamic habenula afferent neurons to AF4.

Mutant transgenic lines

sox1a:*Tg(-8.0cldnb:LY-EGFP)*^{zf106Tg}, *rch*^{u761}:*Tg(-8.0cldnb:LY-EGFP)*^{zf106Tg}, *tcf7l2*^{f55}:*Tg(-8.0cldnb:LY-EGFP)*^{zf106Tg}
*sox1a:*Tg(*(-1.6flh:EGFP)*^{u711}:*Tg(foxd3:GFP)*^{zf15}, *rch*^{u761}:*Tg(-1.6flh:EGFP)*^{u711}:*Tg(foxd3:GFP)*^{zf15},
tcf7l2^{f55}:*Tg(flh:GFP):Tg(foxd3:GFP)*^{zf15}.

Both the *tcf7l2* and the *rch* mutants were generated in an ENU screen by the Wilson laboratory. Characterisation of the *tcf7l2*^{u754} mutant allele was published by Hüsken et al. (2014). The *sox1a* mutants were a gift from Miriam Roussigne and Patrick Bladder.

2.1.2 Microinjection

Microinjection of DNA, RNA and morpholinos was performed using a borosilicate glass capillary needle attached to a Picospritzer III injector. Adult zebrafish were paired with dividers the night before injections. Dividers were removed the following morning and embryos were collected soon after to ensure they were at early 1 cell stage at time of injections. Embryos were aligned against a glass slide inside an upturned petri dish lid. The needle was calibrated to inject 1nl per embryo. Injections were performed into the cell for DNA and RNA and into the yolk for morpholinos. Constructs injected in this study are listed below along with their injection concentrations per embryo.

Construct	Injection concentration per embryo	Plasmid Database Number
CRISPR sgRNA EGFP1 &EGFP2 (Auer et al., 2014)	35-70pg	1379 (sgRNA1) 1387(sgRNA2)
ZFCOCas9 mRNA	75-150pg	1380
Tol2 transposase mRNA	10-25pg	1151
Gbait-hsp70:gal4 (Kimura et al.,2014)	3.5-7pg	1388
UAS:TdTom (Zhang et al.,2012)	5-10pg	1295
UAS:EGFP (Zhang et al.,2012)	5-10pg	1296
Pet1:KalTA4 (tol2 gateway clone)	25pg DNA+25pg tol2 RNA	1254
Sox1a morpholino	8ng (1nl per embryo of 8ng/nl stock conc)	-

Table 2.1: Injection concentrations and plasmid database numbers for DNA/RNA and morpholinos.

2.1.3 Photoconversion of Kaede

Tg(lhx5:Kaede)^{b1204} larvae were anaesthetized and mounted laterally in 1.2% low-melting point agarose. A small number of cells expressing Kaede were photoconverted from green to red (Ando et al., 2002) using the 405nm laser line on a Leica SP8 confocal microscope by selecting a region of interest (ROI). Mounting the larvae laterally ensured that stray light away from the focal plane would only photoconvert the habenular neuropil. Images of the initial photoconverted region were taken. For both tract-tracing and fate map purposes, larvae were removed from the agarose and incubated for 24hpf post conversion then anaesthetized in 0.2% tricaine (MS222, Sigma), placed into Ringer's solution with tricaine, enucleated, embedded in 0.8% low melt agarose with fish water and imaged on a Leica SP8 confocal microscope.

2.1.4 Laser ablation

Parapineal ablations in Tg(foxd3:GFP):Tg(flh:GFP):Tg(-8.0cldnb:LY-EGFP)embryos were performed using an MPopo system (multi photon) attached to a Leica SP8 confocal. Early parapineal ablations were performed between 24-28hpf. Late parapineal ablations were performed between 44-48hpf

Embryos were mounted in multiwell chambers made of araldite on microscope slides in a 1% agarose drop (1% low melting agarose with 0.2% tricaine, PTU fishwater). After agarose had set, embryos were kept submerged in PTU plus tricaine.

A 25x0.95NA Leica water immersion lens (ceramic coated, non coverslip corrected) was used for the ablations with PTU fishwater plus tricaine used as lens immersion medium.

The parapineal was located using the multi-photon microscope, tuned to 910nm with laser power set to 40-60% and the pinhole opened. The parapineal was then ablated by turning “bleachpoint” on and targetting the tg(flh:GFP)signal in the membrane of the parapineal cells (alternatively this was also done using the ROI tool and zooming in as far as possible). The laser power was then turned up to 100% for a duration 750ms-5sec. The result of the ablation was then checked after reverting to low laser power.

At later stages of embryo development, several laser pulses may be required to fully ablate the parapineal. The following day ablated embryos were checked to see if any parapineal cells remain using the confocal microscope. Successfully parapineal ablated embyros were grown to 4dpf and fixed for further processing by immunohistochemical methods to observe the effect of parapineal ablation on the habenula and habenula afferent terminals. Embryos in which only partial parapineal ablation was achieved were classed as “failed ablated” and were also raised and fixed to be processed as controls alongside non-ablated embryos. These failed ablated embryos show that any changes to epithalamic symmetry are specifically a result of parapineal loss and not general damage to surrounding tissues.

2.1.5 Wholemount *in-situ* hybridisation and Antibody labelling

Antibody labelling: Fixation and Dissection

Specimens were deeply anaesthetized in 0.2% tricaine (MS222, Sigma) in fresh water and fixed by immersion in 3-5ml of 4% paraformaldehyde (PFA) in phosphate buffered saline (PBS) with 4% sucrose. Larvae were fixed at 25 °C in an incubator for 1hr per dpf (i.e. 4dpf larvae fix for 4hrs at 25 °C).

For most antibody labelling and FISH, the skin, jaw and yolk of the larvae was removed by pinning larvae to a sylgard dish and micro-dissecting with electrolytically sharpened tungsten wire and fine watchmakers forceps. Dissected larvae were then washed several times in PBS at RT on a shaker and then put stepwise into 100% MeOH and stored at -20 °C for at least 24hrs until needed.

Embryos and larvae, dissected or otherwise, were stained as whole mounts following standard procedures (Shanmugalingam et al., 2000; Turner et al., 2014). In brief, specimens were rehydrated to PBS with Triton 0.5% and after a brief proteinase digestion (concentration dependendent on stage of development of larvae) to improve permeability of the tissue, specimens were incubated with primary antibody overnight at 4ºC in IB (NGS, DMSO,PBTr). Specimens were then washed in PBSTr and incubated with fluorescent secondary antibodies again overnight at 4ºC. After washing in PBSTr, embryos and larvae were mounted in 2% low-melting point agarose in PBS or transferred step-wise into 80% glycerol (25%, 50%, 75%, 80% glycerol/PBS) and either stored at -20 ºC or mounted in 1% low-melting agarose in 80% glycerol/PBS solution and imaged on a Leica SP8 confocal laser scanning system. For a detailed protocol on larval dissection, antibody labeling and mounting for imaging see Turner et al. (2014).

Antibodies and dilutions used were as follows:

Primary antibodies:

Neuropeptide Y (NPY, Sigma, Cat# N9528, dilution 1:1000), rabbit anti-green fluorescent protein (GFP, Torrey Pines Biolabs, Cat# TP401, dilution 1:1000), rat anti-GFP (Nacalai Tesque, Cat# GF090R, dilution 1:1000) and mouse anti-acetylated tubulin antibody (IgG2b) (α-tubulin, Sigma, Cat# T7451, dilution 1:250, labels axons), rabbit anti-calretinin antibody (CR, Swant, Cat# 7697, dilution 1:1000), rabbit anti-γ-aminobutyric acid (GABA ,Sigma, Cat# A2052, dilution 1:1000), mouse anti-synaptic vesicle protein 2 (IgG1) (SV2, DSHB, Cat# AB 2315387, dilution 1:250 labels synaptic neuropil), rabbit anti-DSRed antibody (Living Colours, Clontech, Cat# 632496, dilution 1:300), rabbit anti-RFP (MBL, Cat#PM005, dilution 1:2000).

Secondary antibodies:

Alexa Fluor 488 (Invitrogen, Goat anti-Rabbit Cat# A-11034, Goat anti-Rat Cat# A-11006, Goat anti-Mouse Cat# A-11029, dilution all 1:200), Alexa Fluor 568 (Invitrogen, Goat anti-Mouse IgG Cat# A-11031, Goat anti-Mouse IgG2b Cat# A-21141, dilution all 1:200) and Alexa Fluor 633 (Invitrogen, Goat anti- Mouse IgG Cat# A-21052; Goat anti- Mouse IgG1 Cat# A-21126, dilution all 1:200). To detect anti-acetylated tubulin and anti-SV2 in the same sample, isotype-specific secondary antibodies were used: Alexa Fluor 568 (IgG2b) and Alexa Fluor 633 (IgG1).

Fluorescent *in-situ* hybridization(FISH) with antibody labelling.

The FISH protocol was adapted from Jülich et al. (2005).

Fixation

Embryos were fixed with 4% PFA/PBS overnight at 4°C, washed 2 × 5 min in PBS, 5 min at room temperature (RT), manually dechorionated and then transferred to 25%, 50% and 75% methanol (MeOH) for 5 min each. Embryos were then placed in 100% (MeOH) which was replaced with fresh methanol after 5 min and dehydrated overnight (ON) at –20°C. Embryos were then brought through 75%, 50%, and 25% MeOH for 5 min each at RT and then twice for 5 min in PBST. Embryos were then fixed for 20 min in 4% PFA at RT and wash 2 × 5 min in PBST.

Proteinase treatment

Embryos were digested with proteinase K (5 mg/ml in PBST) at RT for 5 min. Embryos were quickly washed 2× in PBST and fixed in 4% PFA for 20 min. Embryos were washed 2 × 5 min in PBST.

Prehybridization and hybridization

Embryos were incubated 5 min at 55°C in HYB– (50% formamide, 5× SSC and 0.1% Tween-20). The embryos were then changed to HYB+ (HYB–, 5 mg/ml torula (yeast) RNA, 50 µg/ml heparin) and were incubated for at least 1 h at 55°C. Probe was added to the embryos and incubated overnight at 55°C. From this point forward, the tubes were covered in aluminum foil. Probe was removed, and embryos washed in 50% formamide/2× SSC twice for 30 min, washed in 2× SSC for 15 min, and washed in 0.2× SSC for 30 min. All washes at 55°C.

Detection of fluorescein-labeled probe

Embryos were blocked for at least 60 min at RT with 150 mM maleic acid, 100 mM NaCl (pH 7.5) plus blocking reagent (2% Roche Blocking Reagent). Anti-FL POD (Roche) was added at a 1:500 dilution in above solution and embryos were incubated at 4°C ON. Embryos were washed 4 × 20 min in 1× maleic acid buffer and 2 × 5 min in PBS all at RT. Embryos were incubated for 45 min in TSA Plus Fluorescein Solution (Perkin Elmer) (the fluorescein-tyramide substrate was centrifuged briefly before making staining solution and then diluted 1:50 in amplification buffer). Embryos were washed 10 min each in 30%, 50%, 75% and 100% methanol in PBS. To inactivate the POD, embryos were incubated in 1% H_2O_2 in 100% methanol for 30 min at RT. Embryos were then washed 10 min each in 75%, 50% and 30% methanol in PBS and then 2 × 10 min in PBS.

Detection of digoxygenin-labeled probe

Embryos were blocked for at least 1 h at RT as above. Then, the anti-DIG POD antibody (Roche) was added at a 1:1000 dilution in block solution and the embryos incubated at 4°C ON. Embryos were then washed and stained as above with the Cy3-tyramide substrate (Perkin Elmer). After staining the embryos were washed 6 × 10′ in PBST.

β-catenin detection

Embryos were blocked for 60 min at RT in 2% Roche Blocking Reagent. The anti-β-catenin antibody (rabbit polyclonal) was added 1:100 in blocking reagent and incubated at 4°C ON. Embryos were washed 5 × 30 min in PBST, fixed for 20 min in 4% PFA and washed 2 × 5 min in PBST. Embryos were blocked for 60 min in 2% Roche Blocking Reagent and then an anti-rabbit-Alexa647 antibody was added (1:500). Embryos were incubated ON at 4°C, washed 12 × 5 min in PBST and then transferred, incubated 10 min each in 25% and 50% glycerol in PBST. The embryos were then incubated ON in 75% glycerol to make them more amenable to subsequent dissection.

Fixation and Dehydration

Embryos were fixed in freshly thawed 4%PFA overnight at 4°C. Wash 2x5min in PBST at RT. Dehydrate embryos into MeOH using 5min stepwise washes at RT with 25%, 50%, 75%, 100% MeOH in PBST(PBSTween 0.1%). Store embryos in 100%MeOH at -20°C until needed.

Embryos were rehydrated by repeating stepwise washes (100%, 75%, 50%, 25% MeOH in PBST) each for 5min at RT. Wash 2x with PBST at RT.

Permeabalisation and Postfixation

Embryos were digested with proteinase K (10µg/ml in PBST) at RT for
24hpf 10-15min:
30hpf 20min
36-48hpf 25min
48hpf 30min
3dpf 40min (2X PK)
4dpf 40mins (3XPK)
5dpf 40mins(4XPK)
6pf 40mins(5XPK)
(For dissected brains halve the incubation time of the PK digest.)

After PK treatment embryos were rinsed briefly in PBST. Post-fix in 4% PFA for 20min at RT then wash 2x 5min in PBST at RT.

Prehybridization, hybridization and stringency washes

Embryos were prehybridized in HYB+((50% formamide, 5× SSC and 0.1% Tween-20, 5 mg/ml torula (yeast) RNA, 50 µg/ml heparin) for at least 1hr at 55°C. Then all bar 50µl of HYB+ was removed and 2 µl of DIG probe was added to the tubes. The tubes were incubated overnight at 55°C. The probe was reserved for future use and stored at -20°C.

All stringency washes were performed at 55°C.

Embryos were washed in 50% formamide/2xSSCT twice for 30 mins. Then for 15min in 2xSSCT. Detergent was removed for the subsequent washes and embryos were washed in 0.2xSSC for 30mins.

ANTI-DIG Incubation and DIG probe detection

Embryos were blocked for at least 1h at RT in Maleic Acid Buffer solution. Anti-DIG POD(Boehringer) was added at 1:1000 dilution in MAB and tubes were incubated on shaker ON at 4°C. To remove antibody embryos were washed for 4 x20’ in MAB. Then washed in 2x5’ in PBS . To detect the DIG labelled probe the eppendorfs were incubated vertically for 45-60 minutes in TSA Plus Cy3 solution. TSA substrate was briefly centrifuged before diluting 1:50 in the Amplification buffer provided in Perkin Elmer kit. The Cy3 and the eppendorfs containing embryos were covered with tin foil to restrict light. After staining embryos were washed for 6x10' in PBST at RT.

Antibody labelling and detection

Embbryos were incubated in primary antibody ON at 4°C on shaker (primary antibody concentrations as above). Primary antibody was removed and embryos washed with PBST for a minimum of 4 x30' at RT on shaker, extensive washing can be beneficial at this stage. Embryos were incubated with secondary antibody diluted in PBST, ON at 4°C on shaker. Embryos were then washed with PBST for a minimum of 4 x30' at RT on shaker then mounted in agarose and imaged using the Leica SP8 confocal microscope.

2.1.6 Mounting and Confocal Microscopy

For detailed confocal mounting methods see Turner et al., 2013. All imaging was performed on a Leica SP8 confocal with either 25X 0.95NA water immersion or 20X 0.75NA Glycerol immersion lens.

2.1.7 EGFP to Gal4 switching with Crispr/Cas9.

Conversion of transgenic zebrafish EGFP lines to Gal4 was performed according to Thomas Auer's method (Auer et al., 2014) using the modified GBait construct from Kimura et al., 2014. All plasmids including hs:GBait (Kimura) were a kind gift from Thomas Auer. Cas9 transposase mRNA was made using the ZFCOCas9 plasmid, this is a Cas9 optimised for use in zebrafish by the addition of a nuclear localisation signal(Ref).

Generation of Stable Gal4 lines

For the generation of stable Gal4 lines with this method, injection concentrations were the same as in Auer and Kimura studies. Carriers of the EGFP line to be converted were paired to Tg(14xUAS:mRFP,Xla.Cryg:GFP)^{tpl2} carriers with dividers (See 2.1.2). 1nl of injection mix was injected into low 1cell stage embryos giving a total concentration per embryo of

Construct	Concentration per embryo (stable)
sgRNA EGFP1 or2	60-70pg
Cas9mRNA	150pg
Hs:Gbait	7pg

Table 2.2: Injection concentrations for Crispr GFP to Gal4 switching.(See 2.2.7 for synthesis of gRNA and Cas9mRNA methods)

F0 were screened for RFP expression from 24hpf. Healthy embryos positive for RFP within the correct expression domains delineated by the EGFP transgene expression were then raised to adulthood and screened for germline expression by outcrossing to Tg(14xUAS:mRFP,Xla.Cryg:GFP)^{tpl2} carriers. F1 progeny of F0 carriers that had germline transmission and an expression pattern that recapitulated the original EGFP pattern were then raised to create a stable Gal4 transgenic line.

Transient labelling of neuronal morphologies with Crispr/Cas9

For this method, I adapted the Auer/Kimura method to mosaically label individual neurons within known transgene expression domains transiently with membrane RFP. Injections for this method were into EGFP transgenic incrosses with UAS:TdTom plasmid added to the injection mixture. To try and target later-born cell types with this method tol2 transposase mRNA was also sometimes added to the injection mix. The UAS:TdTom construct is inserted into a tol2 mini backbone so addition of tol2mRNA leads to insertion of the UAS:TdTom into the genome so expression persists throughout development albeit still in a mosaic manner. For added mosaicism, I found that the less efficient sgRNAEGFP2 (as reported in Auer et al., 2014) was preferable to the sgRNAEGFP1. Injection concentrations for each individual EGFP line differ so the concentrations below are a guideline. A good approach is to titrate down from the concentrations above using several serial dilutions. Below are the concentrations I used routinely to label Tg(gata2:EGFP)^{bi102} and Tg(-8.0cldnb:LY-EGFP)^{zf106Tg}.

Construct	**Concentration per embryo (transient)**
sgRNA EGFP1 or2	30 pg
Cas9mRNA	75 pg
Hs:Gbait	3.5 pg
UAS:TdTom(Zhang et al., 2012)	5 pg
Tol2 mRNA	10-20pg (optional)

Table 2.3: Injection concentrations for DNA and RNA used in transient mosaic labelling of neurons using Crispr.

Embryos were screened for RFP expression from 24hpf onwards. Embryos with desired expression can either be imaged live on the confocal or fixed and processed for immunohistochemistry. The advantage of antibody labelling is that counterstaining with other antibodies, such as SV2, T-ERK, tubulin or nuclear markers facilitate the identification of brain region, cell type and hodology or labelled neurons.

2.1.8 Anatomical guide to viewing figures in this thesis

SV2 and or acetylated tubulin antibodies have been used throughout this thesis to aid in locating habenula afferent areas. These antibodies label synaptic neuropil (SV2) and axonal processes (tubulin). For the most part this thesis focuses on the zebrafish forebrain (outlined in blue in Figure 2.1). Most of the larval brains are imaged from either a lateral view or from dorsal aspect when looking at the habenulae frequently shown as cropped views of just the epithalus (orange whisker box in dorsal view) . The below images are annotated more fully, throughout the thesis I have used key annotations such as olfactory bulb, pallium, habenula and optic tectum to orientate viewers.

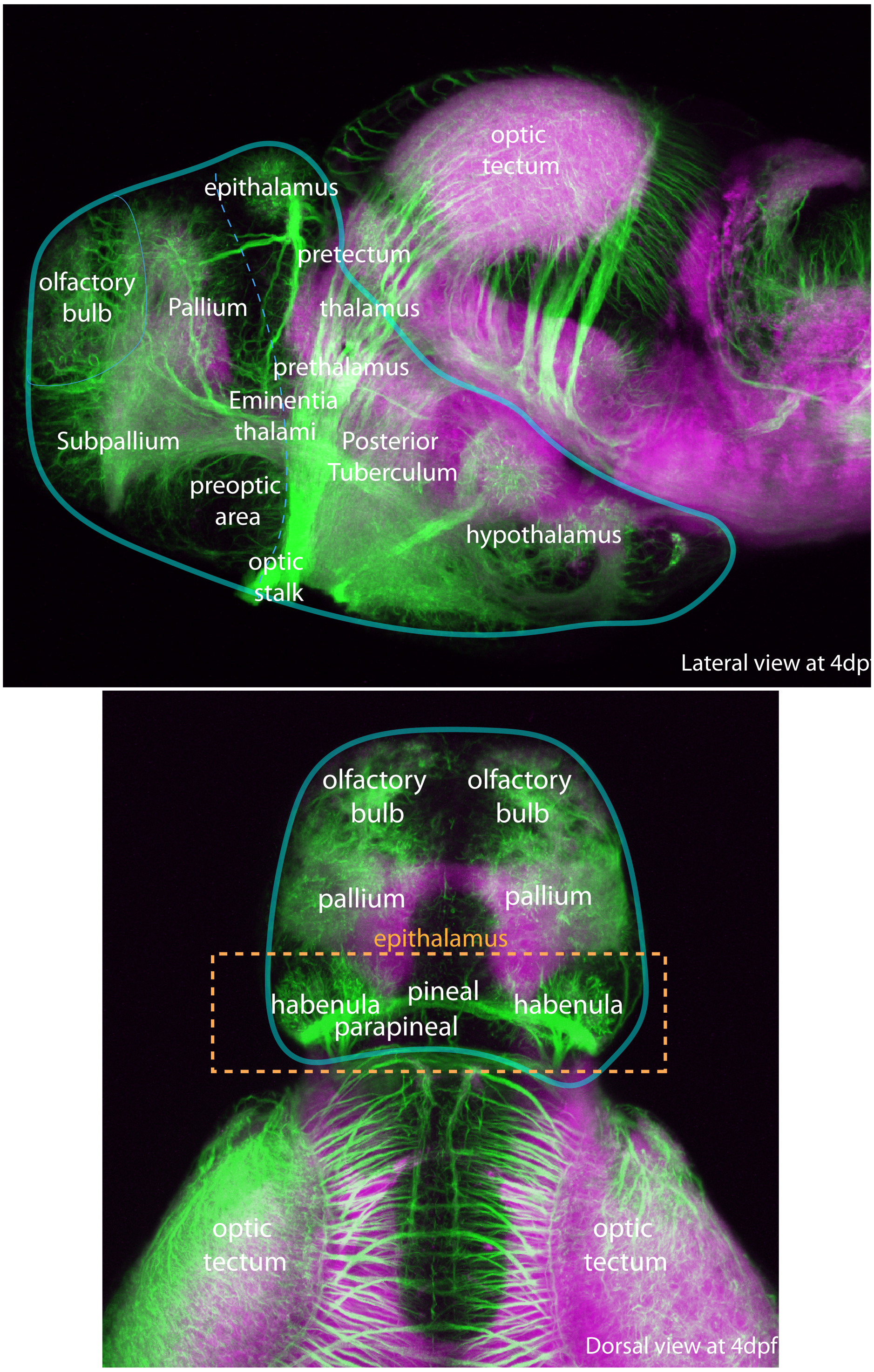

Figure 2.1: Anatomical Guide. Top and Bottom images show 4dpf larval brain labelled with anti-SV2(pink) and anti-tubulin(green). Forebrain is circled in blue. Key areas of interest to this thesis are annotated. Orange whisker box in bottom image shows the cropped view used to view the habenula, pineal and parapineal throughout this thesis.

2.2 Molecular Biology

2.2.1 Genomic DNA extraction from zebrafish embryo and adult fin clips

HotSHOT method (Truett et al., 2000)
Adult fin clips or zebrafish larvae were incubated in base solution (1.25M KOH and 10mM EDTA) 30’ at 95°C; 25µl for individual embryos and 50µl for adult fin clips.
25µl or 50µl of neutralisation solution (2M TrisHCl) was then added and 1µl of was used for PCR template including KASP genotyping.

2.2.2 Restriction enzyme digests

All restriction enzymes used were produced by NEB or Promega and restriction digests were performed as per manufacturer’s instructions. 10 units of enzyme was used per 1µg of plasmid DNA or PCR product. Additionally, 0.1 µg/µl Acetylated bovine serum albumen (BSA) was added to Promega reactions. Reactions were incubated at 37°C for at least 2hrs or ON. Digestions were checked by comparison with undigested plasmid on 1-2% agarose gel.

2.2.3 Digoxigenin (DIG)-labelled RNA probe synthesis for *in-situ* hybridisation

Template DNA was either plasmid DNA linearized with appropriate restriction enzyme digestion or amplified with T3 or T7 promoter overhangs by PCR (Thisse & Thisse, 2008).

Probe	RE (Antisense)	Promoter (Antisense)	Gen Bank Accession number	Plasmid Database Number
Tbr1a	SalI	SP6	AF287006	249
Eom	EcoRI	T7	AF287007	56
Dlx1a	BamH1	T3	V6 7842	538
Egr3	-	T3	CU855695.9	1312
Kctd12.1(lov)	EcoR1	T7	AY120891	705

Table 2.4: DNA templates used to generate probes for ISH.

To digest DNA template 1 µl DNase I (Promega) was added and transcription reaction incubated for a further 15min at 37°C.
In-situ probes for *T-brain 1a* (GenBank accession no. AF287006) and *Eomesodermin* (GenBank accession no. AF287007) used in this study were as published in Mione et al. (2001). The *Dlx1a* probe(GenBank accession no. V67842) was as published in Ellies et al.(1997) and the probe for *leftover (kctd12.1)* (GenBank accession number AY120891) was as published in Gamse et al. (2003).

Probes were quantified using a NanoDrop 2000C and generally used 1:200 in Hyb-.

2.2.4 Genome Walker

Location of the insertion in the enhancher-trap line Tg(gata2:EGFP)^{bi105} was mapped using the Universal Genome Walker™ 2.0 Kit (Clontech). A detailed user manual is available online. Two nested gene-specific primers were used, one for primary PCR(GSP1) and one for the secondary nested PCR (GSP2). These primers should be non-overlapping and anneal to sequences as close to the end of the known sequence as possible. In this instance the tol2 sequence surrounding the gata2:EGFP contruct was used to design primers to amplify the flanking sequences.

2.2.5 DNA purification and Sanger Sequencing

DNA was purified using Qiagen QIAquick PCR purification kit. Eluted in 30 µl of nuclease free H_2O and purity and final concentration was analysed on a NanoDrop 2000C (ThermoScientific).

All sequencing of plasmid and PCR products was performed overnight by SourceBioScience using either stock primers such as M13F or gene specific primers sent with the DNA samples.

2.2.6 Tol2 Gateway cloning

Tol2 Gateway cloning was used to create the Pet1:KalTA4 transgenic construct and line. The Pet1 promoter from the Pet1:GFP construct used in Lillesaar et al., 2012 was subcloned into the 5'entry vector of the tol2 gateway system. This 5' entry vector was combined with the KalTA4 mid-entry vector and a 3' polyA vector to form the Pet1:KalTA4 contruct. All Gateway methods including generation of stable transgenic lines can be found in either Kwan et al., 2007 or on the tol2wiki website: http://tol2kit.genetics.utah.edu/index.php/Main_Page.

2.2.7 Generation of CRISPR gRNA, Cas9 mRNA and tol2 transposase mRNA.

Plasmids containing sgRNA_EGFP1 & sgRNA_EGFP2 template sequence were linearized by digestion with NotI. EGFP1 and 2 gRNAs were synthesised using the HiScribe T7 High Yield RNA Synthesis Kit(NEB). The reaction was incubated for 4hrs or ON at 37°C in a waterbath before DNase I digestion to remove the DNA template.

DNase I digestion was incubated for 15min at 37°C in a waterbath. sgRNA was purified using either RNeasy MiniKit (Qiagen) or Zymo columns.

Tol2 transposase and Cas9 mRNA synthesis

Tol2 PCS2 plamid was linearized with NotI and the pT3TS-nCas9n plasmid (Addgene) (Jao et al., 2013) was linearized with XbaI (Promega) and mRNA synthesised with the mMessage mMachine T3 Transcription Kit (Ambion). Transcription reactions were incubated in a waterbath at 37°C for 2hrs or longer. To digest template DNA, 1 µL of TURBO DNase was added and reaction incubated for a further 15min at 37°C.

The Cas9 plasmid, unlike tol2 transposase, does not contain an SV40 polyA sequence and should be polyadenylated using the polyA tailing kit (Ambion). The PolyA-tailing reaction was set up according to kit instructions and incubated in a waterbath for 1hr at 37°C. 0.5 µL of the reaction before the addition of E-PAP emzyme was kept as minus enzyme control to run on agarose gel to check polyadenylation.

mRNA was purified using either the RNeasy Minikit(Qiagen) or Zymo columns and run against linearized template DNA and non-polyadenylated RNA on a 1% agarose gel to check there was no DNA contamination and that polyadenylation had occurred. The concentration and purity of the mRNA was checked on a NanoDrop 2000 (ThermoScientific) and 260/280 and 260/230 ratios ≥ 2.0 were deemed as pure. The mRNA was then diluted using nuclease free H_2O to a suitable concentration then aliquoted and stored at -20°C or -80°C ready for injection.

2.2.8 KASP genotyping

KASP genotyping assays were designed and produced by LGC Genomics specifically for each mutant line. Allele specific forward primers that include tail sequences specific to two distinct fluorescence resonance energy transfer (FRET) cassettes enable alleilic discrimination of mutant and wt alleles. KASP PCR reactions were set up for each embryo or adult fin clip as follows in a white plastic 96 well PCR plate.

Component	Volume
2 x KASP mastermix	3.89 µL
KASP assay	0.11µL
MQ H_2O	3 µL
DNA	1 µL
Total volume	8 µL

Table 2.5: KASP genotyping

The KASP mastermix* contains both the FAM and HEX FRET cassettes, the ROX passive reference dye, Taq polymerase, free nucleotides and $MgCl_2$ in buffer solution.

PCR conditions

Following PCR spin plate and replace film lid with a fresh lid before reading plate on CFX96 Touch Real-Time PCR Detection System (Biorad). Allelic discrimination plot was generated using Biorad CFX Manager Software.

2.2.9 Transformation of competent *E.Coli* cells.

One Shot TOP10 Competent *E.Coli* cells (Invitrogen) were thawed on ice. One vial of cells (25 µl) was mixed with 2 µl of cloning reaction and incubated on ice for 30min. Cells were then heat-shocked for 30sec at 42°C then placed immediately back on ice for 2mins. 250 µl of S.O.C medium (Invitrogen) was added and tubes shaked at 220rpm at 37°C for 1hr. Cells were then plated on LB agar plates with specific antibiotic(s) and incubated at 37°C ON.

2.2.10 Colony PCR

Single colonies were picked using a sterile pipette tip and added to 50 µl MQ H_2O. 4 µl of this as template was then used to check the insertion by PCR using *Taq* polymerase. To verify the correct insert size the PCR result was run on a 1% agarose gel. Correct colonies were cultured ON by adding 20 µl to

5ml of LB broth with specific antibiotic and incubating ON at 37°C in a shaker (220 rpm).

2.2.11 Plasmid preparation

QIAprep Spin Miniprep Kit (Qiagen) was used to make mini-preps of plasmid DNA. DNA was eluted in 30 µl of nuclease free H_2O. On average 100-300ng/ µl of plasmid DNA was obtained from each 5ml culture. Larger concentrations/volumes of plasmid DNA were prepared by midi or maxi prep by the Biosciences Molecular Biology Unit, UCL.

2.2.12 Image analysis

Confocal ".lif" files were processed using FIJI(Image J) or IMARIS software. Figures and schematics were made using Adobe Photoshop or Adobe Illustrator.

For many of the mosaic z-projections, presented in chapter 5, I have applied a "FIRE" temporal code using FIJI. This assigns different colours to different dorso-ventral depths. The reason for doing this is simply to provide some relief within the image so different aspects of the cells can be more easily observed than with a single colour LUT. The exact dorso-ventro or medio-lateral positional information it communicates is not important as any positional information for a particular cell or process is determined by its position relative to the counterstain, i.e SV2 or DAPI. Panels with this LUT are indicated in the individual figure legends.

Chapter 3: The Entopeduncular Nucleus

3.1 Introduction and adult data

Due to the difficulties in deciphering neuroanatomical structures at embryonic and larval stages we considered it vital to collaborate with neuroanatomists working with adult zebrafish in which neuroanatomy is much better resolved. This study of afferent habenula nuclei in the larvae has been a close collaboration with Monica Folgueira from the University of A Coruña. Our parallel findings in the embryo and larvae (my work) and in the adult (Monica Folgueira's work) were combined into a study of global habenula afferents in zebrafish (Turner et al., 2016). In addition to giving a global overview of habenula afferent circuitry, this study focused particularly on the development and homologous identity of the main habenula afferent nucleus: the entopeduncular nucleus. I have summarised the adult findings within this mini "Introduction" section to this results chapter as they provide information essential to the understanding of the larval experiments that form the "Results" section of this chapter. For clarity, all experiments in adult zebrafish in Turner et al (2016) were performed by Monica Folgueira. All embryonic and larval experiments were performed by myself.

The description of habenula afferent circuitry in zebrafish to date has been limited to a handful of studies. Asymmetric projections from the parapineal (Concha et al., 2003) and the olfactory bulb (Miyasaka et al., 2009) to dHb subnuclei have been well described (See Introduction). Carbocyanine tracing study in the larvae by Hendricks and Jesuthasan (2007) described three main habenulo-afferent areas: the pallium, eminentia thalami and the posterior tuberculum. Afferent areas in the adult were not assessed in that study.

Retrograde labelling from the vHb in adult zebrafish identified the ventral entopeduncular nucleus as the main afferent nucleus for this habenula subnucleus (Amo et al., 2014).

To clarify and expand upon these findings our collaborator, Monica Folgueira, retrogradely labelled habenula afferent nuclei using DiI in 15 adult zebrafish. Afferent nuclei identified by this tracing were confirmed using a combination of reciprocal DiI labelling and, where available, transgenic lines. To assess asymmetry, DiI was applied to either the left or right habenula in each individual and results were annotated accordingly. The main findings from the adult analyses are summarised below (for the full findings see Turner et al., 2016):

Main afferent areas identified in the adult by DiI application to left or right habenula (Monica Folgueira):

- Mitral cells in the dorsomedial region of the olfactory bulb
- Mitral cell collateral fibres in Dp
- Ventral entopeduncular nucleus was strongly labelled in all 15 cases. Both bilateral vENT nuclei were labelled in all cases but some indication of asymmetry in this projection was given by the observation that a higher number of vENT neurons were labelled on the side ipsilateral to DiI application.
- Ventral region of the subpallium (Vv) and the parvocellular peoptic nucleus both showed a few scattered cells in a small number of cases.
- The Nucleus Rostro-lateralis (RL) in the rostral diencephalon were bilaterally labelled following DiI application to either right or left habenula. Due to its location, just ventral to the habenula, spread of DiI from the labelling site in the habenula could potentially account for this labelling.
- Other cells were retrogradely labelled in the posterior tuberculum, periventricular hypothalamus and the median raphe.

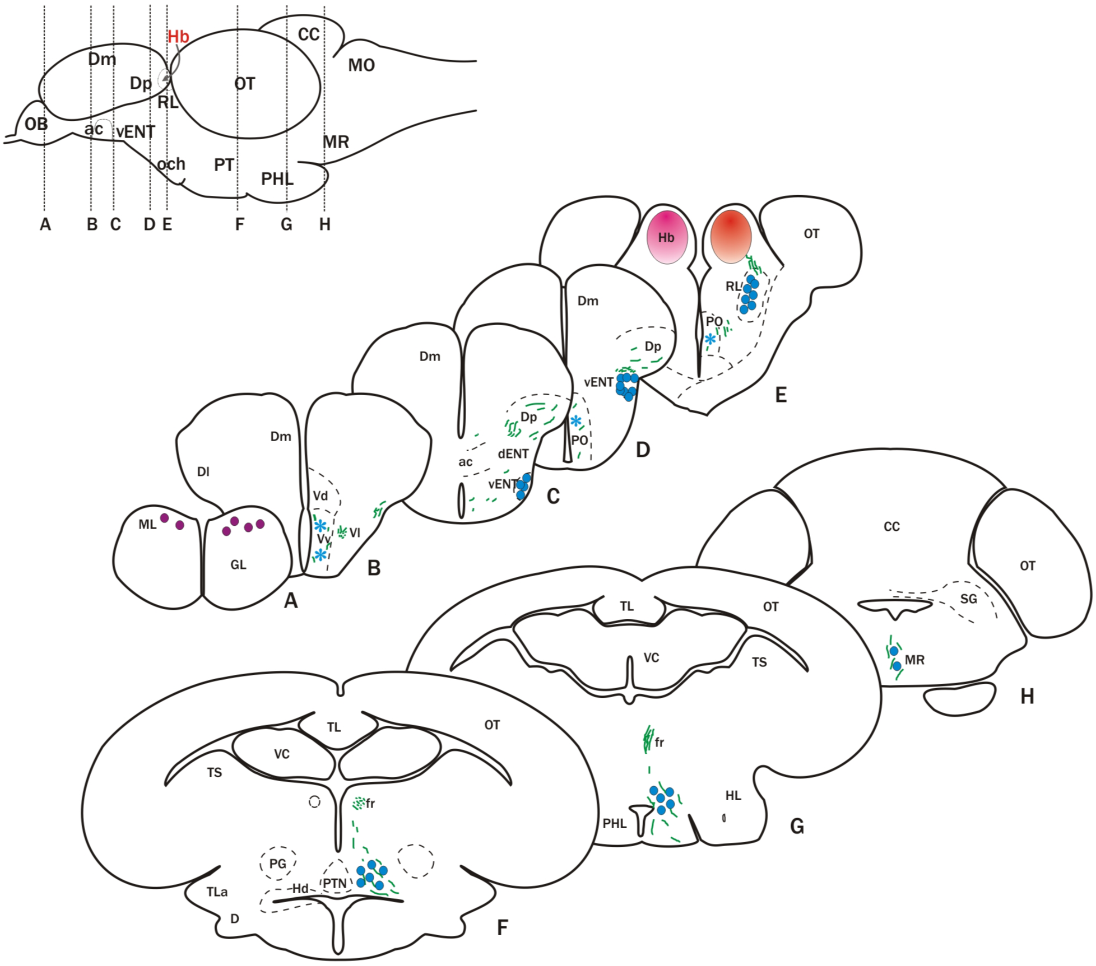

Figure 3.1: **Cells and fibers labeled after DiI application to the habenula.** Schematic at the top left shows a lateral view of the brain indicating position of transverse sections shown in **(A–H)**. **(A–H)** Schematic representation of transverse sections showing labeled fibers (green lines) and neurons (circles and asterisks) after DiI application to the left (pink circle in **E**) or right (red circle in **E**) habenula. Blue circles denote cells that project bilaterally to both habenulae, while purple circles indicate cells project only to the right habenula. Asterisks indicate occasionally labeled cells. Parapineal cells, which project to the left habenula, are not represented. (Figure and legend from Turner et al., 2016).

Reciprocal labelling of habenula afferent areas in the adult (Monica Folgueira).

Olfactory Bulbs

DiI application to left or right olfactory bulbs resulted in the labelling of the lateral and medial olfactory tracts as well as collateral labelling in Dp. Olfactory afferents continue to the habenula and terminate asymmetrically in a small terminal field in the right dorsal habenula subnucleus. These results agree with previous studies in the adult (Gayoso et al., 2011;2012) and larval zebrafish (Miyasaka et al., 2009).

Subpallium and pre-optic area

To confirm the DiI labelling results in subpallial and pre-optic areas, two transgenic lines, Tg(1.4dlx5a-dlx6a:GFP)^{ot1}and Tg(isl1:GFP)^{rw0}, that label large numbers of cells in the subpallium and pre-optic regions were analysed. In both of these transgenics a few GFP+ fibres can be seen to innervate the habenula supporting the tracing results that only very few habenulo-petal cells are present in these areas.

Pallium

Previous studies in larval zebrafish (Hendricks & Jesuthasan., 2007) identified the pallium as a source of habenula afferents (though see correction (Hendricks & Jesuthasan 2011). Both the DiI labellings in this study and analysis of the pan-pallial transgenic line, Et(gata2:GFP)^{bi105} did not corroborate these findings. DiI application to the habenula did not result in any labelling of pallial neurons and no GFP+ processes could be seen in the habenula in ET(gata2:GFP) ^{bi105} The pallial labelling seen in the Hendricks study most likely corresponds to olfactory bulb mitral cells.

vENT

Reciprocal labelling of the vENT resulted in strong labelling of the ipsilateral tract of the habenula commissure. These afferents also crossed in the habenular commissure to innervate the contralateral habenula. The majority of vENT fibres terminated in the ventral habenula but some terminal fields could also be observed in the dorsal habenula. No habenular neurons were labelled indicating that the vENT-habenula connection is not reciprocal.

Parapineal

Parapineal innervation of the left dorsal habenula subnucleus seen at early larval stages (Concha et al., 2003) was confirmed at juvenile stages using the transgenic line Et(gata2:GFP) ^{bi105}. Parapineal fibres still exclusively innervate the left habenula at later stages of development and form terminal fields that spread throughout the left dorsal habenula.

Hypothalamic Lobes

Reciprocal DiI labelling of the posterior hypothalamic lobe led to dense labelling of the projections terminating in the ventral habenula. Some habenula neurons were also labelled in this experiment indicating that this connection may be reciprocal.

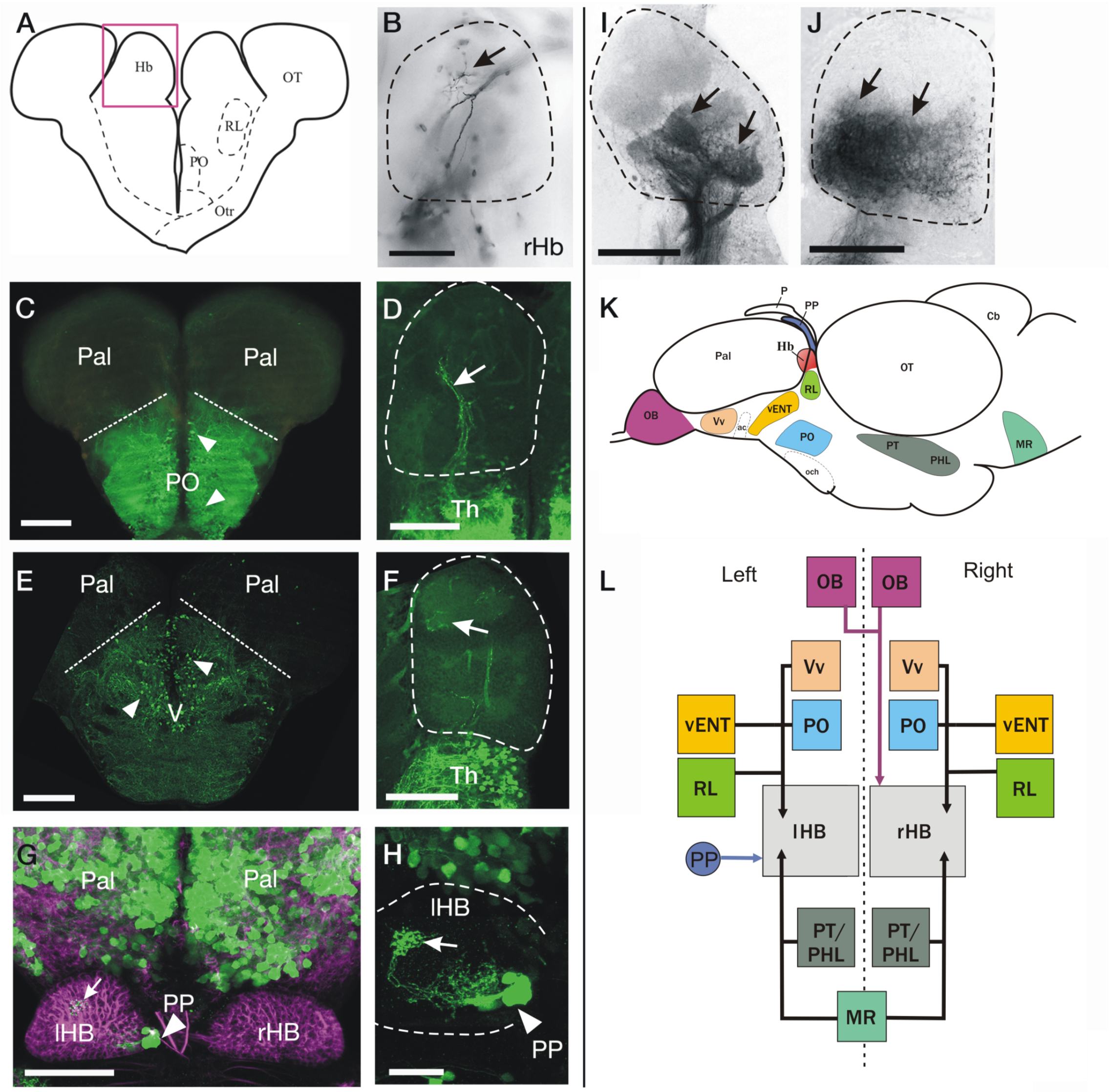

Figure 3.2: Cell populations projecting to the habenula identified by anterograde DiI labeling and/or transgene expression. (A–J) Schematic of a transverse section on the brain at the level of the habenulae **(A).** The pink box approximates the area shown in (B,D,F,I,J). Images are from transverse sections (B–F,I–J) or dorsal views with anterior to the top (G,H) of zebrafish brains. Dotted lines in (B,D,F,H–J) mark the limits of the habenula. Images are of adult brains unless otherwise stated. **(B)** Labeled fibers (arrow) dorsally in the right habenula after DiI application in the olfactory bulb. **(C)** GFP+ neurons (arrowheads) in preoptic areas of a Tg(isl1:GFP)rw0 fish. Dotted lines mark the approximate limit between preoptic areas (ventral) and pallium (dorsal). **(D)** Sparse GFP+ fibers in the right habenula (arrow) of an adult Tg(isl1:GFP)rw0 fish. **(E)** GFP+ neurons (arrowheads) in the subpallium of a Tg(1.4dlx5a-dlx6a:GFP)^{ot1} fish. Dotted line marks the approximate pallial-subpallial boundary. **(F)** Very few GFP+ fibers (arrow) in the habenula of a Tg(1.4dlx5a-dlx6a:GFP)^{ot1}fish. **(G)** GFP expression (green) in 1 month old (1mpf) Et(gata2:GFP)^{bi105} juvenile zebrafish counter stained against tubulin (magenta) showing GFP+ neurons in the pallium and parapineal (PP, arrowhead). Note that the parapineal sends axons that terminate in the left habenula (arrow). Image is a dorsal view, anterior to the top**. (H)** High magnification image of the left habenula shown in

G (after subtracting tubulin channel) showing that GFP+ fibers in the habenula (arrow) originate from the parapineal (PP, arrowhead). **(I)** Confocal image of the habenula showing labeled fibers (arrows) in the habenula after DiI application to the rostral vENT. Although more intense labeling is observed in ventral regions of the habenula, precise habenula subnuclei could be delineated using this method. **(J)** Labeled fibers (arrows) in the ventral half of the habenula after DiI application to the posterior hypothalamic lobe. **(K,L)** Schematics showing a summary of the main afferent areas to the habenula (K: outline of the brain in lateral view, L: boxes diagram). **(K)** The brain nuclei that project to the habenula are shown as colored areas. **(L)** Boxes represent main nuclei projecting to the habenula, while arrows represent projections. Asymmetric projection from the parapineal (PP) to left habenula (lHB) is shown with a blue arrow. Asymmetric projection from mitral cells of the olfactory bulbs (OB) to right habenula (rHB) is shown with a pink arrow. All other afferent areas that seem to innervate both left and right habenula are represented with black arrows. Scale bars: 150 μm in (B–F,I–J); 100 μm in (G), 50 μm in (H). (Figure and legend from Turner et al., 2016).

GFP+ neurons in the vENT of Tg(lhx5:GFP)^{b1205} adult zebrafish innervate the habenula (Monica Folgueira)

Two entopeduncular nuclei: the ventral (vENT) and dorsal (dENT) entopeduncular nuclei, have previously been described in zebrafish (Wullimann et al., 1996). In other teleost species only a single entopeduncular nucleus has been described (Villani et al., 1996[goldfish]; Yañez & Anadon., 1996[trout]). In the adult zebrafish the ventral entopeduncular nucleus extends laterally within the subpallium from the anterior commissure to the telencephalic peduncle. The vENT is composed of smaller more densely packed neurons than the dENT.

The vENT is labelled in the Tg(lhx5:GFP)^{b1205} transgenic line. In transgenic fish, the vENT's elongated morphology is evident (Figure 3.3. Dense GFP+ fibres can also be seen throughout the left and right habenula. Although the Tg(Lhx5:GFP)^{b1205} transgene labels areas other than the vENT, crucially it does not label the dENT and so can be used to distinguish between vENT and dENT. Previous studies describing the anatomy of the zebrafish telencephalon (Ganz et al., 2011; Mueller & Guo., 2009) identify the dENT as the "entopeduncular nucleus proper") and identify the vENT as homologous to the bed nucleus of the stria medularis (BNSM). Our results and those of Amo et al.

(2014) do not support these homologies as DiI labelling experiments identify the vENT as the major habenulopetal telencephalic nucleus.

The dENT is NPY+ and does not innervate the habenula (Monica Folgueira)

The dENT is NPY+ (Castro et al.,2006) and does not extend caudally into the telencephalic peduncle. Very few NPY+ fibres could be seen innervating the habenula. The majority of NPY+ processes innervate Dm. GFP+ cells in the vENT of Tg(lhx5:GFP)^{b1205} fish were NPY-. These same vENT GFP+ cells co-label with DiI following DiI application to the habenula in Tg(lhx5:GFP)^{b1205} fish. We therefore conclude that the vENT and olfactory bulb are the main sources of telencephalic afferents to the habenula in zebrafish, not the dENT.

After establishing these connections in the adult we could now use the Tg(lhx5:GFP)^{b1205} transgenic line and the Kaede allele [Tg(lhx5:Kaede)^{b1204}, (Gao et al., 2012; Zhang et al., 2012)] to look at the development of the vENT at larval stages.

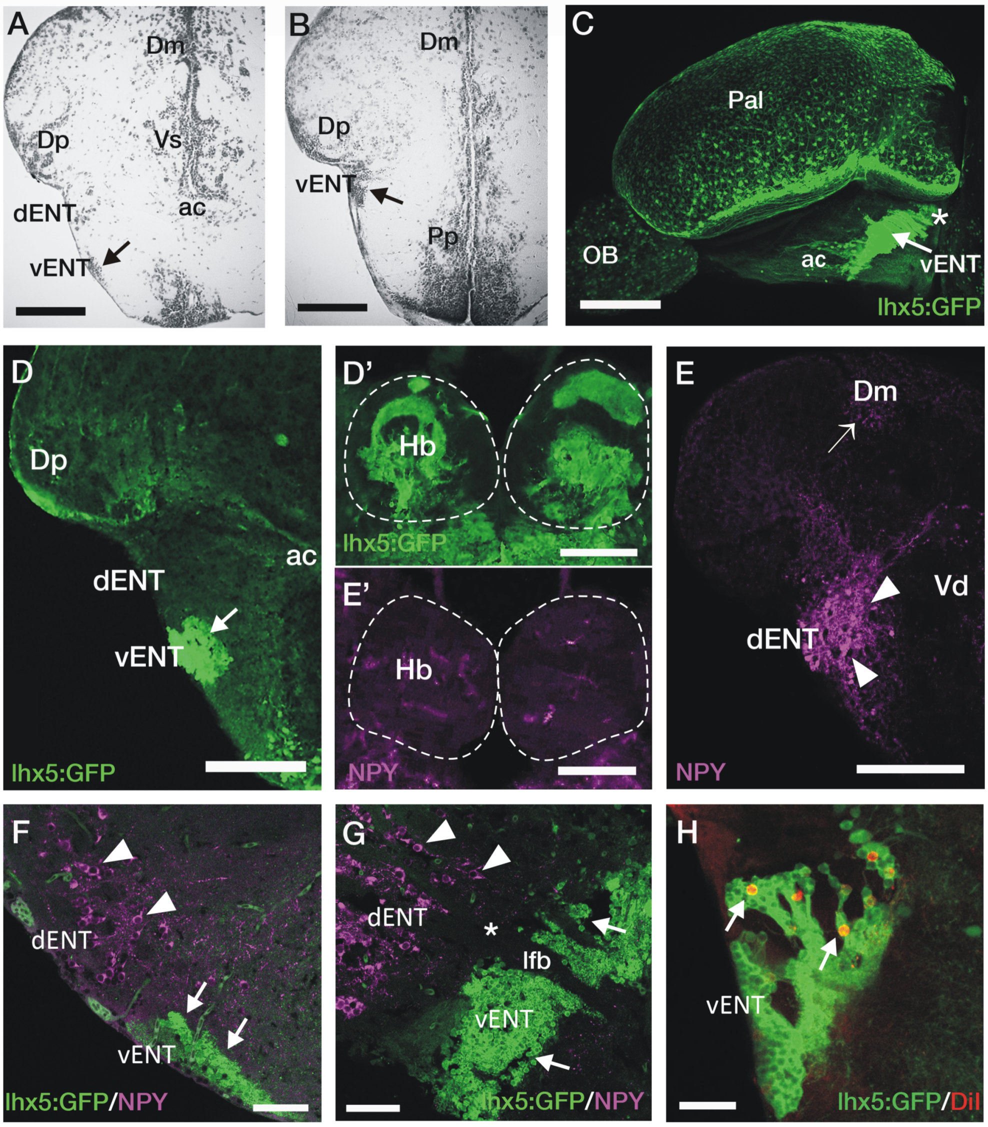

Figure 3.3 GFP+ neurons in the vENT of Tg(lhx5:GFP)^{b1205} adult zebrafish innervate the habenula: Images are transverse sections (A,B,D–F,H), lateral view (C) or parasagittal section (G) of adult zebrafish wild type (A,B,E,E′) or *Tg(lhx5:GFP)*b1205 (C–D′,F–H) brains. **(A,B)** Nissl stained sections showing the cytoarchitecture of the vENT (arrows in A and B) and dENT at anterior and posterior levels. By following serial sections it can be noted that only the vENT extends into caudal areas of the telencephalon (arrow in B). **(C)** Lateral view of intact brain from a *Tg(lhx5:GFP)*b1205 fish (anterior to the left) showing GFP+ cells in the vENT (arrow), among other structures and areas. Note that vENT cells form a band extending from the level of the anterior commissure (ac) into the telencephalic peduncule (indicated with a star). **(D)** GFP+ cells in the vENT (arrow), but not in the dENT, of a *Tg(lhx5:GFP)*b1205 fish. (D′) Dense neuropil of GFP+ fibers in the habenula of a *Tg(lhx5:GFP)*b1205 fish. Dotted lines mark the habenulae. **(E)** NPY+ cells in the dENT and fibers (arrowheads) in the medial area of the pallium (Dm; arrow). (E′) Very few NPY+ fibers are found in the habenulae. Note that some of the labeling observed in the image is caused by autofluorescence of blood vessels. (F,G) Double immunohistochemistry against NPY and GFP in transverse (F) and parasagittal (G; anterior to the left) sections of a brain from a *Tg(lhx5:GFP)*b1205 fish. Note that NPY+ cells are restricted to the dENT (arrowheads). GFP+ cells were observed in

the vENT (arrows). Note in (G) that the dENT (arrowheads) does not extend as far caudal as the vENT (arrows) and there is a clear gap (star) between the two nuclei. Bundles of axons from the lateral forebrain bundle (lfb) travel through both nuclei. (H) Retrogradely DiI labeled cells (arrows) in the vENT of a *Tg(lhx5:GFP)*b1205 fish after tracer application to the habenula. Scale bars: 150 μm in (A,B,D–E′); 250 μm in (C); 100 μm in (F,G) and 50 μm in (H). (Figure and legend from Turner et al., 2016).

Results

From the evidence in the literature described above, the vENT appears to be the main source of afferents to the habenula in adult zebrafish. Since the dENT and vENT were first described by Wulliman et al. (1996) their homologies have been controversial. With this in mind, I set out to investigate the developmental origin of the vENT.

3.2 The Tg(lhx5:GFP)b1205 transgenic line labels habenular afferent areas from larval stages

GFP+ processes can be seen throughout the habenula neuropil in Tg(lhx5:GFP)^{b1205} fish from larval stages

To determine whether the Tg(lhx5:GFP)^{b1205}transgenic line was a suitable tool to look at the development of habenula afferent areas I assessed GFP expression in 4dpf Tg(lhx5:GFP)^{b1205} larvae. At this stage of development, GFP+ processes can be seen throughout the entire habenula neuropil. SV2 antibody labelling in Tg(lhx5:GFP)^{b1205} delineates the neuropil domains of the different habenula subnuclei (Figure 3.4A-A’) and GFP+ axons strongly innervate every subnucleus of the habenula in this line. The main forebrain afferent tracts to the habenula, the stria-medullaris (StMed) and the tract of the habenular commissure (tHc) are also GFP+ (Figure 3.4 C) in this transgenic making it a suitable tool to investigate habenula afferent areas at early stages of development. Having ascertained the suitability of this transgenic line I then looked at GFP expression at earlier stages to see which areas of the forebrain are GFP+ in this transgenic.

At 2dpf (Figure 3.4 B-B’) GFP+ mitral cells are present in the olfactory bulb in Tg(lhx5:GFP)^{b1205} embryos. Additionally, a thick continuous band of GFP+ cells can also be seen in the caudal telencephalon and at the telencephalic/diencephalic boundary (Figure 3.4 B). The tHc can be seen ascending just caudal to this band of GFP+ cells but afferent terminals are yet to elaborate within the habenula. If we look laterally at larval stages (4dpf) many more mitral cells can be seen. The processes from these GFP+ mitral cells can be seen ascending to the habenula via the StMed (as previously described in Miyasaka et al. (2009)). A couple of GFP+ cells can be seen in the pallium. These neurons are likely to be in Dp along with a small neuropil (Figure 3.4 C). This neuropil could be mitral cell collaterals terminating in Dp (as previously described inMiyasaka et al., 2009). At larval stages the band of cells at the telencephalic/diencephalic border has expanded along the rostro-caudal axis and different domains of GFP expression are more easily delineated. Rough divisions showing the proposed identities of GFP+ cells within this band based on subsequent experiments (see Figure 3.5 ,3.6 and 3.7) are shown in the schematics (figure 3B'& C').

The endogenous *lhx5* gene is expressed in the prethalamus in zebrafish (Sun et al., 2015; Jeong et al., 2007; Schlopp et al., 2006) and the caudal extent of the band of GFP in the diencephalon in Tg(lhx5:GFP)^{b1205}embryos also appears to lie anterior to the *zona limitans intrathalamica* as determined by *shh* expression (Sun et al., 2015) and GFP expression in *Tg(-2.7shh:GFP)*^{t10} (Albert et al., 2003) **data from Monica Folgueira** Figure 3.5 -dashed line marks intraencephalic sulcus). The dorsal part of this band of Tg(lhx5:GFP)^{b1205} GFP expression lies within the prethalamus or prethalamic eminence (also known as the thalamic eminence and eminentia thalami (Mueller and Guo, 2009; Puelles, 2007; Wullimann and Mueller, 2004). Studies in the adult have suggested that the vENT originates from the prethalamic eminence (Ganz et al., 2011; Mueller and Guo, 2009) and between 2 and 4dpf we can see an expansion of GFP+ prethalamic cells into the telencephalon (yellow arrow in Figure 3.4 B&C). This group of cells was thus earmarked as the putative larval vENT (Figure 3.4 B'&C'). Ventral to this rostrally expanding domain the bright arching group of GFP+ cells lie within in the preoptic area (Figure 3.4B',C').

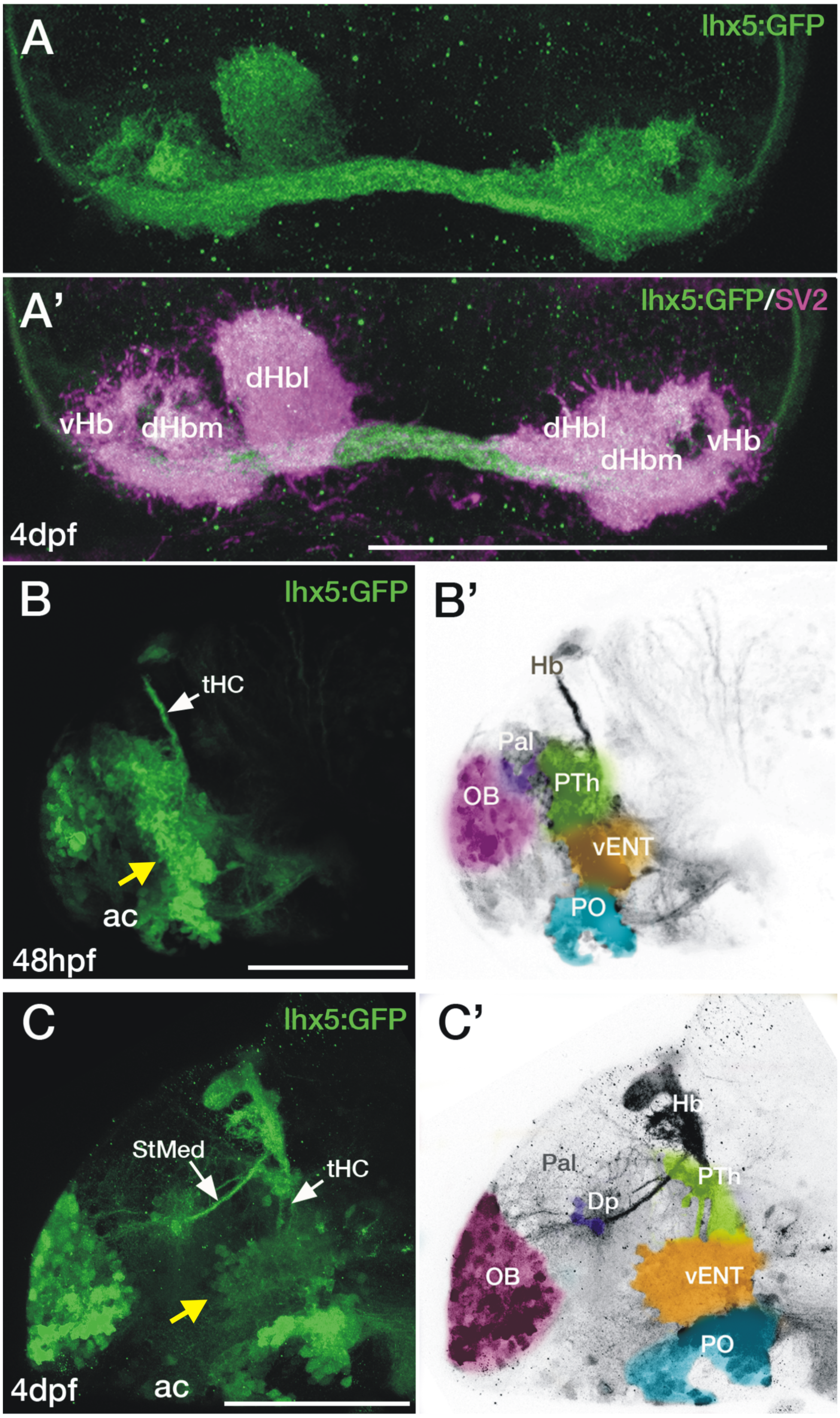

Figure 3.4 GFP+ neurons in the forebrain of Tg(lhx5:GFP)^{b1205} embryos and larvae: Transgene expression in the forebrain of *Tg(lhx5:GFP)*^{b1205} embryos and larvae. **(A,A')** Dorsal views of the habenula of a 4dpf *Tg(lhx5:GFP)*^{b1205} fish labeled

with anti-GFP only **(A)** or anti-GFP (green) and anti-SV2 (magenta) antibodies **(A′)**. GFP+ axon terminals (green) innervate all habenula neuropil domains visualized with SV2 (magenta). **(B–C′)** Lateral views of the forebrain of a *Tg(lhx5:GFP)*^{b1205} fish at 48 hpf **(B,B′)** and 4dpf **(C,C′)**. **(B)** GFP+ cells and processes in 48 hpf *Tg(lhx5:GFP)*^{b1205}. Note that the tract of the habenular commissure is labeled at this stage (tHC, white arrow). Yellow arrow points to putative prethalamic eminence/vENT. **(B′)** Image shown in **(B)** has been converted to gray scale and false colored areas show the different presumptive domains. GFP+ cells and processes form a continuous band at the telencephalic-diencephalic boundary **(B)**, extending from presumptive prethalamus (PTh, labeled in green), through the putative prethalamic eminence/vENT (vENT, labeled in yellow) and preoptic regions (PO, labeled in blue). A number of GFP+ neurons are also present in the olfactory bulb (OB, labeled in pink). **(C)** GFP+ cells and processes in 4dpf *Tg(lhx5:GFP)*^{b1205} fish. Note that at this stage the main afferent tracts to the habenula, the stria medullaris (StMed) and the tract of the habenular commissure (tHC) are visible. Yellow arrow points to putative prethalamic eminence/ vENT. **(C′)** Image shown in **(C)** has been converted to gray scale and false colored areas show the different presumptive domains. There are a number of GFP+ cells rostrally in the OB (pink area), a few GFP+ cells and fibers in Dp (purple). Prethalamus, vENT and preoptic regions are again labeled in green, yellow and blue respectively. Scale bars: All 100 μm.

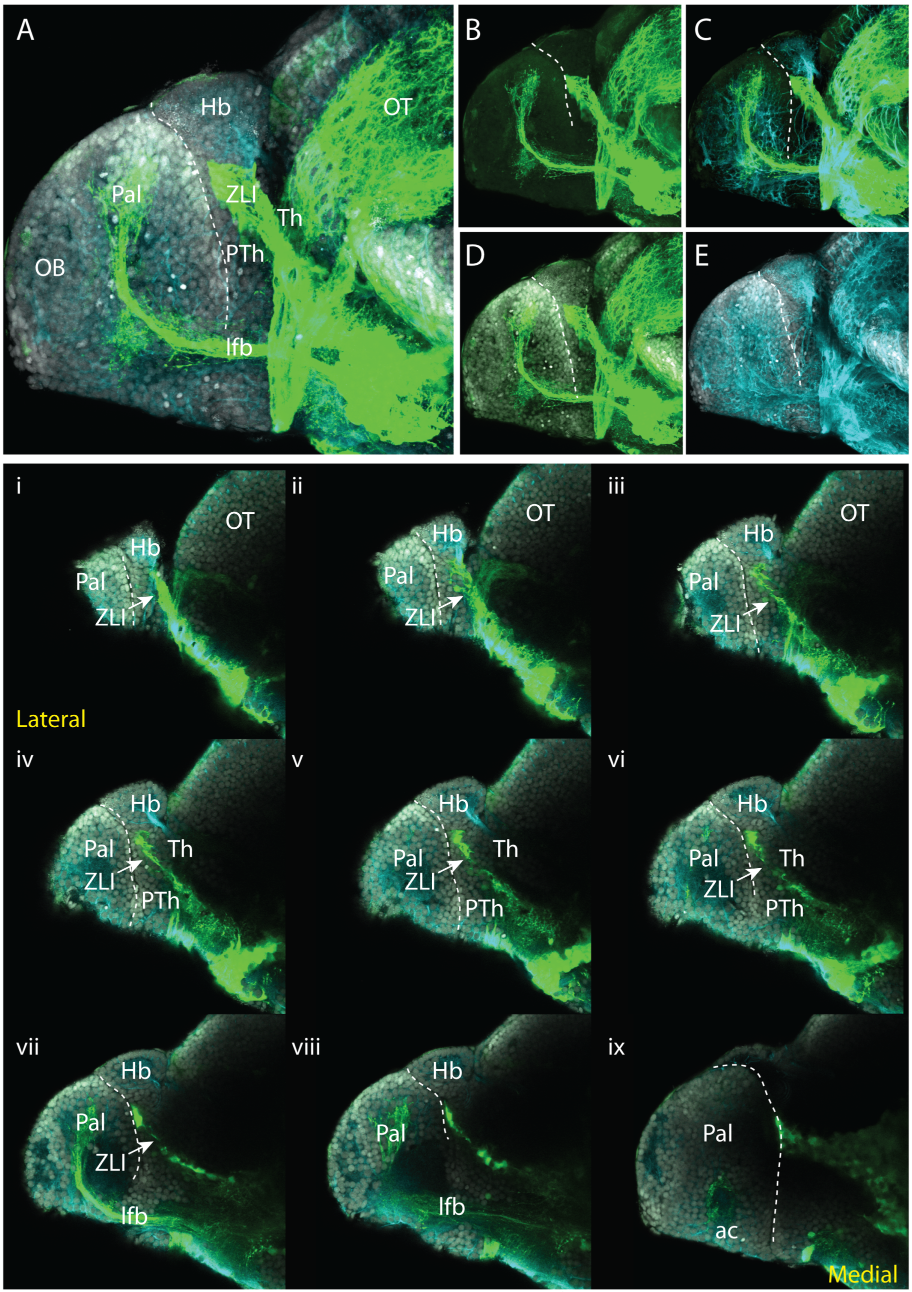

Tg(shh:GFP)/tub/sytox 4dpf Lateral View (immuno by Monica Folgueira)

Figure 3.5: The *zona limitans intrathalamica* as determined by *shh* expression: data from Monica Folgueira Lateral view of a 4dpf *Tg(-2.7shh:GFP)*^{t10} labelled with anti-GFP(green), anti-tubulin(cyan) and Sytox nuclear marker(grey). ((dashed line marks intraencephalic sulcus). **(A-E)** full z-projection. **(I-ix)** single z-slices through the telencephalon and diencephalon showing position of ZLI relative to the intraencephalic sulcus. Cells in the diencephalon ventral to the ZLI are in the prethalamus (also called ventral thalamus) and cells dorsal to it and ventral to the epithalmus are in the thalamus “proper” (also called dorsal thalamus).

3.3 The telencephalic vENT is a major source of habenula afferents, is diencephalic in origin and originates from the prethalamic eminence.

3.3.1 The vENT is a major source of habenula afferents

To examine which developing brain regions are habenula afferent in the larvae, the habenula neuropil of 3dpf Tg(lhx5:Kaede)^{b1204} larvae was photoconverted from green to red using a UV 405nm laser (Fig3.6A) and incubated for 24hrs. Areas afferent to the habenula at this stage of development were retrogradely labelled with red Kaede that had been transported down axons to afferent nuclei. Mitral cells of the olfactory bulb were labelled in n=2/8 conversions. This is in keeping with the innervation of the right dorsal habenula by mitral cells. Some of the labelled cells may not innervate the habenula as a subset of mitral cells use the habenula commissure to cross the midline but show no terminal fields within the habenula (Miyasaka et al., 2009; 2014). In n=6/8 conversions, strong labelling of the region identified as the larval vENT was present supporting the idea that this is the domain from which the vENT derives (Figure 3.6B). In keeping with the adult DiI tracing experiment, a few cells in the preoptic area were retrogradely labelled with red Kaede (n=2/8). In Dp, red Kaede could be detected in the neuropil but not in the cell bodies (Figure 3.6B') supporting the hypothesis that this neuropil corresponds to mitral cell collaterals in this region (Miyasaka et al., 2009;2012).

The results of photo-conversion experiments suggest that the innervation of the habenula by the main forebrain habenula afferent areas, the olfactory bulb and vENT is established early in development. They also help to delineate the position of the presumptive larval vENT at early stages and indicate that it may derive from a domain of *lhx5*:GFP/Kaede expression within the prethalamic eminence.

3.3.2 The vENT expresses tbr1 and straddles the telencephalic/diencephalic boundary at 4dpf.

One of the key factors supporting the hypothesis that the adult vENT derives from the larval prethalamic eminence is that the pallial marker, *T-brain1(tbr),* is expressed in both the adult vENT and larval prethalamic eminence (Ganz et al., 2011). *tbr1* at larval stages is expressed throughout the pallium and olfactory bulbs. Crucially *tbr1* expression also overlaps with GFP expression in the presumptive vENT in Tg(lhx5:GFP)^{b1205} larvae at 4dpf (Figure 3.6C-C”). This *tbr1* expression lends further support to the idea that this group of cells is the vENT. Single z-planes through the lateral (Figure 3.6C’) and more medial parts (Figure 3.6C”) of the vENT co-labelled with GFP and *tbr1* show the morphology of this nucleus better than GFP alone. The nucleus can be seen to surround the lateral forebrain bundle as has been described in the adult (Mueller and Guo., 2009).

3.3.3 The vENT is diencephalic in origin and originates from the prethalamic eminence.

As *tbr1* expression gives better spatial delineation of the vENT than *lhx5*, it was used to trace its developmental origins in Tg(lhx5:GFP)^{b1205} embryos. At 48hpf *tbr1* is expressed throughout the pallium but there is also a small group of *tbr1* cells in the diencephalon (Figure 3.6D-D’). This small triangle of expression in the diencephalon is sandwiched between two *dlx1a* expressing domains that label the prethalamus posteriorly and the pre-optic area anteriorly. The vENT *tbr1a* positive domain is negative for *dlx1a* (Figure 3.6D-F;Wullimann and Mueller., 2004). At larval stages (4dpf) the relative positions of the *dlx1a* and *tbr1* domains are broadly unchanged (Figure 3.6G-J). These results show that the *tbr1*+ area presumed to give rise to the vENT derives from the *tbr1*+/*dlx1a*- prethalamic eminence.

3.3.4 Time-series showing the development of the prethalamic eminence that gives rise to the vENT. (Figure 3.6)

To track the development of the embryonic vENT, *tbr1* expression was tracked over the first three days of development (Figure 3.6K). At 24hpf *tbr1* expression is restricted to the pallium (Figure 3.6Ki). The band of GFP expressing cells at the telencephalic/diencephalic border is also restricted to more dorsal diencephalic regions. By 36hpf (Figure 3.6Kii), the diencephalic GFP expression has spread to more ventral regions and a small group of cells likely to be within the prethalamic eminence have started to express *tbr1*. As development progresses, the number of *tbr1*+ cells in the rostral diencephalon increases. The position of these cells relative to the intraencephalic sulcus (telencephalic/diencephalic boundary) also changes. At 48hpf all of the *tbr1*+ cells lie caudal to the sulcus. Between 48hpf and 72hpf (Figure 3.6Kiii-v) this group of cells expands rostrally so that the *tbr1*+ nucleus straddles the sulcus with the rostral part in the telencephalon and the caudal part still within the diencephalon.

These results show that the *tbr1*+ area presumed to give rise to the vENT derives from the prethalamic eminence and is diencephalic in origin as suggested by previous studies in the adult (Ganz et al., 2011; Mueller and Guo., 2009).

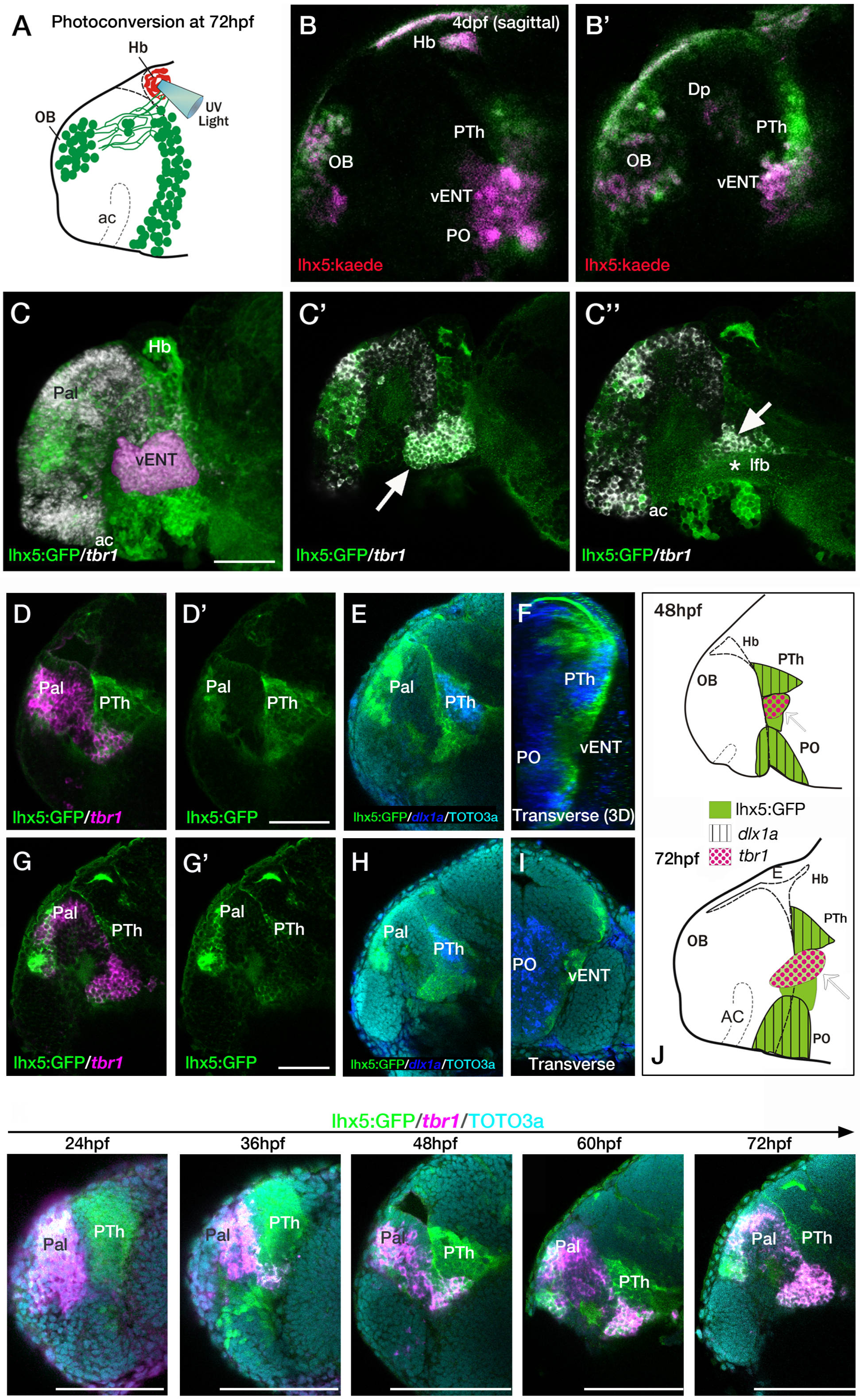

Figure 3.6: The telencephalic vENT is a major source of habenula afferents, is diencephalic in origin and originates from the prethalamic eminence.
Part1: ***The vENT projects to the habenula.*** **(A)** Schematic summarizing experimental setup. Habenula neuropil of 72 hpf *Tg(lhx5:Kaede)*^{b1204} was photoconverted with a

cone of UV light. Photoconversion was made with a lateral approach in order to avoid conversion of areas ventral to the habenula. **(B,B′)** Lateral views of single *Z*-slices of *Tg (lhx5:Kaede)*^{b1204} larvae (B′ is closer to the midline) imaged at 4dpf after photoconversion of the habenula neuropil at 72 hpf. Dotted line marks the anterior intraencephalic sulcus. Some red Kaede cells (magenta in the figure) are observed in the olfactory bulb (OB) and preoptic region (PO), and a few fibers in Dp. A number of red Kaede cells were observed in the domain identified as presumptive larval vENT (arrow in B′). Note red Kaede fibers at the photoconversion area in the habenula (arrowhead in B).

The vENT expresses tbr1 and straddles the telencephalic/diencephalic boundary at 4dpf. **(C–C′′)** Lateral views of *Tg(lhx5:GFP)*^{b1205} inmunostaining against GFP (green) and FISH against *tbr1* (grayscale). In C, the vENT has been false colored in pink. Dotted lines on lateral views mark the anterior intraencephalic sulcus, which runs from the optic recess at the base of the optic stalks ventrally to the pallial/diencephalic boundary dorsally. **(C)** 3D projection of a confocal stack showing *tbr1* and GFP co-expression in the putative vENT (false colored in pink to differentiate from pallial and subpallial *tbr1a* expression). **(C′,C′′)** Single confocal *z*-slices at lateral **(C′)** and medial levels **(C′′)** showing GFP and *tbr1* coexpression in vENT neurons (arrow). Note that the vENT extends from the diencephalon into the telencephalic lobes (dotted line marks the anterior intraencephalic sulcus). At medial levels, the larval vENT surrounds the lateral forebrain bundle (lfb, star in **C′′**), as has been observed in the adult (see **Figure 3.3F**).

Part2: ***The vENT is diencephalic in origin and originates from the prethalamic eminence.*** Lateral **(D,E,G,H)** and transverse views **(F,I)** of Tg(*lhx5:GFP)*^{b1205} fish labeled with anti-GFP (green) and FISH for *tbr1* (pink) **(D–D′,G,G′)** or *dlx1a* (blue) **(E,F,H,I)** at 48 hpf **(D–F)** and 72 hpf **(G–I)**. All images are single confocal z-slices taken from volumes, anterior to the left. **(D–F)** Lateral **(D,E)** and transverse view after 3D rendering **(F)** of Tg(*lhx5:GFP)*^{b1205} 48 hpf larva labeled with anti-GFP (green) and FISH for *tbr1*+ (pink in **D**) and *dlx1a*+ (blue in **E**,**F**). Dotted yellow line in **(D,E)** marks the dorsal limit of the *tbr1*+ domain. **(D)** A group of GFP and *tbr1*+ cells (arrow) are situated in the diencephalon, just caudal to the telencephalic/diencephalic boundary. These cells were identified as prethalamic eminence/prospective vENT. **(D′)** Same image as **(D)** but only showing GFP expression (green channel). Arrow points to prethalamic eminence/prospective vENT. **(E)** GFP and *dlx1a*+ cells in the prethalamus, just dorsal to the prethalamic eminence/prospective vENT (arrow). **(F)** Transverse section shows the relative mediolateral position of the prethalamus, vENT and preoptic areas.

(G–I) Lateral **(G,H)** and transverse section **(I)** of Tg(*lhx5:GFP)*^{b1205} 72 hpf larva labeled with anti-GFP (green) and FISH for *tbr1*+ (pink in **G**) and *dlx1a*+ (blue in **H** and **I**). Dotted yellow line in **(D,E)** marks the dorsal limit of the *tbr1*+ domain. **(G)** The GFP+ vENT expresses *tbr1* extends from the ventrolateral telencephalon to the rostral diencephalon (arrow points to the rostral portion of the vENT, dotted yellow line marks the dorsal limit of the *tbr1*+ domain). **(G′)** Image shown in **(G)** showing just GFP expression (green channel). **(H)** *dlx1a*+ domain in the prethalamus (PTh), just dorsal to the diencephalic portion of the vENT. **(I)** Transverse section shows the GFP+ vENT (green) laterally located and *dlx1a*+ PO (blue) areas more medially. **(J)** Schematic representations of the brain of 48 and 72 hpf larvae showing expression of lhx5:GFP, *dlx1a* and *tbr1* in the prethalamus (PTh), prethalamic eminence (arrow) and preoptic region (PO).

Part3: ***Time-series showing the development of the prethalamic eminence that gives rise to the vENT.*** **(K)** Time series showing *tbr1* expression from 24 to 72 hpf in Tg(*lhx5:GFP)*^{b1205}. **(i)** At 24 hpf, there is no *tbr1* expression in rostral diencephalon; **(ii)** At 36 hpf brain, *tbr1* expression is observed in a subset of the GFP+ cells in the diencephalon (arrow) close to the the telencephalic/diencephalic boundary. These cells are likely to be within the prethalamic eminence/prospective vENT; **(iii–v)** From 48–72 hpf, vENT cells coexpressing *tbr1* and GFP extend into the telencephalic lobes. Scale bars: **(B,C,D′,G′)** 50 μm; **(K)** 100 μm.

3.3.5 Spatio-temporal fate map of the larval prethalamic eminence/prospective vENT and adjacent areas confirms the diencephalic origin of vENT cells

To determine whether the area defined as the vENT in the previous experiment by *tbr1* and *dlx1a* expression derives from the prethalamic eminence, Tg(lhx5:Kaede)^{b1204} fish was used to fatemap the putative vENT and adjacent areas at early stages and follow their development (Figure 3.7).

Presumptive vENT

In order to fatemap the putative vENT the *tbr1*+ area identified in the previous experiment was targeted for Kaede photoconversion. This area was identified at 48hpf using the relative positions of the following anatomical landmarks: the habenula commissure dorsally, and the intraencephalic sulcus anteriorly and the bright arching group of cells ventrally (Figure 3.7A). Post photo-conversion the embryos were allowed to develop in darkness for 24hrs before reimaging. At 72hpf, red Kaede+ cells could be seen in the ventrolateral telencephalon quite far from the initial site of conversion in the diencephalon (n=8/8, yellow arrow in Figure 3.7B). The ventro-lateral telencephalic location of these cells (Figure 3.7B') was consistent with the area of GFP expression defined in the previous experiments as larval vENT. The photoconverted vENT cells also extended axons through the tract of the habenula commissure to terminate in the neuropil of both the ventral (white arrow inset) and dorsal ipsilateral habenula subnuclei (white arrowhead inset) (Figure 3.7B). Some cells could also be seen caudal to the site of photoconversion in hypothalamic regions.

Such migratory populations have been described in previous studies (Mione et al., 2008; Mueller and Wullimann., 2002).

Presumptive Pre-optic region(PO)

A similar approach was taken to fatemap the presumptive preoptic portion of this band of *lhx5* expression. This presumptive PO was targeted using information from the previous experiments of *dlx1a*/GFP co-expression in Tg(lhx5:GFP)^{b1205} embryos. This arching bright group of cells ventral to the presumptive vENT was photoconverted at 48hpf. At 72hpf the red cells in the PO conversions for the most part remained close to the site of photoconversion (n=9/9). A few cells extended into rostral areas but transverse sections show that these cells are located close to the midline consistent with a PO identity (Figure 3.7D-D'). The existence of a minor projection from PO to the habenula was supported by 3 out of 9 conversions showing a small number of red axons projecting to the habenula. Due to the proximity of the PO and vENT populations at 48hpf though these could feasibly be vENT habenulopetal neurons.

Prethalamus

To target and fatemap the putative prethalamic section in Tg(lhx5:Kaede)^{b1204} embryos the region of *dlx1a*/GFP co-expression dorsal to the presumptive vENT was targetted. The photoconversion of these prethalamic cells at 48hpf (Figure 3.7E,E';n=3/3) for the most part resulted in red Kaede+ cells remaining close to the original site of photoconversion or extended caudally into more posterior regions. Unlike the putative vENT cells ventral to this population these cells did not invade telencephalic areas (Figure 3.7F-F").
A summary of all the fatemap results is shown in Figure 3.7G.

Conclusions

This experiment supports the conclusions that the vENT is diencephalic in origin and originates from the prethalamic eminence at early stages before extending into the ventro-lateral telencephalon between 48-72hpf.

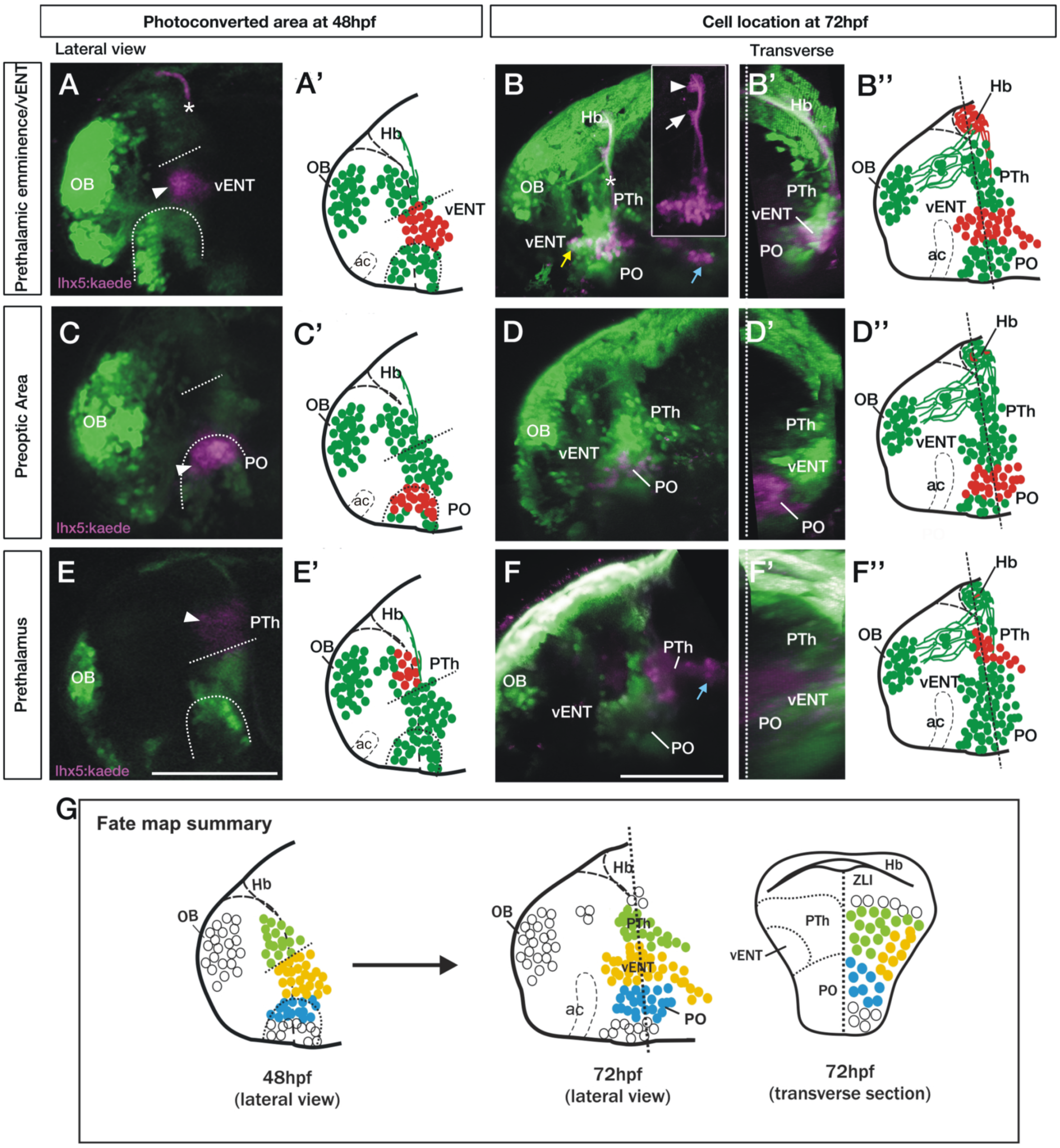

Figure 3.7: Spatio-temporal fate map of the larval prethalamic eminence/prospective vENT and adjacent areas. Images and accompanying schematics show Kaede photoconversion areas in lateral views of 48 hpf *Tg(lhx5:Kaede)*^{b1204} fish (A,A′,C,C′,E,E′) and location of Kaede cells by 72 hpf in lateral view (B–B′′,D–D′′,F–F′′) and transverse sections after 3D rendering (B′,D′,F′). Dotted arch and lines at 48 hpf mark the dorsal limit of the preoptic area and prethalamic eminence respectively. ***Photoconversion in the prethalamic eminence* (*n* = 8). (A–B′′)** Cells were photoconverted from green to red (magenta in

the images) at the diencephalic prethalamic eminence of *Tg (lhx5:Kaede)*^{b1204} embryos at 48 hpf (arrowhead in A, red cells in schematic A′′) and their location was then imaged by72 hpf in lateral view (B and red cells in B′′). Note in (A) that area of photoconversion by 48 hpf is located at the level of the tract of the habenular commissure (marked with a star). **(B′)** is transverse section after 3D rendering. Note that 24 h after photoconversion, red Kaede expressing neurons have expanded from the photoconversion area rostrally into the telencephalon (yellow arrow) and caudally into hypothalamic areas (white arrow). These red Kaede cells send afferent projections to ventral (arrow in B inset) and dorsal halves (arrowhead in B inset) of the habenula and were identified as vENT. Transverse section shows that the vENT occupies a lateral position within the forebrain (B**′). *Photoconversion in preoptic regions (PO)* (*n* = 9)**. **(C–D′′)** Cells were photoconverted in the presumed preoptic area of *Tg (lhx5:Kaede)*^{b1204} embryos at 48 hpf (C,C′). Note that 24 h after photoconversion, most red Kaede cells maintain their relative rostro-caudal positions within the telencephalon and diencephalon (D), and are located ventro-medially relative to the vENT when viewed in transverse section (D′). Most conversions of presumptive PO (*n* = 6/9) did not result in labeling of habenula afferents. ***Photoconversion of the prethalamus (PTh; n = 3)*****.** **(E–F′′)** Cells were photoconverted in the presumed prethalamic area of *Tg (lhx5:Kaede)*^{b1204} embryos at 48 hpf **(E,E′)**. Twenty four hours after photoconversion, most red Kaede cells maintain their positions within the diencephalon and do not expand into the telencephalon **(F)**. A few red Kaede cells expand into caudal areas (white arrow). Transverse section shows that these cells occupy a dorsomedial position **(F′)**. **(G)** Summary of the results of the fate map experiments with *Tg(lhx5:Kaede)*^{b1204}, with the areas of Kaede photoconversion in 48 hpf. Open circles denote cells that were not fate mapped. Level of transverse section is shown in the 72 hpf lateral view of the brain. Scale bars: All 100 µm.

3.4 Characterisation of the larval vENT

3.4.1 The larval vENT contains glutamatergic and calretinin-positive populations of cells.

In rodents, the entopeduncular neuron projection to the lateral habenula is excitatory (Shabel et al., 2012). To determine if this is also the case in zebrafish I used the transgenic line Tg(slc17a6b:DsRed)^{nns9Tg} (Kani et al., 2010; otherwise known as vglut2a:DsRed; Miyasaka et al., 2009). This transgenic expresses DsRed in glutamatergic neurons. In double Tg(lhx5:GFP)^{b1205}: Tg(slc17a6b:DsRed)^{nns9Tg} larvae, GFP in the vENT of colocalises with DsRed indicating that many vENT neurons are glutamatergic (Figure 3.8A-A”). *vglut2a* expression in the adult zebrafish vENT was also reported by Amo et al., 2014.

Individual z-slices through Tg(lhx5:GFP)^{b1205}: slc17a6b:DsRed^{nns9Tg} larvae at 3dpf from lateral (Figure 3.9) and ventral (Figure 3.10) views show the distribution of glutamatergic cells more clearly within the band of GFP+ cells covering the vENT, PTh and PO areas. From a lateral aspect, both the habenula and PO express *vglut2a* strongly (Figure 3.10A-C). Another group of cells just ventral to the habenula is also strongly labelled. Ventral to this group in the PTh there seems to be a gap in *vglut2a* expression. Sections through the vENT in both the lateral and ventral views show many GFP+ cells within the vENT are also glutamatergic although the DsRed labelling in this nucleus is not as strong as in other areas (Fig 3.9i-iii;Figure 3.10iii,iv). Some cells in the PO are also glutamatergic (Figure 3.9iv and Figure 3.10A,B,i,ii).

Calretinin immunoreactivity has also been reported in the ventrolateral telencephalon (Castro et al., 2006) and the prethalamic eminence (Hendricks and Jesuthasan., 2007). There are indeed many *lhx5*:GFP/CR+ neurons within the vENT predominantly in the more medial part surrounding the lateral forebrain bundle (Figure 3.8B-C’). The prethalamus is predominantly calretinin negative.

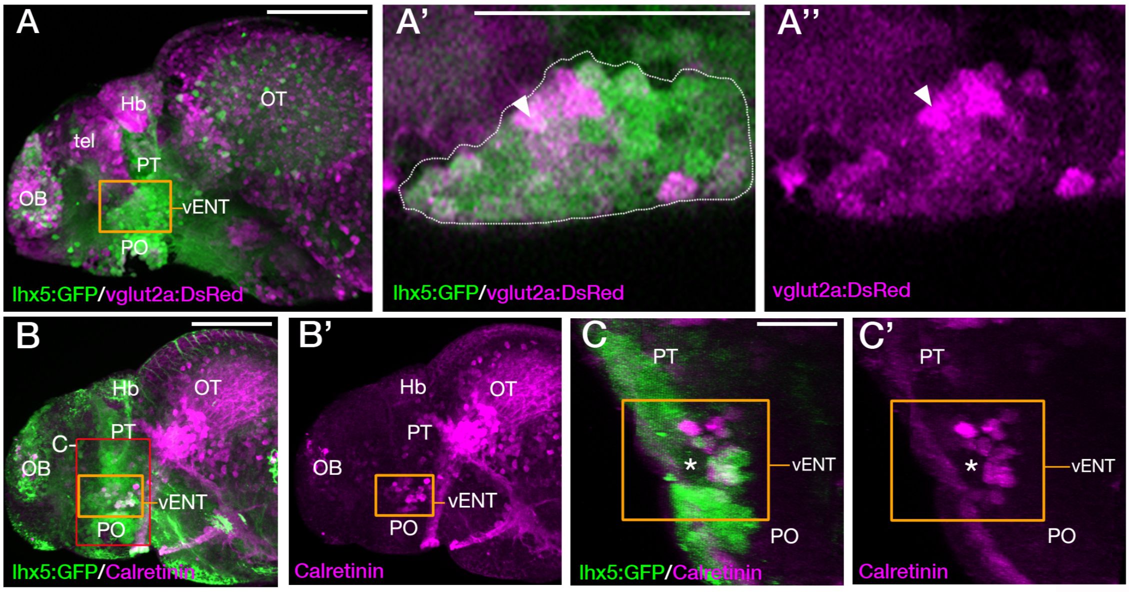

Figure 3.8: The larval vENT contains glutamatergic and calretinin-positive populations of cells. (A,A′′) Confocal images of *Tg(lhx5:GFP)*^{b1205}/ *Tg(slc17a6b:DsRed)*^{nns9Tg} 4 dpf double transgenic larvae labeled with anti-GFP and anti-DsRed antibodies (green and magenta respectively). GFP expression shows the previously identified vENT (orange box in A, enlarged in A′,A′′). Enlarged views of single confocal sections **(A′,A′′)** show co-expression of GFP and DsRed in a subpopulation of cells (arrowheads) of the GFP+ vENT (dotted line in A′ marks). **(B–**

C′) *Tg(lhx5:GFP)b*1205 4dpf larvae labeled with anti-GFP (green) and anti-calretinin (magenta). **(B,B′)** lateral view shows a subset of GFP+ vENT neurons (bound by orange box) express calretinin. **(C,C′)** 3D transverse sections of same larvae**(B)** cropped to area delineated by red box in **(B)**. Calretinin+ and GFP+ neurons within the vENT, which surrounds the lateral forebrain bundle (lfb; asterisk). Scale bars: **(A,B)** 100 μm; **(A′,C)** 50 μm.

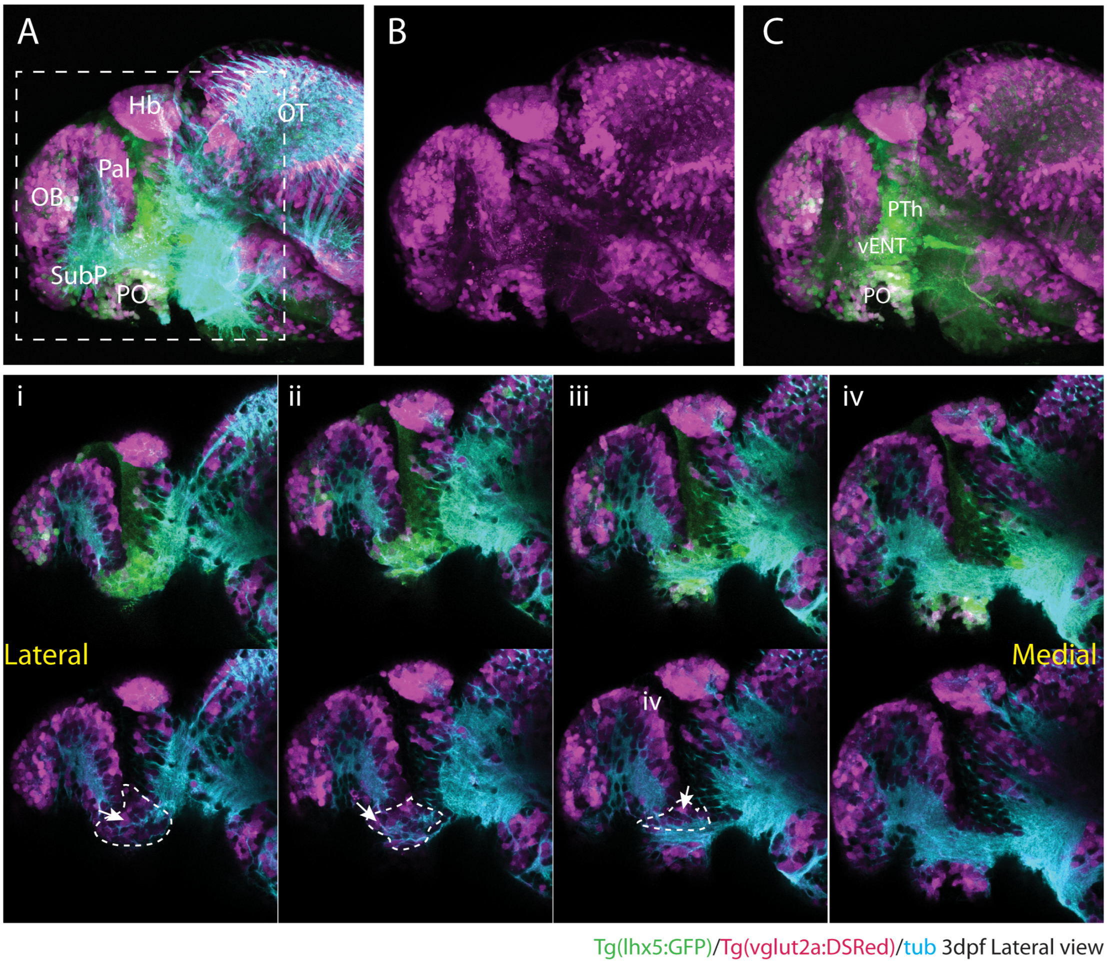

Figure 3.9: Lateral view of a 3dpf Tg(lhx5:GFP)^{b1205}: Tg(slc17a6b:DsRed)^{nns9Tg} brain labelled with **(A)** anti-GFP(green), anti-DSRed(magenta) and anti-tubulin antibodies(cyan). **(B)** Tg(slc17a6b:DsRed)^{nns9Tg} expression only. **(C)** Tg(lhx5:GFP)^{b1205}: Tg(slc17a6b:DsRed)^{nns9Tg}. **(i-iv)** Individual z-slices through Tg(lhx5:GFP)^{b1205}: Tg(slc17a6b:DsRed)^{nns9Tg} larvae dashed line indicates outline of vENT while arrows indicate glutamatergic vENT neurons that co-express GFP and DSred.

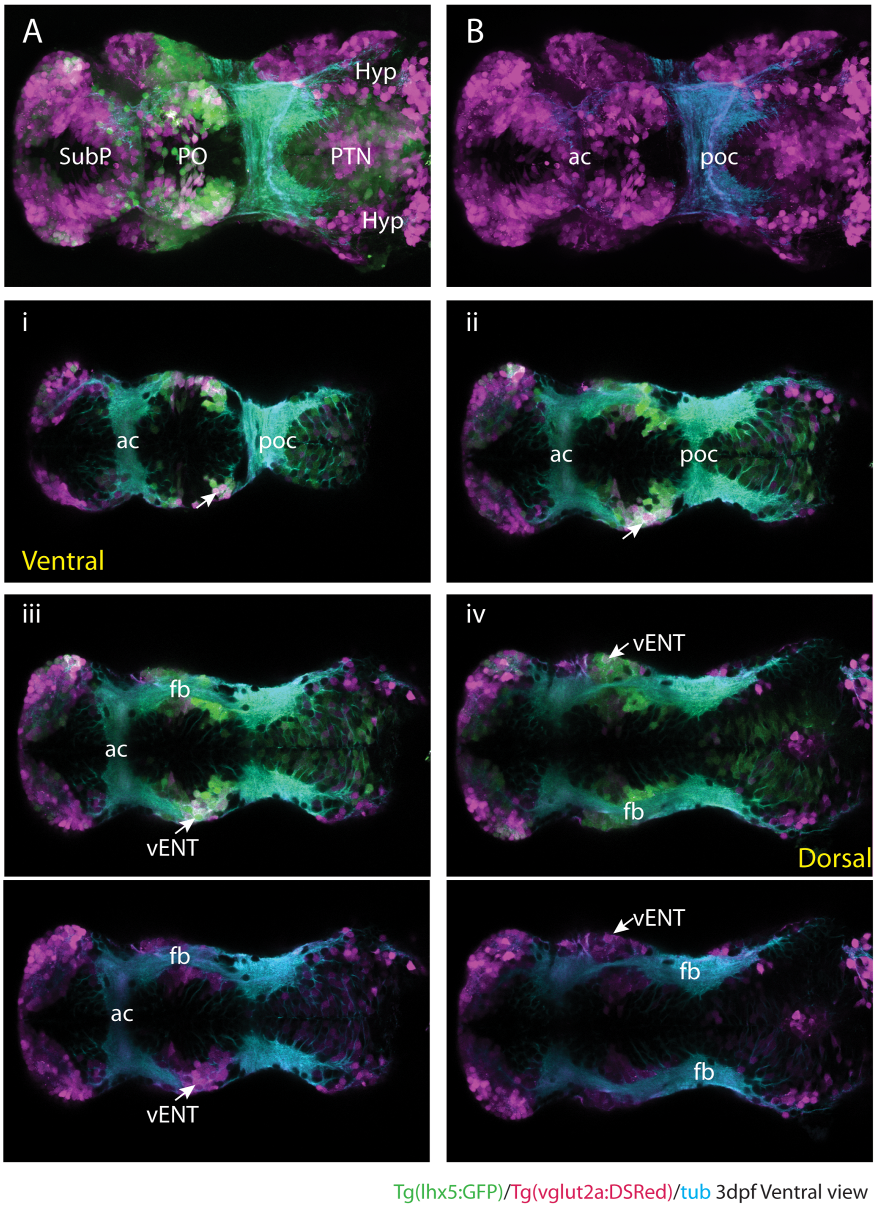

Figure 3.10: Ventral view of a 3dpf Tg(lhx5:GFP)^{b1205}: Tg(slc17a6b:DsRed)^{nns9Tg} brain labelled with **(A)** anti-GFP(green), anti-DSRed(magenta) and anti-tubulin antibodies(cyan). **(B)** Tg(slc17a6b:DsRed)^{nns9Tg} and tubulin expression only. **(i-iv)** Individual z-slices through Tg(lhx5:GFP)^{b1205}: Tg(slc17a6b:DsRed)^{nns9Tg} larvae; arrows indicate glutamatergic vENT neurons that co-express GFP and DSred.

3.4.2 GABAergic neurons in the ENT and adjacent areas.

Co-localisation of anti-GABA and *lhx5*:GFP at 3dpf shows a large group of GFP+ GABAergic cells just ventral to the habenula in the prethalamus (Figure 3.11A, B sections i-v). It is difficult to say which prethalamic nucleus this GABAergic group of cells is at such an early stage as I, VL and VM are all found just ventral to the ventral habenula in the adult and all three nuclei are GABAergic (Mueller 2012). This area may also undergo major morphological changes between larval and adult stages similar to those described for the vHb in Amo et al., 2010. Ventral to this group within the PTh, most neurons within the *lhx5*:GFP+ population are GABA- (Figure 3.11B sections iv-vi). Within the vENT a small number of cells are GABAergic in the most caudal part (white arrows in Figure 3.11v). In PO comparatively, many more GABAergic cells are present (white arrows Figure 3.11section vi). Ventral view of 3dpf Tg(lhx5:GFP)^{b1205} fish labelled with anti-GABA antibody (Figure 3.12) show that the more caudal part of the GFP+ PO is for the most part GABA-. The anterior part of the expression just caudal to the anterior commissure contains more GABAergic cells (white arrows Figure 3.12A'). The part of the vENT dorso-lateral to the lfb seems largely devoid of GABAergic cells (Figure 3.12B').

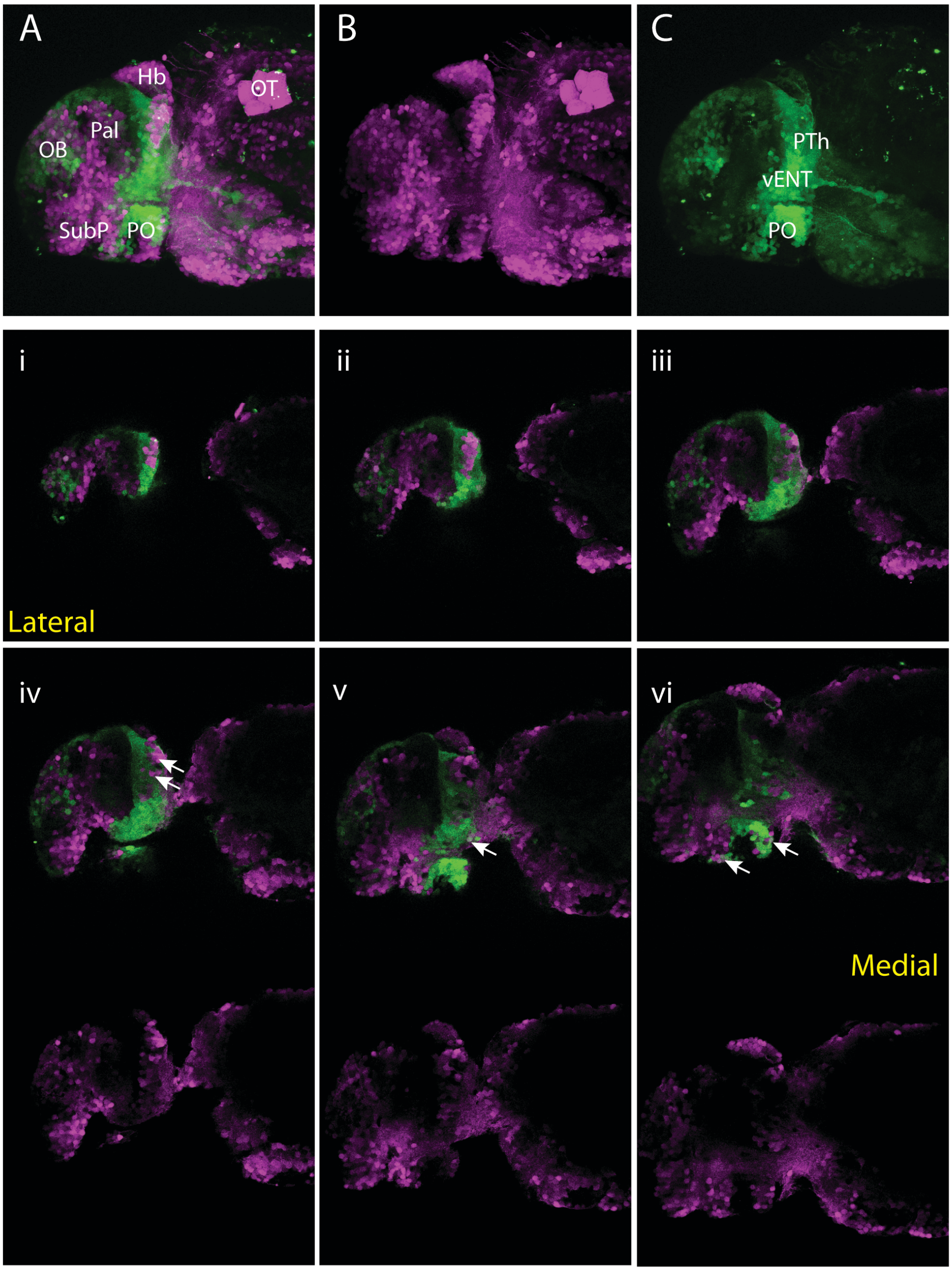

Tg(lhx5:GFP)/GABA 3dpf Lateral view

Figure 3.11 GABAergic neurons in the ENT and adjacent areas (Part I): Lateral view of a 3dpf Tg(lhx5:GFP)^{b1205} labelled with anti-GFP (green) and anti-GABA antibodies (magenta).**(A-C)**Full Z-projection. **(i-iv)** Single z-slices**.** Arrows in i-vi indicate cells that express both GFP and GABA within the prethalamus(iv), vENT(v) and preoptic(vi) areas.

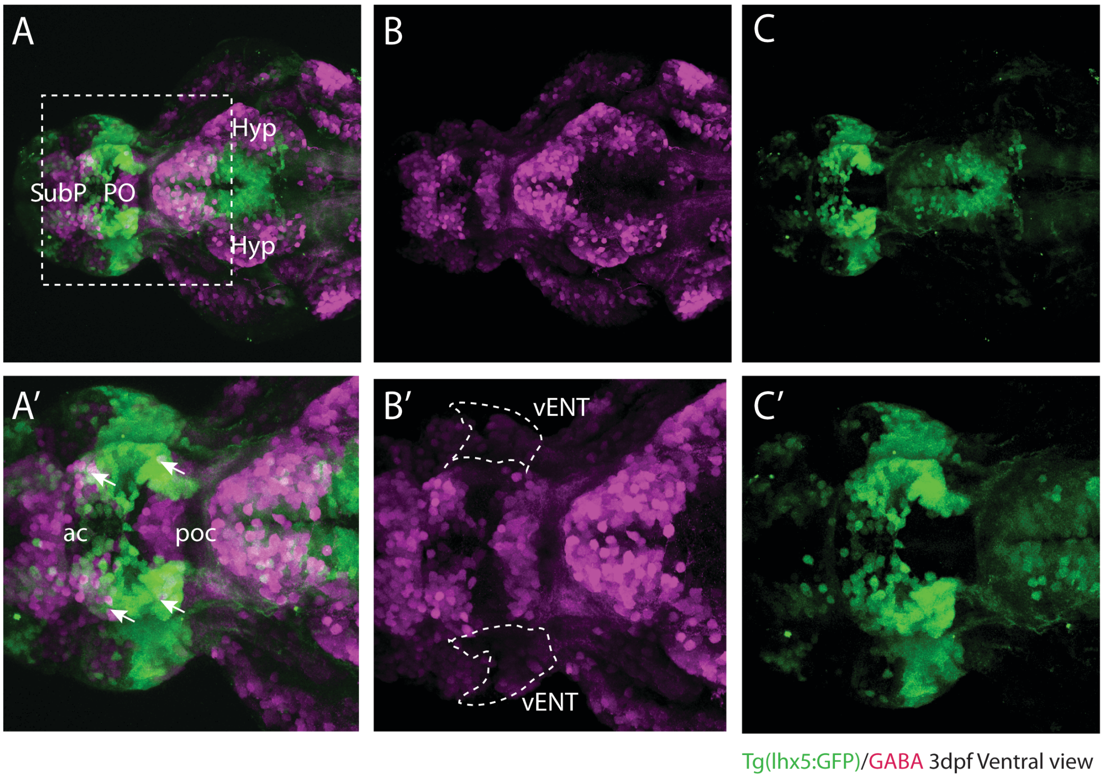

Figure 3.12: GABAergic neurons in the ENT and adjacent areas (Part II): Ventral view of a 3dpf Tg(lhx5:GFP)^{b1205} labelled with anti-GFP (green) and anti-GABA antibodies (magenta). **(A-C)** Entire forebrain. **(A'-C')** High magnification of region surrounded by whisker box in "A". Arrows in A' indicate some neurons in the preoptic area expressing both GFP and GABA. Dashed white line in B' shows approximate location of the vENT, it is largely GABA negative.

3.4.3 *sst* expression in the vENT and adjacent areas. (*FISH and imaging done by Tom Hawkins)*

The habenulopetal entopeduncular nucleus in rodents has been shown to contain neurons expressing the neuropeptide somatostatin (Stephenson-Jones et al., 2016., Wallace et al., 2017). FISH for *somatostatin* (*sst*) in 5dpf Tg(lhx5:GFP)^{b1205} fish show several groups of *sst*+/GFP+ neurons within the forebrain. The dHbm subnucleus shows *sst*+ neurons on both sides (blue boxes Figure 3.13 C,D and E). Ventral to the habenula within the GFP+ prethalamus, no *sst*+ neurons are present. At the midline but dorsal to the vENT in what is presumably the neurosecretory preoptic hypothalamus (NPO)(Herget et al., 2014., Herget and Ryu., 2015) and medial part of EmT bilaterally symmetrical groups of *sst*+ neurons are present that are also *lhx5*:GFP+ (pink boxes Figure 3.13 C,D and E). Within the vENT, some *sst*+ cells are present medial to the lfb (orange boxes Figure 3.13 C,D and E) although some of the very medial cells could be in the pre-optic area. Another small cluster of *sst*+ neurons lie laterally within the ventral telencephalon, caudal to the ac and anterior to the tip of the vENT (yellow boxes Figure 3.13 C,D and E). Some of these cells may also be GFP+. These results indicate that a subpopulation of *sst* positive neurons does exist within the zebrafish entopeduncular nucleus as is the case in mammals (Stephenson-Jones et al., 2016., Wallace et al., 2017).

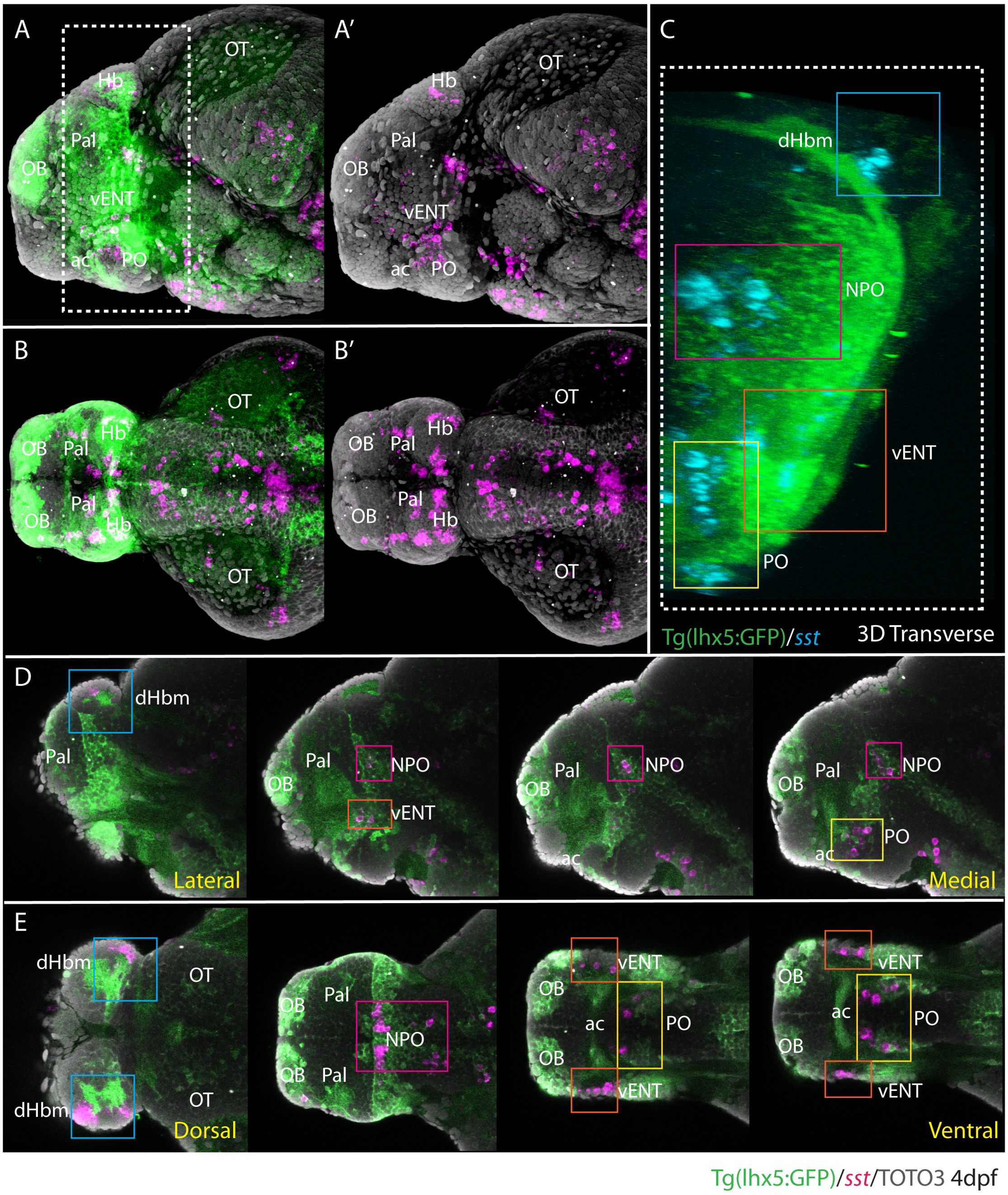

Figure 3.13: *Sst* expression in the vENT and adjacent areas.: Lateral**(A-A’,D)**,Dorsal **(B-B’, E)** and Transverse 3D frontal views **(C)** of a 5dpf Tg(lhx5:GFP)^{b1205}fish labelled with anti-GFP (green), *somatostatin FISH* (magenta and cyan in C) and nuclear marker TOTO3I (grey). **(D)** serial sections through the forebrain of larvae A. **(E)** serial sections through the forebrain of larvae “B”. Blue box surrounds dHbm; pink box surrounds NPO; Orange box surrounds vENT; yellow box surrounds PO.

Main Findings

Using tract tracing and Kaede photoconversion experiments in adult (Monica Folgueira) and larval zebrafish, we have revealed that the main afferent nuclei to the zebrafish habenulae are the olfactory bulb (to right habenula), subpallium, vENT, parapineal (to left habenula), nucleus rostrolateralis (see next chapter), preoptic area, posterior tuberculum, posterior hypothalamic lobe and median raphe. Through fate-mapping and gene expression studies I have shown that the vENT is diencephalic in origin and extends into the telencephalon. I conclude that the vENT is the main afferent telencephalic nucleus of the habenula in zebrafish and is homologous to the entopeduncular nucleus in mammals. These results are discussed in Chapter 6.

Chapter 4. The Nucleus Rostro-lateralis

4.1 Introduction

The left dorsal habenula is light responsive

The asymmetric afferent inputs to the dorsal habenula in zebrafish (Hendricks & Jesuthasan, 2007; Miyasaka et al., 2012., Concha et al., 2003; Turner et al., 2016) alongside its other neuroanatomical asymmetries in gene expression (Concha et al., 2000., Gamse et al., 2003) and efferent projections (Aizawa et al., 2005; Bianco et al., 2008) suggest that the dorsal habenula could also show functional asymmetries. A study performed by Elena Dreosti in our lab confirmed this (Dreosti et al. 2014). Dreosti et al, found that responses to light and odour stimuli by dHb neurons were functionally lateralised. dHb neurons responding to light were predominantly located in the left dHb and those responding to an odour stimulus in the right dHb.

Further experiments in this study using eyeless *chk* mutants and parapineal ablated larvae showed that the asymmetric responses in left dHb neurons are dependent on the eyes.

Ablation of the eyes, either physically by enucleation or genetically using *chk*^{ne2611} eyeless mutants, leads to a reduction in light responses in dHb neurons. The parapineal is a light-sensitive organ that asymmetrically innervates the left dHb. The ablation of the parapineal at 3dpf after parapineal migration and establishment of left dHb identity has occurred did not result in the total loss of visual responses in dHb neurons. These results when taken together indicate that sensory input from the eyes and not the parapineal are required to generate the visual responses in LdHb neurons. Lateralised responses to odour were still present in both the eyeless mutants and parapineal ablated larvae showing that visual input is not required for the establishment of functional asymmetries in the dHb. The reverse is also true as ablation of mitral cell innervation of right dHb by olfactory pit enucleation did not affect the asymmetry of visual responses. Additionally, dark-rearing of larvae had no effect on the establishment of dHb functional asymmetries.

In summary, the key findings of Dreosti et al. (2014) pertinent to this thesis are

1) The eyes and not the parapineal are the most important source of visual sensory input to the dHb.
2) Sensory afferent input relaying olfactory and visual stimuli are not required for the initial establishment of functional asymmetries in the dHb. These are likely to be established by the same genetic patterning mechanisms that underlie the development of anatomical asymmetries seen in the epithalamus in which the parapineal plays a key role.

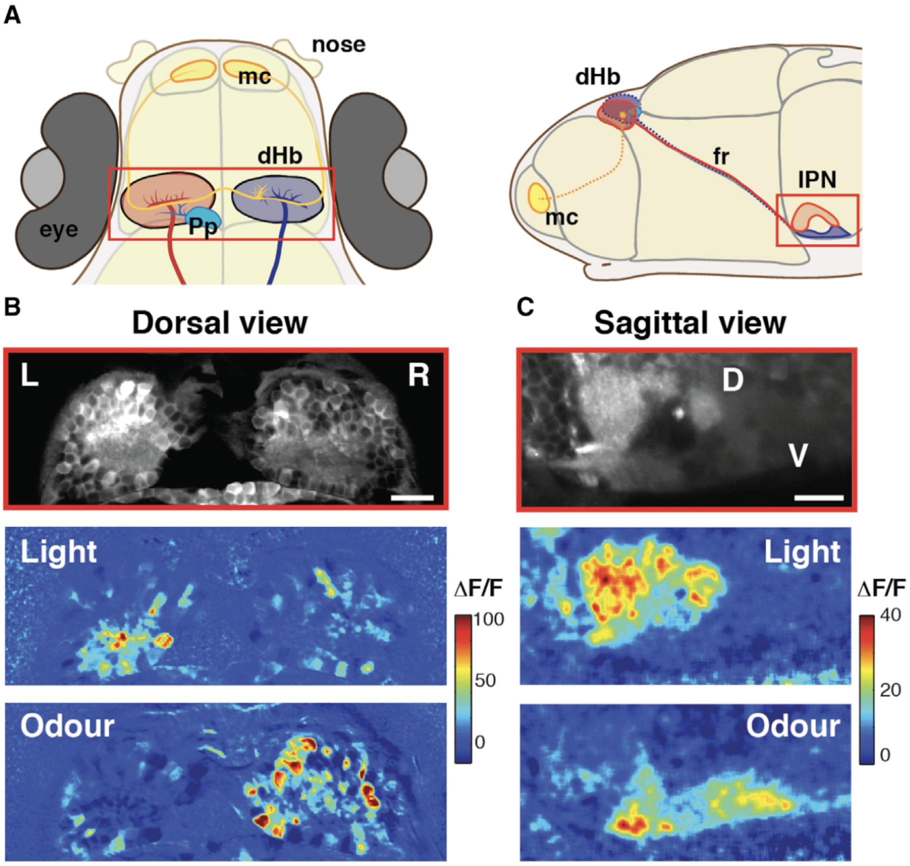

Figure 1. Responses to Visual and Odor Stimuli Are Lateralized in the dHb and Segregated Dorsoventrally in the IPN

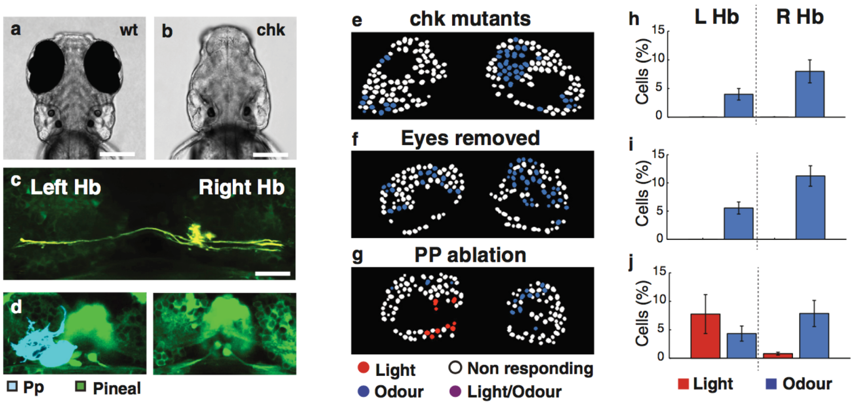

Figure 4. Asymmetric Responses of left dHb Neurons to Light Are Dependent upon the Eyes

Figure 4.1: Dreosti et al. Functional responses to light and odour in the dorsal habenula and IPN of WT larvae (Legend and Figure both from Dreosti et al., 2014): (A) Schematic dorsal and sagittal views of 4 days postfertilization (dpf) zebrafish showing left (red) and right (blue) dHb nuclei and their asymmetric afferents from olfactory mitral cells (yellow) arbor- izing in the right dHb nucleus and parapineal neurons (cyan) arborizing in the left dHb nucleus. Neurons of the left dHb predominantly innervate the dorsal IPN, while neurons of the right dHb innervate the ventral IPN. (B) Example of a two-photon image of a single z plane of the dHb (14

mm below the skin) of a Tg(elavl3:GCaMP5G) 4 dpf fish (top) and corre- sponding color-coded calcium signals that are LR lateralized in dHb neurons in response to a non- lateralized presentation of light (middle) and odor (bottom) stimuli. Each panel is an average of two stimulus trials. The relative change in fluorescence (DF/F) is expressed as a percentage. (C) Example of a two-photon image of a lateral view of the IPN of a Tg(elavl3:GCaMP5G) 4 dpf fish (top) and corresponding color-coded calcium re- sponses to light (middle) and odor (bottom). Each panel is an average of three trails. Responses to light are predominantly localized in the dorsal IPN, while those to odor are localized in the ventral IPN. Note that the dorsal IPN has a higher basal fluorescence (as does the left dHb nucleus). Scale bars, 20 mm. D, dorsal; V, ventral; fr, fascic- ulus retroflexus; IPN, interpeduncular nucleus; dHb, dorsal habenulae; L, left; R, right; mc, mitral cells; Pp, parapineal.

Although Dreosti et al (2014) showed that light stimuli was most likely reaching the habenula via the retina, DiI labelling of the retino-fugal system in larval zebrafish showed no direct projections to the habenula from the retina (Burrill and Easter., 2004). This would indicate that the visual input to the habenula described in Dreosti et al (2014) must be relayed via another afferent nucleus.

Two papers to date, the aforementioned Burrill and Easter (2004) and Robles et al (2014), have traced the retino-fugal pathway in larval zebrafish. Zebrafish retinal ganglion cell (RGCs) axons exit the eye through the optic nerve decussate at the optic chiasm and arborize in distinct arborisation fields (AFs) along the optic tract (See Figure 4.2 for key images from these two studies). These AFs are formed of the neuropil areas of retinorecipient brain nuclei. In addition to the main visual processing centre, the optic tectum, RGC axons project to the hypothalamus, thalamus and pretectal regions (Burrill & Easter.,2004; Robles et al., 2014). The development of the retino-fugal projection was found to be very orderly, requiring no pruning of exuberant projections at later stages (Burrill & Easter.,2004). Identification of the various AFs with retinorecipient nuclei in the adult was done by relative position. Using this method four out of 10 AFs were unambiguously paired with their adult structures: AF-10=Optic Tectum, AF-1= n. suprachiasmaticus & n. preopticus parvicellularis posterioris, AF-3= n. accessorius opticus ventralis, AF-9= n. pretectalis periventricularis pars dorsalis (Burrill & Easter., 2004). Another study by Kubo et al (2014) confirmed this AF-9 pretectal identity and showed this visual area to be optic flow responsive and a driver of horizontal eye movement (Kubo et al., 2014). The identity of the other 6AFs remains ambiguous. Though the fact that the visual information is reaching the habenula via the retina (Dreosti et al.,2014) make one or more of these AFs interesting candidates for the habenular visual afferent nucleus, and so! The hunt begins…

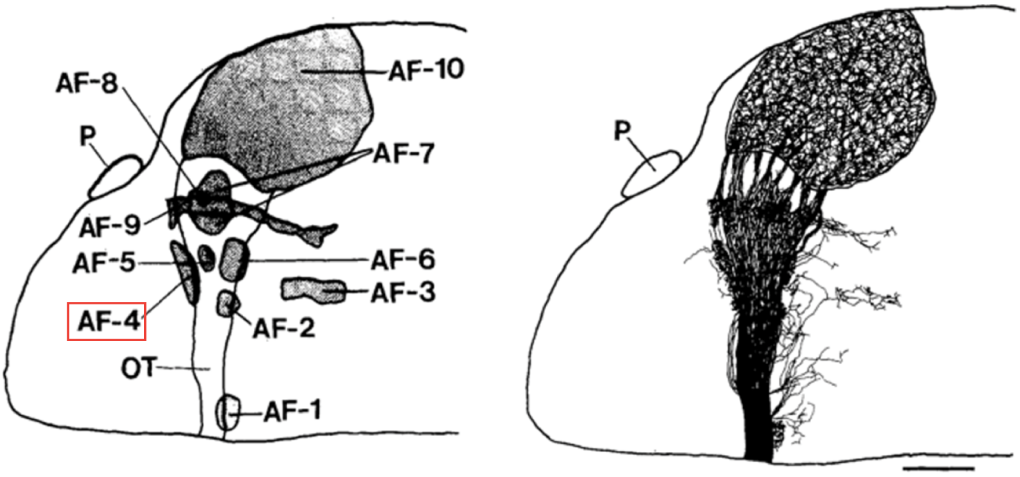

Schematic from Burrill & Easter, 2004

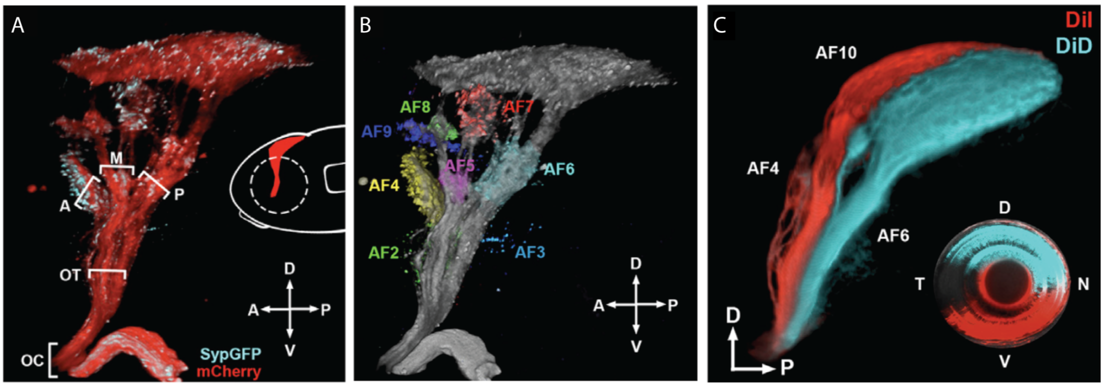

adapted from Robles et al., 2014

Figure 4.2: Arborisation fields of the retinofugal pathway. (TOP) A schematic showing the arborisation fields of the retinofugal projection in the larval zebrafish (adapted from Burrill & Easter, 2004). **(A-C) 3D Model of Arborization Fields Formed by RGC Axons** 3D reconstruction of a fixed 6 dpf larval brain with RGC expression of membrane-targeted mCherry (red) and Syp-GFP (cyan) driven by atoh7:Gal4 driver transgene. Note the optic chiasm (OC), main bundle of the optic tract (OT), and anterior (A), medial (M), and posterior (P) branches formed in the thalamus. The inset shows a schematic side view of larva and removal of the contralateral eye (dashed line) to reveal the optic tract. (B) Lateral view of volume in

(A) with AF1–AF9 pseudocolored in the Syp-GFP channel and overlaid on the mCherry signal in gray. (C) Lateral view of 7 dpf optic tract labeled by injection of DiI (red) and DiD (cyan) into ventral and dorsal hemiretinae. The inset shows the contralateral eye. **Figure and legend Adapted from Robles et al (2014).**

Results

4.2 A prethalamic nucleus is habenula afferent and retinorecipient

4.2.1 The habenular subnuclei

Light responses in the IPN are predominantly restricted to the dorsal IPN (dIPN) (Dreosti et al., 2014). The dorsal habenula subnucleus in zebrafish can further be divided into lateral (dHbl) and medial (dHbm) subnuclei with the lateral subnucleus predominantly innervating the dorsal IPN and the medial subnucleus innervating the ventral IPN (Bianco et al., 2008). As the dorsal IPN is predominantly innervated by habenula neurons located in the left dHbl subnucleus it follows that the visual responsive neurons described in Dreosti et al., 2014 are for the most part located in the lateral subnucleus of the *left* dorsal habenula (Dreosti et al., 2014), from now on abbreviated as LdHbl.

Synaptic-vesicle 2 (SV2) antibody labelling of the habenular neuropil shows the relative size and shape of the neuropil subdomains in the left and right habenula (Figure 4.3 A-D, schematised in E). The largest difference in neuropil size between left and right is in the lateral dHb subnucleus, where the neuropil of LdHbl is larger (labelled with green in Figure Figure 4.3C) than its right-sided counterpart (RdHbl). This left-sided subnucleus is also innervated by the left-sided parapineal nucleus (Figure 4.3D-E). It appears from the both the position of the light-sensitive neurons within the LdHbl and also the outline of the habenula neuropil visible from the images of the Tg(elavl3:GCaMP5G) larvae in Dreosti et al., 2014 (Figures 1B and Figure 2A) that the light-responsive cells surround this same neuropil. These light responsive cells seem to be located directly dorsal to this neuropil and also caudal to it close to the position of the parapineal nucleus just caudal to the habenula commissure. As functional responses to olfactory stimuli seem to cluster around the mitral cell terminals in the right dHbm visualised in Tg(lhx2a:GFP) transgenic larvae, it could follow that visual habenular afferents could show a similarly localised innervation of light responsive LdHbl neurons.

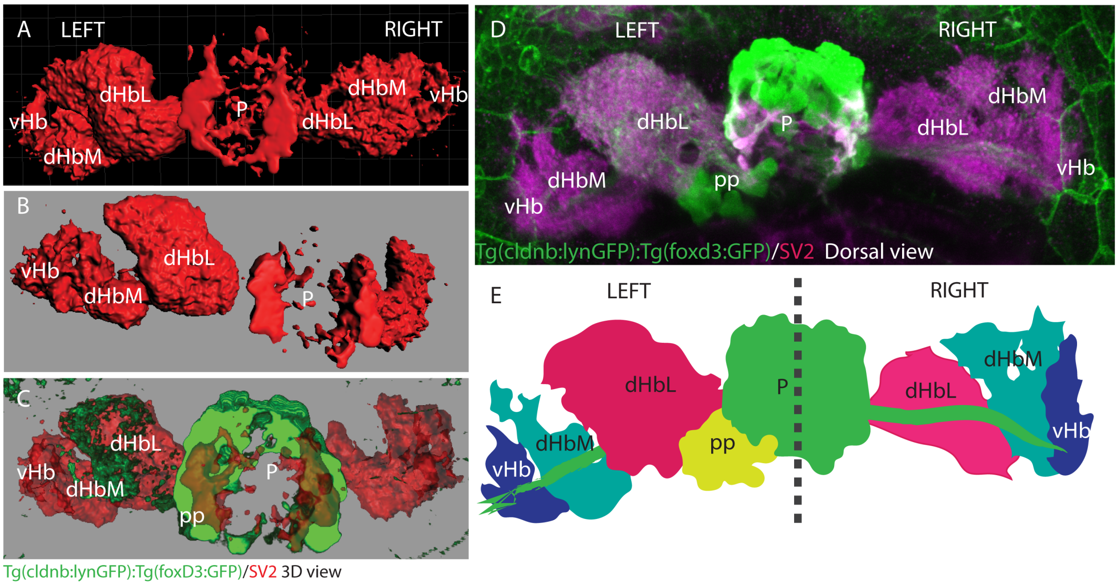

Figure 4.3: The habenular subnuclei: (A-C) 3D surface rendering of GFP (**A** separated & **C** green) and SV2 (**B** separated & **C** red) channels of data shown in a z-projection in **D**: a dorsal view of a 4dpf Tg(cldb:lynGFP):Tg(foxd3:GFP) labelled with anti-GFP (green) and anti-SV2 antibodies (magenta). **E**: Schematic representation of the epithalamus showing the approximate shape of the different habenula subnuclear neuropil and left-side parapineal position.

4.2.2 Tg(cldnb:lynGFP) labels habenula afferents that strongly innervate LdHbl.

The LdHbl neuropil is strongly labelled in the Tg(cldnb:lynGFP) transgenic line (asterisk in Figure 4.4A and B). This transgene expresses lyn:GFP which labels the cell membrane rather than the cytoplasm of the GFP+ cells. Strong GFP expression can be seen throughout the entire telencephalon including the olfactory bulbs, subpallium and pallium. GFP+ axons are visible projecting caudally in the lateral forebrain bundle. In the diencephalon the tHc is GFP+. This tract can be followed ventrally through the prethalamus where a group of prethalamic cells dorsal to the lateral forebrain bundle are visible. There is also an area of neuropil that coexpresses SV2 and GFP in the prethalamus.

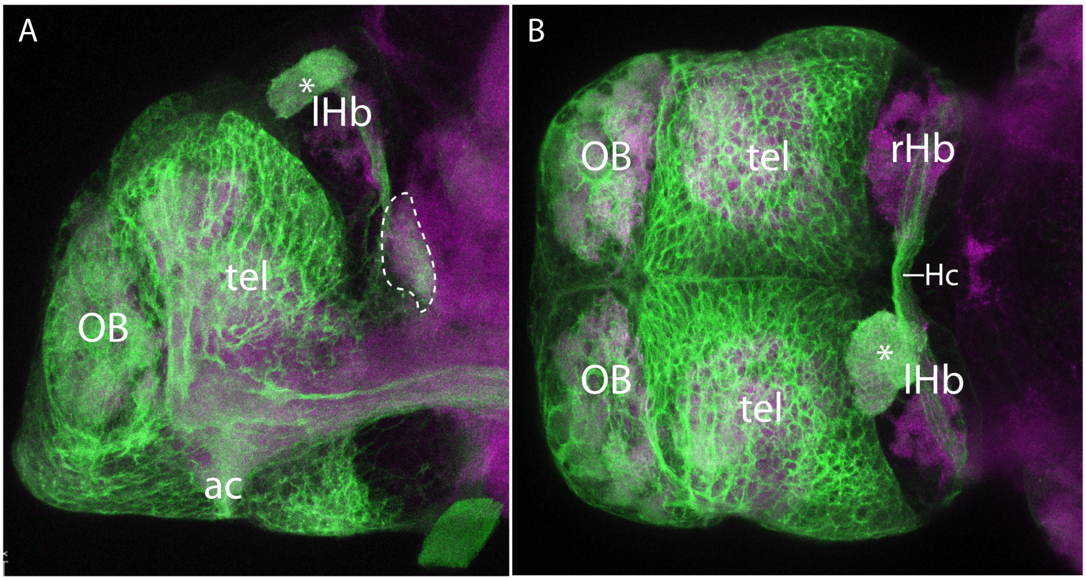

Figure 4.4: Tg(cldnb:lynGFP) labels habenula afferents that strongly innervate LdHbl. (A) lateral (left-side) and **(B)** Dorsal views of a 4dpf Tg(cldb:lynGFP) embryo labelled with anti-GFP (green) and anti-SV2 (magenta) antibodies. Asterisk labels dHbl GFP+ neuropil. Dashed line surrounds PTh neuropil.

4.2.3 Mosaic analysis of Tg(cldnb:lynGFP) cells transplanted into wildtype fry reveals habenulopetal cells that are retinorecipient through contact with AF4.

To determine which group of GFP+ neurons within the Tg(cldb:lynGFP) transgenic line were sending the afferent projection to the left habenula, I used a transplantation approach. I transplanted Tg(cldb:lynGFP) cells into wildtype hosts at blastula stage (Schematic Figure 4.5A). The object of this was to label cells mosaically to be able to see individual cell projection patterns within this dense expression domain.

Only hosts with GFP+ neurons in the diencephalon close to the telencephalic border showed habenula innervation in the neuropil of the left dHb subnucleus (number of hosts showing this projection pattern n=4/20). Figure 4.5 shows two examples of such hosts, in which GFP+ afferent terminals are present in both the left and right dHb (Figure 4.5B&D). When the larvae in Figure 4.4B was imaged from a lateral viewpoint the afferent axons seen ascending to the habenula via the tHc could be traced back to a group of neurons in the prethalamus (marked with a white bracket in Figure 4.5C white arrows in 4.5C’ indicate individual habenula afferent neurons in the high magnification view of the prethalamus). The host in Figure 4.5D-E’ shows many more GFP+ neurons in the prethalamus. The number of afferent axons in the tHc is also increased in this specimen. The denser expression in this host makes it more challenging to trace the habenulo-afferent axons back to the prethalamic cells when looking at the full z-projection and some of the processes travelling to the habenula could originate from more ventrally located vENT cells.

The prethalamic habenulo-afferent neurons sit slightly dorsal and caudal to the entopeduncular nuclei and supraoptic tract. The dendrites of these habenulo-petal prethalamic neurons appear to be located within one of the arborisation fields of the retinofugal pathway. These areas of neuropil are visible with SV2 immunohistochemistry. According to the schematic taken from Burrill & Easter (1994)(Figure 4.5F) this arborisation field seems likely to be “AF-4” in their nomenclature. Axons from the prethalamic cells appear to exit the tangle of dendrites within AF-4 from the dorsal and ventral ends and project up to the habenula via the tHc (small arrows in C’). The relationship between this prethalamic nucleus and AF4 makes it a good candidate to act as a relay nucleus for visual information to the habenula as the dendrites embedded within AF4 could synapse with RGC axons.

In both of the hosts presented in Figure 4.5, in addition to the prethalamic neurons already described, many other cells are GFP+ in the telencephalon and olfactory bulbs. Although it is not possible to completely dismiss the possibility of telencephalic afferents to the habenula in just the two examples shown, the transplant data as a whole did not support this possibility. I found that when transplanted cells were confined to the olfactory bulbs and telencephalon (and excluded diencephalic cells), the left habenula projection was not present (number of hosts showing this innervation pattern n=16/20). Mitral cell innervation of the right habenula neuropil was sometimes seen if the host contained GFP+ neurons in the olfactory bulb, as anticipated from Miyasaka et al (2012). The lack of pallial innervation to the habenula is also discussed in the introduction to Chapter 3 of this thesis and in Turner et al., (2016).

These transplantation experiments provided me with the first clue as to the location of these visual habenular afferent neurons. Chapter 5 contains further detail about the individual morphology and connectivity of these prethalamic neurons. The rest of this results chapter will focus on the characterisation of the prethalamic habenula afferent neurons and their axons.

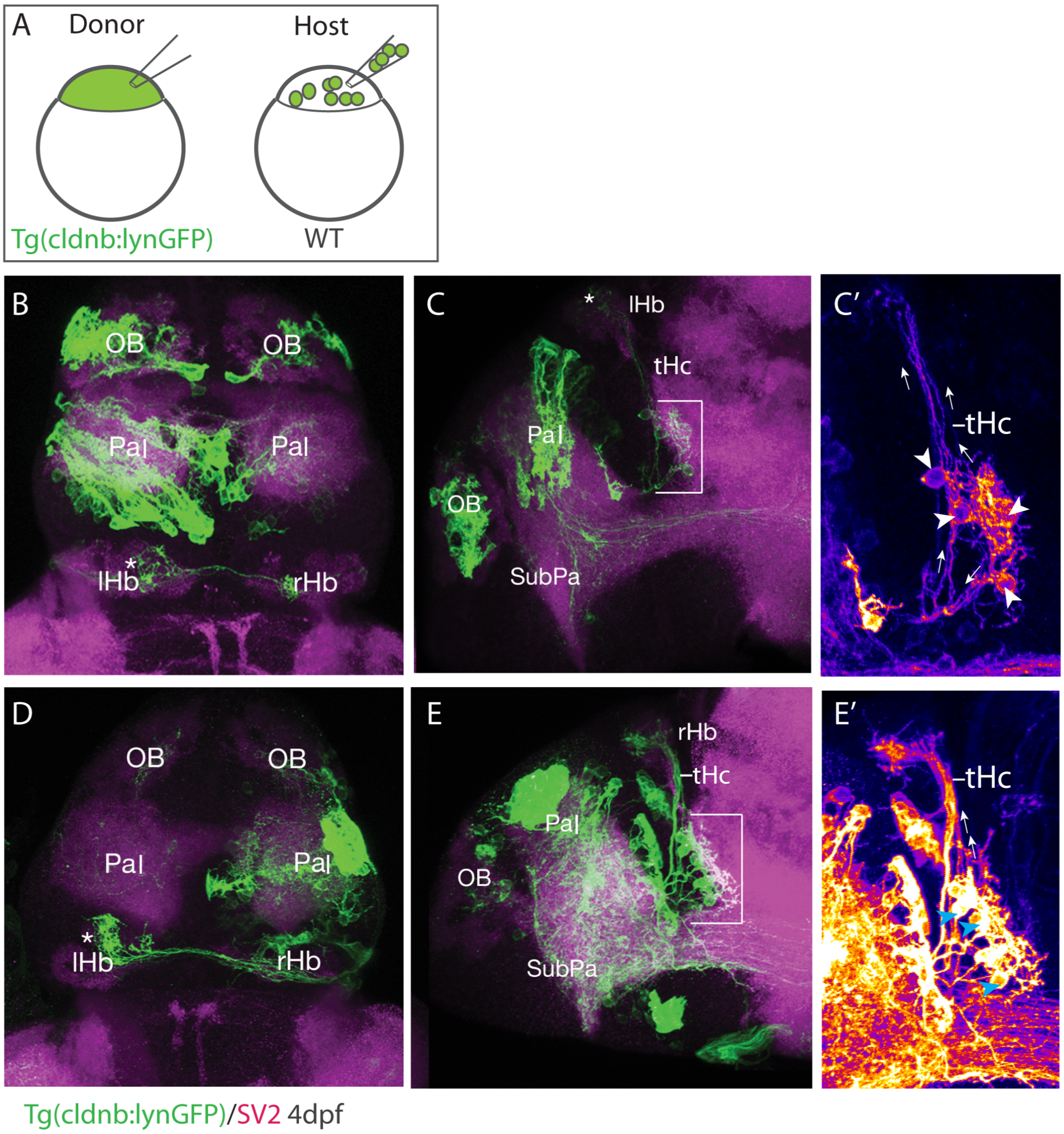

Figure 4.5 Mosaic analysis of Tg(cldnb:lynGFP) larvae: (A) schematic depicting cell transplantation procedure. **(B-E')** Two examples of wildtype larvae transplanted with Tg(cldb:eGFP) cells at blastula stage then fixed at 4dpf and labelled with anti-GFP(green) and anti-SV2(magenta) antibodies. Dorsal **(B)**, lateral **(C)** views of a larvae with GFP+ afferent terminals in the right and left habenula, asterisk marks the LdHbl neuropil. **(C')**High magnification view of (GFP channel shown with a FIRE LUT) (C) centred on 3 GFP+ neurons(arrowheads in C') in the left prethalamus adjacent to AF4(bracket in C) that innervate the habenula. Dendrites of these habenulo afferent prethalamic neurons are embedded in AF4. Small white arrows show axons leaving the prethalamic cells. Some axons ascend directly from the dorsal end of the neuropil created by the prethalamic dendrites, while other axons seem to leave the dendritic neuropil from the ventral side and project ventro-rostrally before turning to ascend to the habenula via the tHc. Dorsal **(D)**, lateral**(E)** and lateral high magnification (GFP channel shown with a FIRE LUT) **(E')** views of another wildtype host. Larvae in (D-E') has more GFP+ afferent terminals in the right and left habenula than larvae(B-C'), asterisk marks the LdHbl neuropil. High magnification view of prethalamus shows more habenula afferent nuclei labelled in this host (blue arrowheads in E'). Dendrites of these habenulo afferent prethalamic neurons are embedded in AF4(arrowhead in E'). Abbreviations: OB, olfactory bulb; Pal, pallium; SubPa, subpallium; lHb, left habenula; rHb, right habenula, tHc, tract of the habenula commisure.

4.2.4 This prethalamic habenulopetal nucleus is also labelled by the Tg(lhx5:GFP/Kaede) transgene

To examine the relative location of the prethalamic nucleus that putatively innervates the LdHbl neuropil to the previously characterised vENT. I examined the colocalisation of fluorescent protein expression between Tg(lhx5:kaede) and Tg(cldb:lynGFP) transgenic fish. As discussed in Chapter 3, the Tg(lhx5:kaede) transgenic line shows kaede+ terminals throughout the entire habenula neuropil, including the LdHbl neuropil labelled by the Tg(cldb:lynGFP) transgene (Figure 4.4 white*). In addition to the LdHbl subnucleus, Tg(cldnb:lynGFP) larvae also show some GFP terminals present throughout dHbm and vHb subnuclei (arrowheads in Figure 4.6C) as is found in Tg(lhx5:kaede).

Close examination of Tg(cldnb:GFP);Tg(lhx5;kaede) double transgenic larvae reveals that the prethalamic area suspected as the source of the LdHbl neuropil is labelled in both transgenic lines (Figure 4.6). The dendrites of the prethalamic neurons described in the transplant experiments (Figure 4.5) form a dense neuropil that overlaps with AF-4 (circled in magenta in Figure 4.6C and schematic). The approximate outline of the vENT delineated by kaede expression is also indicated. The position of the prethalamic, habenular afferent neurons, directly adjacent to AF4 is also indicated. This group of cells seems almost contiguous with the vENT at this stage of development. If we refer back to Figure 3.6C-C’ of this thesis where the vENT is delineated by the more restricted expression of *tbr1* it seems that these cells lie just caudal and slightly dorsal to the *tbr1*+ vENT within the *dlx1a*+ prethalamus (refer to Figure 3.6H). The relative positions of the vENT and this prethalamic nucleus fit with the adult DiI labelling of habenula afferent nuclei (summarised in Figure 3.1 of this thesis and in Turner et al., 2016). The prethalamic nucleus retrogradely labelled with DiI in the adult was identified as the nucleus rostro-lateralis(RL) (Turner et al., 2016). The proximity of the vENT and RL at larval stages suggest a common developmental origin for these nuclei and also represent a major challenge in separating and distinguishing these two nuclei at larval stages. Whether these two nuclei are separate or contiguous at adult stages still remains to be verified.

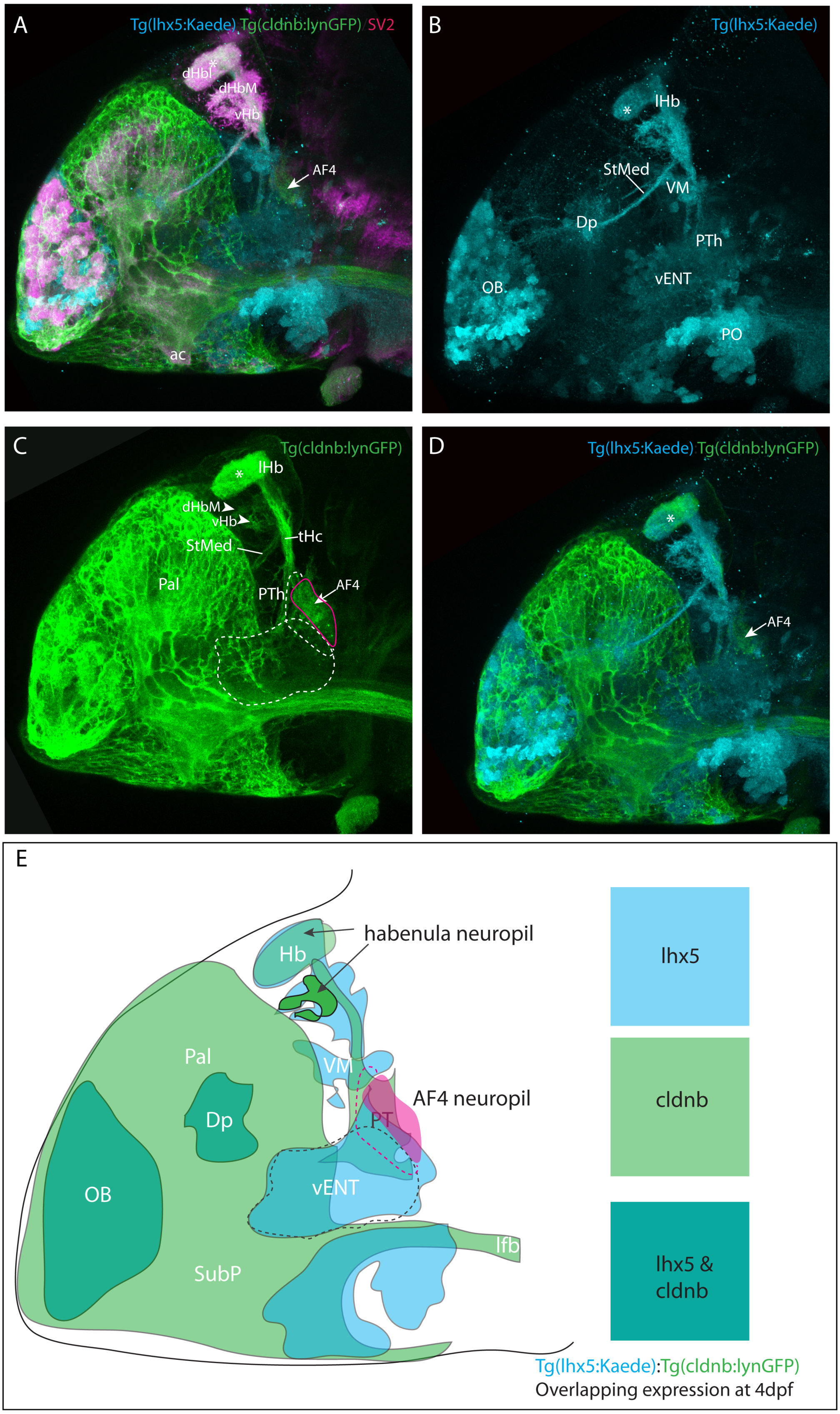
A
Tg(lhx5:Kaede) Tg(cldnb:lynGFP) SV2
dHbl
*
dHbM
vHb
AF4
ac
B
Tg(lhx5:Kaede)
*
lHb
StMed
VM
Dp
PTh
OB
vENT
PO
C
Tg(cldnb:lynGFP)
*
lHb
dHbM
vHb
tHc
StMed
Pal
PTh
AF4
D
Tg(lhx5:Kaede) Tg(cldnb:lynGFP)
*
AF4
E
habenula neuropil
Hb
Pal
VM
AF4 neuropil
Dp
PT
OB
vENT
SubP
lfb
lhx5
cldnb
lhx5 & cldnb
Tg(lhx5:Kaede):Tg(cldnb:lynGFP)
Overlapping expression at 4dpf

Figure 4.6: Colocalisation of Tg(lhx5:kaede), Tg(cldb:lynGFP) and SV2. (**A-D**) Lateral left side view of a 4dpf Tg(lhx5:Kaede):Tg(cldb:lynGFP) larva labelled with anti-kaede (cyan), anti-GFP(green) and anti-SV2(magenta) antibodies. **(E)** Schematic summarises the overlap between the expression patterns of Tg(lhx5:kaede) and Tg(cldb:lynGFP) transgenic lines. The relative positions of the prethalamic habenulo-afferent nucleus relative to the vENT and AF-4 neuropil is depicted.

4.2.5 Tg(cldnb:lynGFP):Tg(atoh7:RFP) larvae show position of GFP+ prethalamic neuropil relative to optic nerve and arborisation fields.

The Tg(atoh7:RFP) transgenic line labels retinal ganglion cells (RGCs) and their projections to the optic tectum. The use of Tg(cldnb:lynGFP):Tg(atoh7:RFP) double transgenic larvae permits visualisation of the position of the prethalamic neuropil relative to the optic tract. This neuropil is present on right (arrow Figure 4.6A-A') and left (arrow Figure 4.7B-B') sides of the brain. Projected images of the expression of the two transgenes show that this neuropil overlaps with the part of anterior branch of the retino-fugal pathway that corresponds to AF4 (as described in Burrill and Easter., 2004 and Robles et al., 2014). Some prethalamic cells surrounding this neuropil seem to be embedded in the area between the anterior and medial branches of the optic tract (Robles at et., 2014).

The close association of cells within the prethalamus and the cells of the caudal vENT with the optic tract is even more obvious in double Tg(lhx5:GFP): Tg(atoh7:RFP) larvae (Figure 4.7C-D') where the GFP labelling is cytoplasmic. The anterior branch of the retino-fugal pathway can be seen growing through the band of *lhx5*:GFP expression (described in Chapter 3) in the diencephalon (anterior branch of optic tract labelled "A" and arrowheads mark prethalamic and vENT cells in Figures 4.7 C' and D'). Lhx5:GFP+ cells in the caudal part of the vENT associate with the optic tract ventral to AF4 at the base of the anterior branch and close to the medial branch. This area could correspond to AF2 (Burrill and Easter.,2004; Robles et al., 2014).

The overlap of the dendrites of habenulo-afferent neurons in the Tg(cldnb:lynGFP) transgenic line with retinal axons at AF4(seen in Figure 4.5) further supports the idea that they could relay visual information to the habenula. In the 3D model of the AFs in Robles et al., 2014 (shown in Figure 4.2 for reference). Transgenic larvae in which all retinal ganglion cells expressed membrane-targetted mCherry and the presynaptic marker synatophysin-EGFP(Syp-GFP) showed “dense clouds” of Syp-EGFP puncta along the anterior branch of the optic tract at AF4 (Figure 4.2A and B). This AF4 recieves input mostly from RGCs located in ventral retina (Figure 4.2C), this information is pertinent to the potential identity of the AF4 associated habenula afferent nucleus and will be discussed later in this chapter.

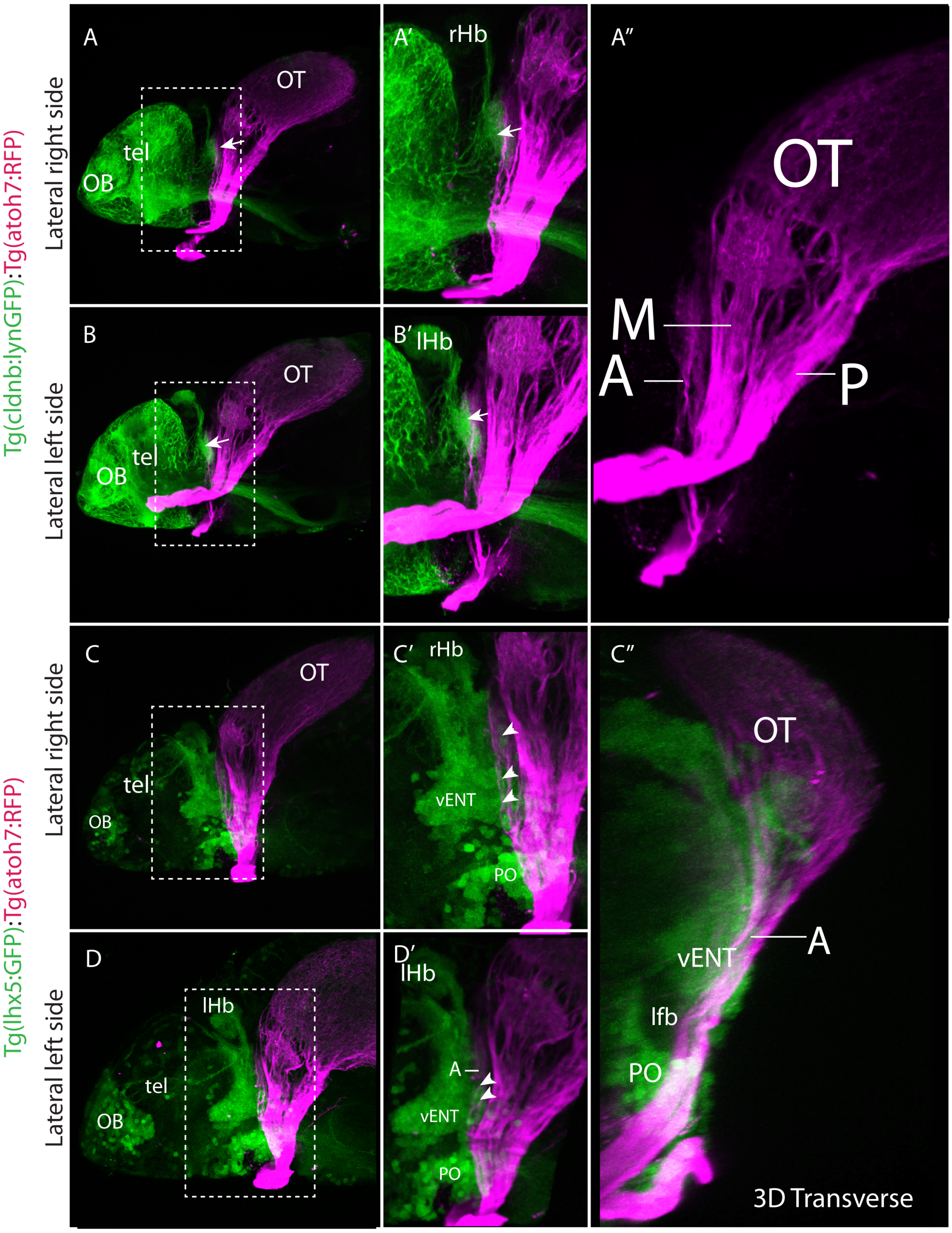

Figure 4.7: Habenula afferent neurons overlap with the anterior branch of the optic tract at AF4. Lateral view of the right**(A-A”)** and left**(B-B’)** side of a Tg(cldnb:lynGFP):Tg(atoh7:RFP) 6 dpf double transgenic fish labelled with anti-GFP and anti-RFP. AF4 neuropil labelled with arrow. High magnification view in (A’) and (B’) shows the neuropil created by dendrites of Tg(cldnb:lynGFP) + neurons in the prethalamus overlaps with the anterior branch of the optic tract. **(A’)** shows a high magnification view of just the optic tract labelled with RFP with the posterior (P), medial (M) and anterior (A) branches of the optic tract labelled . Lateral view of the

right **(C-C’)** and left **(D-D’)** lateral views of a Tg(lhx5:GFP): Tg(atoh7:RFP) 6 dpf double transgenic larva labelled with anti-GFP and anti-RFP. High magnification views of the prethalamus and vENT**(C’ & D’)** show GFP+ cells embedded in anterior branch (labelled A) of the optic tract labelled with arrowheads**.(C”)** Transverse 3D section showing frontal view of (C) shows that some vENT and prethalamic neurons lie lateral to the anterior branch of the optic tract.

4.2.6 The habenulo-afferent prethalamic neurons labelled in Tg(cldnb:lynGFP) are glutamatergic and do not express GABA.

To further characterise the nature of the habenula afferent innervation from the prethalamic neurons labelled in the Tg(cldnb:lynGFP) transgenic line, I looked at the overlap of expression between these cells with makers for inhibitory and excitatory neurotransmitters.

The GFP+ cells surrounding AF4 are not GABAergic (Fig. 4.8A,B). Single z-slices through the prethalamus show that the neurons directly surrounding the AF4 neuropil(white arrows Figure 4.8(Top)i-iv) do not express GABA. A nucleus adjacent to and dorsal to the AF4 associated cells is GABAergic but these cells do not co express membrane GFP. This GABAergic group is likely to be or become one of the GABAergic prethalamic groups: I (intermediate thalamic nuclei), VL (ventrolateral thalamic nuclei) or VM (ventromedial thalamic nuclei) (labelled as VM in Figure 4.11). The fact that the habenular afferent neurons associated with AF4 are not GABAergic helps with their identification as most nuclei within the prethalamus do express GABA(Mueller et al., 2012). It also indicates that this projection to the habenula is most likely excitatory.

After finding that the neurons that we believe innervate the ldHbl do not express GABA, I assessed if they might be glutamatergic. The transgene slc17a6b:DsRed^{nns9Tg} (Kani et al., 2010; otherwise known as vglut2a:DsRed; Miyasaka et al., 2009) expresses DsRed in glutamatergic neurons. In double transgenic Tg(cldnb:lynGFP):Tg(vglut2a:DSRed) larvae many of the prethalamic cells surrounding AF4 are GFP+ and DSRed+ and so are likely to be glutamatergic (arrows in Figure 4.8 Bottom i-iv). These results indicate that the visual afferent prethalamic projection to the habenula is likely to be mostly glutamatergic and excitatory in nature.

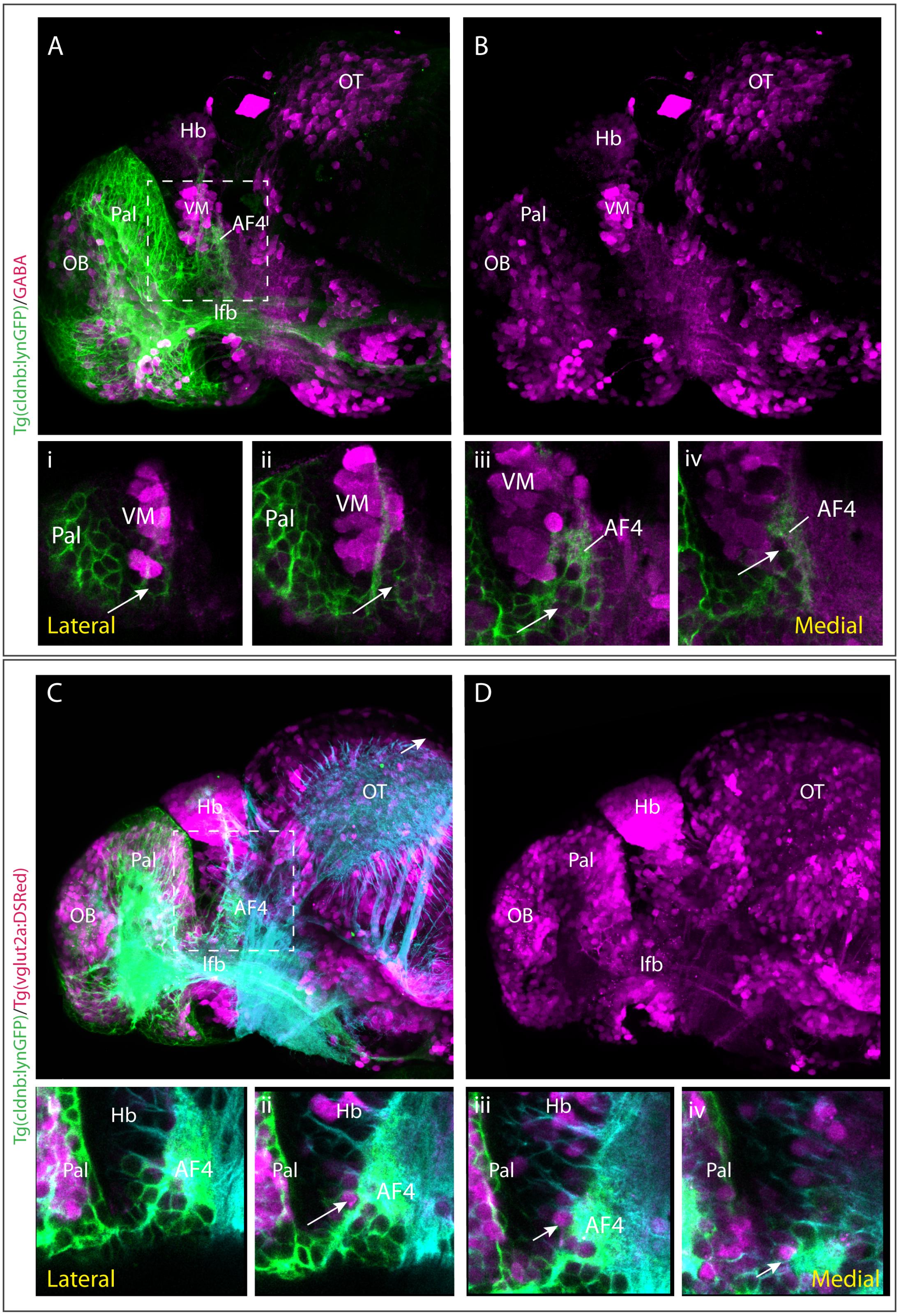

Figure 4.8: The habenulo-afferent prethalamic neurons labelled in Tg(cldnb:lynGFP) are glutamatergic and do not express GABA. Lateral view of a 3dpf Tg(cldnb:lynGFP) larva labelled with anti-GFP and anti-GABA antibodies. **(A)**

GFP (green) and GABA (magenta). **(B)** GABA only (Magenta). **(Top i-iv)** show single z-slices (lateral i; to medial iv) through the prethalamus delineated by dashed box in (A). Arrows show GFP+ cells surrounding prethalamic neuropil(AF4) do not co-express GABA. Lateral view of a 3dpf Tg(cldnb:lynGFP):Tg(vglut2a:DSRed) larva labelled with anti-GFP(green), anti-DSRed(magenta) and anti-tubulin(cyan) antibodies. **(C)** GFP, RFP and tubulin labelling. **(D)** DSRed labelling only. i-iv show single z-slices through the prethalamus delineated by dashed box in **(C)**. (**Bottom i-iv)** show single z-slices (lateral i; to medial iv) through the prethalamus delineated by dashed box in **(C)**. Arrows show GFP+ cells surrounding prethalamic neuropil(AF4) co-express glutamate.

4.3 Discussion:

The nucleus associated with the anterior branch of the retino-fugal pathway and AF4 at adult stages may be the nucleus rostro-lateralis (RL).

In this Discussion section, I will attempt to identify the nucleus equivalent to AF-4 by combining select data from the literature and data sourced from experts directly then in the final discussion Chapter 6, I will elaborate more on the hodology and function of this nucleus and its potential relationship to the vENT.

In our paper on habenula afferents (Turner et al., 2016, Chapter 3 of this thesis), a prethalamic nucleus in the rostral diencephalon was labelled bilaterally following application of DiI to either the left or right habenula. Due to the proximity of this nucleus to the habenula we qualified this observation as the potential for DiI to spread from the labelling site was deemed quite high. The evidence presented in this chapter does support that the retrograde labelling of this afferent nucleus (RL) was not an experimental error. However, we did not look very closely at the possible homologous identities of this nucleus. The following section brings together additional unpublished data(not shown) from our collaborators (Mónica Folgueira and Julián Yáñez) using DiI tracing in the adult that lends further support to the idea that the nucleus associated with AF4 could be the nucleus rostrolateralis: a diencephalic nucleus found in some species of ray-finned fish (Saidel and Butler., 1997).

RL has previously been described in various adult fish species. In zebrafish, the nucleus rostrolateralis was first identified in a study characterising the projections of the subpallium(Vv) (Rink and Wullimann., 2004). DiI application to Vv lead to labelling of cell bodies in the “the rostrolateral nucleus of Butler and Saidel” (Rink and Wullimann., 2004). Transverse sections through adult brains of the two transgenic lines used in this study, Tg(lhx5:GFP) and Tg(cldnb:lynGFP), performed by Monica Folgueira show GFP expression in the area termed RL by Rink and Wulliman(2004).

The description of RL in the freshwater butterfly fish, *Pantodon buchholzi* in Saidel and Butler (1996) states that “The nucleus rostrolateralis occupies the dorsolateral region of the rostral diencephalon. It is bordered by the optic tract laterally, the lateral forebrain bundle ventrally, the nucleus ventromedialis medially, and the habenula caudally. RL consists of a medial cell plate and a lateral neuropil” (Saidel and Butler., 1996). When compared to transverse sections of adult brains with *GAD67* labelling from (Mueller and Guo., 2009) showing the positions of the GABAergic prethalamic nuclei in the adult (VL and VM) these are medial when compared to RL.

From this description, the area associated with AF4 in the zebrafish larvae (in the rostral part of the lateral diencephalon, dorsal to the lateral forebrain bundle, medial to the optic tract and lateral to VM and VL) positionally fits with the description of RL in *Pantodon* (Saidel and Butler., 1997).

Does the connectivity of RL in zebrafish fit with that described in other teleost species? As already stated RL is afferent to the habenula (Turner et al., 2016; This thesis) RL in *Pantodon* receives afferent input from the contralateral ventral retina (Saidel and Butler., 1991) and bilaterally from the optic tectum from its dorso-medial part that also receives input from the ventral retina. (Butler and Saidel, 1992; Saidel and Butler, 1997a).

Unpublished data from Julián Yáñez of DiI labelling of the retina in adult zebrafish shows that RL is efferent to the contralateral retina in zebrafish. This tracing study did not discriminate between dorsal and ventral hemiretinas although DiI labelling of dorsal and ventral retina in zebrafish larvae by Robles et al., 2014 did show that AF4(RL) predominantly receives input from the ventral retina (Robles et al., 2014).

The application of DiI to different regions of the optic tectum in adult zebrafish also by Julián Yáñez resulted in efferent processes (personal communication data not shown) innervating the ipsilateral RL. Mosaic labelling of RL neurons included in my next Results Chapter 5 also show RL to be afferent to the ipsilateral optic tectum and the position of RL dendrites embedded into AF4 seen in the transplantation experiment (Figure 4.4 of this thesis) also suggest it is efferent to the contralateral retina.

In conclusion, the combination of the hodological data presented above coupled with the description of RL's position and morphology in other teleosts leads me to conclude that the prethalamic nucleus conveying visual information to the habenula described in this thesis is the nucleus Rostrolateralis (RL) and will be refered to as such for the remainder of this thesis.

Having determined the potential source and character of the prethalamic LdHbl afferent nucleus, I wanted to look more closely at the asymmetric innervation of the habenula by this nucleus. At what stage of development do the visual afferents start to innervate the habenula and how do these afferents behave when the overall asymmetry of the epithalamus is changed through genetic or physical manipulation?

Chapter 5. The role of the parapineal in RL afferent innervation of the habenula

5.1 Introduction

The parapineal nucleus innervates the left habenula and promotes the elaboration of left-sided habenular identity. If the parapineal is ablated much of the habenula asymmetry is lost and both habenular nuclei display an overtly right-sided phenotype with respect to gene expression and connectivity (Concha et al. 2003; Gamse et al. 2003; Bianco et al. 2008). The asymmetric location of the parapineal is a result of a leftward migration of the early parapineal precursors (Regan et al. 2009). At around 28hpf, bilaterally positioned parapineal precursors detach from the anterior pineal anlage and migrate leftward and slightly ventrally from the dorsal midline establishing a left sided nucleus. This migration is largely complete by 48hpf and parapineal afferents from differentiating parapineal neurons sprout and elaborate in the habenular neuropil, presumably forming connections with left-side habenula neurons.

5.2 Association of prethalamic habenula afferents and the parapineal.

5.2.1 The left dHbL subnucleus is also innervated by the left-sided parapineal.

Parapineal afferents, labelled in the Tg(foxd3:GFP) line, and the Left dHbL Tg(cldb:lynGFP) projection clearly co-localise by 4dpf (Fig 5.1). Although both sets of afferent neurons innervate the LdHbl neuropil, parapineal afferents are restricted to the medio-caudal segment of this neuropil domain (Figure 5.1). It would be interesting to know if parapineal axonal innervation is required for Tg(cldb:lynGFP) afferents to target this particular region of neuropil. The parapineal is a photosensitive nucleus, like the pineal, and so this neuropil could be a point of convergence for visual stimuli on dHb_L neurons.

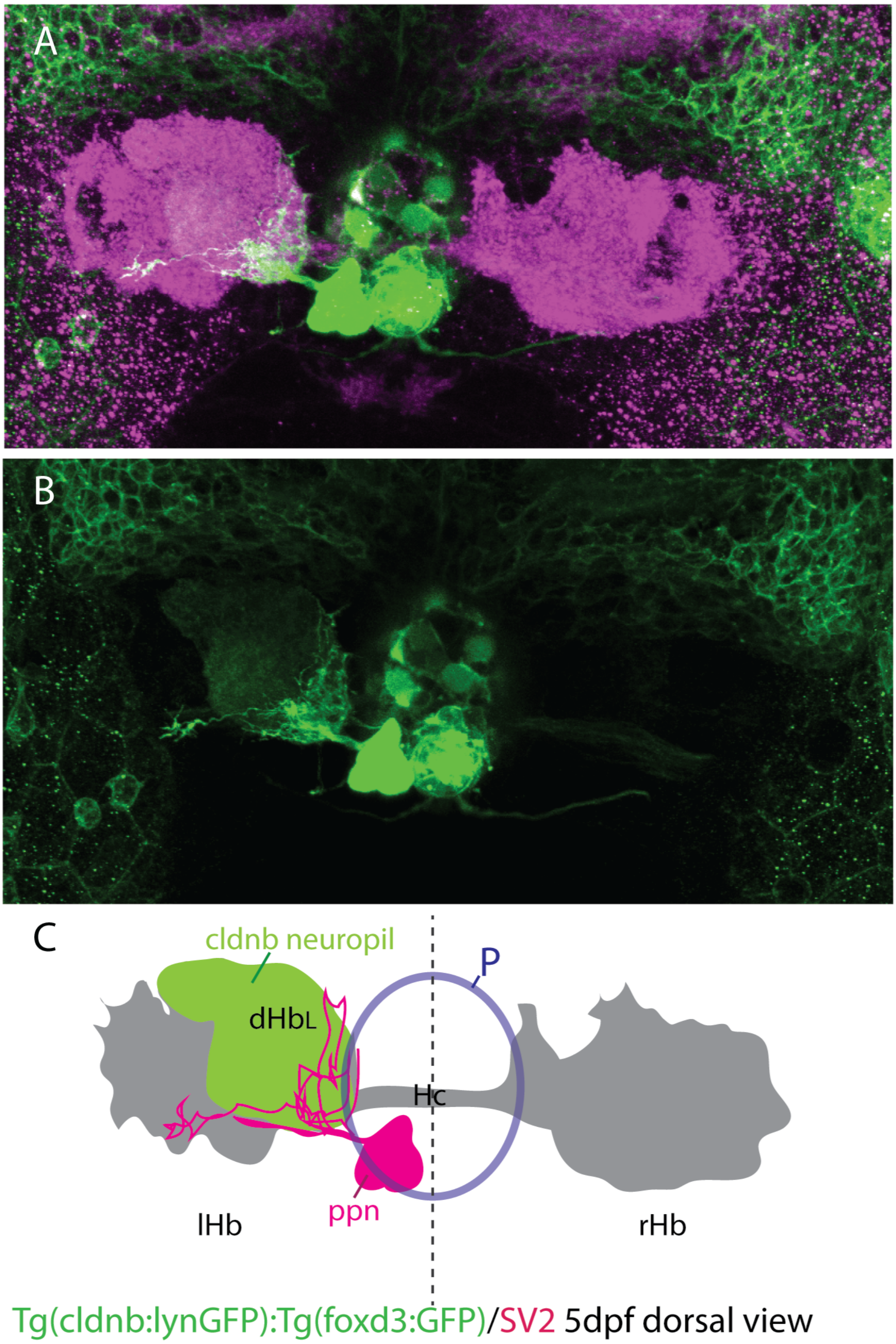

Fig 5.1 Parapineal and cldnb afferent schematic: Dorsal view of a 4dpf Tg(cldnb:lynGFP):Tg(foxd3:GFP) larva labelled with anti-GFP(green) and anti-SV2(magenta) showing the proximity of the parapineal afferents and Tg(cldnb:lynGFP) afferents terminating in the LdHbl subnucleur neuropil.

5.2.2 Prethalamic habenula afferents innervate the habenula around 48hpf after parapineal migration has occurred and when parapineal axons are starting to innervate the $\mathrm{LdHb_L}$ neuropil.

In order to establish the timing of habenula innervation by prethalamic afferents relative to the timing of parapineal migration and dHb innervation, I looked at the development of the asymmetric parapineal projection in Tg(cldb:lynGFP) embryos. At 48hpf there is expression of GFP in the olfactory bulbs and telencephalon (Figure 5.2). By this stage, GFP+ axons are present in the tHc and habenulopetal axons from left and right sides of the brain are meeting at the habenular commissure (Hc). These Tg(cldb:lynGFP) axons have not elaborated any terminal arbours in any Hb neuropil subnuclei by this stage of development (Figure 5.2 B-B').

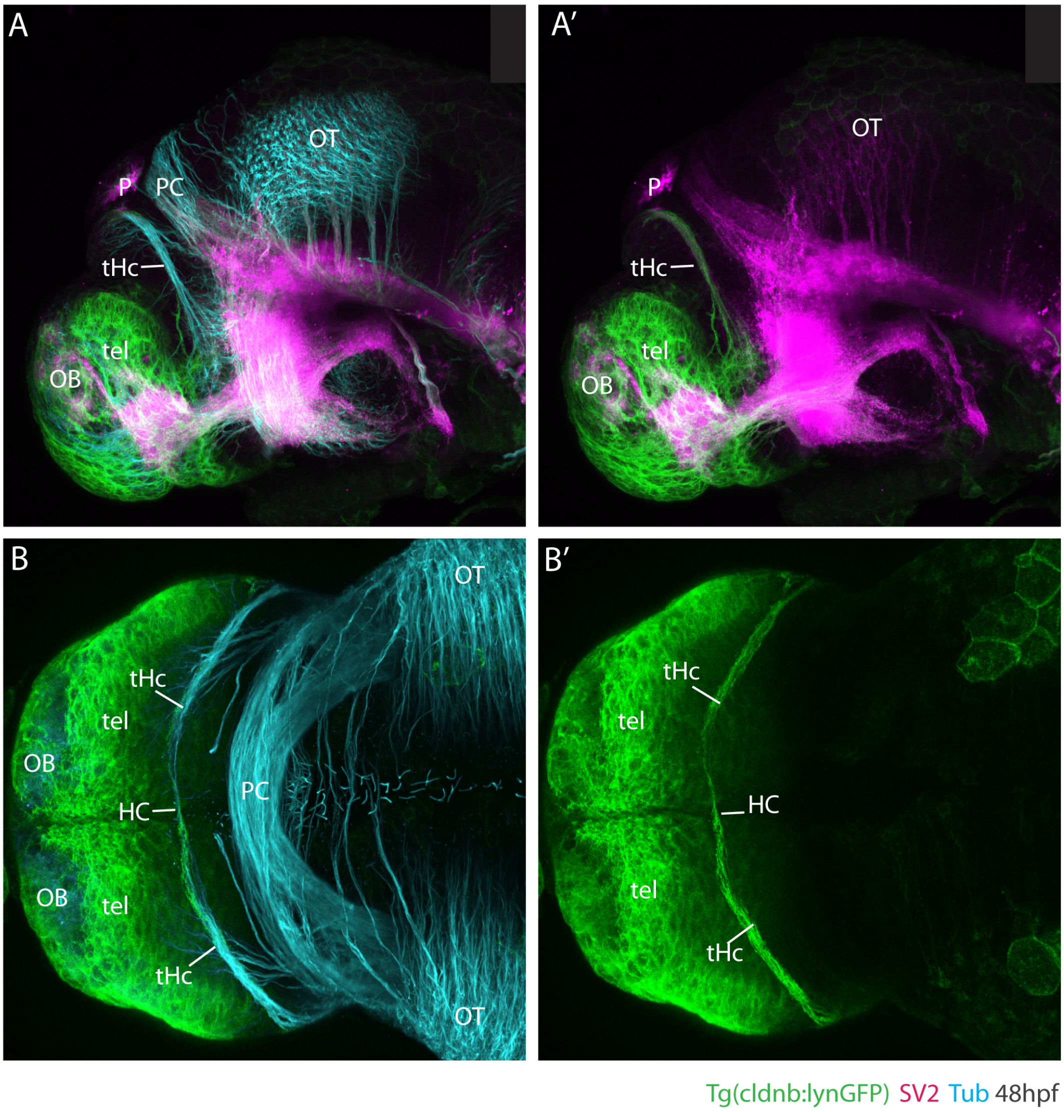

Figure 5.2: Prethalamic habenula afferents innervate the habenula around 48hpf. (A-A’) lateral and **(B-B’)** dorsal view of a 48hpf Tg(cldb:lynGFP) embryo labelled with anti-GFP (green), anti-SV2 (Magenta), and anti-tubulin (cyan) immunohistochemistry.

5.2.3 Tg(cldnb:lynGFP) afferents closely associate with parapineal axons during the innervation of the LdHbl neuropil.

In order to visualise potential interactions of parapineal and other habenulo-petal projections in the left dHbl, I used the Tg(foxd3:GFP) transgenic line that labels parapineal neurons and processes in conjunction with the Tg(cldnb:lynGFP) transgenic line and analysed the interations between parapineal axons and Tg(cldnb:lynGFP) + afferents in the left dHbL. Although both are GFP transgenes, it was possible to distinguish parapineal and thalamic inneveration due to the differences in expression level and anatomical origin of the projections. Indeed, when viewing individual timepoints from timelapse movies of 2 different Tg(cldnb:lynGFP):Tg(foxd3:GFP) embryos it is possible to observe Tg(cldnb:lynGFP)+ terminals closely associating with parapineal axons in the LdHbl neuropil as it is forming (Figure 5.3).

To assess if parapineal axons are specifically required for the Tg(cldb:lynGFP) afferents to target this particular region of neuropil I looked at the effect that various genetic and physical manipulations that disrupt asymmetry in the epithalamus have on the asymmetric projection from the prethalamic afferents. An alternative hypothesis would be that the asymmetric innervation of the LdHbl by prethalamic afferents is because they target left-sided habenular neurons, irrespective of parapineal laterality or functionality. The following section will attempt to tease apart these two possibilities.

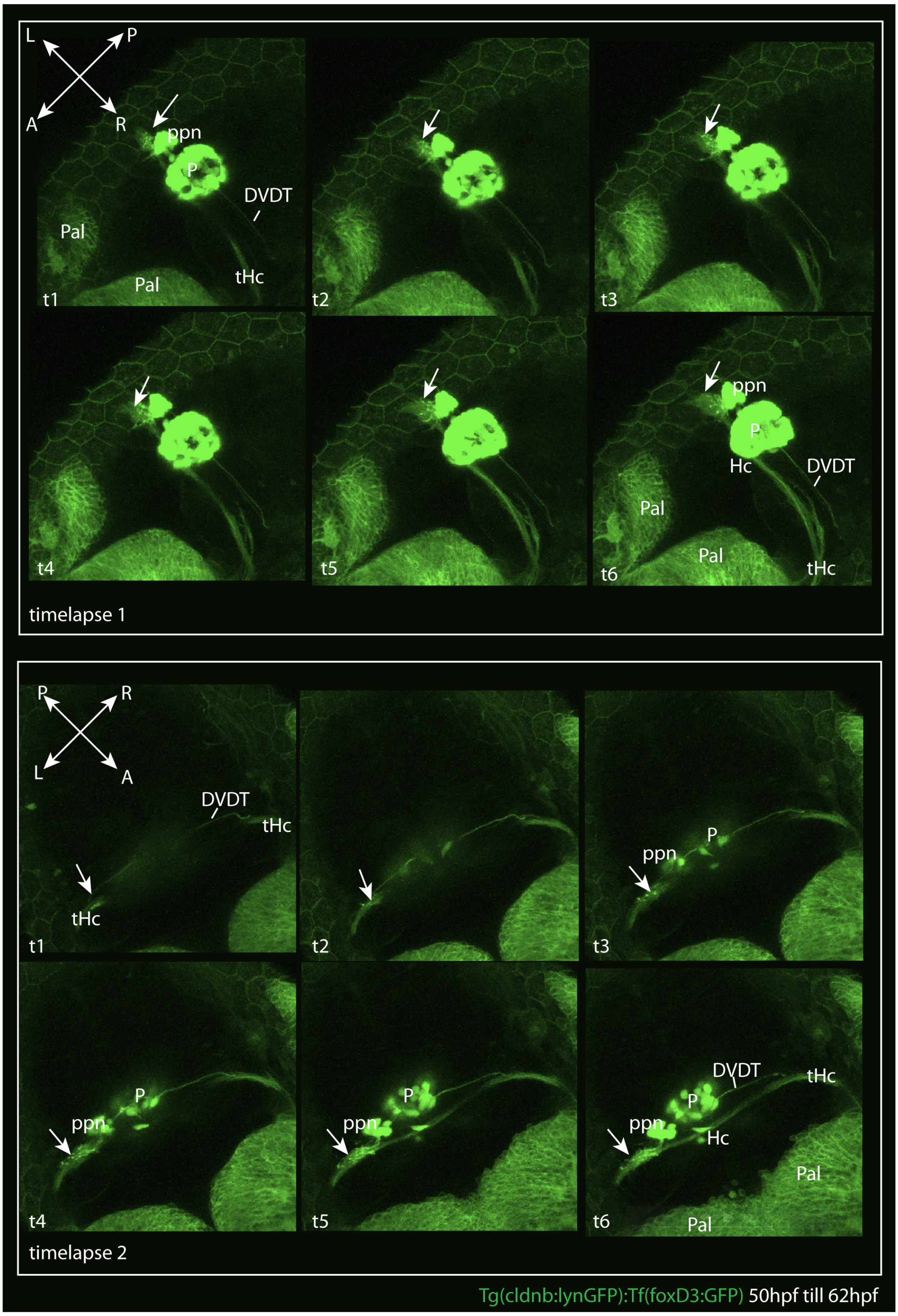

Figure 5.3: Tg(cldnb:lynGFP) afferents closely associate with parapineal axons during the innervation of the LdHbl neuropil. Individual timepoints from timelapse movies of 2 different Tg(cldnb:lynGFP):Tg(foxd3:GFP) embryos spanning 12 hours of development between approximately 50hpf and 62hpf. Arrow indicates Tg(cldnb:lynGFP)+ terminals closely associating with the brighter parapineal axons in the LdHbl neuropil as it is forming.

5.3 Laterality of innervation of dHbL by prethalmic afferents depends on the presence of “early born” left-sided habenula neurons and not the presence or position of the parapineal.

5.3.1 The size and shape of the dHbl neuropil within the wildtype population is consistent between individuals.

The following set of experiments all look at the effect that various genetic and physical manipulations that affect the laterality of the pp and habenula have on the innervation of dHbl by prethalamic afferents. Before starting these manipulations, I looked to see if there was any natural variations in habenula neuropil structure and innervation by Tg(cldnb:lynGFP) afferents within the general wildtype population. This data could then be used to as a standard for comparison for changes to the dHbl neuropil following the different genetic or physical manipulations used to change the asymmetry of the epithalamus. Figure 5.4 shows the size and shape of the Tg(cldnb:lynGFP) LdHbl neuropil (asterisk) and other habenula subnuclear neuropils in 3 different wildtype larvae. Although some variation in the shape of the Tg(cldnb:lynGFP) LdHbl neuropil is present between individuals, overall the relative position and size of the neuropils seem consistent within the wildtype population. The parapineal (labelled by Tg(foxd3:GFP) transgene) is located on the left in all larvae, and parapineal axons always project to the LdHbl neuropil, overlapping with the bulk of Tg(cldnB:lynGFP) habenular innervation. The consistency of this innervation between individuals meant that I could be fairly confident that any changes to the LdHbl neuropil following the planned experimental manipulations would be as a result of changes to epithalamic asymmetry and not due to natural variation within the wildtype population.

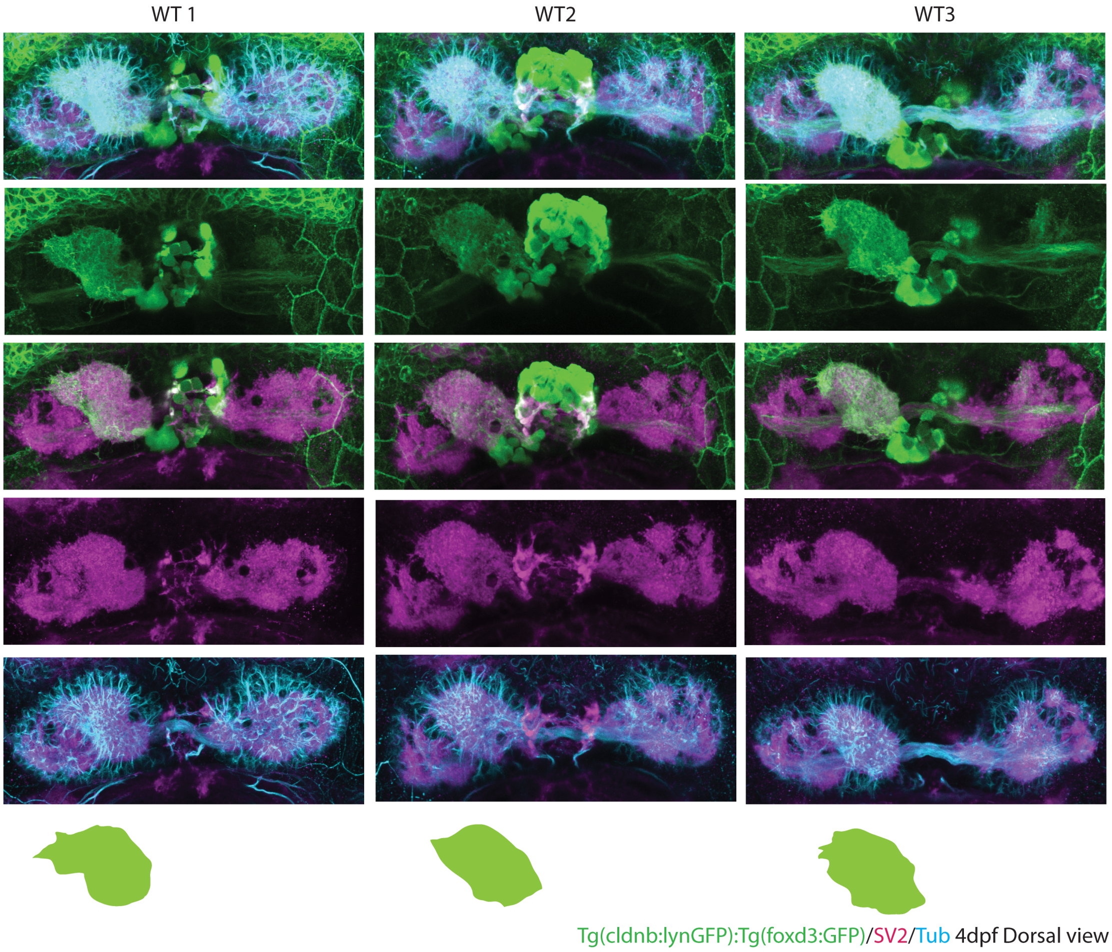

Figure 5.4: Wt diversity of dHbl neuropil. Dorsal view of the epithalamus of 4dpf Tg(cldnb:lynGFP):Tg(foxD3:GFP) larvae labelled with anti-GFP(green), anti-SV2(magenta) and anti-tubulin(cyan) antibodies. This figure shows the size and shape of the Tg(cldnb:lynGFP) LdHbl neuropil(asterisk) and other habenula subnuclear neuropils in 3 different WTs. Last row shows a graphical depiction of Tg(cldnb:lynGFP) neuropil in each wildtype.

To assess changes in habenular lateralisation I used the expression of *kctd12.1*. *Kctd12.1* also known as *leftover(lov*) that encodes a potassium channel tetramerization domain. The expression of *kctd12.1* is restricted to the dHbl subnuclei and correlates with habenula neuroanatomical asymmetry (Gamse et al., 2003 and 2005) and has been shown to be necessary for the asymmetric elaboration of habenula neuropil (Taylor et al., 2011). The following experiments use *kctd12.1* mRNA expression to highlight changes in dHb asymmetry in 3 mutants where asymmetry or parapineal function is affected.

In addition to the genetic manipulation of habenula asymmetry, I also performed parapineal ablations at two different developmental stages to change habenula laterality. The parapineal is required for the elaboration of left-sided habenula character. Ablation of the parapineal at early stages – before its migration and innervation of the LdHb –results in a “double right” phenotype where most neurons in left and right habenula develop with a dHbm character (Gamse et al., 2003., Bianco et al., 2008., Concha et al., 2003). Functionally, parapineal ablated larvae show reduced light responses in both dHb and the dIPN (Dreosti et al., 2014).

5.3.2 In “double left” rorschach mutants, Tg(cldnb:lynGFP) afferents innervate left and right dHbl subnuclei in a symmetric manner

rorschach mutants exhibit “double left (LL)” dorsal habenula subnuclei. Left and right sided dHbl subnuclei are symmetric for the number of cells expressing *kctd12.1* with both left and right habenula showing a “left-typical” level of expression (Figure 5.5B-B’). The parapineal migrates normally to the left in *rch* mutants yet the number of early-born “left sided” or dHbl type neurons is equal on the left and right sides of the brain. Our current understanding of the defect in this mutant is that loss of the *rch* gene results in too many right habenula neurons adopting a dHbl fate resulting in a symmetric double left habenula (personal communication by Ana Faro*).

In *rch* mutants, Tg(cldnb:lynGFP) afferents innervate left and right dHbl subnuclei in a symmetric manner. The symmetric neuropils of *rch* are slightly different in shape (Figure 5.5 A-A”) but similar in size to the LdHbl neuropil in the wt. The parapineal in *rch* mutants migrates normally and is located on the left. However, the r-sided habenula cells in *rch* mutants behave as if they have seen a parapineal signal and adopt left sided character. This result indicates that the presence of the parapineal and its processes were not required for the elaboration of this asymmetric afferent neuropil in *rch* mutants. The Tg(cldnb:lynGFP) afferent innervation seems instead be reliant on the position of “left-sided” dHbl neurons and their processes, as both left and right dHb in *rch* exhibit left-sided character this results in symmetrical GFP+ dHbl neuropils in the *rch* mutant. **rch is an unpublished but well-characterised mutant in our lab. All details of rch phenotype are a personal communication from Ana Faro.*

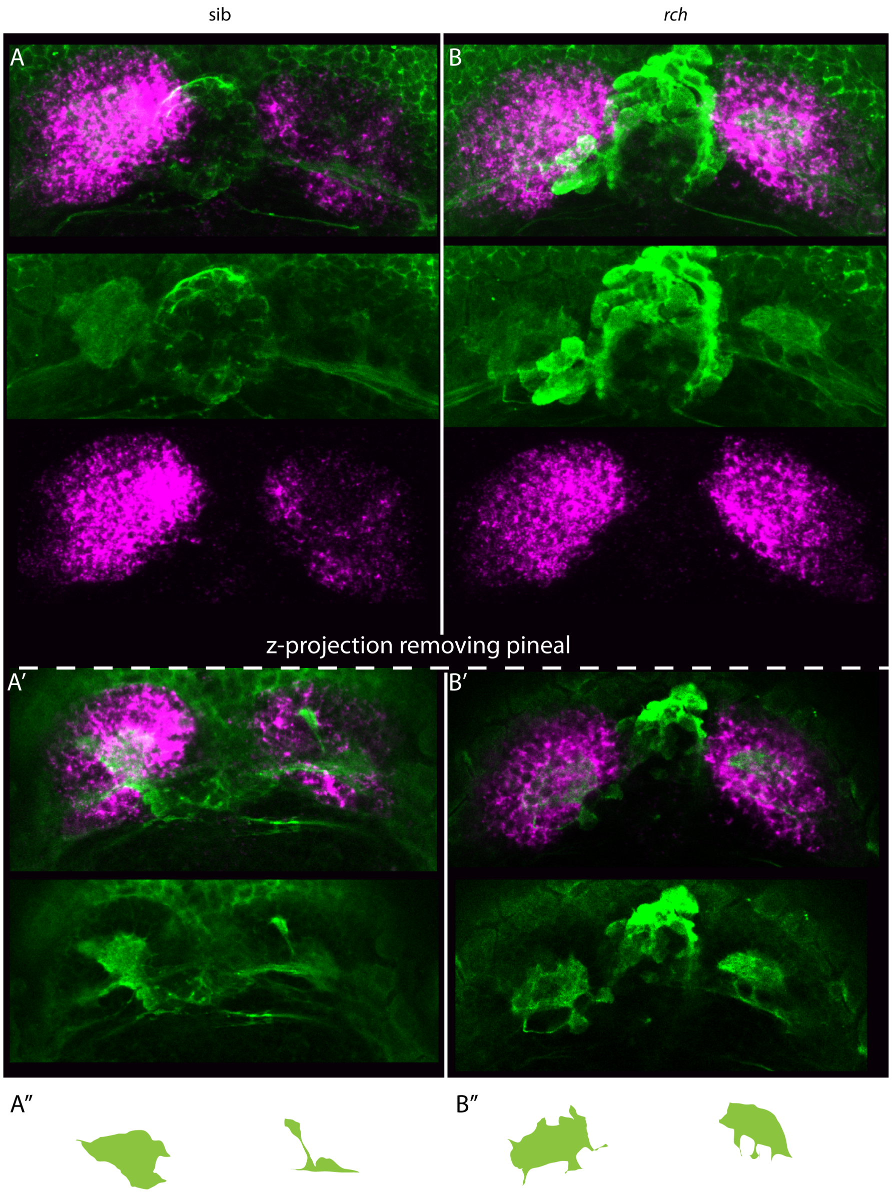

rch:Tg(cldnb:lynGFP):Tg(foxd3:GFP)/*kctd12.1* 5dpf dorsal view

Figure 5.5: In *rorschach* mutants Tg(cldnb:lynGFP) afferents innervate left and right dHbl subnuclei in a symmetric manner
Dorsal view of the epithalamus in 5dpf Tg(cldnb:lynGFP):Tg(foxD3:GFP) *rch* larvae labelled with anti-GFP (green) and FISH Cy3 for *kctd12.1* (Magenta). (A) wt sib (B)

rch-/-. A' and B' Z-projection excluding the pineal and parapineal for easier visualisation of the habenula neuropil. A" and B" graphical depiction of Tg(cldnb:lynGFP) neuropil in wildtype (A") and mutant (B") larvae.

5.3.3 The "double left" Tcf712 mutant also shows symmetric innervation of the habenula by Tg(cldnb:lynGFP) afferents.

tcf712 mutants are symmetric for most dHb markers and both left and right dHb exhibit left-typical character (LL)(Hüsken et al., 2014). The parapineal migrates normally to the left in these mutants as in *rch*. Despite symmetric LL expression of the dHbl marker *kctd12.1* (Figure 5.6B) and also the equivalent dHbm marker, *kctd12.2 tcf712* mutants lack distinct dorsal habenula sub domains. These mutants also lack ventral habenula (Hüsken et al., 2014 and personal communication A.Faro).

In Tg(cldnb:lynGFP):Tg(foxD3:GFP):*tcf712* mutant larvae (Fig 5.6B), expression of *kctd12.1* appears to be symmetric "double left". The Tg(cldnb:lynGFP) strong GFP+ dHbl neuropil (asterisk in Fig4.14A) typically seen in a left habenula is not present in the mutants on either left or right sides, indeed, distinct subdomains appear absent on both sides. This Tg(cldnb:lynGFP) neuropil arrangement in the mutant looks similar to the SV2 antibody labelling seen in *tcf712 -/- larvae* in Hüsken et al., 2014 (Figure 2C'). So, it appears that in this mutant the GFP+ Tg(cldnb:lynGFP) habenula afferents elaborate terminals symmetrically throughout dHbl neuropils on both sides like in *rch* mutants. The morphology of the habenula neuropil or the position of the parapineal do not seem to affect the symmetry of this innervation and as in *rch* the prethalamic afferent innervation of the habenula seems dependent on the position of left side habenula neurons in *tcf712* -/- larvae.

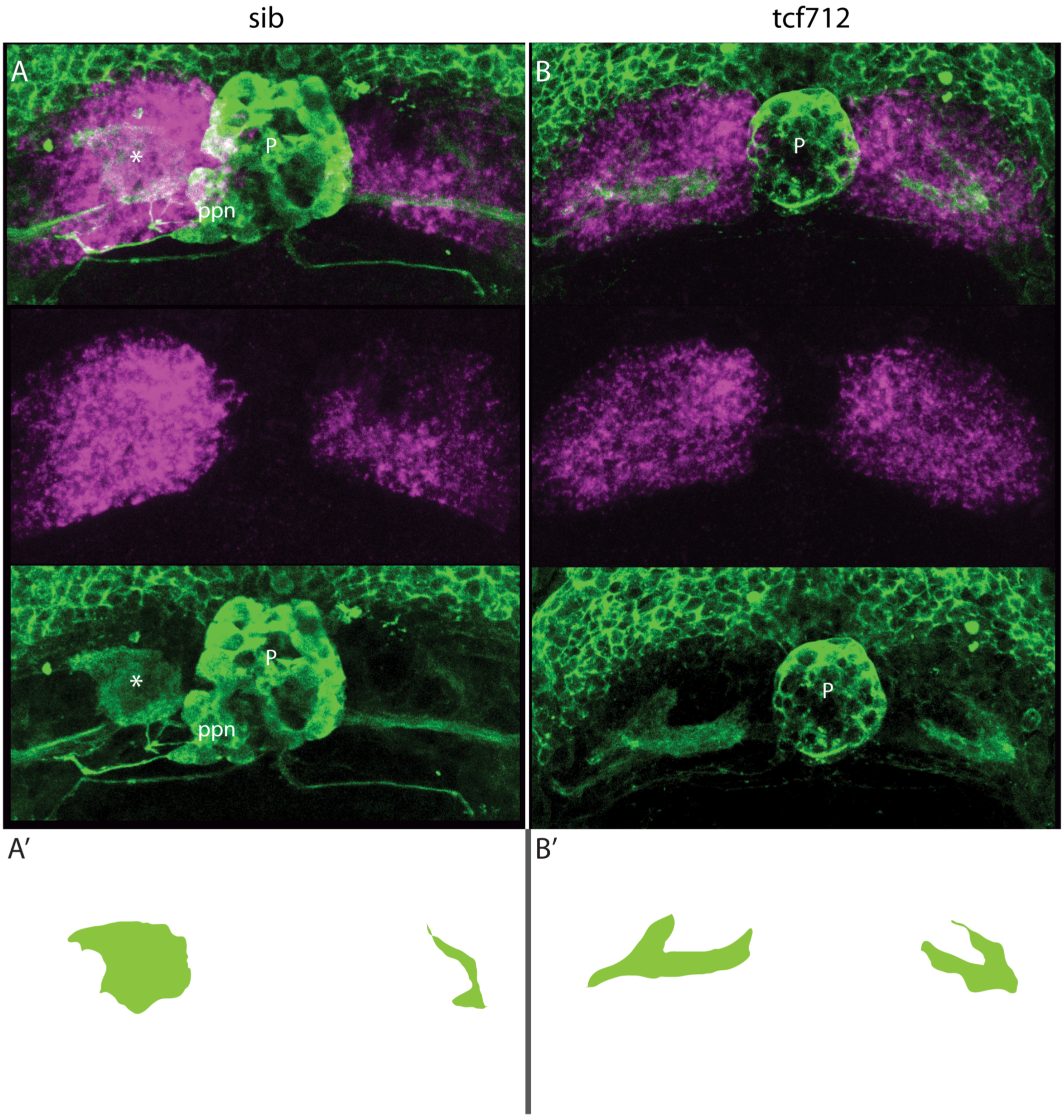

Tcf712:Tg(cldnb:lynGFP):Tg(foxd3:GFP)/*kctd12.1* 5dpf dorsal view

Figure 5.6: ***Tcf712*** **mutants show symmetric innervation of the habenula by Tg(cldnb:lynGFP) afferents.**
Dorsal view of the epithalamus in 5dpf Tg(cldnb:lynGFP):Tg(foxD3:GFP):*tcf712* larvae labelled with anti-GFP (green) and FISH Cy3 for *kctd12.1*(magenta). (A) wildtype sib (B) *tcf712* -/-. (A' and B') graphical depiction of Tg(cldnb:lynGFP) neuropil in wildtype(A') and mutant(B') larvae.

5.3.4 In sox1a “double right” mutants, Tg(cldnb:lynGFP) afferents still asymmetrically innervate the LdHbl but LdHbl neuropil size is reduced.

Loss of *sox1a* using through either morpholino injection or mutation leads to a loss of the ability of the parapineal to impart left-sided character to habenula neurons (unpublished observations personal communication, Ingrid Lekk). In these mutants the parapineal migrates to the left but is not able to induce or support the elaboration of left-sided habenula character and the habenula appears “double right (RR)” with respect to the number of *kctd12.1* expressing neurons and dHb neuropil structure. The *sox1a* mutant is homozygous viable so for this experiment I used a homozygote/heterozygote cross resulting in a 50:50 ratio of *sox1a* homozygote: *sox1a* heterozygote embryos.

Expression of *kctd12.1* is very low in the mutant larvae (Figure 5.7 C and D) but equivalent to the right Hb expression of the het siblings (Figure 5.7A and B). When looking at GFP expression, the LdHbl neuropil is reduced in size and seems more compacted than in the controls (Figure 5.7 C and D). The neuropil in the RdHb is not very pronounced appearing almost absent. The part of the dHbl neuropil closest to the parapineal appears conserved in the mutant where the more distal part is absent (eg Figure 5.7 C). Comparing the shape of the LdHbl neuropil between mutant C and mutant D the shape seems to reflect the *kctd12.1*expression pattern in the left habenula. In D there is more concentrated band of expression as opposed to the more diffuse expression in C and the respective neuropil shapes reflect these differences.

I also used the *sox1a* morpholino to create larvae with “double right” dHbl *kctd12.1* expression. The morphant results largely follow those seen in the *sox1a* homozygous mutants. However, in *sox1a* morphants, the morphology of the Tg(cldnb:lynGFP) dHbl neuropil varies considerably between individual larvae (data not shown). In all morphant larvae the size of the left dHbl neuropil is reduced when compared to the uninjected control group. The level of *kctd12.1* expression, although broadly appearing as double right, also varies between individual morphants. The left dorsal habenulae (dHb) particularly show different levels of expression and high levels of *kctd12.1* can be seen in patches. One thing that is consistent between the morphants is that the position of the LdHbl Tg(cldnb:lynGFP) neuropil always overlaps with the strongest patch of *kctd12.1* expression.

The *sox1a* mutant and morphant experiments taken together support the same conclusion reached in the “double left” mutant experiments: that the laterality and morphology of Tg(cldnb:lynGFP) afferent terminals in *sox1a* mutants, is dictated by the position of dHbl neurons, and not the position of the parapineal. The more extreme morphological phenotypes seen in the *sox1a* morphants could be explained by the more variegated expression of *kctd12.1* seen in these larvae. Although the variegation could reflect a possible dose-dependency in the phenotype. Rather counter-intuitively, the morphants may provide stronger evidence for Tg(cldnb:lynGFP) afferents targeting dHbl sub-type neurons because in these experiments the GFP+ neuropil morphology clearly changes relative to the *kctd12.1* expression pattern.

To conclude, the behaviour of the prethalamic afferents in habenula asymmetry mutants support the idea that the asymmetric afferent innervation is dependent on some feature of the habenular environment rather than a lateralisation intrinsic to the afferent neurons. In all three mutant cases it seems that the afferent axon asymmetry follows whatever character the habenulae have.

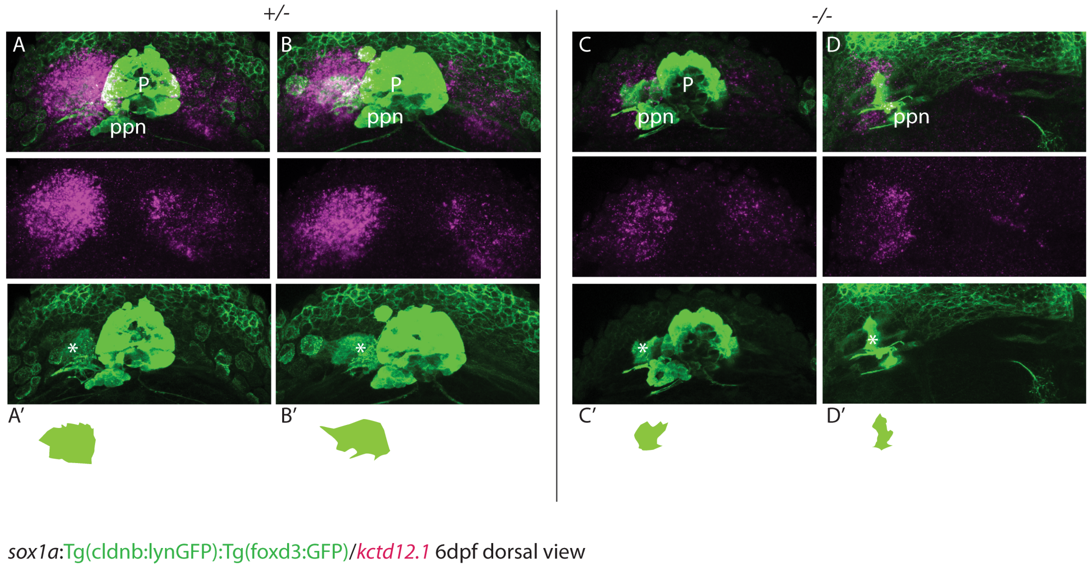

Figure 5.7: Tg(cldnb:lynGFP) afferents still asymmetrically innervate the LdHbl in *sox1a* mutants but LdHbl neuropil size is reduced.
Dorsal view of the epithalamus in 6dpf Tg(cldnb:lynGFP):Tg(foxD3:GFP):*sox1a* larvae labelled with anti-GFP (green) and FISH Cy3 for *kctd12.1* (magenta). (A and B) Het +/- sibling (C and D) *sox1a* -/- mutant. (A' –D') graphical depiction of Tg(cldnb:lynGFP) neuropil in hetrozygous (A' and B') and mutant (C'and D') larvae. Left-sided dHbl neuropil marked with asterisk.

5.3.5 Ablation of the parapineal at early stages affects the morphology and laterality of Tg(cldnb:lynGFP) afferent neuropil .

Parapineal-ablated “double right” larvae (bottom box in Figure 4.21) appear RR for *kctd12.1* expression. The LdHbl Tg(cldnb:lynGFP) GFP+ afferent neuropil is very reduced in size in all 4 embryos shown (and all others observed). The neuropil in embryo 1 appears to be very symmetric between right and left habenulae (embryo 1 bottom box in Figure 5.8). The control failed ablated group are included to show that the overall habenula structure is not damaged during the (attempted) ablation process.

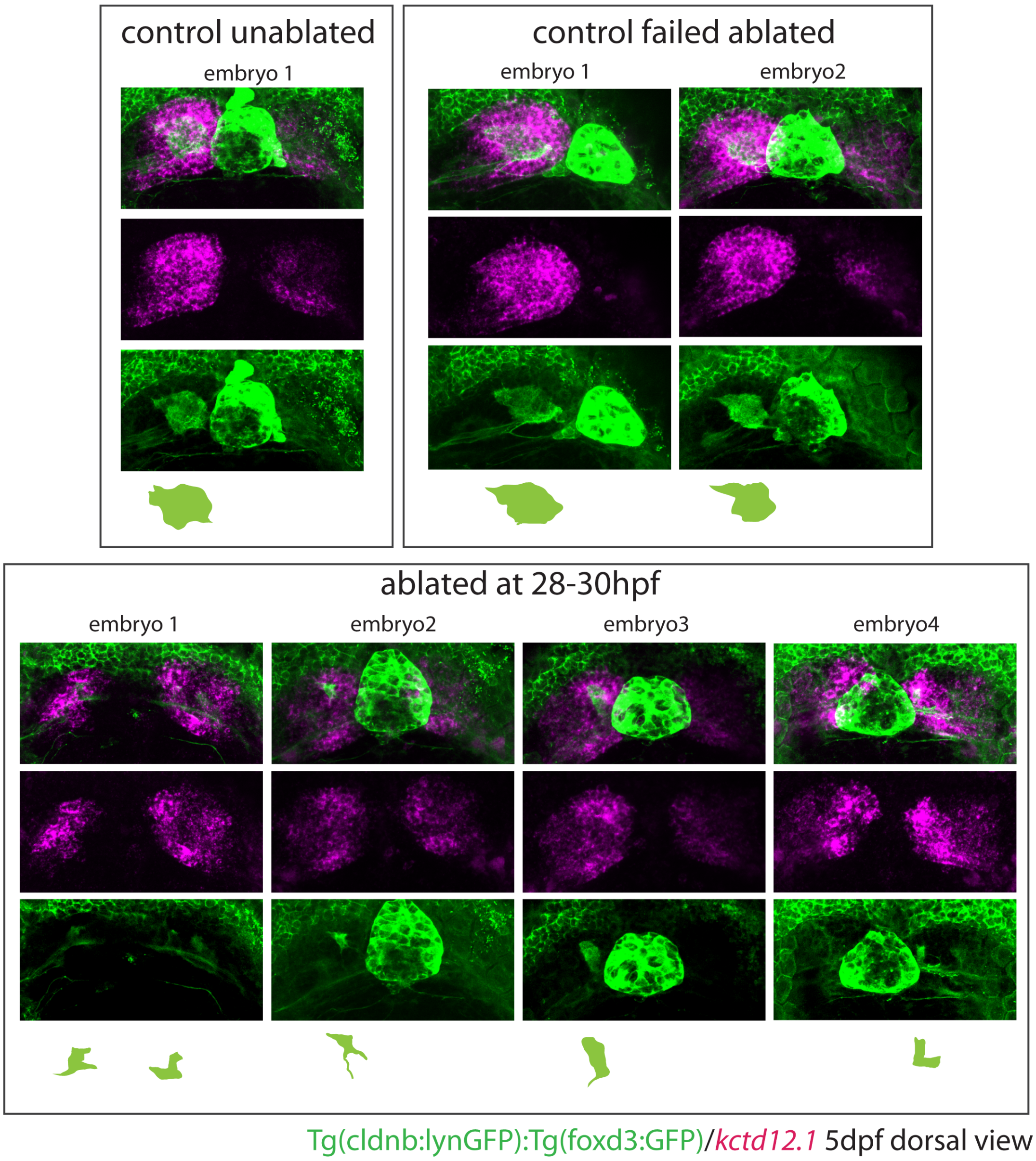

Figure 5.8: Parapineal ablations in Tg(cldnb:lynGFP) embryos at early stage: Dorsal view of the epithalamus in 5dpf Tg(cldnb:lynGFP):Tg(foxD3:GFP):Tg(flh:GFP) larvae labelled with anti-GFP (green) and FISH Cy3 for *kctd12.1* (magenta). The top box shows examples of 4 unablated controls. The middle box shows 4 embryos that underwent parapineal ablation at 28-30hpf where not all parapineal cells were ablated. The bottom box shows 4 examples of embryos that underwent parapineal ablation at 28-30hpf where parapineal ablation was successful.

5.3.6 Loss of the Parapineal at later stages after left Hb identity is established may affect morphology of dHbL Tg(cldnb:lynGFP) afferent neuropil, but not its laterality.

To discriminate between the role of the parapineal in establishing dHbl neuronal fates and a potential role in the formation of afferent circuitry I also ablated the parapineal at later stages of development. Experiments in our lab have shown that ablation of the parapineal after its migration is complete do not have any effect on habenula asymmetry based on *kctd12.1* expression, habenula neuropil morphology and efferent innervation of the IPN (personal communication Ingrid Lekk). To analyse these late stage ablations I have not used FISH for *kctd12.1* to check habenula laterality. Instead I have taken the opportunity to use SV2 to look at any potential changes in overall habenula neuropil morphology following parapineal ablation. Again, the control failed ablation group (top right box; Figure 5.9) is included to show that overall habenula integrity is not altered by this procedure.

The laterality of LdHbl Tg(cldnb:lynGFP) afferent neuropil in the late-ablated larvae (bottom box Figure 5.9) is unaffected, with all larvae showing a GFP+ neuropil in the left dHbl subnucleus. However, the size and morphology of this neuropil does seem to vary considerably between the 3 different ablated embryos, but also between ablated and control embryos (top left box Figure 5.9). The size of the neuropil although altered is not necessarily smaller than in the unablated embryos, embryos 2 shows a large, slightly elongated morphology (bottom box Figure 5.9). The size of the neuropil post ablation in other larvae is smaller than in the unablated controls (embryos 1 and 3, bottom box Figure 5.9). Interestingly the position of the GFP+ neuropil sometimes appears shifted laterally relative to the epiphysis (eg embryo 1).

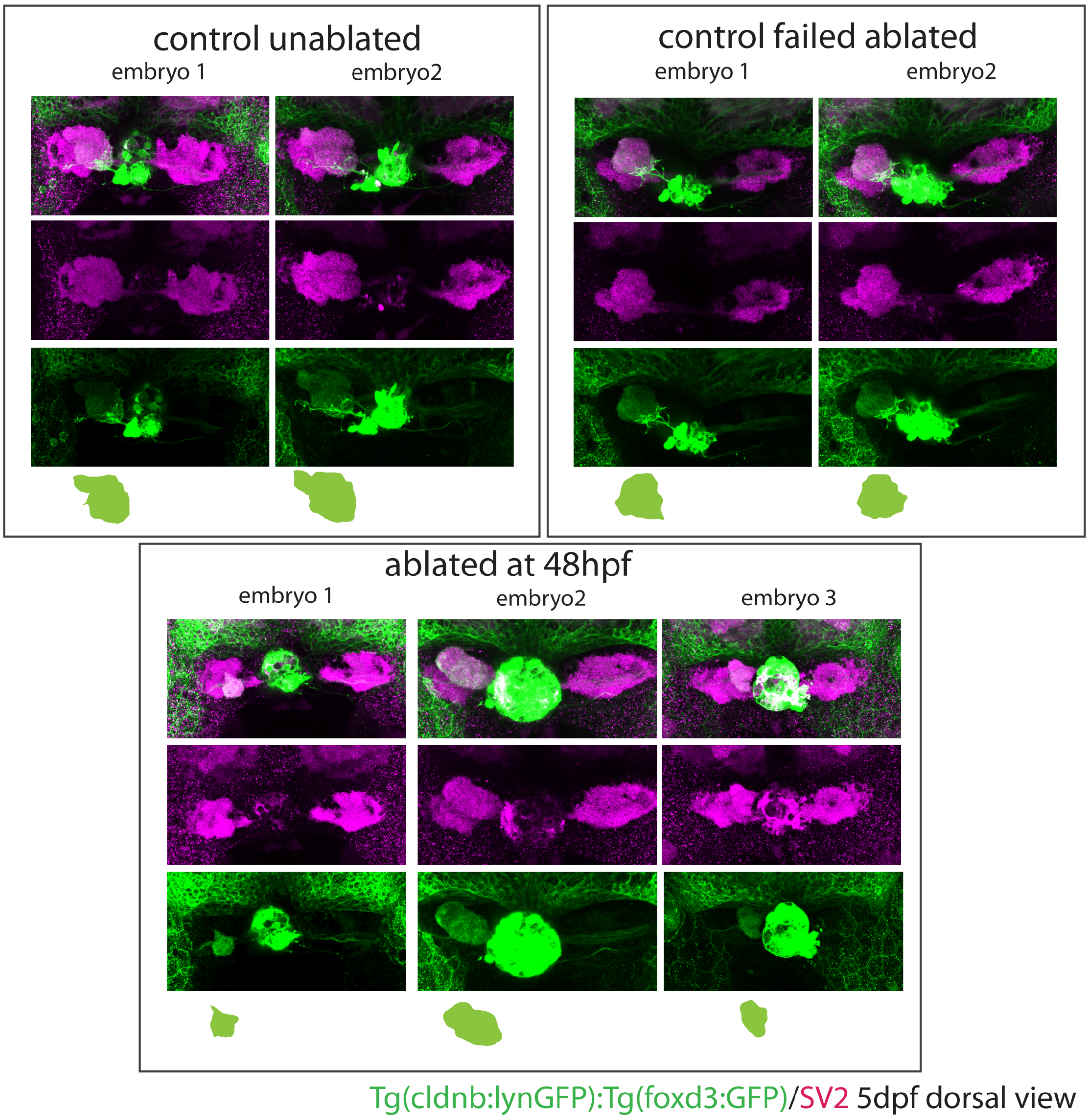

Figure 5.9 Ablation of the parapineal post migration do not affect the laterality of Tg(cldnb:lynGFP) dHbl afferents: Dorsal view of the epithalamus in 5dpf Tg(cldnb:lynGFP):Tg(foxD3:GFP):Tg(flh:GFP) larvae labelled with anti-GFP and anti-SV2 antibodies. The top left box shows examples of 2 unablated controls. The top right box shows 2 embryos that underwent parapineal ablation at 48hpf where not all parapineal cells were ablated. The bottom box shows 3 examples of embryos that underwent parapineal ablation at 48hpf where parapineal ablation was successful. Graphical depiction of Tg(cldnb:lynGFP) neuropil shown below each embryo.

5.3.7 Conclusion of laterality experiments

The late parapineal ablation results support the conclusion of the genetic experiments and the early parapineal ablation experiments that the laterality of the Tg(cldnb:lynGFP) GFP+ afferent neuropil correlates with the laterality of dHbl neurons, as measured by *kctd12.1* expression and habenula neuropil morphology. However, these results also suggest a continuing, late role for the parapineal in shaping or maintaining the shape of the dHbl neuropil.

Figure 5.10 shows a schematic summary of all of the laterality experiments from this chapter. From this summary diagram it is clear that the shape and size of the Tg(cldnb:lynGFP) GFP+ afferent neuropil varies in each condition. Whether this change in shape is a direct consequence of loss of interaction between parapineal axons and other dHbl afferent terminals or is due to changes in dHbl neuron dendritic morphology is not possible to discern from these experiments alone. As functional imaging studies have shown habenula responses to odour and light stimuli are spatially segregated in the habenula (Dreosti et al., 2014; Jetti et al., 2014; Krishnan et al., 2014). When Dreosti et al (2014) looked at sensory responses to odour and light following disruption of dHb asymmetry (using similar genetic and physical manipulations as used in this chapter), they found that changes in epithalamic asymmetry could result in a loss of these sensory responses. Although these prethalamic afferents were not specifically studied in this context it would be interesting to correlate the changes seen in visual responses in the habenula to the shape and laterality changes observed in the Tg(cldnb:lynGFP) GFP+ afferent neuropil in the future.

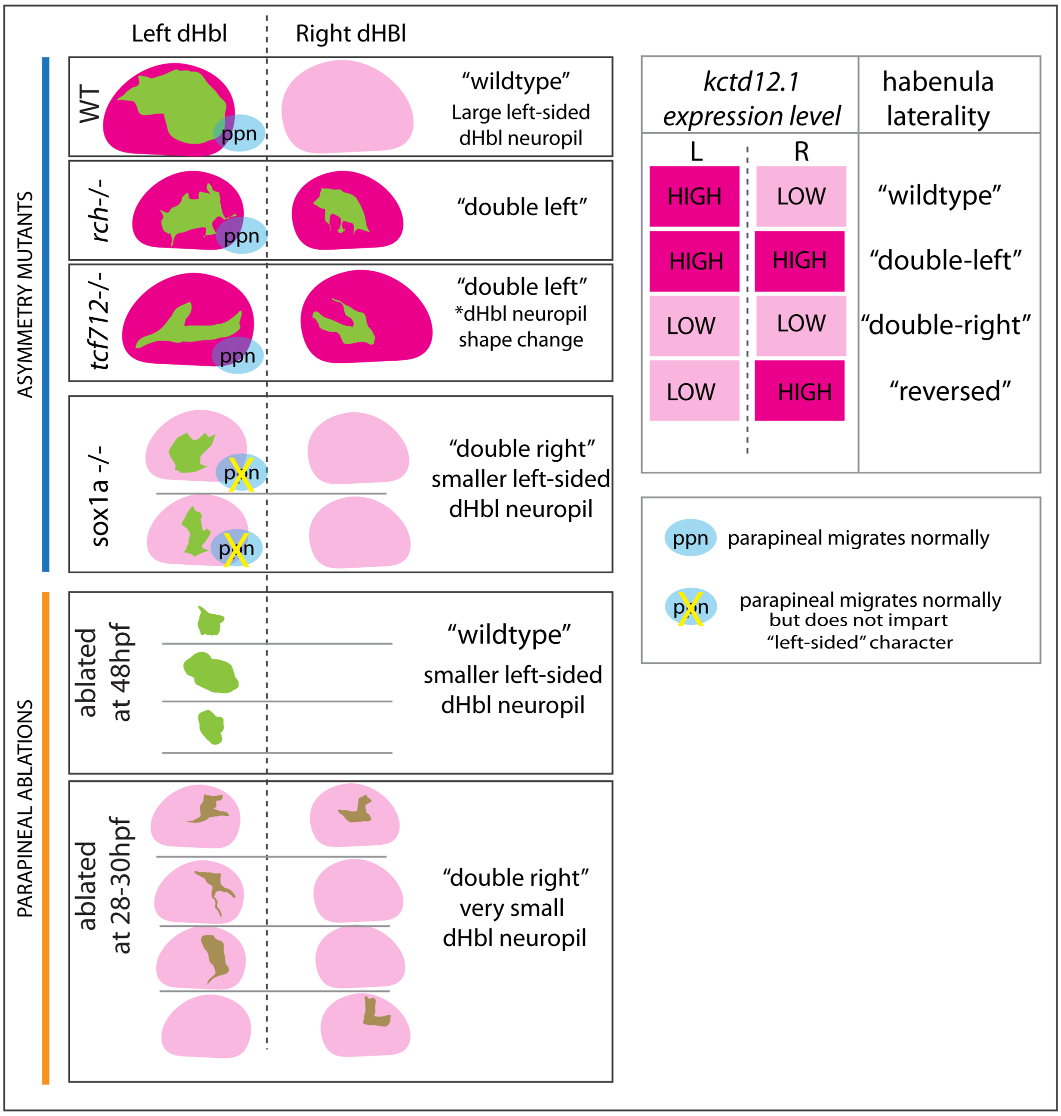

kctd12.1 expression level L	*kctd12.1 expression level* R	habenula laterality
HIGH	LOW	"wildtype"
HIGH	HIGH	"double-left"
LOW	LOW	"double-right"
LOW	HIGH	"reversed"

ppn parapineal migrates normally

ppn parapineal migrates normally but does not impart "left-sided" character

Figure 5.10: Summary of laterality experiments. Pictoral summary of all genetic and physical epithalamic manipulations. Size, laterality and shape of Tg(cldnb:lynGFP) dHbl afferent neuropil shown for each condition in green. *Kctd12.1* expression level in left and right habenula shown for each condition in magenta (high expression level) and pink (low expression level). Key on righthand side shows habenula laterality associated with each combination of *kctd12.1* expression. Laterality of parapineal for each condition shown in blue circle. Yellow cross indicates parapineal is unable to impart "left-sided" habenula character. No parapineal shown for parapineal ablations.

Chapter 6. Development of a new Crispr based method to mosaically label isolated neurons

6.1 Introduction

In the previous two chapters, I presented evidence identifying two of the main habenular afferent nuclei: the ventral entopeduncular nucleus and the nucleus rostro-lateralis. I characterised their developmental origins, hodology and gene expression. This final results chapter will primarily focus on the development of a Crispr based single-cell labelling method. This method uses CRISPR/Cas9 to mosaically label individual neuronal morphologies within a GFP transgenic line. To establish this method, I used a pallial expressing enhancer-trap line. I include in this chapter the mapping of the insertion site for this transgenic line and the characterisation of the expression pattern of this line followed by a description of some pallial cell morphologies highlighted by this labelling technique.

Once established, I used this Crispr technique alongside standard mosaic DNA injections into a pan-thalamic Gal4 transgenic line to mosaically label neurons within vENT and RL. At larval stages these two afferent populations lie adjacent to each other in the prethalamic eminence and prethalamus of the rostral diencephalon. The proximity of these two populations and the lack of transgenes that discretely label only the vENT or RL makes it challenging to analyse their associated circuitry. These mosaic labelling experiments contribute by further characterising the organisation of the habenula afferent nuclei RL and vENT by attempting to categorize the various morphologies and connectivity of the different cell-types present in these nuclei. I also attempt to describe any asymmetries in the innervation of the habenula by RL and vENT afferent neurons.

Finally, I look at some brain regions and neurotransmitter systems potentially afferent to vENT and RL, namely the pallium, serotinergic and dopaminergic systems. I briefly characterise a serotinergic Gal4 transgenic line I generated and show some preliminary data showing the projection patterns of individual raphe neurons. The last section relates to potential points of contact between RL/vENT and dopaminergic neurons. These three preliminary studies reveal potential innervation of vENT neurons by telencephalic, serotinergic and dopaminergic neurons. As the habenula does not appear to have direct pallial, serotinergic or dopaminergic innervation this highlights the important role the vENT could play as a relay nucleus to the habenula.

Results

6.1The Et(gata2:EGFP)^{bi105} transgenic line.

6.1.1 Spatio-temporal expression of *early growth response 3* (*egr3*) during zebrafish brain development.

The Et(gata2:EGFP)^{bi105} transgene shows expression of GFP restricted to the CNS despite using a CNE from the mesodermally expressed *twist1* gene. This suggests that transgene expression is due to a positional effect from transgene insertion close to another gene. We used this transgenic line to rule out pallial innervation of the habenula in our survey of global habenula afferents (Turner et al., 2016) and have subsequently been using the line to look at the development of the telencephalon/pallium in zebrafish, from embryonic stages through to adulthood (in collaboration with Monica Folgueira and Tom Hawkins and as a follow up to Folgueira et al. 2012). After an initial description of the transgene expression and mapping of the insertion, I will focus on this transgenic line purely as a tool used to establish a technique to mosaically label cells within EGFP transgenic lines. This technique uses Crispr/Cas9 and is an adaptation of the method originally published by Thomas Auer (2014) using modifications to this technique developed by Kimura et al (2015).

6.1.2 The Et(gata2:EGFP)^{bi105} transgenic line labels the pallium at larval stages.

GFP expression in 4dpf Et(gata2:EGFP)^{bi105} transgenic larvae is present in many diverse areas of the brain that I describe below in anterior to posterior sequence. There is dense expression throughout the pallium (Pal; Figure 6.1:A-C”). GFP positive (GFP +ve) neurons are also present in a small subpallial nucleus (SubP), ventral to the olfactory bulbs and just anterior to the anterior commissure (ac; Figure 6.1A-A’,B-B’). In the epithalamus a subset of neurons in the left-sided parapineal nucleus (parapineal) express GFP (Figure 6.1C-C’). In the ventral diencephalon some GFP +ve cells are present in the bilateral preglomerular complex (PG), lateral tuberal regions (PT), and in the midline posterior-tuberal nucleus (PTN). And finally, for the forebrain, there are many GFP +ve cells present in the hypothalamic lobes (HL; Figure 6.1B-B’). In the midbrain, a group of cells is labelled in the pretectum (PrT), just anterior to the optic tectum. Caudal to these cells, a subset of neurons in the periventricular grey zone of the optic tectum (PGZ) are labelled (Figure 6.1A-A’, C-C’). These cells extend processes to innervate more superficial layers of the optic tectum and terminate in the SFGS. In the hindbrain, several cells are labelled in the superior raphe (SR) and areas of the reticular formation (RF) (Figure 6.1B-B’) and caudally in areas of the medulla oblongata (MO).

GFP expression in Et(gata2:EGFP)^{bi105} is cytoplasmic and not in the plasma membrane, thus long axons have minimal expression, despite this, the high density of even lightly labelled GFP-positive axons means that several tracts and neuropil areas are labelled in several areas of the brain. In the telencephalon, the anterior commissure and the forebrain bundle (forebrain bundle) are labelled (Figure 6.1B-B’). Caudally there is GFP expression in the superficial neuropil of the optic tectum (OTn) (Figure 6.1A-A’,C-C’). Most of these fibres can be followed and originate from cells located in the deep PGZ. However, the possibility that some fibres have other origins cannot be ruled out. Ventrally in the diencephalon, the horizontal commissure (chor) is labelled. Finally, at caudal levels there are GFP+ fibres labelled in the medial (MLF) and Lateral (LF) longitudinal fascicles.

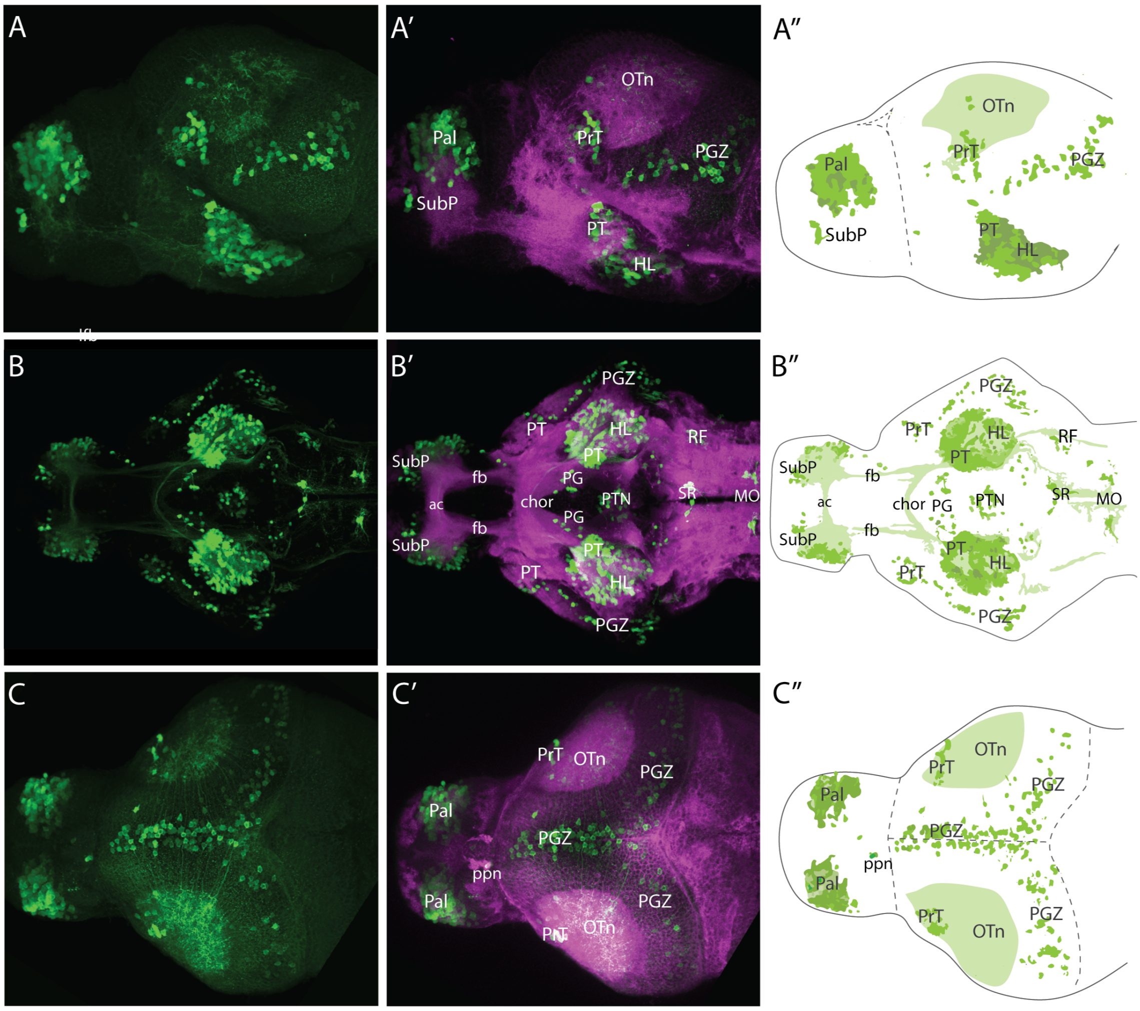

Figure 6.1: Et(gata2:EGFP)^{bi105} GFP expression at 4dpf. Lateral(A-A”), Ventral (B-B”) and Dorsal(C-C”) views of a 4dpf Et(gata2:EGFP)^{bi105} larvae labelled with anti-GFP and anti-SV2 antibodies. Major areas of GFP expression are annotated in the schematics (A”,B” and C”).

6.1.3 Tg(gata2:EGFP)^{bi105} traps the expression of *egr3*

I mapped the position of the transgene insertion in Et(gata2:EGFP)^{bi105} using the Genome Walker kit (Clontech). This method enables the amplification and sequencing of unknown regions of genomic DNA adjacent to known sequences (eg. from insertions). As this transgenic line was made using the Tol2-transposase system, I designed primers specific to the *tol2* sequence to amplify adjacent genomic regions. Several PCR fragments amplified using the nested adaptor-linked PCR (from the kit) were Sanger sequenced. Genomic sequence adjacent to the *tol2* sequence in each sequenced fragment was queried using BLAST against the zebrafish genome (zv9 genomic assembly). I amplified and sequenced four separate genomic fragments of varying lengths. All four of these sequences aligned to the same region of chromosome 8 (Figure 6.2A,B). The insertion site was confirmed using PCR from genomic DNA using primers specific to the EGFP of the construct and the newly sequenced adjacent genomic sequence. I then confirmed the linkage of the insertion site to several previously mapped simple-sequence length polymorphisms (SSLPs) on chromosome 8 (Figure 6.2A) using traditional mapping methods.

These results show that the insertion of the tol2 transposase construct that generated the Et(gata2:EGFP)^{bi105} transgenic line lies approximately 7kb upstream of the first exon of *Early Growth Response 3* (*egr3)* (Figure 6.2B), an immediate early gene encoding a zinc finger transcription factor (Yamagata et al., 1994; Li et al., 2007)). Fluorescent *in-situ* hybridisation for *egr3* overlaps with GFP expression in the telencephalon from 24hpf (Figure 6.2C-C''). At this stage there is already *egr3* mRNA expression in the optic tectum midline, but no GFP protein is observed (Figure 6.2C'-C"). By 60hpf *egr3* mRNA expression overlaps with GFP protein in the pallium, subpallium and optic tectum (PGZ) of Et(gata2:EGFP)^{bi105} embryos. *egr3* mRNA expression is harder to detect in the pretectal and parapineal GFP+ve cells perhaps because of a lower GFP+ cell density when compared to pallial and PGZ domains. Expression of *egr3* in medaka is similar to zebrafish, with strong expression in the telencephalon, optic tectum and hypothalamus (Deguchi et al., 2009). In summary, these results show that the Et(gata2:EGFP)^{bi105} insert maps near the *Egr3* first exon and GFP expression is nested within *Egr3* mRNA expression. These results, in concert, are strongly suggestive that the same *cis*-regulatory elements acting to control *Egr3* expression are also actively regulating GFP expression in Et(gata2:EGFP)^{bi105}.

Egr3 is an immediate early gene encoding a transcription factor. In mice *Egr3* expression is induced by synaptic activity and is required for normal hippocampal long-term potentiation (LTP) and for hippocampal and amygdala-dependant learning and memory (Li et al., 2007) and hippocampal long-term depression (LTD) (Gallitano-Mendel et al., 2007). In humans, *EGR3* has been linked to schizophrenia, SNPs in both *EGR3* and its target ARC (another activity dependent synaptic plasticity protein) show a significant association with schizophrenia (Huentelman et al., 2015) supporting other GWAS studies (Yamada et al., 2007; Gallitano-Mendel et al., 2008;Kim et al., 2010; Guo et al., 2010).

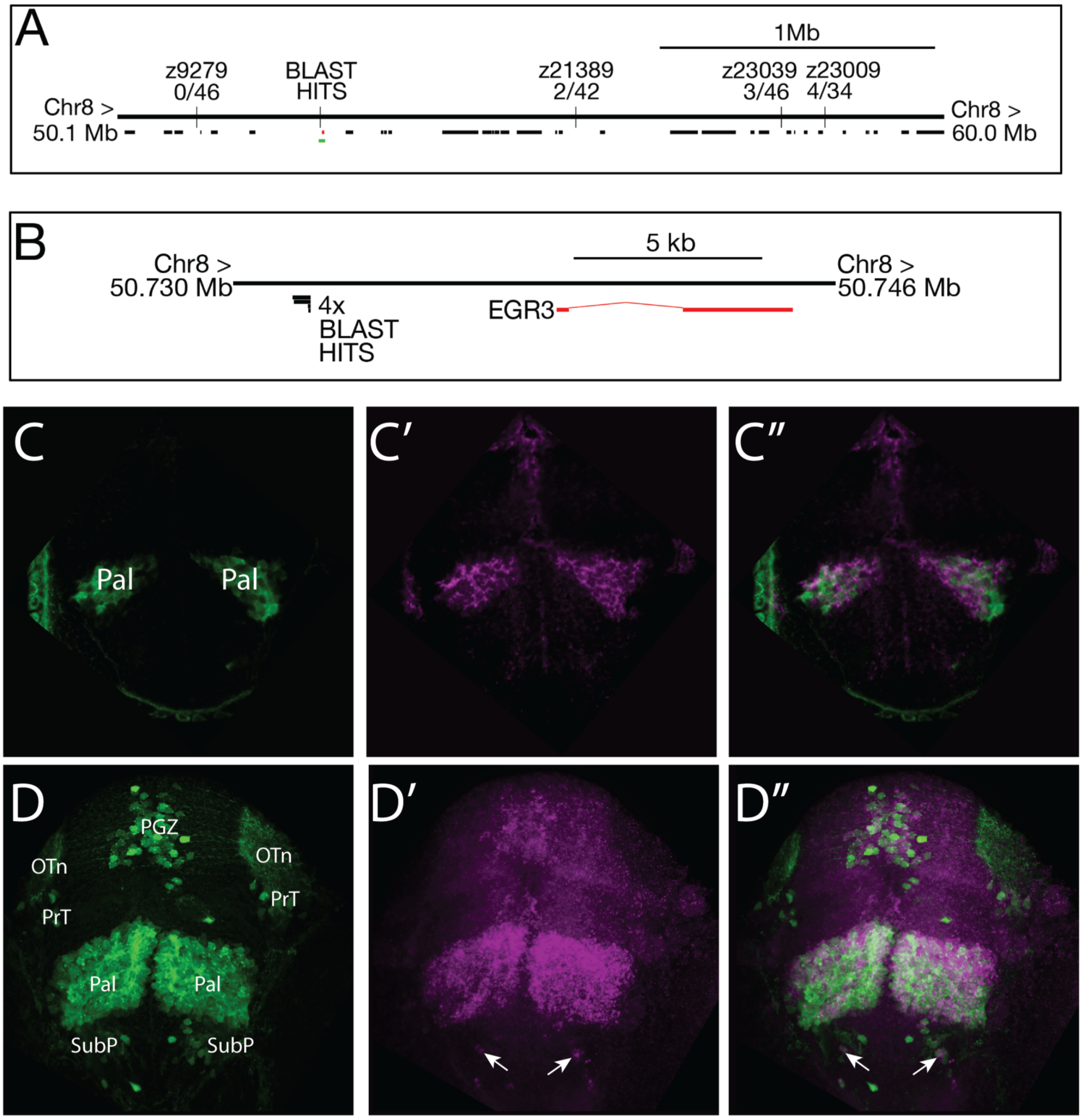

Figure 6.2: Et(gata2:EGFP)^{bi105} is egr3. Et(gata2:EGFP)^{bi105} insertion mapping showing the position of Genome Walker blast hits and relative position of linkage markers(A) and *Egr3*(B).(C-C") Et(gata2:EGFP)^{bi105} GFP expression and *Egr3* overlap in the telencephalon and optic tectum at 24hpf(C-C') and 60hpf(D-D").

6.2 Using CRISPR/Cas9 to generate mosaic transgene expression for neuroanatomical studies.

In its simplest form the injection of just the sgRNA_EGFP (gift from T.Auer; Auer et al., 2014) and Cas9 mRNA will result in an “erosion” of the GFP expression pattern (Figure 6.3C). Note how mosaic the optic tectum has become compared to the full transgenic expression (compare Figure 6.3B to 6.3C). This erosion approach is very simple and thus can be useful to observe individual cell behaviour and morphology in transgenics lines where the density of expression would normally mask such detail. This method is a good alternative to other mosaic labelling techniques such as cell transplantation where cells from a fluorescent donor embryo at blastula stage are transplanted into a host embryo. Cell transplantation is technically challenging and only a few transplants can be completed per session resulting in low experimental numbers. The erosion of GFP using Crispr can also be preferable to simple mosaic injections of promoter drived DNA constructs since this type of injections commonly results in ectopic expression outside the tissue or cell type of interest when used in transience.

The ability to resolve individual cell morphologies depends very much on the initial brightness and the cellular localisation of the EGFP transgene. To label cells even more sparsely within the domain of transgene expression and improve the level of morphological cellular detail, we made a simple modification to the EGFP/Gal4 switching method described in Auer et al., (2014). This labelling method uses the addition of both the modified bait construct from Kimura et al., (2014) and 5XUAS:TdTom (Zhang et al., 2012) DNA to the injection mix. This enabled us to label neuronal morphologies much more robustly within EGFP transgenic expression patterns in a very mosaic manner (Schematised in Figure 6.3A part iii). We also experimented with adding tol2mRNA to this cocktail to increase the efficiency of genomic integration of 5XUAS:TdTom to increase the efficiency of labelling later born cell types. **All of this work has been done in collaboration with Tom Hawkins**.

6.2.1 How the method works

Simultaneous Crispr/Cas9 induced cleavage of the both the Gbait construct at the bait sequence and EGFP in the genome (Figure 6.3Ai) of the embryo leads to the "erosion" of EGFP (Figure 6.3B and C). Homologous DNA repair also results in the inefficient integration of the bait plasmid into the EGFP locus resulting in a switching of EGFP for Gal4 in some transgene loci. The addition of the hs promoter (Kimura et al., 2014) to the bait construct increases "knock-in" efficiency, as both forward and reverse integration will lead to Gal4 expression (Figure 6.3ii). The addition of the membrane targeted 5XUAS:TdTom (Zhang et al., 2012) DNA to this injection mixture allows the entire morphology of the transiently Gal4 expressing neurons to be visualised. The relative inefficiency of both the EGFP/Gal4 switching coupled with the additional mosaicism resulting from the low concentration DNA injections leads to highly mosaic labelling (Figure 6.3Aiii). This makes it useful for examining individual cell morphologies within existing EGFP transgenic lines without needing to create the equivalent stable Gal4 transgenic line.

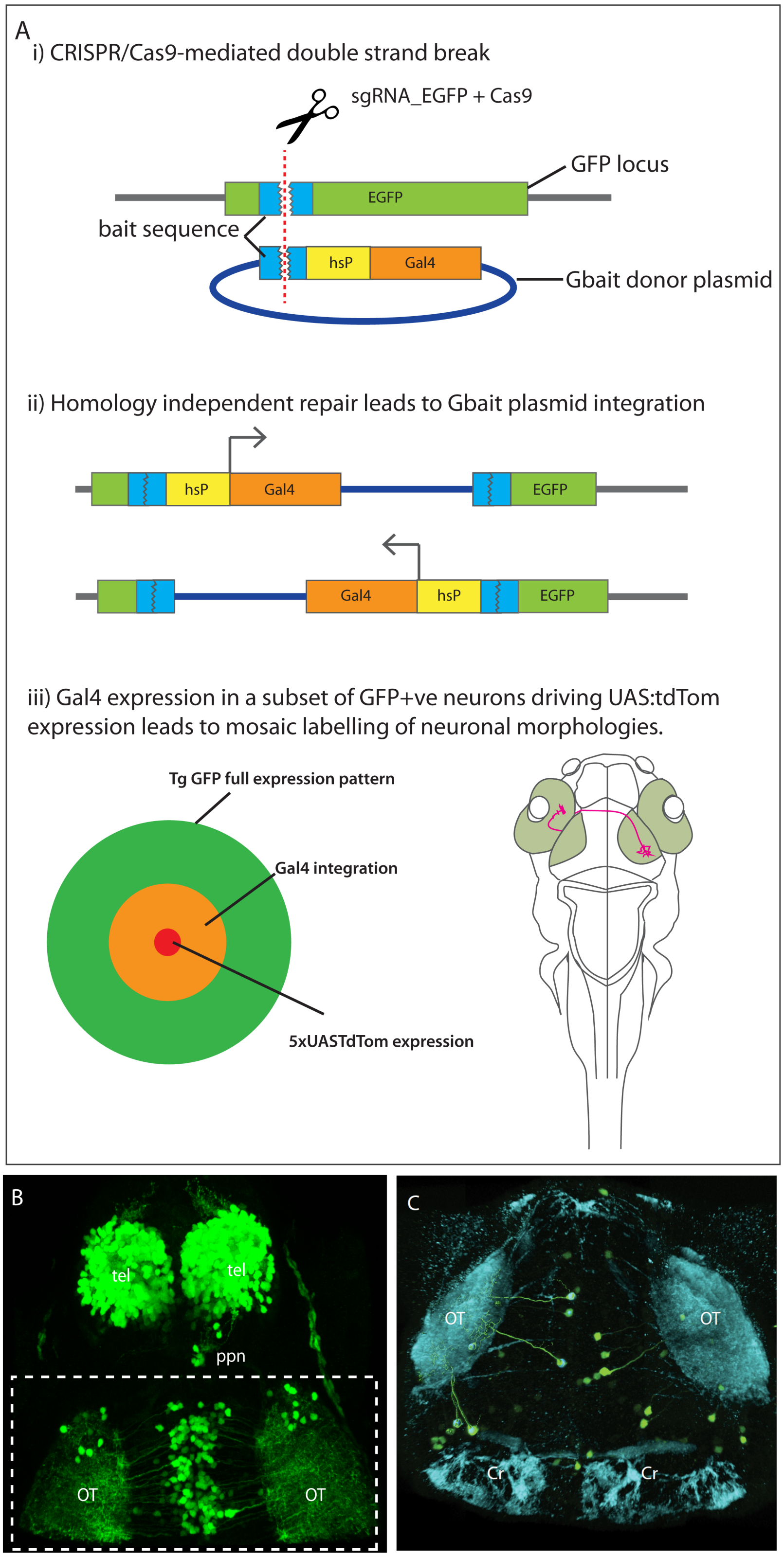

Figure 6.3: Crispr/ Cas9 switching methodology. (A) Schematic depicting the Crispr/Cas9 EGFP/Gal4 switching method pioneered by Auer er al., 2014 using the modified bait construct with heat-shock (hs) basal promoter (Kimura et al., 2014). (i) The action of sgRNA_EGFP and Cas9 cut both bait sequence in the GFP locus and

Gbait donor plasmid. (ii) Homology independent DNA repair leads to integration of Gbait plasmid into EGFP locus. Both forward and reverse integrations can occur (iii) Addition to this injection mixture of 5xUASTdTom DNA with or without *tol2* mRNA leads to very mosaic labelling with TdTom of neurons within the original EGFP expression pattern. Size of circles within the target reflect number of neurons labelled (B) Dorsal view of an uninjected control Et(gata2:EGFP)^{bi105} 4dpf larvae showing full EGFP expression pattern. (C) Dorsal view of the optic tectum of a "Crispered" Et(gata2:EGFP)^{bi105} 4dpf larvae injected with sgRNA_EGFP1 (Auer et al., 2014) and Cas9mRNA.

6.2.2 The UAS:TdTomato transgene enables beautiful labelling of neuronal morphologies, enabling axons and dendrites to be traced over long distances.

To demonstrate the efficacy of the UAS:TdTomato (Zhang et al., 2012) fluorophore to label neuronal morphologies I include this image of a single mechanosensory neuron in the tail of a 4dpf zebrafish (Figure 6.4). The neuron labelled here has the morphology of Rohon-Beard neuron (Sagasti et al. 2005). Rohon-Beard neurons are analogous to the trigeminal neurons that detect mechanothermal sensory stimuli in the head in both function and morphology. This Rohon-Beard neuron elaborates a dendritic arbour that covers the entire tip of the tail. The cell body is located in the dorsal spinal cord in what will become the dorsal root ganglion. This neuron sends an axon rostrally into the hindbrain (not shown). This neuron was imaged *in vivo* and demonstrates the exquisite resolution of neuronal morphology achievable with these constructs.

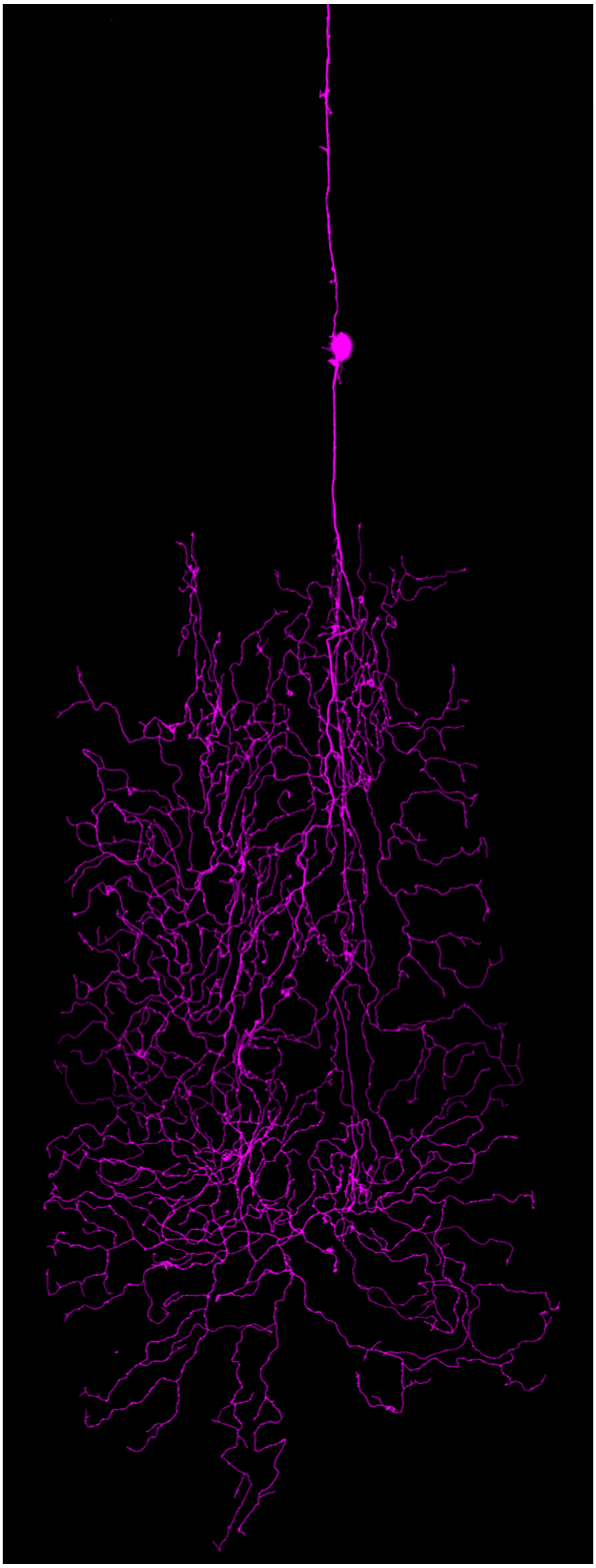

Figure 6.4: UAS:TdTomato . Lateral view of a live 4dpf Et(gata2:EGFP)^{bi105} larva injected with Crispr cocktail (see methods). Image is composed of 5 overlapping confocal stacks assembled in photoshop. The mechanosensory cell, likely to be a Rohon-Beard neuron pictured is labelled with 5xUAS:TdTomato.

For the initial establishment of this labelling technique, I used the Et(gata2:EGFP)^{bi105} enhancer-trap line. The results of the mosaic analysis of Et(gata2:EGFP)^{bi105} form part of a larger study on pallial development (Collaboration with Monica Folgueira and Tom Hawkins). “Crispering” of this enhancer-trap line in addition to establishing this labelling technique also revealed some interesting morphologies and projection patterns of pallial neurons.

6.3 The vENT could act as a relay nucleus from the telencephalon to the habenula.

Mosaic labelling of telencephalic neurons using Crispr show the different morphologies of dorsally and ventrally located telencephalic neurons and reveal potential area of convergence between telencephalic and vENT neurons within the lateral forebrain bundle.

6.3.1 Morphologies of pallial neurons Part I: dorsal cell types

Following injection of the Crispr EGFP converting cocktail at the one cell stage, the resulting mosaicism shows the arrangement of some of the dorsal pallial neurons that surround the central core of telencephalic neuropil demarcated by SV2 expression (Figure 6.5 A and B). Some of these dorsally located cells show a monopolar morphology (Figure 6.5 C) with a single process extending towards the neuropil core before extending dendrites that form a dense tangle with the dendrites of adjacent neurons ramifying through the telencephalic neuropil. In Figure 6.5 A, some processes can also be observed to innervate the contralateral telencephalic neuropil core. However, this specimen does not have sufficiently mosaic expression to trace whether this innervation comes from these same monopolar cells projecting through the anterior commissure, although some processes are visible within the anterior commissure.

The second type of cell morphology observed in the dorsal pallium is a multipolar morphology that resembles a basket shape. These neurons sit either just at the dorsal surface or inside of the central neuropil core. The cells extend multiple processes directly from the cell body that appear to encase small areas of neuropil or groups of somata (Figure 6.5 C).

In addition to the dorsal pallial neurons labelled in larvae 6.5 A and A1 B both of these specimens (Figure 6.5 A and B) show some processes projecting to caudal regions through the forebrain bundle. In the case of larva B, when checked slice by slice, these caudal projections appear to emanate from the more ventrally located cells at the midline (centrally located yellow coloured neurons in the first panel Figure 6.5 B). Further examples of this class of ventral projecting neuron are presented in the following section (Figure 6.6).

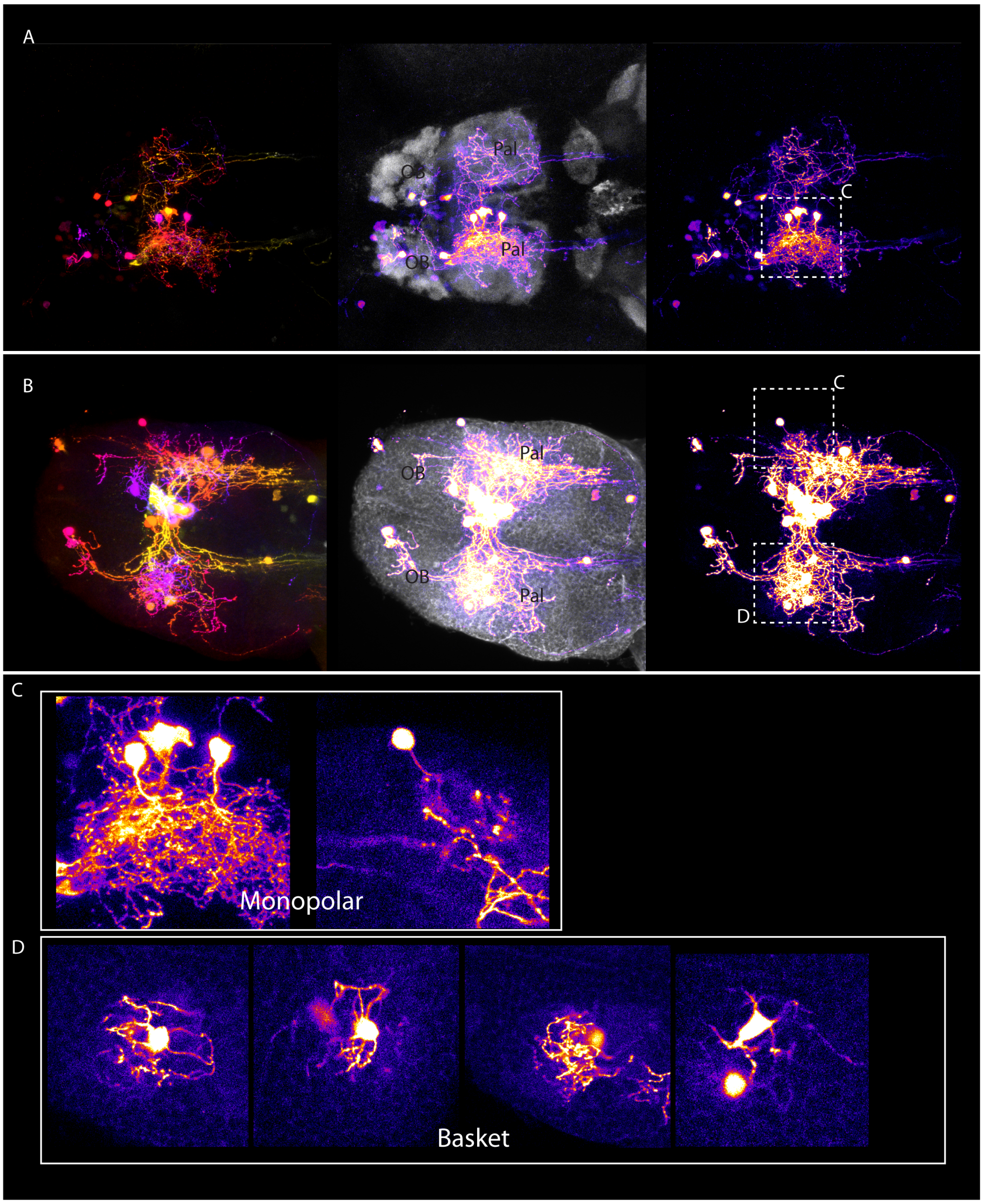

Tg(gata2:EGFP)^{bi105} RFP(FIRE LUT)/SV2 or T-ERK 5dpf

Fig 6.5: Morphologies of pallial neurons Part I- Dorsal cell types. Dorsal views of 4dpf Et(gata2:EGFP)^{bi105} larvae injected with Crispr cocktail. Labelled with anti-RFP (FIRE temporal depth colour code and FIRE LUT **(A&B)**, anti-SV2(grey channel larva A) and anti-TERK (grey channel larva B). **(C&D)** Close-up of dorsal pallial neurons grouped into "monopolar" (C) and basket (D) cell morphologies.

6.3.2 Morphologies of pallial neurons Part II: projecting neurons

Ventrally located pallial neurons extend axons bilaterally down both forebrain bundles and innervate multiple downstream targets including the vENT (Figure 6.6 A, C and arrow in F& G), preglomerular complex (PG), lateral posterior tuberal areas (PT), midline posterior tuberal nucleus (PTN) and the hypothalamus (Hyp). Two examples of this ventrally located “projection” neurons cell class are shown in Figure 6.6 (Figure A2 A and C). Their cell bodies lie at the level of the AC with their cell bodies just anterior or dorsal to the AC. They exhibit a cascading morphology with dendritic processes that project within a small dorso-ventral plane throughout the ac and ipsilateral adjacent neuropil domain. Their dendritic processes also appear to be spiny (Figure A2 arrow in E). Both of these cells extend a single process across the midline in the ac to innervate the contralateral vENT. Cell “A” does not extend a contralateral axon past the vENT but cell “C”. Although the position of their cell body and morphologies of Cell “A” and Cell “C” are similar they show distinct innervation patterns.

In addition to these neurons that project to multiple caudal areas I observed one very peculiar “projecting” cell (Figure 6.6 B) with a cell body located within the AC. This cell exhibits almost cocoon-like dendrites, tightly wrapped within the ac itself. It sends one process rostrally into the contralateral pallium at the border with the olfactory bulb and another caudally through the lateral forebrain bundle to the posterior tuberculum (PT).

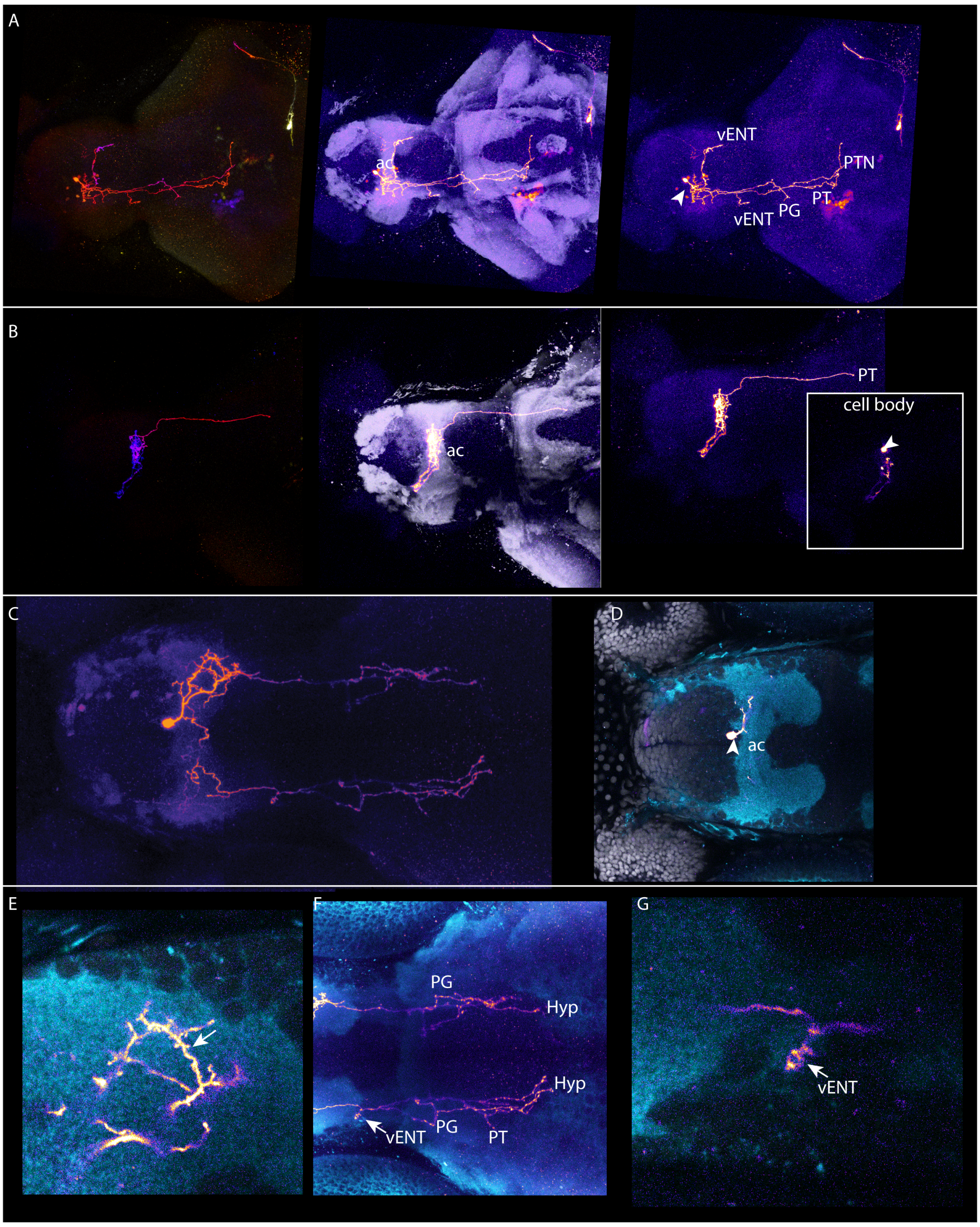

Tg(gata2:EGFP)^{bi105} RFP(FIRE LUT)/SV2 5dpf

Figure 6.6: Morphologies of pallial neurons Part I- Ventral cell types. Ventral views of 4dpf Et(gata2:EGFP)^{bi105} larvae injected with Crispr cocktail. Labelled with anti-RFP (FIRE temporal depth colour code or FIRE LUT **(A-G)**, anti-SV2(grey A&B; cyan in C-G) **(D-G)** Close-up details of larvae (C).Arrow in D shows spines on dendrite. Arrow in F &G show branching in the area of the lfb adjacent to the vENT.

6.3.3 Pallial neurons elaborate terminals within the lateral forebrain bundle at the level of the vENT.

The lateral forebrain bundle could be a point of connection between pallial and vENT neurons. Some neurons elaborate terminals within the neuropil of the lateral forebrain bundle at the level of the vENT (dashed box Fig.6.7 B and C). As described in Chapter 3 the vENT cells surround the lateral forebrain bundle (also called the supraoptic tract in Wilson et al., 1990) between the anterior and post optic commisures. These findings indicate that the vENT neurons surrounding this neuropil and also extending processes into it are well placed to act as a relay between the telencephalon and the habenula. In addition to these putative vENT terminals, some axons extend straight through the vENT region of the lateral forebrain bundle to caudal regions without elaborating any collaterals.

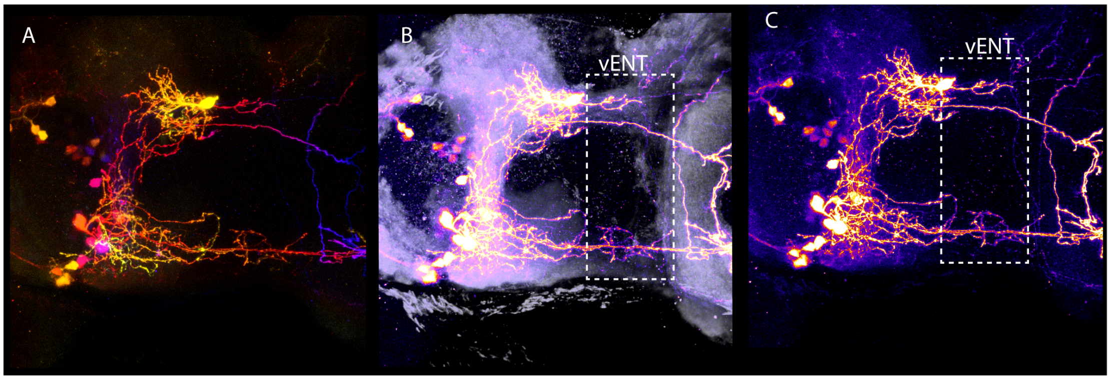

Tg(gata2:EGFP)^{bi105} RFP(FIRE LUT)/SV2 5dpf

Fig 6.7: **Pallial neurons elaborate terminals within the forebrain bundle at the level of the vENT.** Ventral views of **a** 4dpf Et(gata2:EGFP)^{bi105} larvae injected with Crispr cocktail. Labelled with anti-RFP (FIRE LUT) **(A-C)**, anti-SV2 (grey B). Whisker box in “B” and “C” delineates the area of the lateral forebrain bundle surrounded by vENT neurons. Pallial neurons can be seen to elaborate terminals within this region.

Despite having a few misgivings about exuberant labelling with the Crispr/Cas mosaic labelling method, the lack of alternative Gal4 transgenic lines drove me to use this technique to try to mosaically label vENT and RL neurons.

6.4 Mosaic analysis of Tg(cldnb:lynGFP) using Crispr reveals the complex morphology and innervation patterns of habenula afferent vENT neurons.

Transient switching of lynGFP to Gal4 in Tg(cldnb:lynGFP) embryos works well and labels neurons within the Tg(cldnb:lynGFP) GFP expression pattern robustly and mosaically. The lynGFP sequence is not recognised by the more efficient sgRNAEGFP1 guide RNA (Auer et al., 2014) but is targeted by the sgRNAEGFP2. This guide is less efficient but for my purpose of labelling just few cells, a lower efficiency can be beneficial as it results in even more mosaic labelling with UAS5xTdTom (I do not visualise the native GFP in these larvae so the mosaicism of GFP is not important). The 1000+ injections I performed in the Tg(cldnb:lynGFP) line unfortunately did however confirm my earlier impression that this technique preferentially labels earlier born cell-types within the GFP expression. This proved to be particularly problematic when trying to label vENT and RL neurons that only start to develop post 48hpf. The incidence of hitting these cells – compared to labelling pallial/subpallial and olfactory bulb cells – was extremely low.

Outside of the mitral cells of the olfactory bulb (of which I labelled many) I only succeeded in labelling 2 habenulo-petal neurons out of thousands of labelled neurons. These cells show incredibly beautiful and complex morphologies. They also show that these forebrain afferents innervate the habenula subnuclei in an asymmetric manner similar to the mitral cell (Miyasaka et al., 2012) and parapineal innervation (Concha et al., 2003). This is expected, given the distribution of GFP in the habenula neuropil of Tg(cldb:lynGFP) larvae (Figure 4.3). Lateral differences in afferent circuit microarchitecture probably contribute to the functional lateralisation seen in the habenula and its efferent nuclei (Dreosti et al., 2014., Jetta et al., 2014). Despite very low cell numbers, these cells warrant our full attention and detailed description, in an ideal world there would be several hundred of them to describe; we will have to accept the small numbers we have, for now.

The first habenula afferent neuron labelled following Crispr conversion of the Tg(cldnb:lynGFP) transgenic line that I will describe is a right-sided vENT neuron(Figure 6.8). This vENT neuron really illustrates the complexity of habenula afferent neuronal morphologies and innervates both ventral and dorsal habenula subnuclei in an asymmetric fashion. In addition to the habenula, this vENT neuron innervates AF4 and the midbrain. The vENT cell body straddles the telencephalic/diencephalic border (arrow in Figure 6.8) and extends a process ventro-caudally that bifurcates when it reaches the lateral forebrain bundle. One branch extends caudally for a short distance before ramifying throughout a neuropil that is most probably AF4 (dashed circle in Figure 6.8B) before ascending through the tract of the habenula commissure to innervate the habenula (green arrowheads in Figure 6.8 B,C,D,E and F). The process (axon) originating from this neuron then ramifies in the right ventral habenular subnucleus before projecting a further process that crosses the midline in the habenular commissure and terminates in the left dHbl subnucleus (Figure 6.8C). The several pallial neurons labelled in this specimen do not project to the habenula (Fig 6.8D, E and F) and all terminals seen in the habenula emanate from this single vENT neuron. The complexity of this cell makes it difficult to be sure if a single dendrite/axon branches into AF4 and gives rise to an axon or if an axon and a dendrite originate from the cell body and traverse the various tracts side by side

The vENT neuron in Figure 6.8 also innervates more caudal regions in the ventral diencephalon or midbrain. The long process (axon/dendrite) of this vENT neuron is indicated with a blue arrowhead in Figure 6.8, after bifurcation, this process briefly extends rostrally into the caudal telencephalon before looping back on itself and projecting down the lateral forebrain bundle (blue arrowhead in figure 6.8 A,B,G-G” and H). It is possible to follow this axon until it reached the preglomerular complex whereupon a very bright neuron obscures its trajectory (Figure 6.8 G-G’). Although it is possible that this axon turns medially at this point I believe it is traceable back into the midbrain and could terminate in the vicinity of the superior raphe (Figure 6.8G”-H).

The vHb is afferent to the median or superior raphe and innervated by the vENT (Amo et al., 2014., Turner et al., 2015). Amo et al (2014) suggested a putative projection from median raphe back to vENT based on observation of Lillesaar et al (2009) data, although this innervation was not explicitly described in this paper. They suggested that the vENT-vHb-MR may constitute a ternary (three-part) neural circuit. If the projection to the MR from this vENT neuron does exist this would indicate a possible reciprocal connection between habenulopetal vENT neurons and the median raphe.

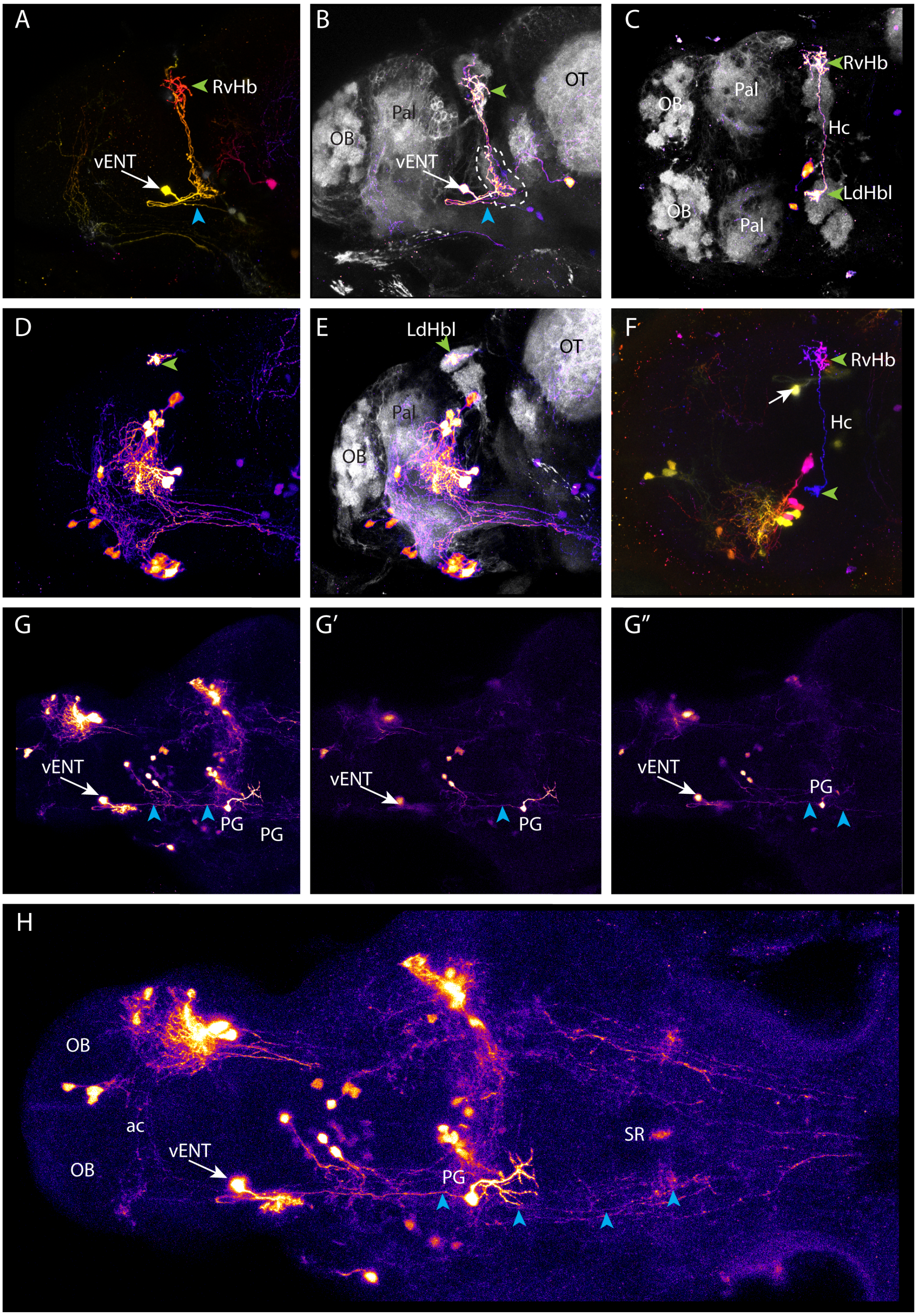

Figure 6.8: Tg(cldnb:lynGFP) Crispr vENT neuron. Lateral (A,B,D-F), Dorsal(C) and ventral(G-H) views of a 4dpf Tg(cldnb:lynGFP) larva injected with Crispr cocktail labelled with anti-RFP (FIRE temporal depth colour code A and F; or FIRE LUT B,-E,

G-H) and anti-SV2(grey B,C and E). White arrow indicates vENT neuron cell body. Green arrowheads label Hb terminals. Blue arrowheads label process extending down the lateral forebrain bundle to the midbrain.

The second habenula afferent neuron labelled following Crispr conversion of the Tg(cldnb:lynGFP) transgenic line that I will describe lies in the telencephalon most probably within the dorso-medial part of the vENT (white arrow Figure 6.9). Again, this vENT neuron illustrates the complexity of habenula afferent neuronal morphology and connectivity. The cell in Figure 6.9 shows a more symmetric innervation of the habenula than the vENT neuron in Figure 6.8, elaborating terminals in the left and right dHbm subnuclei. In addition to the habenula the neuron extends multiple processes that terminate in the pallium and subpallium.

This cell is quite ambiguously located, and without clearer anatomical cues, I do not feel totally confident in placing it in the vENT as when viewed from a dorsal aspect (Figure 6.9C-D) the cell body is not totally lateral within the telencephalon and so could potentially be in the preoptic area. This neuron is bipolar, a ventral process projects ventrally into the lateral forebrain bundle where it splits into several branches. These processes extend within the neuropil domain (delineated by SV2 expression) in the tract of the ac that connects the lateral forebrain bundle to the ac in the subpallium. The processes terminate ventrally at the level of the rostral border of the ac (yellow arrowhead Figure 6.9).

This neuron also extends a process dorsally into the pallium. This axon splits into two where it meets the stria medullaris, one branch ascends up to the habenula and innervates the ipsilateral left dHbM subnucleus and then crosses the midline through the habenula commissure to innervate the contralateral right dHbm subnucleus (green arrowheads in Figure 6.9). In both the left and right dHbm the axon elaborates small terminals that form a triangular shape in the section of neuropil caudal to the habenula commissure. Although this “triangular” innervation looks quite symmetric, the axon actually extends slightly further laterally within the RdHbM neuropil and extends another small terminal process. The fact that this cell innervates the dorsal habenula (homologous to the medial habenula) rather than the vHb may support the idea that it is not entopeduncular.

The opposite branch of this axon projects rostro-ventrally within the pallial neuropil. This axon sends out two dorso-rostral projections that terminate in the dorsal pallium just caudal to the olfactory bulb (orange arrowhead in Figure 6.9). The final branch of this axon descends into the subpallium and terminates within the neuropil domain of the ac (orange arrowhead Figure 6.9) almost in touching distance of the other subpallial processes (yellow arrowhead). Apart from the habenula, the connections of this neuron are all within the left telencephalic lobe.

Despite being an effective and useful technique to perform clonal analysis in transience where a suitable Gal4 line is not available, the very low incidence of labelling later-born cells was a severe limitation for my experiments. As the GFP should be permanently “switched” to Gal4 in the genome and so Gal4 should show the same spatio-temporal expression as the original GFP expression. I hypothesised that the reason that very few later born cells types were being labelled with this method was the loss of the UAS:TdTom over time. To counteract this I started to add tol2 transposase mRNA to the Crispr cocktail to insert the UAS:TdTom, which is flanked by mini tol2 sites, into the genome. Anecdotally, I do think this increases the efficiency of this labelling technique although overall mosaicism also decreases. I did not continue using this method of mosaic labelling as a potentially suitable Gal4 line finally came along, however I think that tol2 should be considered as a possible addition to the injection mix, when labelling of later-born neurons is desired.

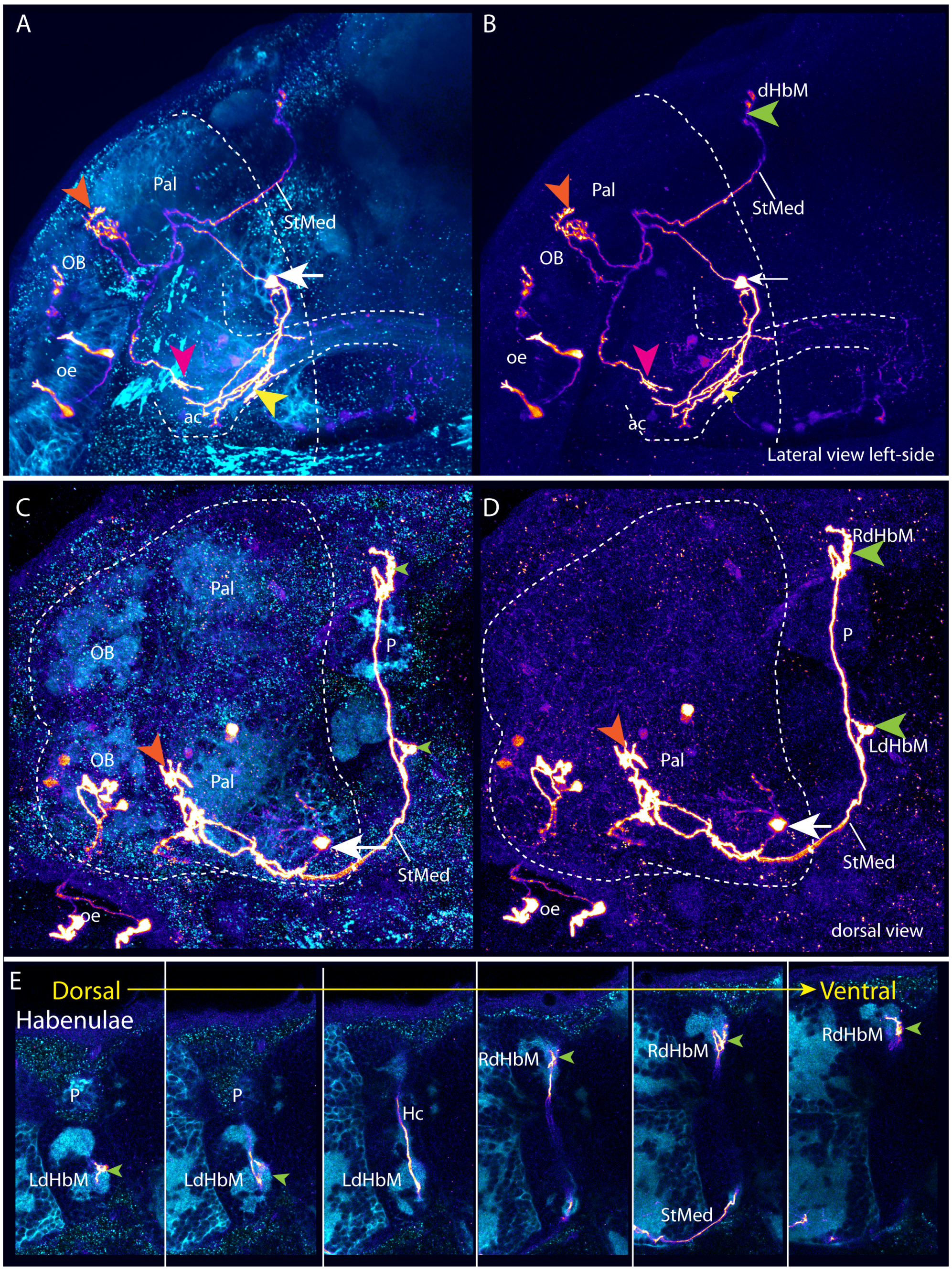

RFP(FIRE LUT)/SV2 6dpf

Figure 6.9: Tg(cldnb:lynGFP) Crispr dHbM afferent neuron. Lateral (A,B,), Dorsal(C-E) views of a 6dpf Tg(cldnb:lynGFP) larva injected with Crispr cocktail labelled with anti-RFP (FIRE LUT) and anti-SV2(cyan). (E) Single z-slices through the habenula from dorsal(left) to ventral(right). White arrow indicates neuron cell body probably in vENT. Green arrowheads label Hb terminals. arrowheads label process extending down lateral forebrain bundle to midbrain.

6.5 Mosaic analysis of RL and vENT neurons using the Gal4^{s1020t} transgenic line

The Et(-0.6hsp70l:Gal4-VP16)s1020t (from now referred to as Gal4^{s1020t})transgenic line (Scott et al., 2007) is essentially a “pan-thalamic” line (Figure 6.10). To assess the expression of the Gal4^{s1020t} enhancer trap line Gal4^{s1020t} carriers were crossed to the UAS:RFP transgenic and the larvae were labelled with anti-RFP and anti-SV2 to visualise neuropil, for context.

Examination of Gal4^{s1020t}:UAS:RFP larvae from a lateral aspect show diencephalic Gal4/RFP expression in the the vENT and prethalamus, areas described above as afferent to the habenulae: (Figure 6.10A-A’). Single z-slices through this larva show that the whole vENT is labelled in the Gal4^{s1020t} transgenic line including the rostral half of this nucleus that by this stage resides in the ventro-lateral telencephalon. Other RFP+ cells are located in the diencephalon with strong expression throughout the prethalamus, thalamus and posterior tuberculum. Some expression is also visible in the preoptic area. RFP expression can also be seen in the habenula (Figure 6.10B-C) most of this expression is in the habenula neuropil but some habenula neurons are also RFP+ (arrowhead in Figure 6.10C), This means the Gal4^{s1020t} transgenic line is not ideal for identification of habenula afferents as the habenula intrinsic population needs to be considered/eliminated for the interpretation of afferents.

Data provided kindly provided to me by Lucy Heap and Ethan Scott shows that this Gal4 transgenic line labels habenula afferent neurons. The *Gal4^{s1020t}* transgenic line, in a UAS:Kaede background was crossed to a UAS line that drives expression of synaptophysin-GFP (Heap et al., 2013) (UAS:synatophysin GFP or UAS:syn-GFP). The larva in Figure 5.7D the Kaede protein was photoconverted from green to red, so the Gal4/Kaede expressing cells were labelled in red while their presynaptic terminals were labelled in green. Syn-GFP strongly labels the entire habenula neuropil (Figure 6.10D) There does not appear to be any red kaede expression in the habenula itself, only synaptic terminals labelled in green, although without access to the original data this is difficult to confirm.

These initial studies ascertained that the main afferent areas of interest are indeed labelled in the Gal4^{s1020t} transgenic line . To further explore the possibilities of this transgenic line for the study of habenular afferents, I used a mosaic labelling approach to try to target single afferent neurons in both RL and the vENT by injecting a mixture of UAS:TdTom DNA and tol2mRNA. Most injected larvae show small clones or groups of cells close to each other rather than single cells. As such, this study falls unsatisfyingly short of really nailing the habenula afferent circuitry through the description of individual cellular morphologies. Key findings on vENT and RL cytoarchitecture and connectivity are summarised in the following sections.

To mosaically label neurons in habenula afferent nuclei, Gal4^{s1020t} embryos were injected at one cell stage with 5XUAS:TdTom and tol2mRNA. Embryos were raised till 5dpf then labelled with anti-RFP and anti-SV2 antibodies to provide a neuropil counterstain allowing visualisation of key landmarks; the habenular subnuclei, optic tract and lateral forebrain bundle. Screening for larvae with habenula innervation was performed post-immunohistochemistry when the RFP signal was strongest so that very mosaically labelled brains were not inadvertedly discarded. Larvae that showed RFP+ terminals in the habenula were selected and imaged by confocal microscopy.

The border between EmT and ventral thalamus/prethalamus is very difficult to ascertain at 5dpf, even with molecular markers, so for the remainder of these results I will refer to cells that lie within the Tbr-1/entopeduncular part of EmT as vENT and the rest of the EmT as prethalamus.

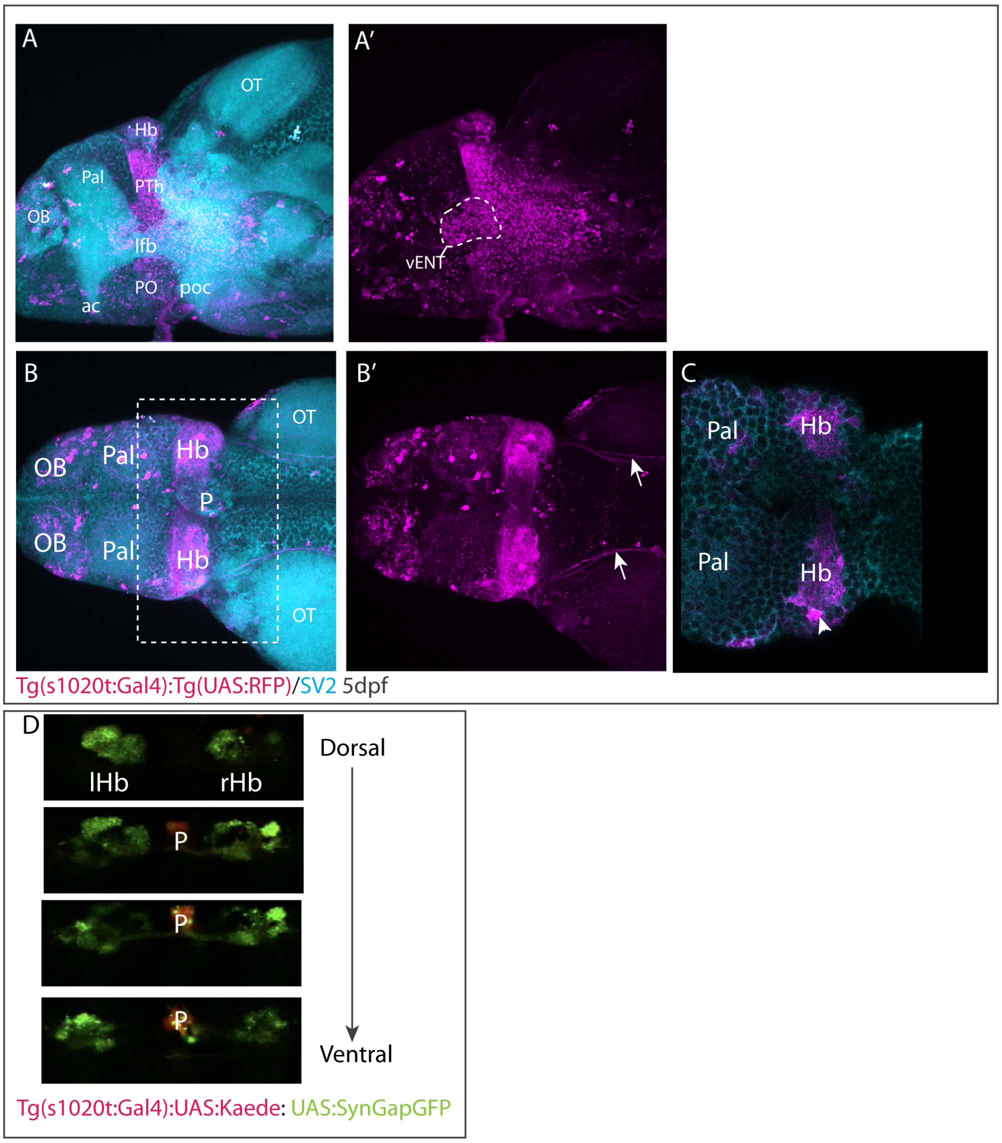

Figure 6.10: Synaptic targets of the "pan-thalamic" Gal4^{s1020t} line revealed by a pre-synaptic marker.: Lateral**(A-A')** and dorsal **(B-C)** views of a 5dpf Gal4^{s1020t}:UAS:RFP labelled with anti-RFP(magenta) and anti-SV2(cyan)(A,B and C) and RFP only(A' and B'). **(C)** single z-slice through the habenula of larvae in (B) showing RFP+ neurons in the left habenula (arrowhead). **(D)**Dorsal view of a 6dpf live *Gal4^{s1020t}; UAS:Kaede; UAS:syn-GFP* transgenic larvae. Anterior to the top. Photoconverted Kaede is shown in red, and syn-GFP is shown in green (**Data in Panel "D" from Ethan Scott and Lucy Heap)**.

6.6.1 Larvae with RFP+ neurons in the prethalamus and vENT show afferent terminals throughout all of the habenula subnuclei

Mosaic labelling experiments with the Gal4^{s1020t} transgenic line help to confirm my earlier findings that the main populations afferent to the habenula in zebrafish lie directly ventral to the habenula in the diencephalon in prethalamus/EmT/vENT regions close to the border with the telencephalon. Figure 6.11 shows an example of what these habenula afferent populations look like when viewed dorsally. The Gal4^{s1020t} larvae in Figure 6.11 shows afferent terminals throughout all habenula subnuclei(Figure 6.11C-C’). Smaller z-projections through prethalamic (Figure 6.11D) and vENT(Figure 6.11E) regions show the organisation of these afferent cells that follow the curve of the anterior-intraencephalic sulcus.

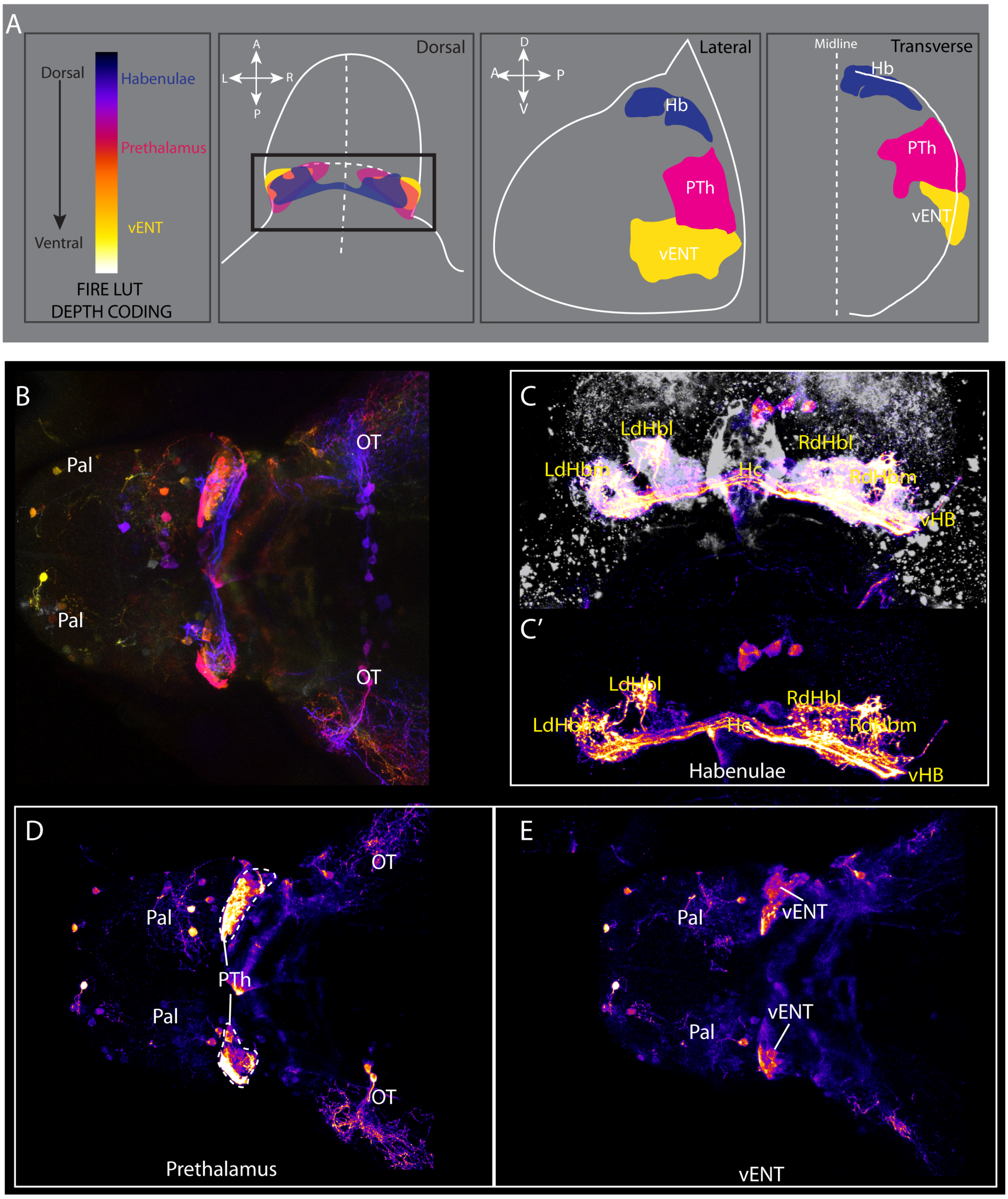

s1020t injected with UAS:TdTom Drosal view 4dpf

Figure 6.11: Larvae with RFP+ neurons in the prethalamus and vENT show afferent terminals throughout all of the habenular subnuclei: **(A)** Schematic showing the dorso-ventral depth FIRE colour code. This false colouring allocates different colours to different DV positions of cells within the z-stack and allows the visualisation of the 3 main areas of interest within the same z-projection. From dorsal to ventral; Habenula afferent terminals (purple), the prethalamic group (magenta/red) and the more ventral entopeduncular region (yellow) shown from dorsal, lateral and transverse frontal viewpoints. **(B-E)** Dorsal view of a brain from a 5dpf Gal4^{s1020t} larva injected with 5XUAS:TdTom and tol2mRNA at 1 cell stage and labelled with anti-RFP (FIRE LUT), anti-SV2 (grey in B;cyan in D) and DAPI (grey in D and F). **(B)** Full z-projection with false colouring to show different DV position of

cells. **(C)** Z-projection of habenula neuropil visualising RFP and SV2 showing afferent terminals throughout the habenula. **(C')** Z-projection of only the habenula neuropil visualising RFP alone. **(D)** Z-projection of prethalamus. **(E)** Z-projection through vENT/prethalamic eminence. The larvae shown in this figure, has cells labelled with RFP in both the prethalamus (red) and vENT(yellow) and shows afferent terminals throughout all of the habenula subnuclei.

6.6.2 The prethalamic nucleus is both habenula and tectal afferent and contains neurons with two distinct morphologies.

Larvae with prethalamic neurons labelled also have afferent terminals innervating the optic tectum (Figure 6.12 A&C). The afferent neurons in this larva are all located directly ventral to the habenula. A 3D transverse section shows the DV position of the afferent neurons (Figure 6.12B-B'). This larva has cells labelled in the prethalamus and shows strong labelling throughout all the habenula subnuclei (Figure 6.12F &G) including LdHbl (Figure 6.12G arrowhead).

Two distinct morphological cell classes innervating the habenulae are present in the pre-thalamus. A Z-projection through only the prethalmus shows the arrangement of these afferent neurons relative to the neuropil areas associated with the optic tract (Figure 6.12D). The first class of neuron has an elongated teardrop shape (schematised by blue outlined cells in schematic Fig 6.12E). Their cell bodies are positioned medially and could be in contact with or close to the ventricular surface. These neurons extend processes to contact the prethalamic neuropil adjacent to the tHc and ventral to the vHB. Their cell bodies are positioned rostral and ventral to the LdHbl. The way in which the shape of the cells arch caudally to contact the neuropil seems to follow the curve of the intraencephalic sulcus indicating that these cells lie within the rostral-most part of the "thalamus" and could form the more dorso-medial, proliferative part of the eminentia thalami which at the most rostral levels should lie almost directly ventral to the habenula (Wullimann and Mueller 2004).

The second class of cells surround this same area of neuropil but show a rounded morphology (schematised in orange in Figure 6.12E). Their cell bodies abut the neuropil as they cluster around it. Temporal depth coding shows that the rounded cells surrounding the neuropil (orange outline in schematic Figure 6.12E) lie caudal and very slightly ventral to the elongated cell group. Higher magnification of this area (Figure 6.12D) shows that the elongated cell processes extend through the centre of the cluster to reach the neuropil of the optic tract.

6.6.3 Prethalamic afferents show asymmetries in habenular subnuclear innervation.

As the small number of right-sided neurons (arrowhead in Figure 6.12C) are not habenula afferent, the afferent processes seen in the habenula (Figure 6.12F-G) derive from left-sided prethalamic neurons only (Figure 6.12D). Although the habenula is innervated quite broadly by these afferent axons, these left-sided prethalmic afferent neurons do show some asymmetry in their innervation of some habenular subnuclei. This larva shows more terminal elaboration and innervation in the right (contralateral) habenula. Afferent terminals are present throughout all of the RHb subnuclei, including a strong rostrally elongated terminal in the RdHbl that extends past the neuropil domain delineated by SV2. In the left habenula the LdHbl shows a terminal field of low intensity in the rostral half of this neuropil (Figure 6.12 F and G) possibly emanating from just a single afferent process. The areas of neuropil caudal to the commissure in dHbm show quite symmetric amounts of innervation (encircled in Figure 6.12F). This result indicates that there is some asymmetry in this projection. With the density of cells present in the prethalamus it is not possible to determine whether the two morphologically distinct cell types are both afferent to the habenula and if so, show similar habenula innervation patterns.

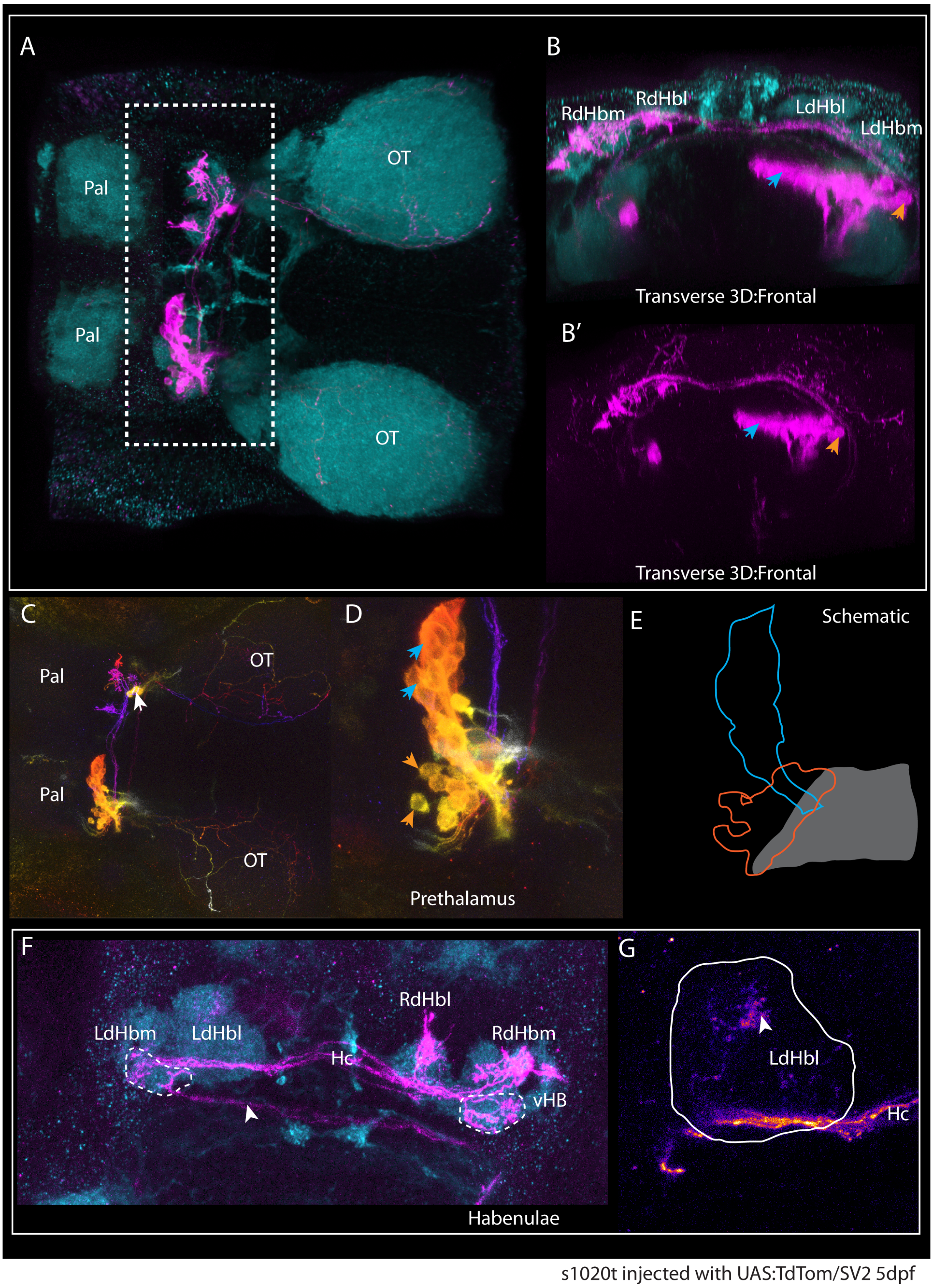

Figure 6.12: Prethalamic afferents show asymmetries in habenular subnuclear innervation.: Dorsal views of the brain of a 5dpf Gal4^{s1020t} larva injected with 5XUAS:TdTom and tol2mRNA at 1 cell stage and labelled with anti-RFP (Magenta in A,B,B'and F) or FIRE LUT (C,D and G) and SV2 (cyan in A,B and F). **(A)** Z-projection of larvae with prethalamic afferents labelled. This larva has 3 cells labelled in the

right prethalamus and many more in the left prethalamus. **(B)** Transverse 3D section of A through diencephalon (crop planes denoted by white dashed box in A) showing relative D-V positions of labelled cells with SV2 (cyan) and RFP (magenta). **(B')** same as B visualising RFP only. **(C)** Z-projection with false colouring to show different DV position of cells. As well as habenula innervation this larva has axons innervating the optic tectum. **(D)** Close up of the left prethalamus showing the two different morphological cell clusters. **(E)** Schematic of prethalamic cell arrangement relative to optic tract neuropil(grey). Neurons within this prethalamic population can be grouped into two distinct cellular morphologies, small rounded cells directly adjacent to the neuropil (orange outline in schematic "E" surrounds this sub-population). The second cell morphology are the teardrop shaped cells (cyan outlines in schematic "E" surrounds this subpopulation). This subpopulation have their cell bodies positioned more medially and extend a long process through the group of cells surrounded by orange outline to contact the same neuropil(grey in schematic E). **(F)** Z-projection of habenula only visualising RFP (magenta) and SV2 (cyan) showing innervation of habenula subnuclei by RFP+ afferent axons. **(G)** RFP+ (FIRE)terminals in habenula show innervation of multiple habenular subnuclei by these afferents. White dotted lines encircle symmetrical terminals posterior to the habenula commissure. White arrowhead shows axons crossing in the posterior commissure originating from prethalamic cells in C marked with white arrow. A small terminal in the LdHbl subnucleus is present in this larva (white arrowhead in G). Blue arrows label the teardrop shape prethalamic cells throughout figure. Orange arrows label rounded prethalamic cell cluster throughout figure.

6.6.4 Connectivity of the vENT and RL

The lateral views of a mosaically labelled Gal4^{s1020t} larva presented in Figure 6.13 and 6.14, show the efferent connectivity of vENT and RL and the spatial arrangement of a subset – albeit a large subset – of vENT/RL neurons and their processes. Processes from vENT/RL neurons can be seen projecting to the dorsal and ventral habenula, optic tectum, subpallium, posterior tuberculum and ventrally to preglomerular complex and inferior hypothalamic regions. The processes from the RFP+ cells within the vENT/RL form two laminar neuropils at their caudal edge (Figure 6.14), one lateral and one medial. Axons leaving these two laminar neuropils project to distinct brain regions. If we look back at previous experiments, such as Figure 4.4 and Figure 4.6, the sum of the lateral and medial neuropils at the caudal edge of the vENT and RL could form AF4.

Lateral Neuropil

The lateral neuropil at the caudal edge of the vENT/RL nucleus (Figure 5.10bi) runs parallel with axons in the optic tract. Cells align along the anterior edge of this neuropil (white arrowheads Figure 6.13, Gii) and their processes turn dorsally to innervate the optic tectum. There is also a caudal projection from the dorsal tip of this neuropil where processes project back into the posterior tuberculum and inferior hypothalamus and in into the post optic commissure (green arrows Figure 6.13D). Some RL cell bodies lie anterior to the lateral neuropil (arrowheads in Gi) but others (Gii) seem sandwiched between the lateral and medial neuropil. Arrowhead in Gii shows a neuron with slightly different morphology that lies parallel to the lateral neuropil and has a single short fat process. The neurons associated with this lateral neuropil could be RL neurons that have been shown to be tectal afferent in several teleost species.

Medial Neuropil

Some RFP+ cells can be seen sandwiched in between these lateral and medial neuropils (Figure 6.13D and E) and seem to contribute processes to both. The larvae in Figure 6.13 and b also shows the arrangement of vENT neurons (arrowheads in Giii and iv) that extend processes into a larger more medial neuropil(orange neuropil in Figure 6.14C seen in section 6.14Dii and iii). Habenulopetal afferents leave this tangle of processes and coalesce into the tract of the habenula commissure. Some vENT neurons project their processes ventrally into the dorsal part of the lateral forebrain bundle referred to as the supra-optic tract (Wilson and Easter., 1997)(Figure 6.13Giii and Giv). This results in the neuropil having an almost triangular shape when viewed laterally (Figure 6.14C and Dii and Diii). The large tangle of processes that form the medial neuropil of the vENT could be formed by vENT neurons such as the neuron described in Figure 6.8.

A close up of the habenula shows terminals throughout the vHb and dHb in this larvae (Figure 6.13C). When these habenuopetal axons are traced back to their cells of origin it seems that there are two different populations of neurons sending these habenula afferents in this larva:

- The posterior group of axons labelled with a blue arrow in Figure 6.13 exit from the medial neuropil. The arrangement of these processes is reminiscent of the transplanted Tg(cldnb:lynGFP) cells in Figure 4.4C and C’) and this medial neuropil could be AF4.
- Rostrally located vENT neurons appear to send axons to the habenula more directly without entering this medial neuropil (yellow arrows in figure 6.13 and 6.14).

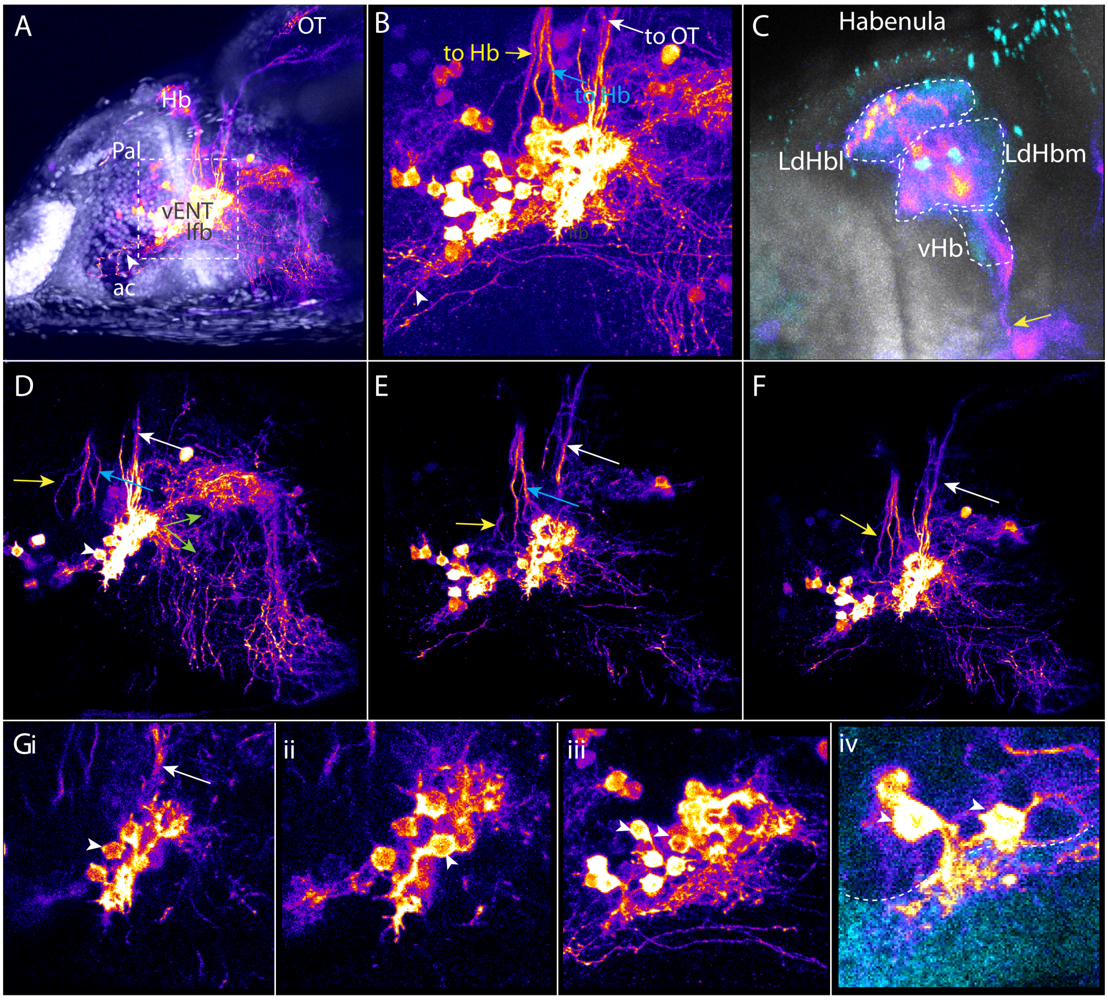

s1020t injected with UAS:TdTom/SV2/DAPI 5dpf

Figure 6.13: Connectivity of the vENT and RL (Part I). Lateral views of the forebrain from a 5dpf Gal4^{s1020t} larva injected with 5XUAS:TdTom and tol2mRNA at 1 cell stage and labelled with anti-RFP (FIRE LUT), SV2 (cyan) and DAPI (grey). Yellow and blue arrows show habenulopetal axons. White arrow shows axons ascending to optic tectum. Green arrows show axons innervating posterior tuberculum and intermediate hypothalamus. **(A)** RFP and DAPI nuclear staining shows the position of RFP+ neurons relative to the intraencephalic sulcus and the lateral forebrain bundle. Arrowhead shows vENT axons extending rostrally through the lateral forebrain bundle into the neuropil of the subpallium close to the ac. **(B)** Higher magnification view of larva in (A) visualising RFP only. View focussed on the vENT and RL (delineated by whisker box in “A”). Yellow and blue arrows label habenulopetal axons. White arrow shows axons ascending to optic tectum. **(C)** Close up of the habenula showing afferent terminals throughout the dHb and vHb. Mini z-projections**(D-F)** and single z- slices**(Gi-iv)** through caudal part of vENT/RL visualising RFP+ cells only. These z-projections show the connectivity of RL (white, blue and green arrows in D,E and G) and vENT(yellow arrows D-G). **(D)** RL cell bodies (white arrowhead) align along the anterior edge of a lateral neuropil. Processes exit this lateral neuropil dorsally to innervate the optic tectum (white arrow) and also project caudally into the neuropil of the posterior tuberculum and

ventrally down to the inferior hypothalamus (green arrows). Arrangment of RL cell bodies and lateral neuropil also shown in single z-slice in Gi and Gii. **(E)** Mini Z-projection through the medial part of RL showing habenula afferent processes leaving RL/caudal vENT. A group of habenulo-afferent processes leave RL from the dorsal end of a dense tangle of processes that form a more medial neuropil (blue arrow E and Giii) while some others seem to come from more ventral parts of the vENT(yellow arrows D-F). Some RL cell bodies lie anterior to the lateral neuropil (arrowheads in Gi) but others (Gii) seem sandwiched between the lateral and medial neuropil. Arrowhead in Gii shows a neuron with slightly different morphology that lies parallel to the lateral neuropil and has a single short fat process. This larvae also shows the arrangement of vENT neurons(arrowheads in Giii and iv) that extend processes into a more medial neuropil. The arrangement of these two neuropils is further elaborated on in the accompanying Figure 5.10b.

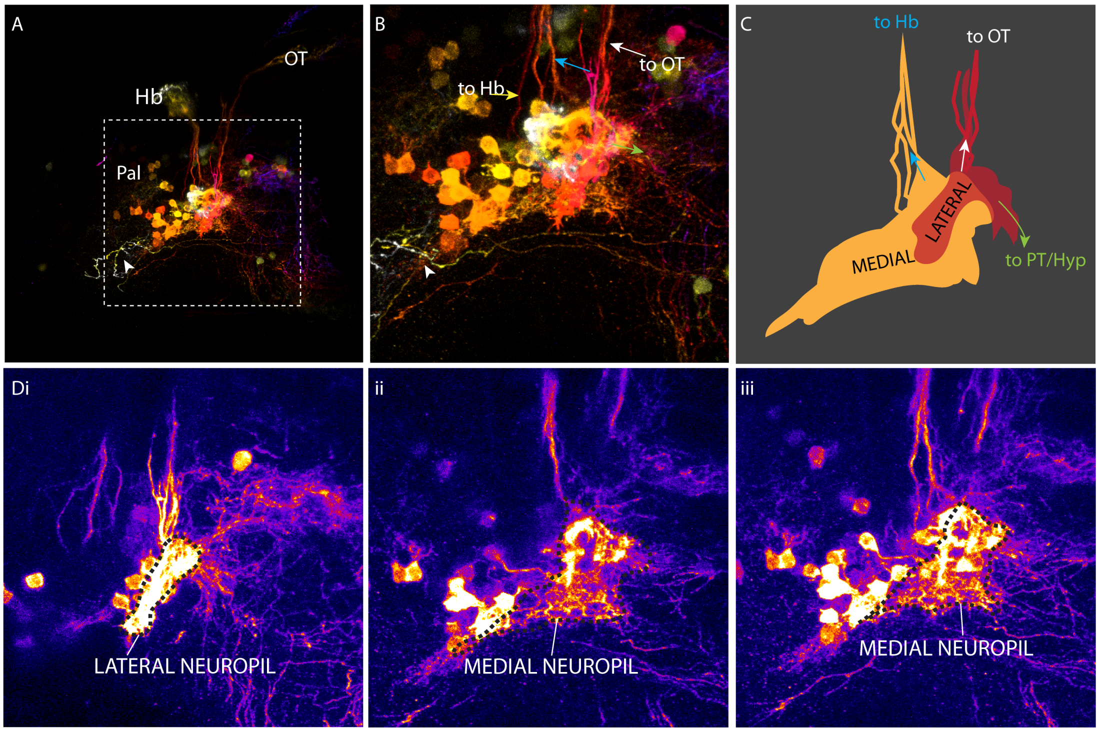

s1020t injected with UAS:TdTom/SV2/DAPI 5dpf

Figure 6.14: Processes from vENT and RL neurons create two neuropil laminae at their caudal edge. This figure shows the same larvae as Figur 5.10a **(A)** Z-projection of RFP channel with false colouring to show different medio(yellow/white)-lateral(purple/red) position of cells. Arrowhead shows vENT axons extending rostrally through the lateral forebrain bundle into the neuropil of the subpallium close to the ac. **(B)**High magnification of whisker box in (A). Yellow and blue arrows show habenulopetal axons. White arrow shows axons ascending to optic tectum. Green arrows show axons innervating posterior tuberculum and intermediate hypothalamus. **(C)** Schematic of the two lamina neuropils formed by RL and vENT neurons. Axons leave the lateral neuropil(red) and ascend to the optic tectum and project caudally to posterior tuberculum and intermediate hypothalum.

Habenulopetal axons leave the medial neuropil(orange) dorsally(blue arrow). **(Di-iii)** Single z- slices through caudal part of vENT/RL visualising RFP+ cells only show the shapes of the lateral neuropil(Di) and medial neuropil(Dii and Diii) circled with a black dashed line.

Figure 6.15 shows a larva with more mosaic labelling of the vENT than those shown earlier, this allows better discrimination of individual cell morphologies within this nucleus. Some cells located in the dorsal part of the vENT close to the intraencephalic sulcus (yellow arrowheads in Figure 6.15 D) seem to be the source of the habenula afferents (yellow arrows in Figure 6.15). These axons seem to ascend directly to the habenula rather than first entering through the medial neuropil similar to the more rostral group described in Fig 6.13 and 6.14 above. Their axons innervate the right habenula fairly broadly and terminals are present in all subnuclei although innervation of the rostral part of the RdHbm seems the strongest. It was not possible to see the innervation pattern in the left habenula in this larva.

This larva also has strong labelling of a neuron whose dendrites run parallel to the caudal edge of the vENT (white arrowhead in Figure 6.15D). This neuron has a similar morphology to the cell sandwiched between the medial and lateral neuropil in Figure 6.13 Gii with a thick dendritic process, like the tap root of a tree. Just before the tip of this thick process splits into two this neuron extends an axon that grows dorsally to innervate the optic tectum (white arrow in Figure 6.15). When the serial optical sections of this specimen are checked sequentially it is possible to see that the thick process originating from this cell runs dorso-ventrally along the very caudal edge of the vENT, and the small processes that come off this major branch enter the neuropil of the optic tract.

Another cell of interest in this larva has its cell body located laterally within the vENT, just at the telencephalic/diencephalic border (Figure 6.15, box in C; close up in F). This neuron is located quite ventrally within this part of the vENT, very close to the lateral forebrain bundle. This neuron may be bipolar as when serial optical sections are checked, one process seems to leave the cell body dorsally and meet the habenulo-petal cells (yellow arrowhead in Figure 6.15D) and another process ventrally towards the lateral forebrain bundle. After entering the lateral forebrain bundle the thick principle process splits into four branches, two processes turn rostrally within the lateral forebrain bundle and continue until they are level with the tip of the lateral migrating vENT cells. These processes have a simple morphology and show little further branching. The other two processes turn caudally and then dorsally to cover the medial lamina neuropil. Their processes extend to the caudal edge of the vENT and show further branching. With DAPI nuclear labelling it is possible to see cell bodies embedded within the lateral forebrain bundle that this cell may contact. Please see the the latter part of this chapter for a description of the location of pallial, dopaminergic and serotinergic afferent processes relative to the vENT/RL.

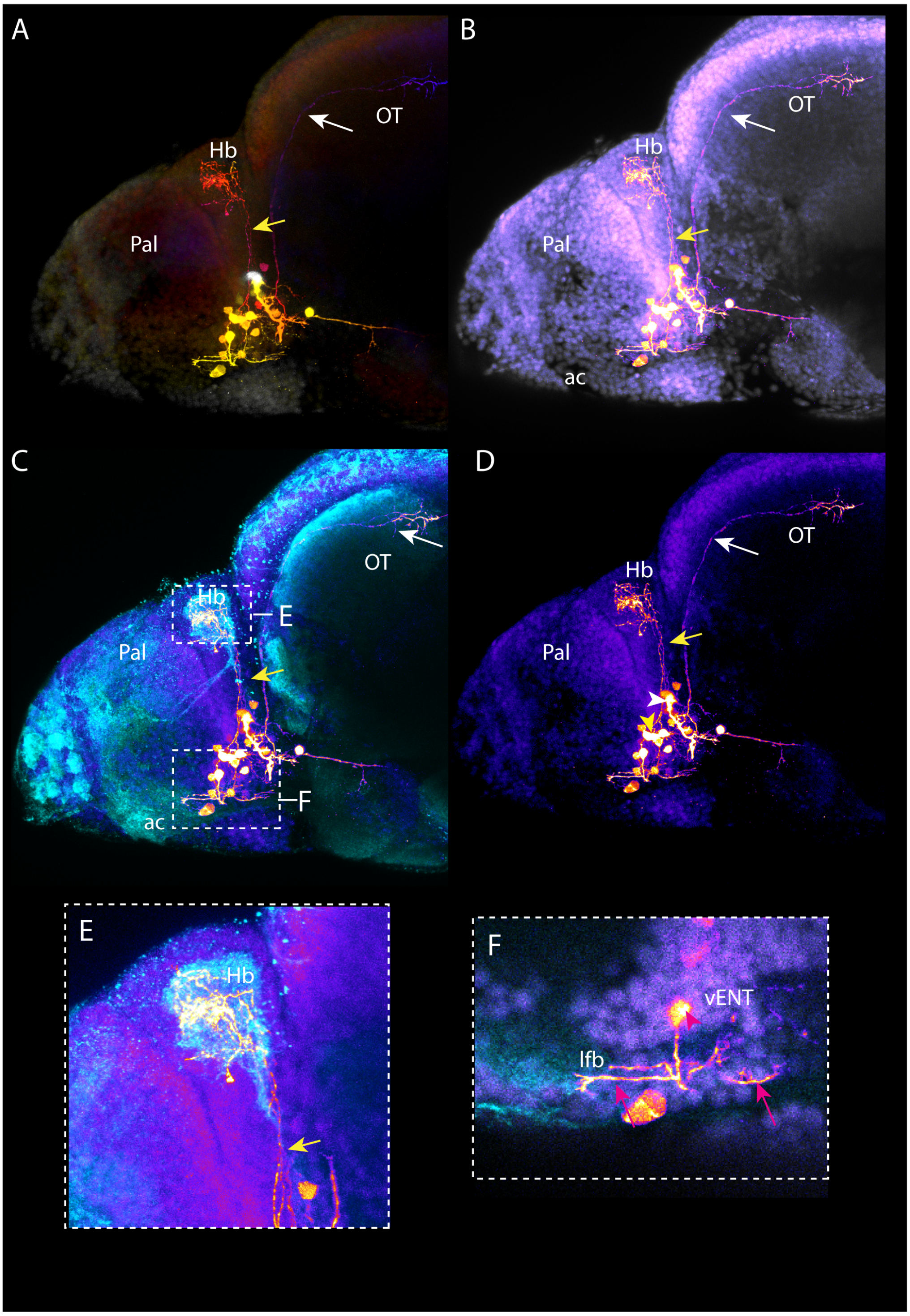

s1020t injected with UAS:TdTom/SV2/DAPI 5dpf

Figure 6.15: Connectivity of the vENT and RL (PartII). Lateral views of the left side of the forebrain and anterior midbrain of a 5dpf Gal4^{s1020t} larva injected with 5XUAS:TdTom and tol2mRNA at 1 cell stage and labelled with anti-RFP (FIRE LUT) , SV2 (cyan) and DAPI (grey). (A) Z-projection of RFP channel with false colouring to show different medio-lateral position of cells. Yellow arrow labels habenulopetal axons (E) Close up of the habenula (dashed box in C) showing afferent terminals throughout the dHb and vHb. Yellow arrow marks the tHc (F) The dendrites (pink arrows) of a single vENT neuron (pink arrowheads) extending through the lateral forebrain bundle (lateral forebrain bundle delineated by SV2 labelling) and back into the medial laminae of the vENT neuropil. DAPI nuclear staining shows that some cells are present embedded within this fibre tract and the vENT dendrites seem to contact some of these cells.

6.7 Summary of observations from mosaic labelling experiments. (Schematised in Figure 6.16 & 6.17)

- Habenular afferent neurons in the vENT and RL can innervate multiple habenular subnuclei. (Figures: 6.8, 6.9, 6.12, 6.15)
- Habenular afferent neurons from vENT/RL show asymmetric innervation of habenular subnuclei similar to other afferent populations such as mitral cells (Miyasaka et al., 2012) and the parapineal (Concha et al., 2003). (Figures: 6.8, 6.9, 6.12, 6.15)
- Larvae that show habenular innervation all have neurons labelled in the most anterior part of the diencephalon just caudal to the intraencephalic sulcus in the prethalamus/prethalamic eminence. (Figure 6.11)
- Neurons within the vENT/RL anlage innervate: the subpallium, the habenula, the optic tectum and caudal diencephalic regions such as the posterior tuberculum, preglomerular complex and anterior hypothalamus. (Figures: 6.13, 6.14)
- Many habenula-afferent neurons within RL and vENT show dendritic innervation of AF4. (Figures: 4.5, 6.8, 6.12,6.13-15)
- A subclass of RL neurons innervate the optic tectum. (Figure 6.13, 6.14-16)
- Some vENT neurons extend processes ventrally into the lateral forebrain bundle. (Figures 6.13-16)

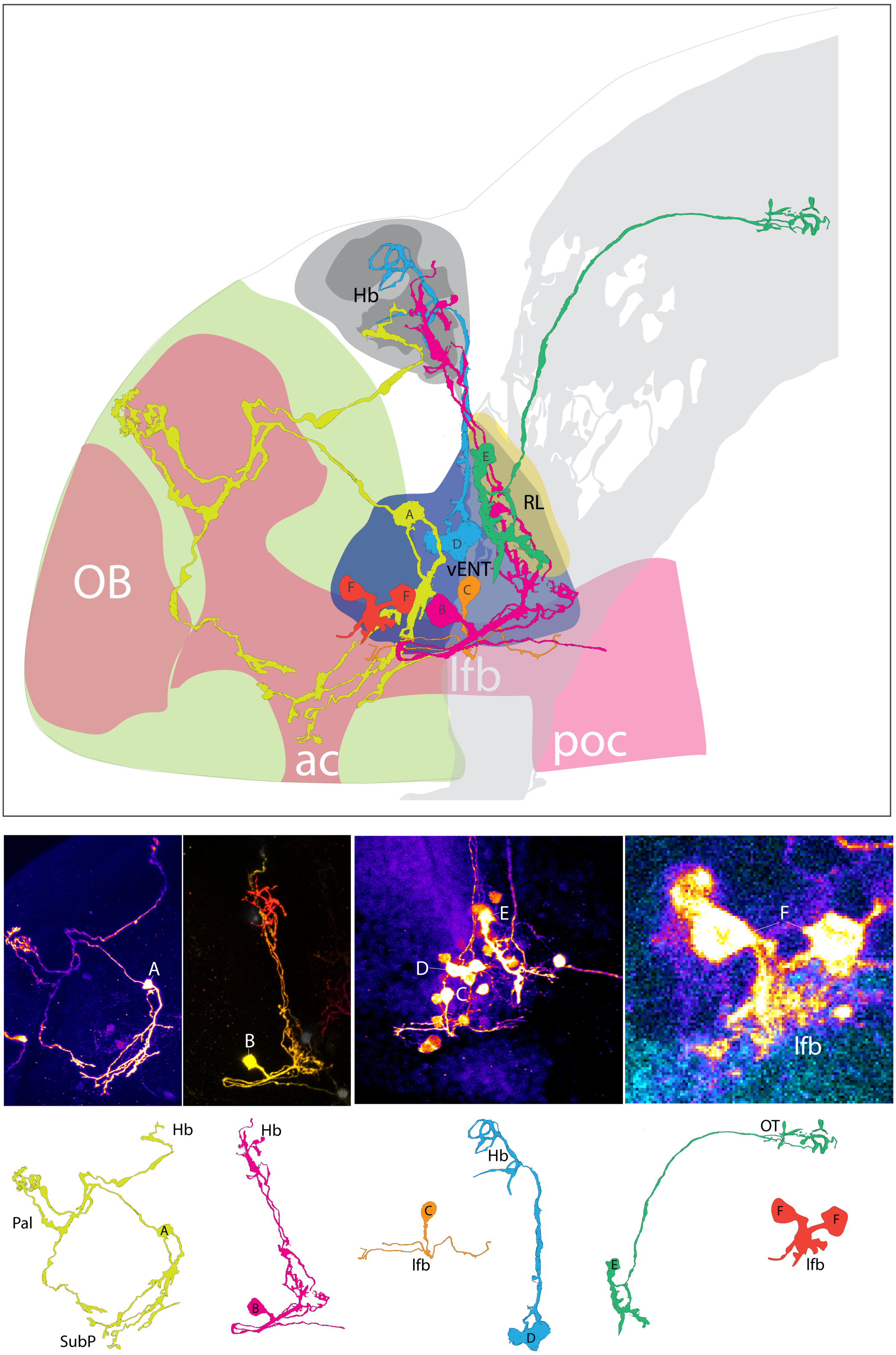

Figure 6.16: Morphologies of individual vENT and RL neurons. (**Top**) Traced neurons superimposed onto schematized brain of a 4dpf larvae viewed laterally. This schematic shows the relative positions of vENTand RL and the

rough positions of mosaically labelled individual neurons within these structures. (**Middle**)original images used to trace the cells. (**Bottom**)Traced cells in isolation showing their morphology. The connectivity of these neurons, where known, is shown.

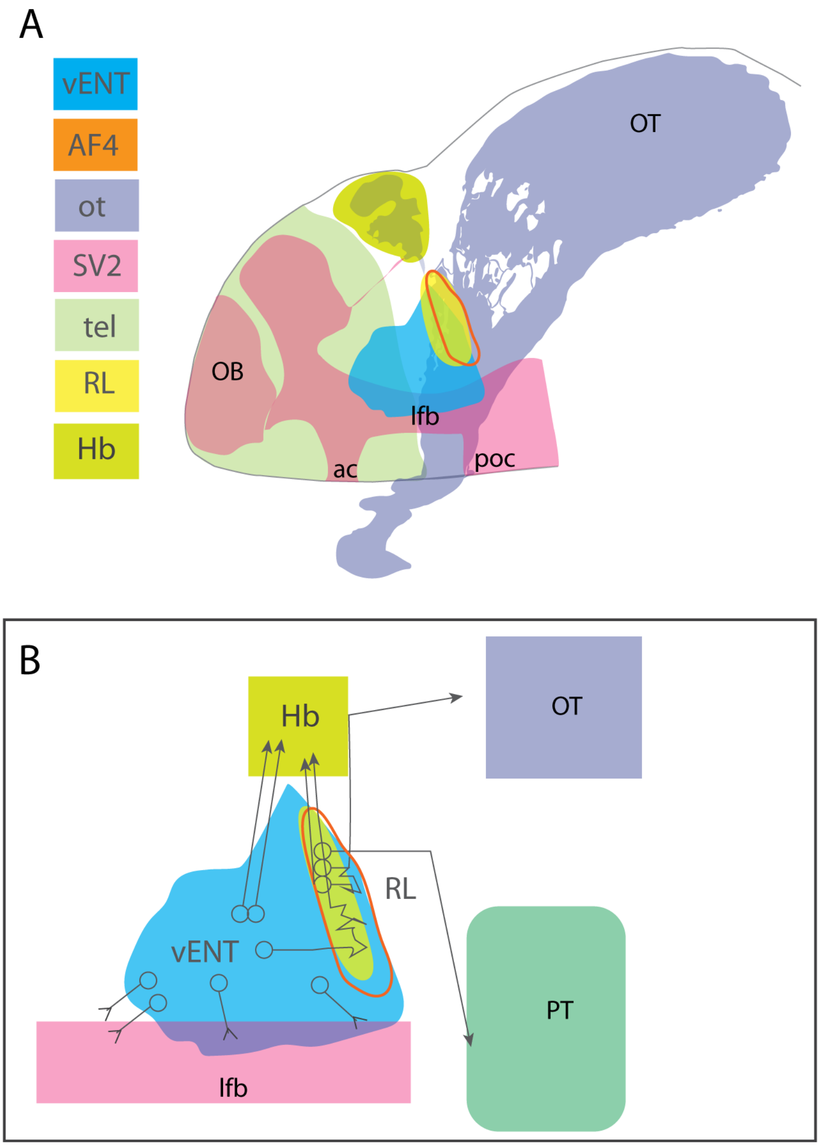

Figure 6.17: Schematic summarising relative position and connectivity of vENT and RL. (A)Schematic showing a lateral view of a 4dpf larva showing the relative positions of AF4, RL and vENT at this stage of development. (B) Circuit diagram summarising and schematising the connectivity of vENT and RL derived from mosaic labelling experiments presented in this chapter. The neuropil areas are presented as scribbled lines. Different cell types that project to the habenula either directly or via the medial neuropil(AF4) are depicted as hollow circles.

6.8 Future Perspectives

Both mosaic labelling approaches used in this thesis to describe vENT and RL neurons have their drawbacks. For the Crispr switching approach the efficiency of labelling these later born neurons is fairly low, though the level of mosaicism is high. For the more straightforward Gal4/UAS the amount of mosaicism achieved is not sufficient to describe the morphology of individual neurons though the efficiency of labelling vENT/RL neurons is much higher than with the Crispr based method. Perhaps with future labelling techniques a more harmonious balance between mosaicism and efficiency could be struck. If/when it arrives it would be good to register the mosaically labelled brains to a standard brain using the algorithms developed by the Burgess(Randlett et al. 2015) lab, as well as introducing some synaptic markers to the injection mix. Coupled with functional imaging of the vENT/RL and the habenula this would start to build a more detailed model of the function and cytoarchitecture of these afferent nuclei.

6.9 The *vENT* receives serotonergic innervation from the raphe

The vENT has been shown to be the major source of afferents to the vHb in adult zebrafish (Amo et al.,2014). The main efferent target of vHb neurons is the median raphe (MR) in the ventral hindbrain (Amo et al., 2010). Amo et al (2014) showed that the vENT in the adult zebrafish receives serotonergic innervation. This suggests the possibility that there exists a vHb-MEDIAN RAPHE-vENT circuit where serotonergic signalling from MR could feedback onto the vENT and thus vHb, or perhaps modulate vENT input to the vHb. To explore this possibility, I examined the output of the MR by using already characterised genomic elements that label the projection neurons of the MR.

Tg(Pet1:KALTA4) labels serotonergic raphe neurons

I used the *pet1* promoter (plasmid provided by Bally-Cuif lab) and made a Tg(Pet1:KalTA4) line using the tol2 gateway system (Kwan et al.,2007). Lillesaar et al., (2009) beautifully characterised the serotonergic raphe projections in larval, juvenile and adult zebrafish using a GFP transgenic line driven by this same regulatory elements of the *pet1* gene, which specifically labels the raphe population of serotonergic neurons. To use this transgenic to label individual raphe neurons and look at their projection patterns and morphologies, The Tg(Pet1:KalTA4) when crossed to the Tg(cry1:eGFP:UAS:RFP) line similarly labels the median and inferior raphe and ventro lateral serotonergic groups described in the GFP transgenic in Lillesaar et al. (2009). I have assessed the full expression pattern of Tg(Pet1:KALTA4) fish at larval stages(Figure 6.18) and then went on to use the transgenic line to mosaically label serotonergic raphe neurons. As the original description of the full raphe projections is so comprehensive in the Lillesaar paper (2009) I will focus predominantly on the single cell results of pertinent to this thesis.

In Pet1KalTA4/UASRFP larvae, large numbers of RFP+ fibres course into the telencephalon via the forebrain bundle (Figure 6.18 A-A' and C–C'). As described in Chapter 5 of this thesis, the vENT surrounds the forebrain bundle and elaborates processes within the forebrain bundle. The vENT, although not specifically mentioned or labelled in Lillesaar et al., 2009, is likely to receive serotonergic innervation from the raphe, as sections through the adult telencephalon show dense GFP+ processes within the ventrolateral telencephalon (Lillesaar et al., 2009 Fig7B-C). Amo et al., 2014 also mention this reciprocal median raphe-vENT connection in their paper. On this evidence, it seems likely that there is MR innervation of the vENT. To examine this in more detail I separated the ventral view shown in Figure 6.18 C-C' into individual z-slices. In the resulting slices, it is easier to observe that RFP-positive (probable serotonergic) fibres travelling in the forebrain bundle appear to defasiculate within the PO/ vENT region (inside dashed white box Figure 6.19iii-vii). This may indicate the sprouting of collaterals and the formation of synapses with vENT neurons in this neuropil.

The positions of the raphe terminals relative to the neuropil domains described in the vENT in the previous section seem promising and suggest that SR neurons could feedback onto the vENT. To confirm this, the next step would be to label the SR processes with a presynaptic marker such as syn-GFP and look at whether synapses are present within the lateral forebrain bundle and other neuropil areas surrounding the vENT, where the dendritic processes of vENT cells are known to reside. To look at the projection patterns and morphology of individual serotonergic raphe neurons Tg(Pet1:KALTA4):Tg(cry1:GFP:UASRFP) embryos were injected with 5XUAS:EGFP (Zhang et al., 2012) at 1 cell stage.

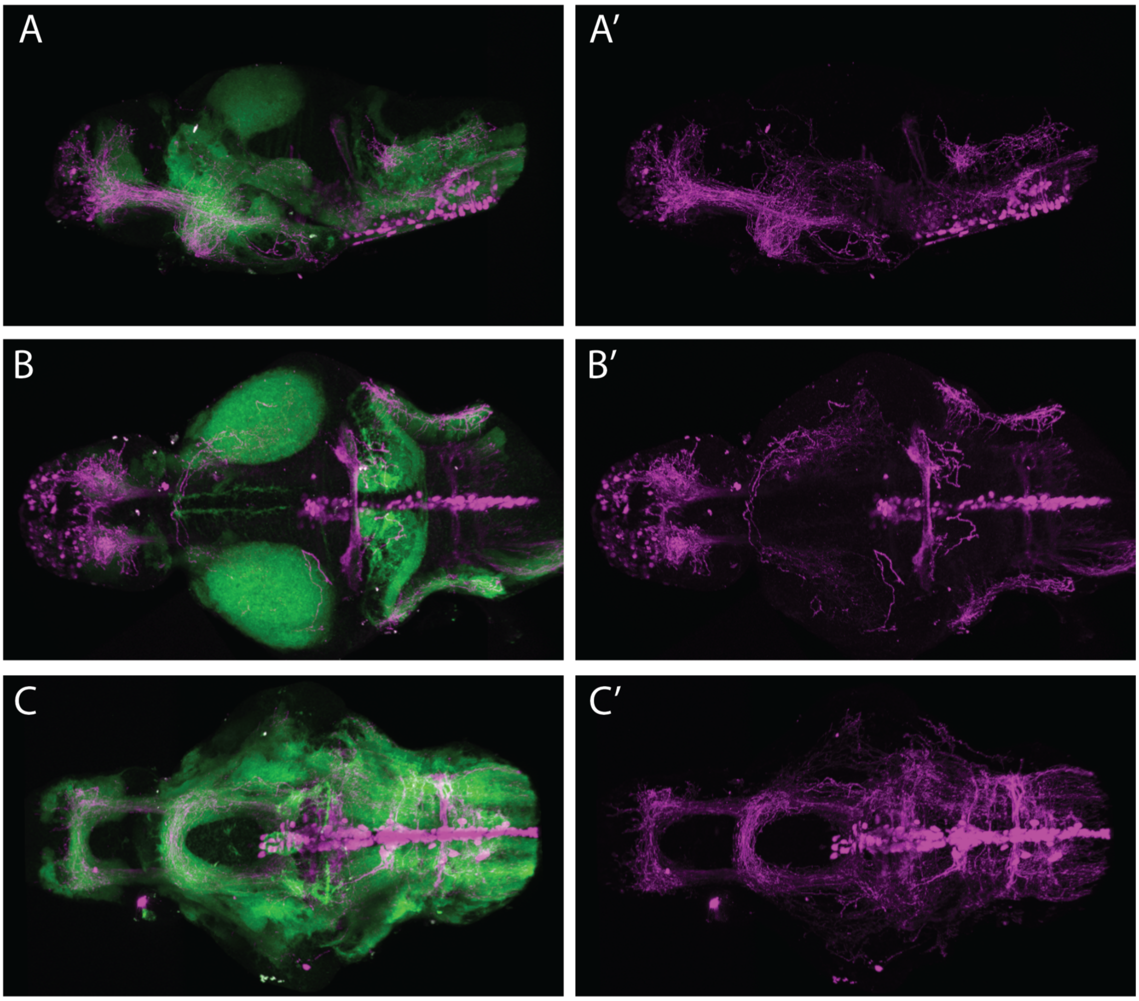

Pet1:KalTA4:UAS:RFP/SV2 4dpf lateral, dorsal and ventral views

Figure 6.18: Tg(Pet1:KALTA4) labels serotonergic raphe neurons. Lateral (A-A'), Dorsal (B-B') and Ventral views (C-C') of brains of 4 dpf Tg(Pet1:KALTA4)/UAS:RFP transgenic larvae labelled with anti-RFP (magenta) and anti-SV2 antibodies (green).

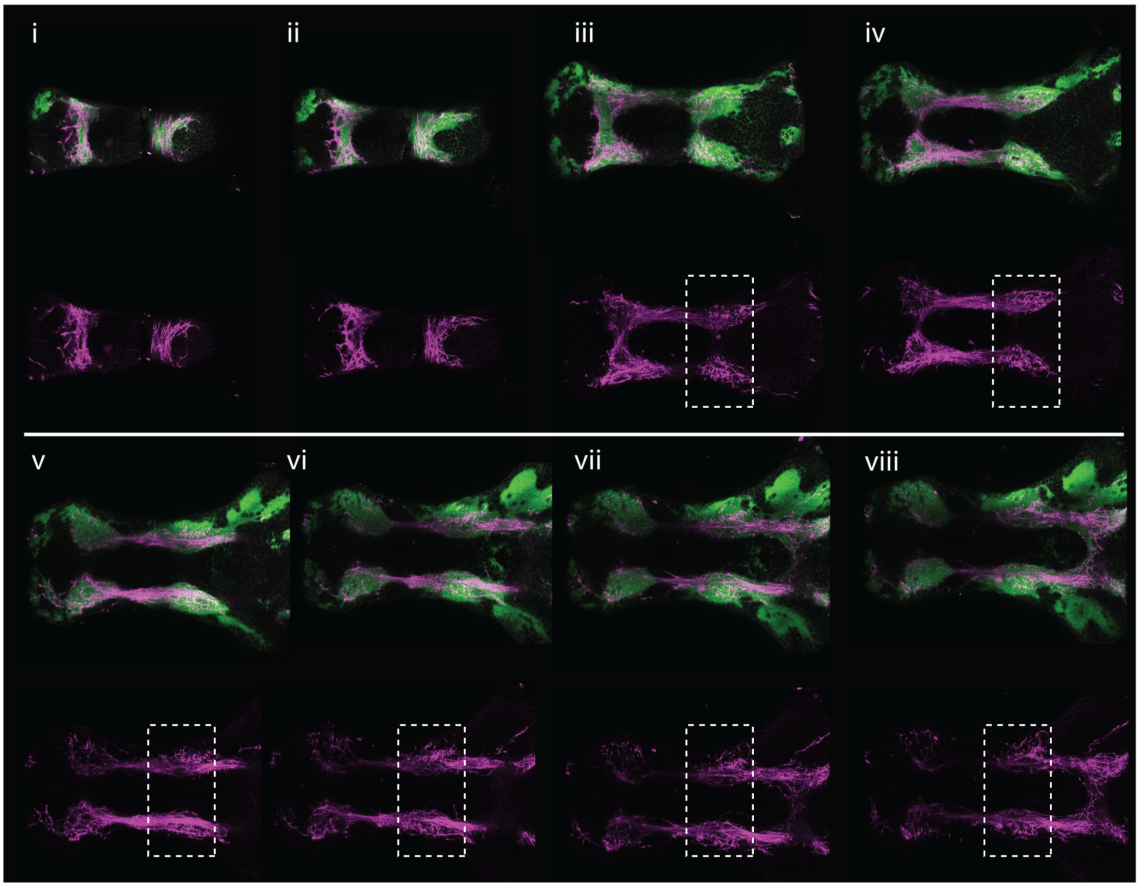

Figure 6.19: Ventral view of of a 4 dpf Tg(Pet1:KALTA4)/UAS:RFP larva shows serotonergic processes densely innervating the forebrain. Ventral view of the forebrain of a 4 dpf Tg(Pet1:KALTA4)/UAS:RFP transgenic labelled with anti-RFP (magenta) and anti-SV2 antibodies (green), presented as serial sections from ventral (i) to dorsal levels (xii). Dashed white box indicates approximate level of vENT relative to serotonergic fibres coursing in the lateral forebrain bundle.

Mosaic labelling of serotinergic vENT afferent neurons

These preliminary results indicate that serotonergic MR neurons do elaborate terminals within the neuropil areas associated with vENT neurons. These serotonergic connections could provide feedback onto the vENT-vHb-MR circuit. Figure 6.20 shows three examples of this possible vENT innervation. Figure 6.21 by contrast shows an MR neuron that also innervates the telencephalon but does not send any collaterals to the vENT. A brief description of each larvae is given below.

1) **Larva A** is very mosaically labelled, showing a single MR process visible running rostrally in the forebrain bundle. At the caudal end of the lateral forebrain bundle this process branches within the neuropil area into which many vENT neurons extend processes. After forming this triangular elaboration, the two branches of this MR axon both enter the telencephalon where one turns dorsally into the pallial neuropil and the other arborises throughout the ac and both contra and ipsilateral subpallial neuropil.

2) **In Larvae B**, several MR neurons are labelled. Close examination of the area of the lateral forebrain bundle at the level of the vENT reveals a tangle of GFP-positive processes that are elaborated in the telencephalic neuropil just where the lateral forebrain bundle enters the subpallium and meets the tract of the anterior commissure. Many vENT neurons in the rostral and ventral parts of this nucleus also extend processes within this subpallial neuropil domain (Figure 6.20 B). A single z-section through the dorsal part of the lateral forebrain bundle at the level of the vENT (Figure 6.20 Biii) shows that the GFP-positive fibres run in the dorsal part of the lateral forebrain bundle, some processes can also be seen terminating in the lateral part of the dorsal lateral forebrain bundle (arrows in Figure 6.20 Biii). The dorsal part of the lateral forebrain bundle is covered by a neuropil formed by the dendritic processes of vENT cells (See Figure 6.13-14).

3) **Larvae C**, viewed dorsally, shows the DV extent to which serotonergic fibres innervate the telencephalon (Figure 6.20 C FIRE LUT). These processes extend up into the dorsal pallium where one process shows a tiny teardrop shaped terminal. Within the lateral forebrain bundle at the level of the vENT collaterals branch off the main processes that innervate the pallium are also present in this specimen.

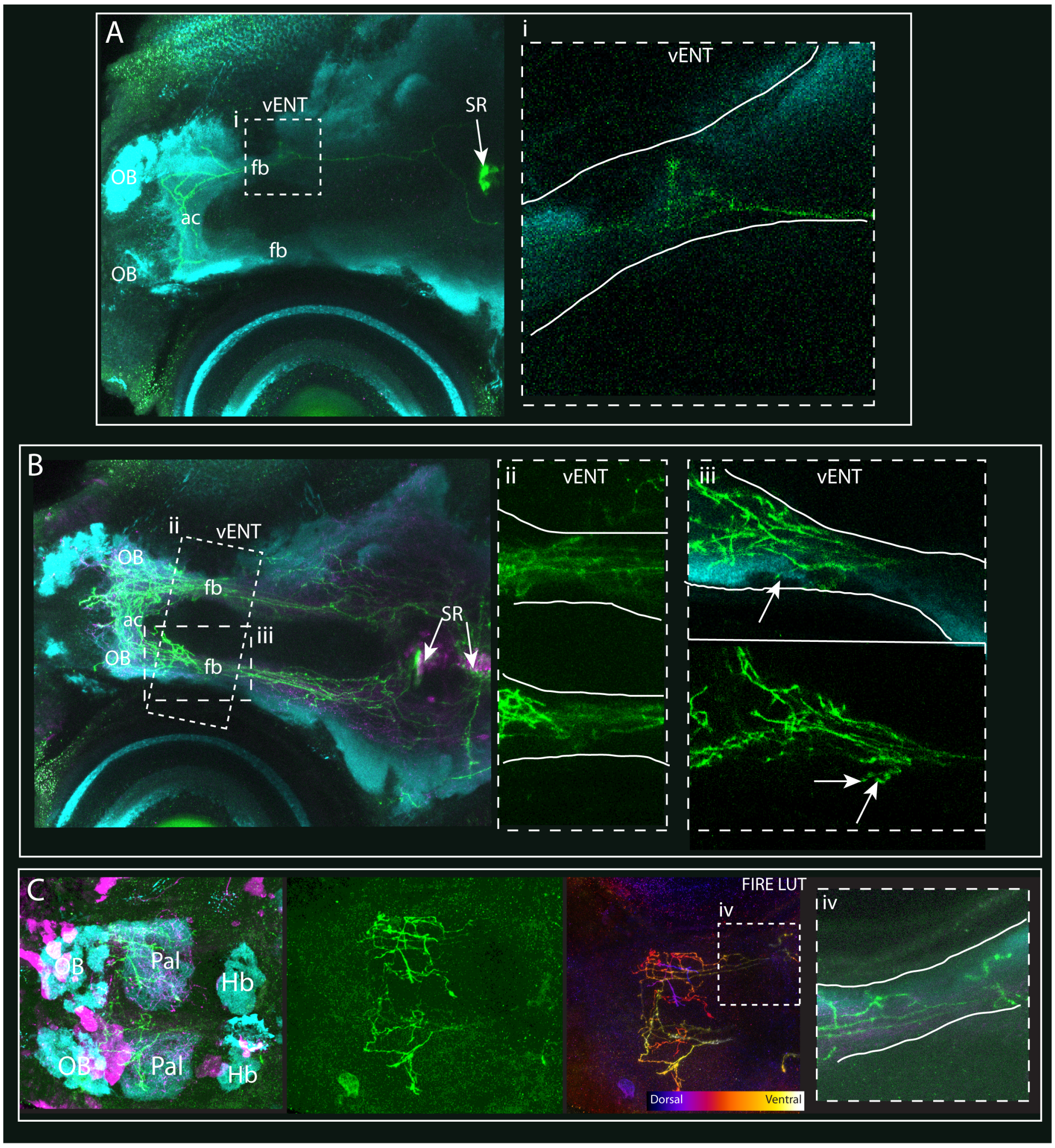

Petl:KalTA4:UASRFP injected with UAS:EGFP/SV2 4dpf

Figure 6.20: Mosaic labelling of raphe neurons: vENT. Ventral (A and B) and dorsal (C)views of the head of a 4 dpf Tg(Pet1:KALTA4):UAS:RFP transgenic larva that was injected with UAS:EGFP at 1 cell stage. The specimen was labelled with anti-RFP (magenta),anti-GFP (green) and anti-SV2 (cyan) antibodies. (i-iii) close up views of the lateral forebrain bundle at the level of the vENT (iii) Fire LUT spatial coding to show the DV position of GFP+ serotonergic terminals in the telencephalon.

The larva in Figure 6.21 shows the morphology of a single MR neuron that does not send collaterals to the vENT. This neuron extends a process laterally to join the lateral fiber bundles and then grows rostrally to innervate the telencephalon and olfactory bulbs. This projection pattern suggests the neuron is positioned in the dorsal part of the MR, based on Lillesaar's description (2009):

> "From the MR, two main projection patterns were observed: the projections of eGFP- positive neurons located ventrally were directed toward rostrally immediately after leaving the raphe area, whereas those of neurons located dorsally were initially directed laterally to join lateral fiber bundles. Based on retrograde tracing in adult brains (see below), the main target areas of these two fiber tracts are likely to be hypothalamus and forebrain, respectively."

Another cell in the VL raphe population is labelled directly lateral to this MR neuron. The processes of this cell are fainter but can be followed anteriorly to the posterior tuberculum. If we focus on the telencephalon (inset Figure 6.21) we can see that this axon branches into three rami just where it enters the telencephalon through the lateral forebrain bundle. These branches spread throughout the neuropil in the pallium and form large end terminals within the pallial neuropil, and also within the posterior part of the olfactory bulb. A faint process can be seen coursing through the ac and into the contralateral telencephalon (arrow in Figure 6.21iii).

Some strange oval bright globules are present in the RFP (asterisks in Figure 6.21 ii), These are most likely tastebuds as these have been shown to use serotonin as a neurotransmitter in several species of vertebrates, including several teleost species (Kim and Roper., 1995. Eram and Michel.,2005. Toyoshima et al., 1984).

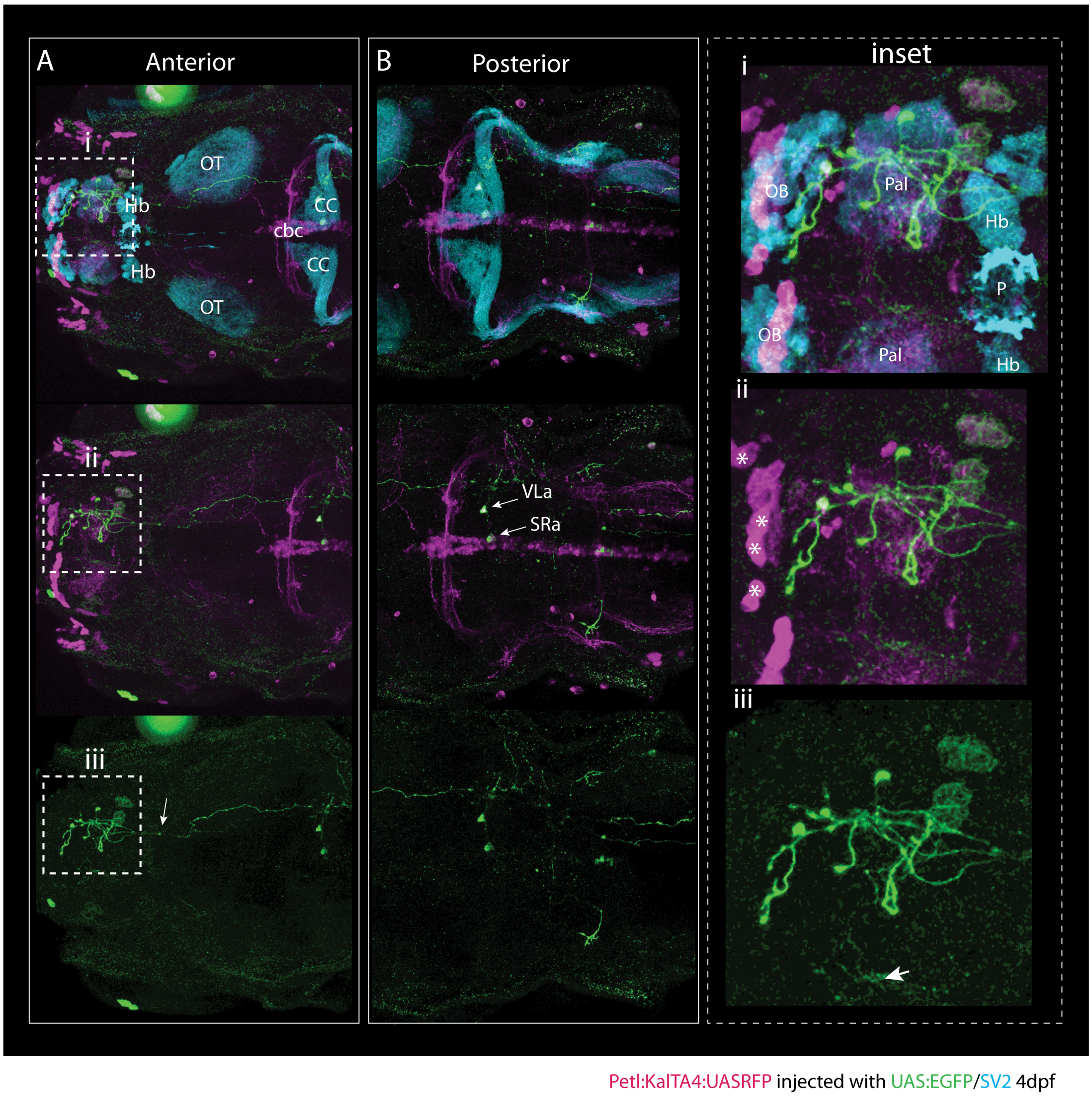

Figure 6.21 Mosaic labelling of raphe neurons: Median Raphe. Dorsal views of the head of a 4 dpf Tg(Pet1:KALTA4)/UAS:RFP larva injected with UAS:EGFP at 1 cell stage and labelled with anti-RFP magenta),anti-GFP (green) and anti-SV2 (cyan) antibodies. Data is presented in two parts (anterior brain and posterior brain and in various combinations of staining: SV2/RFP/GFP (top), RFP/GFP only (middle) and GFP alone (bottom). The inset shows an area of the telencephalon (indicated by the dashed area in the left hand column) in detail.

In summary, the preliminary results from my mosaic labelling of serotonergic neurons do show a potential reciprocal projection from the median or superior raphe to the vENT. However, this branching within the lateral forebrain bundle at the level of the vENT is not shown by all median raphe neurons that innervate the forebrain.

6.10 Dopaminergic neuron somata surround AF4 and AF2 and elaborate processes into these arborisation fields.

In the rat reciprocal, dopaminergic projections exist between the ventral tegmental area and the lateral habenula (Jhou et al. 2009; Hong et al. 2011). The ventral tegmental area also provides indirect feedback to the lateral habenula via its afferent pallidal and striatal nuclei. The zebrafish does not have DA releasing areas that are homologous to the VTA and substantia nigra pars compacta (Amo et al., 2014). Instead, zebrafish have two clusters of dopaminergic neurons in the posterior tuberculum and posterior tuberal nucleus (Rink and Wullimann., 2002). To look at dopaminergic innervation of the zebrafish habenula and the vENT/RL I used the *Tg(slc6a3:EGFP)* transgenic line that labels dopaminergic but not noradrenergic neurons (Xi et al., 2011).

The *Tg(slc6a3:EGFP)* transgenic line expresses GFP under the control of cis-regulatory elements of the dopamine transporter (DAT) gene *slc6a3.* GFP+ neurons are present in this transgenic line in the olfactory bulb, pallium, preoptic area, prethalamus, pretectum and throughout the ventral diencephalon including the posterior tuberculum and hypothalamus (Figure 6.22 A-A''). I found no direct projection from GFP+ dopaminergic neurons to the habenula at 3dpf in the *Tg(slc6a3:EGFP)* line. This is in contrast to a study by Kastenhuber (2010) where dopaminergic and noradrenergic neurons were labelled with an anti-TH antibody where some direct dopaminergic projections to the habenula can be observed in their data but were not commented on in this study. The anti-TH antibody also labels noradrenergic neurons so these TH+ fibres could derive from the locus coeruleus, as in mammals both the MHb and LHB receive monoaminergic input from this nucleus (Herkenham & Nauta., 1977; Wilson & Bianco., 2009).

Dopaminergic neurons and their processes are visible in the prethalamus/prethalamic eminence in the *Tg(slc6a3:EGFP)* line. The cell bodies of dopaminergic GFP+ neurons surround the AF4 and AF2 neuropil areas and elaborate processes within these arborisation fields. These AFs are also innervated by RL and vENT neurons and so could make contact with these habenulo-afferent nuclei and provide indirect feedback to the habenula from dopaminergic signalling centres. Additionally, a very dense network of GFP+ neurons and their processes are visible in the posterior tuberculum. This area is also contacted by RL/vENT neurons (Figure 6.13 and 6.14).

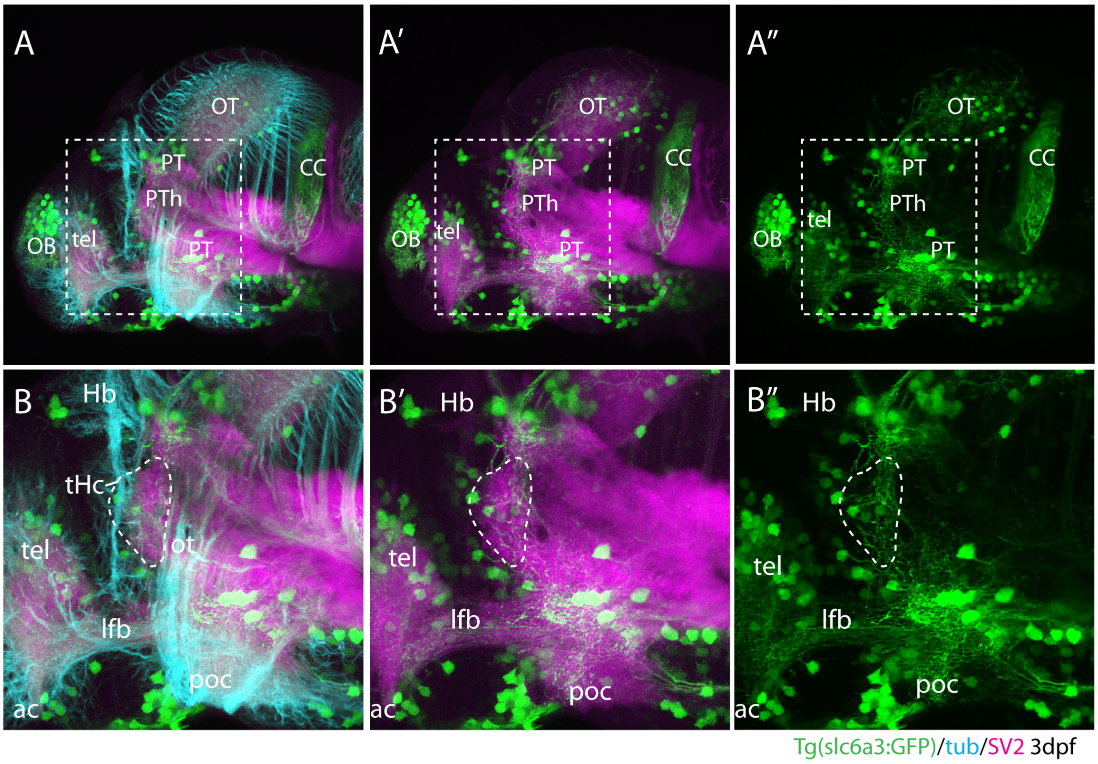

Figure 6.22: Dopaminergic neurons surround AF4 and AF2 and elaborate processes into these arborisation fields.
A-A'' Lateral view of a 3dpf Tg(slc6a3:EGFP) larvae labelled with anti-GFP(green), anti-SV2(pink) and anti-tubulin(cyan) antibodies. B-B" close-up of forebrain area delineated by whisker box in A-A". Dopaminergic neuron somata surround the arborisation fields of the retino-fugal pathway and elaborate processes into these neuropil domains (labelled with SV2). AF4, also targeted by RL and vENT neurons is circled with a dashed white line (B-B"). AF2 another arborisation field innervated by RL and vENT neurons also shows strong dopaminergic innervation.

Figure 6.23 shows the schematic summarising vENT and RL circuitry from Figure 6.17 with the potential serotonergic, dopaminergic and pallial inputs discussed in this chapter to vENT and RL added.

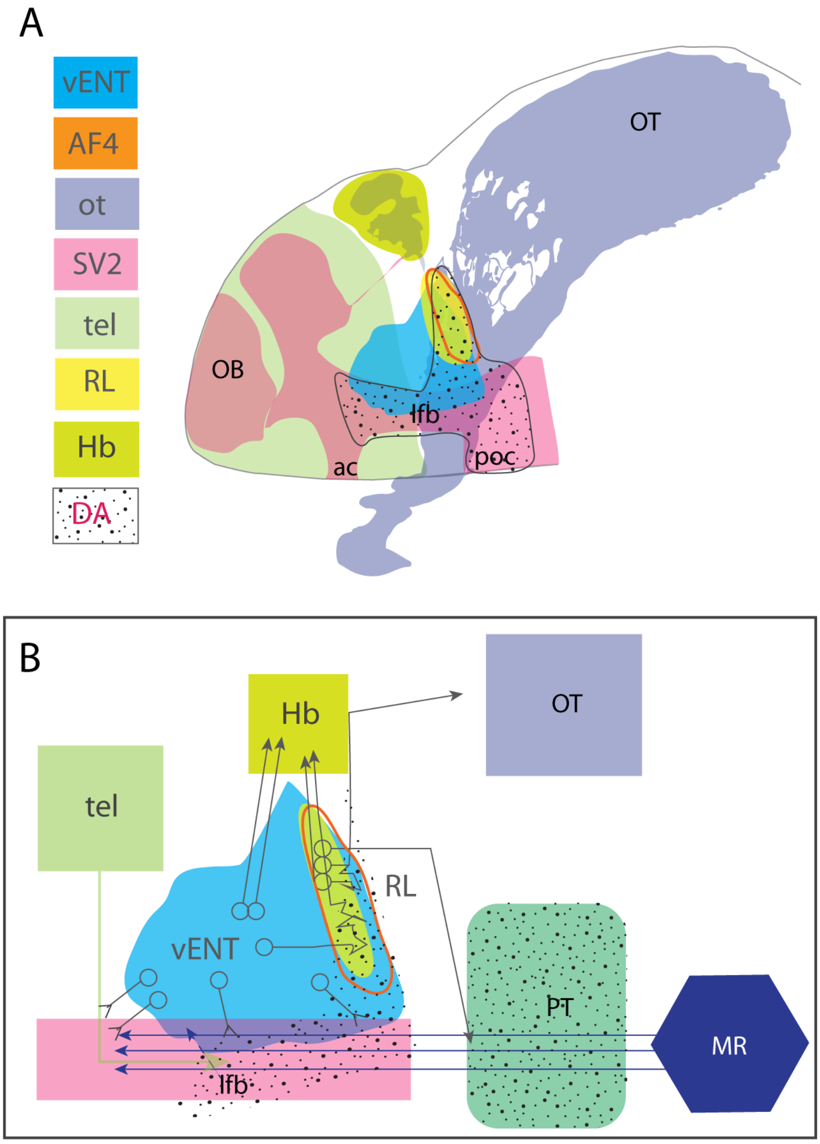

Figure 6.23: Schematic summarising pallial, serotonergic and dopaminergic afferents to vENT and RL. (A)Schematic showing a lateral view of a 4dpf larva showing the relative positions of AF4, RL and vENT at this stage of development. (B) Circuit diagram summarising and schematising the connectivity of vENT and RL derived from mosaic labelling experiments presented in Chapter 5. Different cell types that project to the habenula either directly or via the medial caudal neuropil (AF4) are depicted as hollow circles. Pallial, serotonergic and dopaminergic neurons all elaborate terminals within the neuropil areas surrounding vENT and RL. As dendrites of vENT and RL neurons also ramify through these same neuropil, vENT/RL neurons are well placed to act as a relay centre providing important input/feedback onto habenula neurons from dopaminergic, serotinergic and telencephalic centers.

In conclusion, the neuropil areas surrounding the vENT and RL that include AF4, AF2, the lateral forebrain bundle and the post-optic commissure/posterior tuberculum seem like an interesting area for future study. With input from serotonergic, monoaminergic, retina and pallium into these neuropils the surrounding vENT and RL neurons that also ramify processes within them (See 6.13-15) are well placed to integrate and relay information from all these centres to the habenulae.

Chapter 7. Discussion

In this thesis, I have set out to define afferents of the habenula in both larval and adult zebrafish. To achieve this goal, I have used a combination of DiI tract tracing, kaede photoconversion and analysis of transgenic lines in which habenula afferent neurons are labelled. These experiments have revealed that the main afferent nuclei to the habenula are the olfactory bulb (to right habenula), subpallium, vENT, parapineal (to left habenula), nucleus rostrolateralis, preoptic area, posterior tuberculum, posterior hypothalamic lobe and median raphe (Turner et al., 2016). This thesis has mainly focused on the identification and characterisation of two of these afferent areas: the ventral entopeduncular nucleus and the nucleus rostrolateralis. I have also made and characterised the serotinergic Pet1:KalTA4 transgenic line to try to identify reciprocal superior/median raphe projections back to the vENT.

Additionally, I have shown that both in adults (Turner et al., 2016), and larvae, using Et(gata2:EGFP)^{bi105} which broadly labels the pallium, that no pallial afferents innervate the habenula, as had previously been suggested by Hendricks and Jesuthasan (2007). I have also used this transgenic line to establish a method to mosaically label individual neuronal morphologies within a GFP transgenic line using CRISPR/Cas9. I have used this and other methods to mosaically label neurons within vENT and RL and characterise the organisation of these afferent nuclei, the morphology and connectivity of the different cell-types present in these nuclei and attempt to describe any asymmetries in their innervation of the habenula.

Apart from the major technical challenge of mosaically labeling habenular afferent neurons, which I have alluded to earlier in this thesis, another problem has been the physical proximity of the vENT and RL nuclei at larval stages and their controversial homologies in both the larvae and adult. As such this discussion will focus on the possible homologies and functions of these two habenulopetal nuclei. I have separated the discussion into two sections, “vENT” and “RL”.

7.1 The zebrafish vENT is the homolog of the conserved vertebrate ENT (GPi in primates)

My studies have helped to refine our understanding of the nuclei originally termed the ventral entopeduncular nucleus. The dorsal and ventral entopeduncular nuclei were first described in zebrafish by Wullimann et al. (1996) in his topographical atlas of the zebrafish brain. The homologies of these two nuclei have been somewhat controversial. A study by Castro et al. (2006) used the distribution of calretinin immunoreactive neurons relative to other neuropeptides and neurotransmitter-synthesising enzymes to define homologies of forebrain nuclei between zebrafish, other teleost species (a group that have an everted telencephalon) and other vertebrates. Castro et al. (2006) postulated that the dENT in zebrafish represents the caudal extension of Vl as they share the same NPY immunoreactivity. They also hypothesised that the dENT likely projects widely to the dorsal pallium and not the habenula. In Turner et al., (2016), working with my co-authors, I confirmed this finding, we also found that the dENT projects to the pallium. Castro et al. (2006) concluded that the vENT is the entopeduncular nucleus “proper” as they found processes from the vENT ascending to the habenula, as had also been described in the trout (Yáñez and Anadón, 1996) and goldfish (Villani et al., 1996).

In contrast to Castro et al. (2006), two other studies presented evidence that the dENT is the ENT “proper” and the vENT was rechristened as the “bed nucleus of the stria medullaris” (Mueller and Guo., 2009; Ganz et al., 2011). These homologies were based on the gene expression of the nuclei and not on their hodology. Analysis of the distribution of *GAD67*-expressing cell populations in the adult zebrafish forebrain found the dENT to be *GAD67*+ and suggested from the morphology of these cells that they might be pallidal GABAergic projection neurons. The dENT was easily distinguishable from the

GAD67- “former” vENT/BNSM. The whole entopeduncular complex was deemed not to be derived from the larval eminentia thalami as proposed by Wullimann and Mueller., 2004. Mueller and Guo (2009) defined the GAD67+ portion of the entopeduncular complex as a derivative of the subpallium and homologous to the entopeduncular nucleus of mammals (GPi in primates). The GAD67- vENT was described as the derivative of the larval EmT by the same authors. The larval EmT described as Calretinin (CR) positive and habenula afferent was proposed to be homologous to the CR+ thalamic eminence of the fetal mouse brain (Abbott and Jacobowitz, 1999), and Cajal’s nucleus of the stria medullaris in the rat (Risold and Swanson, 1995). What does the existing literature have to say about these different brain structures purportedly homologous to the vENT?

7.1.1 The bed nucleus of the stria medullaris (BNSM)

The BNSM, in the rat, is described as a densely packed enkephalinergic nucleus in the septal region. This group of neurons is described as distinct from other enkephalinergic groups in other septal nuclei such as; the lateral septal nucleus, the bed nucleus of the stria terminalis, the septofimbrial*, triangular nuclei* in the posterior septal region and also in the bed nucleus of the anterior commissure (*these posterior septal nuclei are afferent to the MHb in mammals). This nucleus is described as forming the most caudal extension of the septal region that may receive input from the fornix and be afferent to the medial habenula (although no tracing of the connections of this nucleus was performed in this study)(Risold and Swanson., 1995). The location of septal nuclei or a septal region remains to be defined in zebrafish, particularly at larval stages. Expression of the enkephalinergic markers *penka* and *penkb* like *somatostatin* lie within the neurosecretory preoptic hypothalamus (NPO)(Herget et al., 2014., Herget and Ryu., 2015). This diverse group of neurons lie slightly dorsal and medial to the vENT(see Chapter 3 Figure 3.13). Like the proximity of RL and the vENT the distinction between the vENT and neurons within the NPO at larval stages may be too close to call. The neuron labelled in Figure 5.6 with a medial/dorsal position close to/within the vENT could fit the description of a BNSM neuron as it projects through the stria medullaris to innervate the dorsal habenula.

7.1.2 EmT or thalamic emminence

The fatemap experiments and gene expression studies shown in Turner et al (2016) and presented in this thesis support the hypothesis that the vENT in zebrafish derives from the prethalamic eminence. The thalamic eminence in the mammalian brain is only observed in late embryonic and fetal stages but has been described as a distinct structure in other vertebrates including teleosts and urodeles, where it has been shown to project throughout the ipsilateral diencephalon and is thought to be involved in processing olfactory information. In mammals at the later stages of fetal development the EmT is continuous dorsally with the ventral thalamus. It is possible that the EmT acts as an organizing centre for the thalamus during its early development and may then ultimately be transformed into specific thalamic/hypothalamic structures in the adult (Abbott and Jacobowitz, 1999).

The vENT, and not the dENT, is afferent to the habenula. When hodology was used to test the homologies of the dENT and vENT, the vENT was found to be afferent to the vHb following tracer application by Amo et al. (2014). The reciprocal DiI experiments done in the adult by Monica Folgueira and the kaede photoconversion experiments in the larvae I have presented here (Fig 3.7) have built on this finding to show that only the vENT, and not the dENT, is afferent to the habenula. This evidence confirms the vENT as the homolog of the conserved vertebrate ENT and I believe the nucleus should be called as such. The location of the dENT and its developmental origins are yet to be confirmed in the larvae, but, given the hodological evidence that this nucleus does not project to the habenula it should be renamed to avoid further confusion.

7.1.3 The vENT is diencephalic in origin in all vertebrates

In mammals, the ENT has been described by Puelles to be pallidally derived (Puelles et al., 2000). Ganz et al., (2011) showed that the dENT in zebrafish expresses both the pallidal marker *nkx2.1b* in addition to *GAD67* (Mueller and Guo., 2009). The BNSM or vENT expresses the pallial marker tbr1 and is negative for the subpallial marker *dlx2a.* The pallidal identity of the dENT made it seem a more likely candidate to be the entopeducular nucleus “proper” in zebrafish, indeed this was the conclusion reached by Mueller and Guo (2009) and Ganz et al (2011). However other evidence suggests that the vertebrate ENT is likely to be diencephalic in origin in all vertebrates. The fate-mapping and gene expression data in Chapter 3 demonstrate that the vENT originates from the prethalamic eminence, as defined by the expression of *lhx5* and *tbr1* at 24-48hpf (Wullimann and Mueller., 2004; Mueller and Guo., 2009;Ganz et al., 2011; Lauter et al., 2013., Turner et al., 2016 and present results). In rat, the ENT is likely derived from an area in the diencephalon associated with the ventral diencephalic sulcus (Marchand et al., 1986). The EmT in *Xenopus*, mouse and chick also express *lhx5* and *tbr1* and contribute neurons to the basal telencepalon (Puelles et al., 2000; Brox et al., 2004; Abellán et al., 2010) as we have shown in zebrafish. These results all support a diencephalic, not pallidal origin, for the ENT.

7.1.4 Conservation of ENT circuitry

In mammals, the ENT modulates motor behaviours through its connections with the lateral habenula. This circuitry is highly conserved, as a similar pallidal circuit has been described in the lamprey (Yáñez and Anadón, 1994; Yáñez et al., 1999; Stephenson-Jones et al., 2011, 2012, 2013). The mammalian ENT is composed of both glutamatergic and GABAergic neurons, but its projection to the habenula has been shown to be excitatory (Shabel et al., 2012, 2014). This is also true for this same projection in lamprey (Stephenson-Jones et al., 2013). My results extend these findings to demonstrate that the same is true in zebrafish larvae (Turner et al., 2016, this study) and also in the adult where Amo et al (2014) showed that most ENT neurons express *vglut2a*. In the larvae (this study) as in adults (Mueller and Guo., 2009) few GABAergic cells are present in the ENT (labelled BNSM in Mueller and Guo., 2009).

The zebrafish ENT projects to the vHB (Amo et al., 2014, Turner et al., 2016 and this study) shown by gene expression and hodology to be the homolog of the mammalian lateral habenula (Amo et al., 2010). The vHb (Amo et al., 2010) and mouse lateral Hb (Pollack Dorocic et al., 2014) both extend glutamatergic projections to the median (superior) raphe.Two factors suggests that the vHb, median or superior raphe and ENT may constitute a three-part circuit: 1. The presence of serotinergic axons in the adult zebrafish ENT (Amo et al., 2014) and 2. The observation that the ENT area in Pet1:GFP transgenic adults also show GFP processes (Lillesaar et al., 2009). My mosaic labelling of serotinergic neurons, using the Tg(Pet1:KalTA4) transgenic line (See Chapter 6), also support this theory. Serotinergic terminals from superior/median raphe branch within the lateral forebrain bundle close to vENT dendrites and the medial vENT neuropil. This proximity suggests that the median raphe is afferent to the vENT. This evidence is still fairly weak being only preliminary data. Further analysis using synaptic markers would be required to confirm this and the Tg(Pet1:KALTA4) transgenic line provides the tools to undertake this analysis.

7.1.5 The function of vENT-vHb-MR circuitry

Amo et al. (2014), showed that the tonic neuronal activity of vHb neurons could play a role in active avoidance learning by encoding a negative reward expectation value. Inactivation of the vHb-MR pathway in zebrafish impairs the reinforcement learning of active avoidance and stopped the increase in the tonic firing rate of vHb neurons that results from associated of the conditioned and unconditioned stimuli at the early stages of active avoidance learning. The normal activity of this vHb-MR circuit transfers this negative reward expectation value to the reinforcement learning sytem to enable adaptive active avoidance (Amo et al., 2014). Photobleaching of ENT-vHb afferents (which acts to silence this afferent projection) in a different zebrafish study also resulted in a defect in active avoidance behaviour in response to an inescapable stressor (Lee et al., 2010). Activation of ENT inputs to LHb in mouse using optogenetics also causes avoidance of environments associated with the optogenetic stimulation (Shabel et al., 2012). Thus, this conserved ENT-vHb/LHb-MR circuitry seems to play a crucial role in the modulation of motor behaviours in response to both fear and reward across the vertebrate phylum (Amo et al., 2014., Aizawa et al., 2011).

7.1.6 Heterogeneity of cell-type and projection patterns of GPi/ENT neurons in mammals

Hetrogeneity of cell-types in the ENT/GPi is supported by both anatomical and physiological studies. In mice, ENT neurons have been shown to co-release GABA and glutamate onto LHb neurons (Shabel et al., 2012,2014). Despite co-releasing GABA, these projections are proposed to have a net excitatory effect on LHb neurons (Hong and Hikosaka, 2008; Shabel et al., 2014; Stephenson-Jones et al., 2016). Using RNA seq of hundreds of individual ENT neurons in the mouse, Wallace et al. (2017) identified 3 separate classes of ENT neurons. These classes were conserved within the GPi of humans. The three classes are composed of: a) A purely glutamaterigic LHb afferent neurons that express parvalbumin, b) A somatostatin (*Sst)* positive LHb afferent neuron that co-release GABA and, c) glutamate and a purely GABAergic class of ENT neuron that acts as the classic motor output nucleus of the GP and projects to motor thalamus but not the LHb (Wallace et al., 2017).

I have found *Sst*-positive cell in the area defined as ENT (Figure 3.13). These neurons seem to surround the lateral forebrain bundle in the ventral part of the ENT. There is also a larger, more medial group of *sst*-positive neurons in the medial part of the prethalamus/eminentia thalami (pink box Figure 3.13), adjacent to the diencephalic border. My mosaic labelling of cells in this area did not show whether these *sst*+ cells are habenula afferent, though this experiement was not comprehensive. From the literature it is possible that this medial group of *sst*+ cells could to belong to the neurosecretary preoptic area (Herget et al.,2014; Herget and Ryu.,2014). In the rat lateral habenula a dense *sst*+ terminal field is present (Vincent and Brown 1986). In zebrafish, some *sst* expression is present in the neuropil area of the dHb but as several dorsal habenula neurons are *sst*+ it is impossible to know the cellular origin of the *sst* puncta: it could be ENT or habenula (or elsewhere). Looking specifically at the innervation patterns of the various forebrain *sst*+ populations in zebrafish could help to further resolve homologies between the zebrafish and mammalian ENT/GPi. It would be especially interesting to determine if these cells are also capable of co-releasing GABA and glutamate in the vHb as shown in rat (Shabel et al., 2012,2014).

7.1.7 LHb and the dopaminergic system

In addition to LHb efferent projections onto serotinergic raphe neurons, the LHb in mammals projects to GABAergic rostro-medial tegmental neurons (Jhou et al., 2009). Phasic activation of LHb neurons leads to repression of midbrain dopaminergic (DA) neurons in the ventral tegmental area (VTA; Matsumoto and Hikosaka, 2007). The Hb-VTA pathway is thought to mediate aversive behaviours and overactivation of this pathway has been linked to depression (Shabel et al., 2012, Li et al., 2011,2013). As discussed in Amo et al (2014) the zebrafish does not have DA releasing areas that are homologous to the VTA and substantia nigra pars compacta. Instead, zebrafish have two clusters of dopaminergic neurons in the posterior tuberculum and posterior tuberal nucleus (Rink and Wullimann., 2002). Interaction between the zebrafish vENT-vHb-MR system and dopaminergic system remains to be examined. DA positive cells in the subpallium are present in larval zebrafish and some Tyrosine Hydroxylase+(TH+) processes are present within the lateral forebrain bundle. In the diencephalon, DA neurons are present in the ventral thalmus, posterior tuberculum and hypothalamus. Processes from these ventral diencephalic groups seem to heavily innervate the large area of neuropil caudal to the ENT, dorsal to the poc (Figure 1C and F in Kastenhuber et al., 2010 and Figure 6.22), as ENT neurons also do (Figure 6.13-14). TH-positive fibres detected using an anti-TH antibody, can also be seen in the stria medullaris and tHc with small neuropils in the vHb and dHb (Figure1H in Kastenhuber et al., 2010). It would be interesting to determine the source of these DA afferents and any points of convergence between DA neurons and ENT-vHb circuitry. This would serve to further clarify homologies between zebrafish and mammalian habenula associated circuitry.

7.2 RL is the visual habenula afferent nucleus in zebrafish

As stated in the Introduction, towards the very end of my doctorate, two studies identifying the same visual afferent circuit that my own work has determined have been published. One study has recently been published in Neuron (Zhang et al., 2017) and another published in BMC Biology (Cheng et al., 2017). What identity did these two complimentary studies ascribe to the visual afferent nucleus (termed RL in this thesis)?

7.2.1Afferent nuclei identity and stated homology

Zhang et al (2017)

Zhang et al (2017) state that the Retina-EmT-L-dHb pathway is evolutionarily conserved:

> "the EmT and dHb in zebrafish are homologous to the bed nucleus of the stria medullaris (BNSM) (Mueller and Guo, 2009; Risold and Swanson,

> 1995) and the MHb (Amo et al., 2010; Okamoto et al., 2012) in mammals, respectively. The BNSM is the posterolateral part of the medial division of the bed nucleus of the stria terminalis (BNST) (Risold and Swanson, 1995). Similar to our findings about the afferent and efferent of the EmT in zebrafish, it was reported that the BNST in rodents receives RGC axonal projections (Itaya et al., 1981) and innervates the MHb (Dong and Swanson, 2006; Hikosaka et al., 2008)."

This statement although very forcefully put is, at the very least, over simplistic and potentially incorrect. The references used to justify these statements are also quite misleading as the data in Zhang et al., (2017) for the most part does not correlate with the descriptions of the afferent nuclei described in these papers or their projections to MHb. The conflation of the BNST with the BNSM to extrapolate the existence of a homologous light preference circuit in mammals is also misleading. I will discuss the anatomy of the BNST below to illustrate why. The Hikosaka et al., (2008) reference is a review focussed predominantly on the lateral habenula circuitry that barely mentions the BNST and its afferent connections to the MHb: it just includes a small projection from BNST to both MHb and LHb in a general diagram of habenula afferent and efferent nuclei.

The area described by Zhang et al., (2017) as EmT where these dHb afferents are situated is not within the lateral *tbr*+ domain of the EmT (Wullimann and Mueller., 2004) that surrounds the lateral forebrain bundle that Mueller and Guo (2009) label as BNSM and we (Turner et al., 2016) and Castro et al (2006) define as the vENT or ENT "proper". Based on their position relative to the habenula these afferent neurons are not even necessarily within the medial part of the EmT as defined by (Wullimann and Mueller., 2004) as their lateral position directly ventral to the habenula makes them more likely to be within the ventral thalamus/prethalamus. Without many anatomical landmarks, the identity of these neurons would need to be checked using gene expression for specific markers of EmT and PTh. The calretinin+ cells projecting into the optic tract at AF4 (Figure 6D from Zhang et al., 2017 compare with blue box in Figure 7.1) are not, in my opinion, included in what Mueller and Guo (2009) refer to as the BNSM in the adult, or at least are the dorsal/caudal extension of this nucleus as the main group in both the larvae (yellow box in Figure 6.1) and in the adult (Castro et al., 2006) surround the lateral forebrain bundle. The most dorsal group of CR+ cells (orange box in Figure 7.1) seem to associate with AF9 (Burrill and Easter., 1996).

.

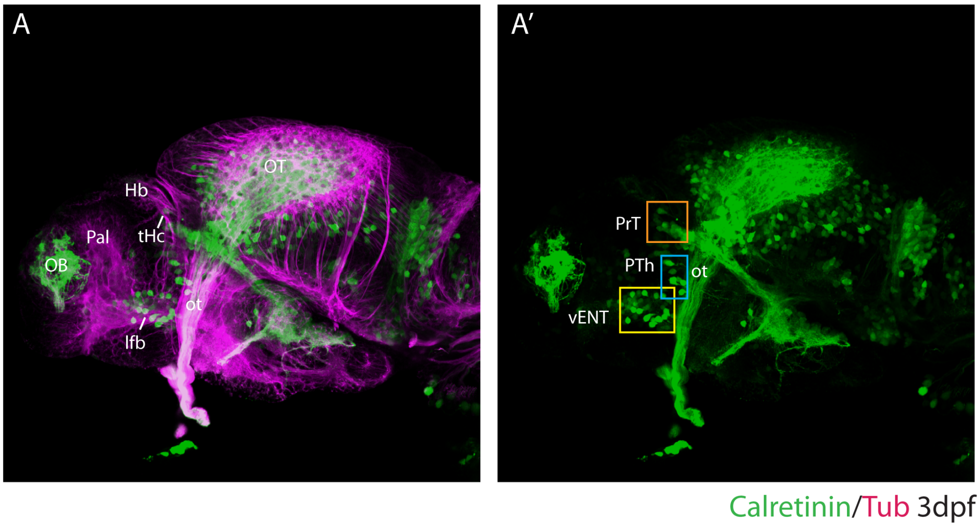

Figure 7.1: Calretinin expression at 3dpf labels a subset of neurons in the vENT, prethalamus and pretectum. (A-A’) Lateral view of a 3dpf zebrafish larvae labelled with anti-Calretinin(green) and anti-Tubulin(magenta) antibodies. Calretinin positive neurons are visible within the vENT, prethalamus (PTh) and pretectum (PrT).

What is the BNST and where is it in zebrafish?

The stria terminalis in humans serves as a major output pathway of the amygdala carrying fibres to septal nuclei and hypothalamic and thalamic areas of the brain. Ju and Swanson (1989) described the bed nucleus of the stria terminalis in rat as “an extremely complex mass of gray matter”. The BNST is a heterogeneous cell mass with relation to its cytoarchitecture and neuropeptide expression. It forms the ventral subdivision of the septal region and surrounds the anterior commissure just before it crosses the midline. Using thionin staining to describe the cellular organization of the BNST Ju and Swanson (1989) divided the BNST into 15 “relatively distinct” cell groups or nuclei that are embedded within an undifferentiated matrix of scattered nuclei. The BNST is divided by the vertical stria terminalis into anterior and posterior divisions. The anterior division forms a continuous cell mass traversed by the anterior commissure. The posterior division lies caudal to the dorsal and commissural bundles of the stria terminalis (Ju and Swanson, 1989a and 1989b).

Wullimann and Mueller (2004) state in their paper on the identification and morphogenesis of the EmT during zebrafish development that there is “practically no information on the *adult* fate of the developmentally clearly defined EmT in mammals. It has, in fact, even been claimed that the EmT may act as a transitory calretinin-rich signalling center (Abbott and Jaco- bowitz, 1999). Alternatively, the early mammalian EmT has been said to give rise to the bed nuclei of both stria medullaris and (extratelencephalic) stria terminalis (Puelles et al., 2000).”

Comparative gene expression studies in chick and mouse suggested the adult derivatives of the EmT in mouse include the bed nucleus stria medullaris, as well as posterior parts of the bed nucleus stria terminalis complex (Puelles et al., 2000 derived from evidence from Ju and Swanson,1989; see also the Paxinos and Watson, 1991 atlas). This lead Puelles to suggest a fundamental genetic difference between the Tbr-1-positive part of BNST, the part that gives rise to the BNSM/vENT and the Dlx-2/Nkx-2.1- positive part of BNST (Puelles et al., 2000).

The Dong and Swanson (2006) paper used by Zhang et al., 2017 to infer a homologous light-preference circuit in rat actually only looks at the connectivity of one nucleus within the **anteromedial** group of the BNST, the dorsomedial nucleus (BSTdm). Even if you assumed that this BNST nucleus is a part of the “posterior parts of the bed nucleus striae terminalis complex (Puelles et al., 2000)”, which logically you wouldn’t as it is stated to be part of the anteromedial group. The description of the projection patterns of the BSTdm nucleus is very different to the relatively simple projection pattern of the “EmT” neurons described in the zebrafish by Zhang et al., (2017). The BSTdm group in rats project very widely: “The BSTdm generates the densest known inputs to the neuroendocrine system from any part of the cerebral hemispheres” (Dong and Swanson., 2006). This nucleus does project to the habenula, mainly to the LHb with a small projection continuing into MHb. No mention of a role in visual behaviours is suggested and the connections of the BSTdm with inputs from striatal derived amygdala, and widespread efferent connections to the neuroendocrine system suggest a role in the regulation of fluid balance homeostasis through regulating drinking behaviour and sodium appetite (Dong and Swanson, 2006).

Itaya et al (1981) do describe an extrageniculate projection to the posterior part of the BST and to the anterodorsal and anteroventral thalamic nuclei in the rat. This retinal input to the limbic system has only been described in three mammals (Itaya et al., 1981). Some projections of the posterior part of the septal region, including from the posterior part of the BST, terminate in the MHb (Swanson and Cowan., 1979). Irrespective of the existence of RGC projection to the BST and BST projections to the habenula, it is still important to determine if the BST does actually derive from the EmT in zebrafish and where the BST actually is in larval zebrafish which has not been attempted by Zhang et al., (2017). Conserved molecular marker analysis in adult zebrafish ascribes the ventralmost part of Vs and Vp in the caudal subpallium as homologous to the pallidally derived part of the amygdala/homologous to the BST. This area is distinct from the ventro-lateral BNSM (vENT) and expresses different markers consistent with a subpallial origin (Ganz et al., 2011).

Cheng et al., (2017)

In their discussion Cheng et al (2017) also proposed that the identity of this thalamic nucleus could be the nucleus Rostro-lateralis citing our study on habenular afferents (Turner et al., 2016). Like us they found no projection to the IPN from this nucleus in contrast to Saidel’s description of RL connectivity in the butterfly fish (Saidel., 2013). They also query the Zhang et al., (2017) claim that this nucleus is the thalamic eminence that gives rise to the BNSM as using their vENT specific transgenic they can see this nucleus is distinct from the vENT and also state that the presence of GABAergic cells make it unlikely to be the glutamatergic BNSM. They do however concur that it is possible that this nucleus is another derivative of the thalamic eminence but that this had not yet been demonstrated by lineage tracing experiments (Cheng et al., 2017).

7.2.2 Possible adult identities of AFs (Burrill and Easter 2004)

The original description of the development of the AFs in larval zebrafish done by Burrill and Easter (1996), who attempted to ascribe adult identities to the 10AFs. These identities were allocated based on the relative positions of the AFs to each other and to the optic tract, not on their cytoarchitecture, as the nuclei that contribute to these AFs had not yet migrated into their adult positions within the superficial neuropil. Four of the AFs including AF10/the optic tectum were unambiguously paired with their adult identities. Unfortunately, AF4 and AF2 were not included in this group. In fact, the ambiguity of AF2 identity even had repercussions for the assignments of the other AFs resulting in 6 possible assignments for these remaining AFs.

According to Burrill and Easter's AF allocation the most likely candidate for AF2 is nVL (n. ventrolateralis thalami), an alternative is nAOD (n.accessorius opticus dorsalis). AF4 is probably nPSp (n.pretectalis superficialis pars parvicellularis) but alternatives are: nI (n.intermedius thalami), nA (n.anterioris thalami), nAOD or nVL. However, unlike some other AFs where the adult identity is clear, such as AF10 is the optic tectum, the allocated adult identities for both AF2 and AF4 were declared as quite ambiguous and so require further identification in the adult.

The first paper to identify RL in the zebrafish (Rink and Wullimann., 2004) came out in the same year as Burrill and Easter (2004) and so RL would not have been available as a candidate retinorecipient nucleus. In the 1month pf sections of Tg(cldnb:lynGFP) nPSp is also strongly labelled but nVL, and nI are not (Figure 4.18D). VL is labelled in Tg(lhx5:GFP) 1 month pf sections. nI and nVL are both GABAergic nuclei in the adult (Mueller and Guo., 2009; Mueller., 2012) and the prethalamic neurons surrounding AF4 at early stages are predominantly not GABAergic. Coupled with the fact that this AF4 receives input mostly from the ventral retina (Robles et al., 2014; Zhang et al., 2017) similar to nRL in *Pantodon* (Saidel and Butler., 1991) and its position relative to the Hb, VM/VL, optic tract and lateral forebrain bundle. AF4's afferent and efferent connections, including reciprocal connections with ventral telencephalon (Rink and Wullimann., 2004), eye and optic tectum make me believe that it is a good candidate for the source of these prethalamic afferents to the habenula. I also potentially see efferent projections from RL to the preglomerular complex (Figure 5.19F) as discussed in Saidel and Butler (1996). One thing I do not see from my mosaic labelling of prethalamic habenular afferents is an efferent projection from "RL" to the IPN via the fasiculus retroflexus as has been described in *Pantodon* (Saidel.,2013) so I cannot determine if RL is an extension of the epithalamus as Saidel suggests.

7.2.3 Is RL the caudal part of the ENT or a separate nucleus?

It is very clear from much of the data presented in this thesis (Summarised in Figure 5.23) and Cheng et al., (2017) DiI labelling, just how closely related the vENT and the RL are at larval stages and an association between the entopeduncular nucleus and RL has been described for *Lepisosteus* [Northcutt and Butler, 1993] and the two osteoglossomorph species *Pantodon* and *Osteoglossum* [Butler and Saidel, 1991, 1992]. (Rupp and Northcutt., 1998). RL has also been identified in *Xiphoporus helleri* but named as the "lateral entopeducular area" (Saidel and Butler., 1996). It is possible that RL could simply be the caudal extent of the vENT although the different organisation and projection patterns of the two cell groups seen in my mosaic labelling experiments do suggest that they are separate nuclei that both project to the habenula. This question is still being addressed by ongoing experiments in the adult by Monica Folgueira.

7.2.4 Is RL an adaptation in fish that hunt with ventral retina?

> "Ray-finned fishes display a spectacular range of evolutionary diversification, which is also reflected in the structure of their brains [Bath, 1962]. The differentiation of specific brain areas is determined both by the genealogical relationships and the ecological adaptations of each species. Vision plays a dominant role in the behavioral repertoire of most ray-finned fishes. With the exception of the optic tectum, the remaining nuclei that receive primary retinal projections are located in the diencephalon. The visual system of fishes has been shown to be particularly dynamic with respect to evolutionary changes [Northcutt and Wullimann, 1988; Wullimann and Meyer, 1990; Butler et al., 1991; Wullimann et al., 1991]." (Rupp and Northcutt., 1998)

Anne Butler and Bill Saidel's theory of the potential function of the RL fits well with both the circuitry of RL in zebrafish and the other species this nucleus has been described in. It also makes sense in light of the functional and behavioural data presented in Zhang et al. (2017) and Cheng et al., (2017), although it potentially provides a different interpretation of these results.

In *Pantodon,* where most of the work of RL has been focused, the circuitry of RL suggests that it is concerned with mapping some visual function occurring in the aerial field and integrating that afferent visual information with some visuomotor activity through its connections with the preglomerular complex and torus longitudinalis (Saidel and Butler., 1996). The African butterfly fish *Pantodon,* like zebrafish, and several others that possess substantial RL nuclei in their diencephala is a surface feeder. The association of this nucleus, RL with RGCs with large dendritic fields in the ventral retina could be an adaptation for surface feeding, where prey/food appearing in the dorsal visual field could be detected as a darkcircle surrounded by light. Inputs from these RGCs could be a basic stimulus for feeding and through connections through the DDC and midbrain monoaminergic nuclei provides a useful stimulus to the DDC to increase the excitability of motor systems prior to feeding and potentially increase the likelihood of successful prey capture. Being a surface feeder is not a prerequisite for having a RL though and so this adaptation could be seen more generally as an adaptation to increase motivation in response to a specific visual stimulus (Saidel and Butler., 1996., Saidel., 2013). This idea would not be incongruous with RLs perceived role in light-preference behaviours (as described in Zhang et al., 2017).

Undoubtedly, more work is required to correctly and definitively allocate the different AFs described at larval stages with their adult counterparts. These experiments are currently ongoing in our lab and will hopefully further clarify the identity of these rather ambiguous diencephalic nuclei at larval stages. Additionally, the identity of “septal” habenula afferents still need to be determined in the zebrafish.

To conclude I think that the dHb afferent neurons described in Zhang et al., (2017) based on their mosaic analysis are most likely the same neurons located directly ventral to the habenula around the tHc, slightly dorsal, and just caudal to the vENT in the prethalamus. They contact RGC terminals at AF4 and are afferent to the dHb and optic tectum (also seen in Zhang et al., 2017 but not elaborated on) and are the same cells described in this thesis that have been described as belonging to the nucleus rostro-lateralis. I think that the asymmetries in this projection to the habenula may have been overstated in these other studies as I see very heterogeneous innervation of the habenula in my mosaic labelling experiments and most afferent neurons seem to innervate more than one habenula subnuclei. I think that ultimately the functional asymmetries seen are dictated by the physical differences in size of the habenula subnuclear neuropils that result in the ability to synapse with more and ultimately excite more habenula neurons in the left dHb where the neuropil is much larger.

Reference List

Agetsuma, M. et al., 2010. The habenula is crucial for experience-dependent modification of fear responses in zebrafish. *Nature Neuroscience*, 13(11), pp.1354–1356.

Aizawa, H. et al., 2005. Laterotopic representation of left-right information onto the dorso-ventral axis of a zebrafish midbrain target nucleus. *Current biology*, 15(3), pp.238–243.

Amo, R. et al., 2010. Identification of the Zebrafish Ventral Habenula As a Homolog of the Mammalian Lateral Habenula. *Journal of Neuroscience*, 30(4), pp.1566–1574.

Appelbaum, L. et al., 2009. Sleep-wake regulation and hypocretin-melatonin interaction in zebrafish. *PNAS*, 106(51), pp.21942–21947.

Barth, K.A. et al., 2005. fsi Zebrafish Show Concordant Reversal of Laterality of Viscera, Neuroanatomy, and a Subset of Behavioral Responses. *Current Biology*, 15(9), pp.844–850.

Bianco, I.H. & Wilson, S.W., 2009. The habenular nuclei: a conserved asymmetric relay station in the vertebrate brain. *Philosophical Transactions of the Royal Society B: Biological Sciences*, 364(1519), pp.1005–1020.

Bianco, I.H. et al., 2008. Brain asymmetry is encoded at the level of axon terminal morphology. *Neural Development*, 3, p.9.

Braford, M.R., Jr, 2009. Stalking the Everted Telencephalon: Comparisons of Forebrain Organization in Basal Ray-Finned Fishes and Teleosts. *Brain, Behavior and Evolution*, 74(1), pp.56–76.

Bromberg-Martin, E.S. & Hikosaka, O., 2011. Lateral habenula neurons signal errors in the prediction of reward information. *Nature Neuroscience*, 14(9), pp.1209–1216.

Concha, M.L. & Wilson, S.W., 2001. Asymmetry in the epithalamus of vertebrates. *Journal of Anatomy*, 199(1-2), pp.63–84.

Concha, M.L. et al., 2000. A nodal signaling pathway regulates the laterality of neuroanatomical asymmetries in the zebrafish forebrain. *Neuron*, 28(2), pp.399–409.

Concha, M.L. et al., 2003. Local tissue interactions across the dorsal midline of the forebrain establish CNS laterality. *Neuron*, 39(3), pp.423–438.

Dirian, L. et al., 2014. Spatial regionalization and heterochrony in the formation of adult pallial neural stem cells. *Developmental Cell*, 30(2), pp.123–136.

Dreosti, E. et al., 2014. Left-right asymmetry is required for the habenulae to respond to both visual and olfactory stimuli. *Current biology : CB*, 24(4), pp.440–445.

Facchin, L., Argenton, F. & Bisazza, A., 2009. Lines of Danio rerio selected for opposite behavioural lateralization show differences in anatomical left–right asymmetries. *Behavioural brain research*.197(2009)pp.157-165.

Facchin, L., Burgess, H.A., et al., 2009. Determining the function of zebrafish epithalamic asymmetry. *Philosophical Transactions of the Royal Society B: Biological Sciences*, 364(1519), pp.1021–1032.

Facchin, L., Duboue, E.R. & Halpern, M.E., 2015. Disruption of Epithalamic Left-Right Asymmetry Increases Anxiety in Zebrafish. *Journal of Neuroscience*, 35(48), pp.15847–15859.

Folgueira, M., Anadón, R. & Yáñez, J., 2004. Experimental study of the connections of the telencephalon in the rainbow trout (Oncorhynchus mykiss). II: Dorsal area and preoptic region. *Journal of Comparative Neurology*, 480(2), pp.204–233.

Folgueira, M.N. et al., 2012. Morphogenesis underlying the development of the everted teleost telencephalon. *Neural Development*, 7(1), pp.1–1.

Folgueira, M.N., Anad n, R.N. & Y ez, J.N., 2004. An experimental study of the connections of the telencephalon in the rainbow trout (Oncorhynchus mykiss). I: Olfactory bulb and ventral area. *Journal of Comparative Neurology*, 480(2), pp.180–203.

Furlan, G. et al., 2017. Life-Long Neurogenic Activity of Individual Neural Stem Cells and Continuous Growth Establish an Outside-In Architecture in the Teleost Pallium. *Current biology : CB*, 27(21), pp.3288–3301.e3.

Gamse, J.T., 2005. Directional asymmetry of the zebrafish epithalamus guides dorsoventral innervation of the midbrain target. *Development*, 132(21), pp.4869–4881.

Gamse, J.T. et al., 2003. The parapineal mediates left-right asymmetry in the zebrafish diencephalon. *Development*, 130(6), pp.1059–1068.

Ganz, J. et al., 2011. Subdivisions of the adult zebrafish subpallium by molecular marker analysis. *Journal of Comparative Neurology*, 520(3), pp.633–655.

Glick, S.D. et al., 2006. 18-Methoxycoronaridine acts in the medial habenula and/or interpeduncular nucleus to decrease morphine self-administration in rats. *European journal of pharmacology*, 537(1-3), pp.94–98.

Groenewegen, H.J. & Van Dijk, C.A., 1984. Efferent connections of the dorsal tegmental region in the rat, studied by means of anterograde transport of the lectin Phaseolus vulgaris-leucoagglutinin (PHA-L). *Brain Research*, 304(2), pp.367–371.

Gutiérrez-Ibáñez, C. et al., 2011. Variation in asymmetry of the habenular nucleus correlates with behavioural asymmetry in a cichlid fish. *Behavioural brain research*, 221(1), pp.189–196.

Hendricks, M. & Jesuthasan, S., 2007. Asymmetric innervation of the habenula in zebrafish. *Journal of Comparative Neurology*, 502(4), pp.611–619.

Hendricks, M. & Jesuthasan, S., 2011. Asymmetric innervation of the habenula in zebrafish. *Journal of Comparative Neurology*, 519(18), pp.3815–3815.

Hennigan, K., D'Ardenne, K. & McClure, S.M., 2015. Distinct midbrain and habenula pathways are involved in processing aversive events in humans. *The Journal of Neuroscience*, 35(1), pp.198–208.

Herkenham, M. & Nauta, W.J., 1977a. Afferent connections of the habenular nuclei in the rat. A horseradish peroxidase study, with a note on the fiber-of-passage problem. *Journal of Comparative Neurology*, 173(1), pp.123–146.

Herkenham, M. & Nauta, W.J.H., 1977b. Afferent connections of the habenular nuclei in the rat. A horseradish peroxidase study, with a note on the fiber-of-passage problem. *Journal of Comparative Neurology*, 173(1), pp.123–145.

Hétu, S. et al., 2016. Asymmetry in functional connectivity of the human habenula revealed by high-resolution cardiac-gated resting state imaging. *Human Brain Mapping*, 37(7), pp.2602–2615.

Hikosaka, O., 2010. The habenula: from stress evasion to value-based decision-making. *Nature Reviews Neuroscience*, 11(7), pp.503–513.

Hikosaka, O., Nakamura, K. & Nakahara, H., 2006. Basal ganglia orient eyes to reward. *Journal of neurophysiology*, 95(2), pp.567–584.

Hong, S. & Hikosaka, O., 2008. The globus pallidus sends reward-related signals to the lateral habenula. *Neuron*, 60(4), pp.720–729.

Hong, S. et al., 2011. Negative reward signals from the lateral habenula to dopamine neurons are mediated by rostromedial tegmental nucleus in primates.*The Journal of Neuroscience*,31(32),pp.11457-11471.

Ichijo, H. et al., 2016. An Evolutionary Hypothesis of Binary Opposition in Functional Incompatibility about Habenular Asymmetry in Vertebrates. *Frontiers in neuroscience*, 10, p.595.

Ichijo, H. et al., 2015. Lateralization, maturation, and anteroposterior topography in the lateral habenula revealed by ZIF268/EGR1 immunoreactivity and labeling history of neuronal activity. *Neuroscience research*, 95, pp.27–37.

Jhou, T.C. et al., 2009. The rostromedial tegmental nucleus (RMTg), a GABAergic afferent to midbrain dopamine neurons, encodes aversive stimuli and inhibits motor responses. *Neuron*, 61(5), pp.786–800.

Kastenhuber, E. et al., 2010. Genetic dissection of dopaminergic and noradrenergic contributions to catecholaminergic tracts in early larval zebrafish. *Journal of Comparative Neurology*, 518(4), pp.439–458.

Lawson, R.P. et al., 2014. The habenula encodes negative motivational value associated with primary punishment in humans. *Proceedings of the National Academy of Sciences*, 111(32), pp.11858–11863.

Lillesaar, C. et al., 2009. Axonal projections originating from raphe serotonergic neurons in the developing and adult zebrafish, Danio rerio, using transgenics to visualize raphe-specific pet1expression. *Journal of Comparative Neurology*, 512(2), pp.158–182.

Mathuru, A.S. & Jesuthasan, S., 2013. The medial habenula as a regulator of anxiety in adult zebrafish. *Frontiers in neural circuits*, 7, p.99.

Matsumoto, M. & Hikosaka, O., 2008. Representation of negative motivational value in the primate lateral habenula. *Nature Neuroscience*, 12(1), pp.77–84.

McCallum, S.E. et al., 2012. α3β4 nicotinic acetylcholine receptors in the medial habenula modulate the mesolimbic dopaminergic response to acute nicotine in vivo. *Neuropharmacology*,63(2012),pp.434-440.

Miyasaka, N. et al., 2009. From the Olfactory Bulb to Higher Brain Centers: Genetic Visualization of Secondary Olfactory Pathways in Zebrafish. *Journal of Neuroscience*, 29(15), pp.4756–4767.

Morley, B.J., 1986. The Interpeduncular Nucleus. *International Review of Neurobiology*. Elsevier, pp. 157–182.

Mueller, T., 2012. What is the thalamus in zebrafish?*Frontiers in Neuroscience*,6. pp.1–14.

Mueller, T. & Wullimann, M.F., 2009. An Evolutionary Interpretation of Teleostean Forebrain Anatomy. *Brain, Behavior and Evolution*, 74(1), pp.30–42.

Mueller, T., Wullimann, M.F. & Guo, S., 2008. Early teleostean basal ganglia development visualized by ZebrafishDlx2a,Lhx6,Lhx7,Tbr2 (eomesa), andGAD67 gene expression. *Journal of Comparative Neurology*, 507(2), pp.1245–1257.

Northcutt, R.G., 2011. Do Teleost Fishes Possess a Homolog of Mammalian Isocortex? *Brain, Behavior and Evolution*, 78(2), pp.136–138.

Northcutt, R.G., 2008. Forebrain evolution in bony fishes. *Brain Research Bulletin*, 75(2-4), pp.191–205.

Okamoto, H., Agetsuma, M. & Aizawa, H., 2012. Genetic dissection of the zebrafish habenula, a possible switching board for selection of behavioral strategy to cope with fear and anxiety. *Developmental Neurobiology*, 72(3), pp.386–394.

R Baldwin, P., Alanis, R. & Salas, R., 2012. The Role of the Habenula in Nicotine Addiction. *Journal of Addiction Research & Therapy*, 01(S1).

Randlett, O. et al., 2015. Whole-brain activity mapping onto a zebrafish brain atlas. *Nature Publishing Group*, 12(11), pp.1039–1046.

Regan, J.C. et al., 2009. An Fgf8-dependent bistable cell migratory event establishes CNS asymmetry. *Neuron*,61,pp.27-34.

Rink, E. & Wullimann, M.F., 2004. Connections of the ventral telencephalon (subpallium) in the zebrafish (Danio rerio). *Brain Research*, 1011(2), pp.206–220.

Rothenaigner, I. et al., 2011. Clonal analysis by distinct viral vectors identifies bona fide neural stem cells in the adult zebrafish telencephalon and characterizes their division properties and fate. *Development*, 138(8), pp.1459–1469.

Roussigné, M., Blader, P. & Wilson, S.W., 2012. Breaking symmetry: The zebrafish as a model for understanding left-right asymmetry in the developing brain. *Developmental Neurobiology*, 72(3), pp.269–281.

Sagasti, A. et al., 2005. Repulsive Interactions Shape the Morphologies and Functional Arrangement of Zebrafish Peripheral Sensory Arbors. *Current Biology*, 15(9), pp.804–814.

Salas, R. et al., 2010. BOLD Responses to Negative Reward Prediction Errors in Human Habenula. *Frontiers in human neuroscience*, 4, p.36.

Savitz, J.B. et al., 2011. Habenula Volume in Bipolar Disorder and Major Depressive Disorder: A High-Resolution Magnetic Resonance Imaging Study. *Biological Psychiatry,*69, pp.336-343.

Shabel, S.J. et al., 2012. Input to the lateral habenula from the basal ganglia is excitatory, aversive, and suppressed by serotonin. *Neuron*, 74(3), pp.475–481.

Shibata, H. & Suzuki, T., 1984. Efferent projections of the interpeduncular complex in the rat, with special reference to its subnuclei: a retrograde horseradish peroxidase study. *Brain Research*, 296(2), pp.345–349.

Stephenson-Jones, M. et al., 2012. Evolutionary conservation of the habenular nuclei and their circuitry controlling the dopamine and 5-hydroxytryptophan (5-HT) systems. *Proceedings of the National Academy of Sciences*, 109(3), pp.E164–E173.

Sutherland, R.J., 1982. The Dorsal Diencephalic Conduction System: A Review of the Anatomy and Functions of the Habenular Complex. *Neuroscience and biobehavioral reviews*, 6(1), pp.1–13.

Tay, T.L. et al., 2011. Comprehensive catecholaminergic projectome analysis reveals single-neuron integration of zebrafish ascending and descending dopaminergic systems. *Nature communications*, 2, p.171.

Varga, V., Kocsis, B. & Sharp, T., 2003. Electrophysiological evidence for convergence of inputs from the medial prefrontal cortex and lateral habenula on single neurons in the dorsal raphe nucleus. *The European journal of neuroscience*, 17(2), pp.280–286.

Wullimann, M.F. & Mueller, T., 2004a. Identification and morphogenesis of the eminentia thalami in the zebrafish. *Journal of Comparative Neurology*, 471(1), pp.37–48.

Wullimann, M.F. & Mueller, T., 2004b. Teleostean and mammalian forebrains contrasted: Evidence from genes to behavior. *Journal of Comparative Neurology*, 475(2), pp.143–162.

Yamaguchi, T. et al., 2013. Distinct Roles of Segregated Transmission of the Septo-Habenular Pathway in Anxiety and Fear. *Neuron*, 78(3), pp.537–544.

Yamamoto, N. et al., 2007. A New Interpretation on the Homology of the Teleostean Telencephalon Based on Hodology and a New Eversion Model. *Brain, Behavior and Evolution*, 69(2), pp.96–104.

Yañez, J. & Anadón, R., 1996. Afferent and efferent connections of the habenula in the rainbow trout (Oncorhynchus mykiss): an indocarbocyanine dye (DiI) study. *Journal of Comparative Neurology*, 372(4), pp.529–543.

Yañez, J. et al., 2009. Pineal projections in the zebrafish (Danio rerio): overlap with retinal and cerebellar projections. *Neuroscience*, 164(4), pp.1712–1720.